COPPER MATTE VACUUM PURIFICATION

by

André Allaire

A thesis submitted to the faculty of Graduate Studies and Research in partial fulfillment of the requirements for the degree of Doctor of Philosophy.

Department of Mining and Metallurgical Engineering,
McGill University,
Montréal, Canada.

May, 1991

To my wife, Patricia.

Abstract

An investigation of copper matte vacuum purification was undertaken. A mathematical model using monatomic, diatomic sulphide and diatomic oxide vapours of the impurities was developed to explain the vacuum refining process. The model was used to predict the overall refining rates for variables such as temperature, matte grade, oxygen activity and chamber pressure of the melt.

A series of experiments was undertaken to characterize the dust produced during vacuum refining of copper matte. An attempt to selectively condense the vapours produced during the vacuum refining experiments was carried out. From these experiments, it was found that :

1) The main mineralogical species in the dust were lead sulphide (PbS), zinc sulphide (ZnS) and metallic lead (Pb).

2) More than 80 % of the copper present in the dust was due to splashing. A dust of 1 to 2 % copper can be produced by reducing matte splashes.

3) The fifty percent passing size of the dust (dry sieve screening) was found to be 80 microns. However, scanning electron microscopy showed that the grains of dust were clusters of sub-micron particles homogeneously condensed.

4) It was demonstrated that selective condensation of ZnS from the vapour mixture was possible by controlling both the temperature of the condenser and the total chamber pressure.

The "Lift-Spray" vacuum refining process was used to refine 15 to 40 kg batches of molten copper matte containing 35 to 78 % copper. The removal rates of lead, bismuth, arsenic, antimony, selenium, nickel and silver were measured under different levels of matte grade, chamber pressure, lifting gas flow rate and dissolved oxygen content in the melt. The ranges of the variables under study were from 10 to 600

pascals chamber pressure, 0 to 40 normal milliliter per second of lifting gas flow rate and 10^{-16} to 10^{-7} atmosphere of oxygen activity. The duration of the experiments varied between 40 and 60 minutes and it was found that:

1) Increases of the rates of refining of 60 percent, compared to still melt experiments, were possible in the pilot LSV apparatus, for the lifting gas flow rate range under study.

2) Percent removal of up to 99 % of the lead, 97 % of the bismuth, 100 % of the arsenic and 73 % of the antimony were recorded under certain experimental conditions.

3) No removal of selenium, nickel or silver was recorded during the experiments.

4) The removal rates of lead and bismuth were insensitive to the oxygen content of the melt and the percent copper in the matte.

5) The removal rates of arsenic and antimony became negligible when the percent copper in the matte increased from 65 to 80 % copper.

6) The removal rates of arsenic and antimony increase with increasing oxygen activity in the melt.

7) The removal rate of lead, bismuth, arsenic and antimony decreased with increasing pressure, but all responded differently with respect to pressure changes from 10 to 600 pascal.

In conclusion, LSV refining of copper matte was shown to be a promising process. Furthermore, scale-up to industrial size is now possible. The scale-up dimensions compare well to the dimensions of the RH degassing unit presently used in the steel industry.

Résumé

Une étude sur la purification sous vide de la matte de cuivre a été entreprise. Un modèle mathématique, utilisant les vapeurs monoatomiques, monosulphuriques et monooxidiques des impuretés, a été proposé pour expliquer l'affinage sous vide de la matte. Le modèle a été utilisé pour prédire le taux d'épuration des impuretés lorsque des variables tel que la température du bain, la teneur en cuivre de la matte, l'activité de l'oxygène dans le bain et la pression totale ont été variées.

Une série d'expériences a été faite pour déterminer les charactéristiques de la poussière produite durant l'affinage de la matte de cuivre. Des essais pour condenser de façon sélective les vapeurs produites ont été faits. De ces expériences il a été démontré que:

1) Les principales espèces minérales dans la poussière sont le sulphure de plomb (PbS), le sulphure de zinc (ZnS) et le plomb metallique (Pb).

2) Plus de 80 % du cuivre contenu dans la poussière provient des éclaboussures et une poussière de 1 à 2 % de cuivre peut être produite sans les éclaboussures.

3) Par tamisage à sec, il a été trouvé que le d_{50} de la poussière est de 80 microns. Toutefois, des images par microscope à balayage électronique ont montré que les grains de poussières étaient des agrégats de plusieurs grains plus petits que 1 micron.

4) Il a été demontré qu'il est possible de condenser le sulphure de zinc (ZnS) séparément du mélange de vapeurs produites à l'affinage en controllant la température du condenseur et la pression totale dans la chambre à vide.

Le procédé d'affinage sous vide "Lift-Spray" a été utilisé pour purifier des lots de matte contenant 35 à 78 % de

cuivre. Les taux d'épuration du plomb, bismuth, arsenique, antimoine, selenium, nickel et de l'argent ont été mesurés à différentes teneurs en cuivre de la matte, pressions atmosphériques, taux d'injection du gaz à élévation et niveau d'oxygène dissout dans la matte. La pression totale de la chambre à vide a été variée de 10 à 600 pascal, le taux du gaz de 0 à 40 mililitre par seconde et l'activité de l'oxygène dans le bain de matte de 10^{-16} à 10^{-7} atmosphère.

Les expériences d'affinage sous vide ont duré entre 40 et 60 minutes et il a été démontré que:

1) Le taux d'affinage sous vide dans l'appareil LSV est 60 pourcent plus élevé que pour des expériences dans des bains statiques.

2) Des pourcentages d'élimination maximum de 99 % pour le plomb, 97 % pout le bismuth, 100 % pour l'arsenic et 73 % pour l'antimoine ont été enregistrés durant les expériences.

3) Aucune élimination n'a été observée pour le sélénium, le nickel et l'argent durant les expériences.

4) Les taux d'élimination du plomb et du bismuth ne sont pas fonction de l'activité de l'oxygène dans le bain et du pourcentage de cuivre dans la matte.

5) Les taux d'élimination de l'arsenic et de l'antimoine augmentent avec l'activité de l'oxygène dans le bain.

6) Les taux d'élimination de l'arsenic et de l'antimoine deviennent négligeables quand le pourcentage de cuivre dans la matte augmente de 65 à 80 %.

7) Les taux d'élimination du plomb , du bismuth, de l'arsenique et de l'antimoine diminuent avec l'augmentation de la pression totale du système, mais ils démontrent tous des comportements différents.

Pour conclure, le procédé "Lift-Spray" est très prometteur pour le traitement de la matte de cuivre et il est maintenant possible de calculer la taille d'un appareil pour application industrielle. La grandeur de l'appareil se compare bien aux dimensions d'un appareil de dégazage de type "RH" utilisé dans l'industrie de l'acier.

Acknowledgements

I was very fortunate to have the support and help of many people during the course of my graduate studies at McGill university. I wish to express my gratitude to all the members of the McGill Metallurgical Department who made my studies interesting and enjoyable.

I want to make a special mention of professor Ralph Harris, my thesis supervisor. Under his guidance and through many challenging discussions, I improved my technical skills and developed my full potential. I appreciated his being available and eager to discuss my work or helping me in the laboratory.

I want to further thank my fellow graduate students, Javier Jara, Francesco Dimayuga and Ernie Mast for interesting feedback. Also thank you to Frank Buijen, an exchange student from the Netherlands, for writing the LSV computer simulation program.

Financial support for my studies and for the Lift-Spray vacuum refining project was provided by Noranda Inc. and NSERC. Needless to say that none of this work would have been possible without their support.

I appreciated the time taken by the personnel of the Noranda Technology Center for the project follow up, the sample assays and their views on the project. More specifically thank you to Dr. Dan Poggi and to Hans Persson of the technology center.

It was a pleasure to meet with J.Dutrizac, our contact with NSERC who continuously provided useful comments and challenging questions.

Table of Contents

List of Tables

List of Figures

List of Symbols

A	Surface Area Available for Evaporation (m^2)
$D_{i,G}$	Diffusion Coefficient of Species i in the Gas ($m^2 s^{-1}$)
$D_{i,L}$	Diffusion Coefficient of Species i in the Liquid ($m^2 s^{-1}$)
g	Gravitational Acceleration ($m\ s^{-2}$)
j	Number of Atoms in Polyatomic Species
K_E	Evaporation Mass Transfer Coefficient ($m\ s^{-1}$)
K_G	Gas Phase Mass Transfer Coefficient ($m\ s^{-1}$)
K_L	Liquid Phase Mass Transfer Coefficient ($m\ s^{-1}$)
K^{eq}	Equilibrium Constant of the Reaction
K_{ov}	Overall Mass Transfer Coefficient ($m\ s^{-1}$)
l_c	Diameter of Droplet (m)
M	Molar Mass ($kg\ kgmole^{-1}$)
$\dot{n}''_b$	Molar Flux of Bulk Species($kgmole\ m^{-2}s^{-1}$)
$\dot{n}''_i$	Molar Flux of Element i ($kgmole\ m^{-2}s^{-1}$)
N_b	Molar Concentration of Bulk Liquid ($kgmole\ m^{-3}$)
N_i	Molar Concentration of species i in Liquid ($kgmole\ m^{-3}$)
P_b	Pressure of Evaporating Bulk Species (Pa)
P_i	Pressure of Species i (Pa)
P_i^o	Equilibrium Vapour Pressure of Pure Species (Pa)
$P_{i,\infty}$	Vapour Pressure of Species i in the Bulk Gas Phase (Pa)
R	Universal Gas Constant ($Joules\ kgmole^{-1}\ K^{-1}$)
s	Surface Renewal Rate (s^{-1})
T	Temperature (K)
t_e	Exposure Time of a Liquid Element to the Surface of the Liquid Phase (s)
V	Total Volume of the Melt (m^3)

X_i	Mole Fraction of Species i in Liquid
α	Accomodation Coefficient
δ	Density (kg m^{-3})
δ_{eff}	Effective Film Thickness (m)
θ	Penetration Time (s)
ϕ	Olette's Activity Coefficient
γ	Raoultian Activity Coefficient
ψ	Constant Relating the Vapour Pressure to the Molar Concentration in the Liquid (kg m^2 $kgmole^{-1}$ s^{-2})
σ	Surface Tension (kg s^{-2})

CHAPTER 1

Introduction

1.1 Background

Approximately 90% of the world's primary copper is produced through the concentration, matte smelting and electro -refining of copper sulphide ores (1). Of major concern to today's copper industry is the control of the impurity levels in cathode copper. The sources of relatively pure copper ores are being depleted. Impure, lower quality copper concentrates (7) are appearing in today's market place. Increasing levels of impurities, such as bismuth, arsenic and antimony are becoming problematic for two reasons. Firstly, these are not being efficiently removed during the matte smelting processes hence, larger residuals are reporting in the anode copper (7). Secondly, the copper electrolytic refinery can only tolerate finite levels of these impurities for they tend to contaminate the electrolyte, resulting in decreased cathode purity (1,2).

In the 70's, the copper industry underwent modernization in an attempt to make the copper smelting processes more cost efficient, to reduce metal fume plant emissions, and to increase sulphur recovery levels. The new modern matte production methods, such as flash smelting, Mitsubishi process and Noranda Reactor, utilize tonnage oxygen and the heat evolved during the oxidation of the sulphide

concentrates to produce higher grade copper mattes, as well as higher sulphur dioxide concentrations in the off gases. These new processes are more fuel efficient, less labor intensive and thus, more cost effective than conventional reverberatory matte smelting methods. However, these processes result in higher impurity concentrations in the high grade copper matte as well as a shorter copper converting time. The end result is increased levels of bismuth, arsenic and antimony in the blister copper (2,3,4).

Several options exist to control the impurity levels in the blister copper. Noranda Inc., Horne Smelter, for example, controls the impurity levels via the blending and selection of the concentrates charged to the smelting unit which results in a maximum elimination of impurities (21). It is well known that smelters schedule their converting charges for maximum volatilization and "slagging-off" of impurities (21). Volatilized products condense in the flue duct to form dust. The dust can then be bled from the circuit, instead of recirculated, to create an additional output for the volatilized impurities (17). Finally, impurities can be slagged off the blister copper during fire refining (15,16).

An option, not yet commercialized, is the application of vacuum refining of copper matte to the removal of impurities during copper matte smelting. The advantages of vacuum refining copper matte are as follows:

1-Removal of all volatile impurities from the matte, such as lead, zinc, bismuth, arsenic, antimony and possibly selenium and nickel with commensurate improvements in final cathode quality.

2-Reduction of the emissions of metal fumes in the smelter leading to a healthier working environment.

3-Reduction of the plant emission of lead, cadmium and arsenic dust from the smelter stack into the atmosphere.

1.2 Vacuum Refining of Copper Matte

The author has previously carried out a study on vacuum refining of copper matte in simple batch experiments. The matte was contained in standard straight sided alumina crucibles (52). The objective was to measure the evaporation rates of bismuth, arsenic, antimony and lead from copper matte melts over a range of matte grades, melt temperatures and chamber pressures.

It was concluded that the vacuum refining experiments followed first order kinetics during the initial stages of refining after melt degassing. The overall evaporation rate coefficients were measured for each impurity as a function of the operating parameters. To achieve the maximum removal rates (melt side mass transfer control), matte grades of 65 % copper or less, and chamber pressures less than 100 pascal were required. The removal rates were relatively insensitive to temperature since they were controlled by transfer in the liquid phase.

The study demonstrated the feasibility of vacuum refining copper matte to remove lead, bismuth, arsenic and antimony. The removal rates were measured and scale-up calculations to commercial size were performed. The calculations predicted refining rates too slow for vacuum refining of quiescent industrial size copper matte ladles. It was concluded that in

order to reduce refining time, larger surface areas were required.

A process called "Lift-Spray Vacuum Refining" (LSV) is being developed at McGill University to create larger evaporation surface areas in an attempt to reduce the refining time.

1.3 Objective of This Study

The overall objective of this investigation was to examine the feasibility and commercial validity of using the LSV process to refine copper matte. To achieve this objective the experimental work was divided into two sections; the characterization of the vacuum refining dust and the "Lift-Spray" vacuum refining of copper matte melts.

The characteristics of the dust produced during refining were scrutinized both, to obtain information leading to the recovery of the valuable metals present in the dust and to limit the extent of copper entrainment. The objectives of this section were :

1-To identify the major mineralogical species in the dust.

2-To quantify the amount of copper present in the dust and determine the mechanism by which it was transported from the melt.

3-To investigate the possibility of fractional condensation of the vapours produced during vacuum refining of copper matte.

The objectives of the LSV refining of copper matte section were to :

1-Measure the rate of evaporation of lead, bismuth, arsenic, and antimony as function of variables such as matte grade, oxygen activity, chamber pressure and melt temperature.

2-Measure the surface area generated in the LSV process as a function of the lifting gas flow rate and to show that surface areas available for evaporation in the LSV process are larger than in straight walled crucible.

3-To develop a mathematical model to predict the overall refining rates as a function of the operating parameters such as matte grade, chamber pressure, sulphur and oxygen activity in the melt, and test the model against experimental data.

CHAPTER 2

Literature Survey

2.1 Introduction

Several techniques can be used to increase the removal of the group Vb elements (Bi, As, Sb) during the pyrometallurgical treatment of copper sulphide concentrates. This chapter briefly reviews the existing and the newly emerging methods.

The elimination methods that will be discussed in this chapter are as follows:

a) Prior to smelting the copper concentrates, the removal of bismuth, arsenic, antimony and lead can be achieved by sulphidation or chlorination in a rotary kiln or, by roasting the concentrates.

b) During the copper matte making stage, removal of bismuth, arsenic, antimony and lead can be achieved by bleeding the flue dust from the smelting and converting vessels or by vacuum refining the copper matte.

c) Once the matte has been converted to blister copper, the removal of bismuth, arsenic, antimony and lead can be accomplished by either slagging-off the impurities using a sodium carbonate flux or by vacuum refining the blister copper.

2.2 Sulphidation or Chlorination in a Rotary Kiln

Impurities, in particular arsenic, can be volatilized from copper concentrates by adding sulphur (sulphidation) in a tight rotary kiln furnace and heating the concentrate between 500 and 900 ^{o}C. At these temperatures, the complex minerals decompose and evaporate in the form of sulphide species (46).

If the content of bismuth, antimony and lead is very high in the concentrate, simultaneous chlorination (addition of a chlorinating agent) with sulphidation is required for evaporation of these elements in the form of gaseous chloride species (46).

The proceeding techniques would be especially advantageous if the concentrate required drying prior to smelting since both the drying and impurity evaporation process could be combined into a single unit. This would only involve the additional expenditure of energy required to raise the temperature between 500 and 900 degrees celsius.

2.3 Roasting of Copper Concentrates

Impurity elimination from copper concentrates, in particular arsenic and antimony, is possible in the roasting step prior to matte smelting (32,33), since metallic, sulphidic and trioxide arsenic and antimony have high vapour pressures and boiling points lower than the melting point of chalcopyrite. During the roasting operation, care must be taken to maintain reducing conditions (low oxygen pressures, 10^{-13} to 10^{-16} atm.). This is crucial in order to avoid the oxidation of the arsenic or antimony compounds in the concentrate to non volatile As_2O_5 or Sb_2O_5 oxides.

By recirculating the concentrate, the residence time in the roaster can be increased to maximize volatilization time (46). High temperatures will maximize volatilization as well.

The removal efficiency of arsenic and antimony depends on the mineralogy of the concentrate. Imris (33) has shown that arsenic is vaporized more easily than antimony. Thus, roasting is not suitable for purifying all copper concentrates.

2.4 Bleeding and Processing the Flue Dust Produced during the Smelting and Converting Operations

Large proportions of the lead, bismuth and antimony input to the smelter are evaporated and condensed into the flue dust during the smelting and converting of the copper concentrate. This is especially true for the converting process where high gas volumes and high melt temperatures are used (17). The dust is usually recirculated to the smelting unit. However, if the dust is all or partly bled from the circuit, an additional output is created to remove these impurities from the smelter. This dust will require a separate hydrometallurgical or pyrometallurgical treatment to recover the metal values.

This method is presently used by Noranda Inc, Horne Smelter, in Québec, which ships part of the converter's dust to their lead smelting facilities for lead and copper recovery (17).

2.5 Sodium Carbonate Fluxing of Blister Copper to Remove Group Vb Elements

Impurities can be eliminated from blister copper by producing a basic slag using sodium carbonate (soda ash) (29). Under oxidizing conditions, i.e., high dissolved oxygen content in copper, arsenic and antimony will dissolve in a synthetic soda slag according to the reaction (29):

$$2\ (\underline{As}\text{ or }\underline{Sb}) + 5\ \underline{O} + Na_2CO_{3(l)} = 2\ Na(As\text{ or }Sb)O_{3(l)} + CO_{2(g)}$$

However, this process can also be used for the removal of Pb and Se under reducing conditions, i.e., low dissolved oxygen content in the molten Copper.

This method is not problem free:

1- Bismuth is not fluxed out with arsenic and antimony.
2- The copper content of the slag is high, 10% or more.
3- The slags are very corrosive and lead to high refractory wear.
4- The slags are water soluble and thus secondary treatment of the synthetic slag is required.
5- Soda ash is difficult to handle, toxic and corrosive.
6- The kinetics of reaction are limited by liquid phase melt transport, so large surface areas are required.

2.6 Vacuum Refining of Blister Copper Melts

Vacuum refining of molten copper metal to remove bismuth, arsenic and antimony has been studied by several authors. A summary of these results are presented in Table 2.1. The studies covered a large range of melt temperatures, chamber pressures and melt area to volume ratios.

The results of these previous studies showed that 40 to 90 % bismuth, 0 to 50 % arsenic and 0 % antimony could be removed from a melt with temperatures ranging from 1423 to 1623 K, a refining time of 40 to 120 minutes and chamber pressures from 5 to 30 pascals.

Three authors, Danovitch (36), Ozberk (2) and Harris (6), did pilot scale studies in which the surface area for evaporation and the melt volume were measured. These kinetic studies showed that the removal rate of bismuth ranged from 1.0 to 18 X 10^{-5} ms^{-1}, the removal rate of arsenic ranged from 0.0 to 3.5 X 10^{-5} ms^{-1} and the removal rate was negligible for antimony.

In summary, those studies found that bismuth removal was controlled by a combination of liquid and gas phase control. The removal rates of arsenic and antimony were controlled by evaporation at the interface. Thus, only bismuth could be eliminated rapidly enough to render it feasible for

commercial operations.

Table 2.1: Previous Studies for the Removal of Bismuth, Arsenic and Antimony from Copper Melts (6).

Source Ref.	Weight of Cu	Temp.	Press.	$k_{Bi}^{exp.}$	$k_{As}^{exp.}$	$k_{Sb}^{exp.}$
	(kg)	(K)	(Pa)	$10^5 (ms^{-1})$	$10^5 (ms^{-1})$	$10^5 (ms^{-1})$
Danovitch (36)	23 to 35	1500 to 1740	7 to 160	1.6 to 7.4	2.o t o 3.5	<0.5
Ozberk (37)	34	1423 to 1623	8 to 13	1.1 to 3.1	<0.1	<0.1
Kametami (9)	0.6 to 6.0	1473	130 to 270	$\frac{2 \text{ to } 12}{A/V}$	$\frac{2 \text{ to } 25}{A/V}$	$\frac{4 \text{ to } 25}{A/V}$
Bryan (34)	4.0	1473 to 1573	3 to 27	$\frac{50}{A/V}$	——	——
Ohno (83)	0.5	1468 1573	1 to 13	6.1 to 12.3	——	——
Ohno (83)	0.15	1473 1573	0.1 to 1	8 to 26	——	——
Komorova (6)	0.03	1473	1	$\frac{10 \text{ to } 22}{A/V}$	$\frac{10 \text{ to } 25}{A/V}$	$\frac{10 \text{ to } 20}{A/V}$
Streltsov (6)	0.04	1473	13 to 67	$\frac{2.8}{A/V}$	——	——
Kameda (6)	0.03	1373 1473	13	$\frac{20 \text{ to } 64}{A/V}$	$\frac{3 \text{ to } 30}{A/V}$	$\frac{10 \text{ to } 20}{A/V}$
Harris (6)	35	1450 to 1610	3 to 30	2.6 to 17.5	0.5 to 2.9	<0.1

Note: When the area over volume ratio (A/V) of the melt is unknown, it is not possible to calculate an experimental mass transfer coefficient. The slope of the logarithm of the concentration versus time curve needs to be divided by A/V to be meaningful.

2.7 Vacuum Refining of Copper Matte Melts

Studies on vacuum refining of copper matte are not abundant. Only four were found in the literature survey, Ayhan et al. (62), Kametami et al. (9,70), Player (5) and Bryan et al. (34). These along with the author's previous kinetic study of the vacuum refining of copper matte (52), are summarized in Table 2.2.

Bryan et al. (34) carried out two experiments in a tube furnace, where 20 gram samples of Cu_2S doped with bismuth were subjected to vacuum. The sample was heated to 1443 K and a vacuum pressure of 10 pascal was maintained for one hour. One experiment showed an 81 % removal of bismuth, while the other showed none.

Bryan lacked a value for the activity coefficient of bismuth in white metal or copper matte and erroneously concluded that bismuth removal would be considerably slower in copper matte as compared to metallic copper.

Player (5), studied the removal rate of lead and arsenic from copper matte. The experiments were done on matte containing 46 % copper. Both the laboratory trials and the pilot plant experiments (up to two ton melts) were performed and evaporation rates between 8.0 and 20 X 10^{-5} ms^{-1} for arsenic, at temperatures between 1273 and 1523, and pressures between

40 and 130 pascal, were recorded. Under the same experimental conditions, the lead evaporation rate was found to be slower than arsenic by a factor of 1.2 to 2.2 .

Player did not study the evaporation of bismuth and antimony, nor did he measure the effect of matte grade on the kinetics of refining.

Kametami et al. (9,70) studied the removal of lead, zinc, bismuth, arsenic and antimony from copper matte melts. The study was two fold. In the first part, 100 gram samples of matte were placed under vacuum for one hour at a temperature of 1473 K and a pressure of 60 pascal. It was observed that the fraction removed of the five impurities was between 60 and 100 % for a matte grade of 45 % copper. When white metal (71% copper) was subjected to the same experimental conditions; there was no removal of arsenic, nil to 60 % antimony removal, nil to 80 % bismuth removal and 90 to 100 % lead and zinc removal. The results from the three white metal experiments were very scattered and inconclusive.

The second part of Kametami's study was carried out in an apparatus simulating the D.H. vacuum degassing process used in steel making (9,70). The experiments were carried out on 4 kg melts of copper matte, at a set temperature of 1473 K, a pressure of 60 pascal and a total vacuum refining time of one hour. As in part I, the area to volume ratios of the melts

were not known.

The D.H. vacuum refining work clearly showed that the removed fractions of all impurities were proportional to the stirring rates of the melt. For a 45 % copper matte grade, removal of up to 80 % of bismuth, arsenic and antimony were measured. One experiment was carried out on 71 % copper white metal in which 60 to 80 % of all five impurities were removed.

Kametami's work on vacuum refining copper matte clearly showed that for 45 % copper grade, bismuth, arsenic and antimony removal was possible at the pressure and temperature studied. The removal was proportional to the mixing rate, thus the kinetics were liquid phase controlled. However, the kinetic data required to scale up the process to commercial size were not available. The effects of matte grade and chamber pressure on the removal rates were not studied in detail.

Ayhan et al. (62) studied the vacuum purification of lead-copper matte (30 % copper and 12 % lead) to remove lead, zinc, tin, bismuth, arsenic and antimony. The summary of his 300 kg pilot scale work is presented in Table 2.2. Ayhan did not study the effect of matte grade on the kinetics, however the effect of temperature was clearly observed. It is interesting to note that the rate of refining of antimony increased with temperature but the rate of refining of

bismuth and arsenic decreased with temperature. The experiments further showed that the evaporation rates of bismuth and antimony were liquid phase controlled. However, the removal rate of antimony was slower due to a blend of liquid and gas phase control.

The present author previously carried out a study on the kinetics of elimination of lead, bismuth, arsenic and antimony from copper matte melts (52). The study was done over a range of copper matte contents, melt temperatures and chamber pressures.

Seven kilogram batches of copper matte were melted in alumina crucibles of 0.14m in internal diameter (nominal melt surface area = 1.54×10^{-2} m^2). The vacuum chamber was depressurized after the melt reached the desired temperature. Treatment times varied from 40 to 60 minutes depending on the specific experiment. Molten matte samples were taken every 5 to 10 minutes without breaking the vacuum. The matte samples were sent to the Noranda Technology Center in Pointe-Claire, Québec, for lead, bismuth, arsenic and antimony analysis.

The ranges of variables under study were as follows; the matte grade varied from 35 to 73% copper, the temperature ranged from 1373 to 1523 K and the total chamber pressure fluctuated between 50 to 130 pascal during the experiments.

It was found that the bismuth removal was between 88 to 98%, the arsenic removal was between 60 and 93%, the antimony removal was between 40 and 92% and the lead removal was between 70 and 96% of the initial concentrations.

The plots of the natural logarithm of the concentration of the impurities versus time showed that the refining experiments followed first order kinetics. The overall evaporation rate coefficients were measured for each impurity as a function of operating parameters. The study demonstrated that for matte grades less than or equal to 65% copper and chamber pressures less than 100 pascal, the refining rates were maximum (liquid phase mass transfer control). The removal rates were thus relatively insensitive to temperature fluctuations since they were controlled by transport in the liquid phase.

The study demonstrated the feasibility of vacuum refining copper matte to remove Bi, As, Sb and Pb and gave the refining rates and operating conditions needed for scale up of the process to commercial size.

Such calculations were performed to evaluate the time required for the still vacuum refining of a 40 ton ladle of copper matte. It was found that even at maximum refining rates (liquid phase control) the refining time was approximately 10 times too slow for industrial applications.

Thus, it was concluded that large surface areas were required during the vacuum refining process.

Table 2.2: Previous Studies for the Removal of Bismuth, Arsenic and Antimony from copper Matte Melts.

Source	Weight	Temp.	Press.	%Cu	$K_{Bi}^{exp.}$	$K_{As}^{exp.}$	$K_{Sb}^{exp.}$
	(kg)	(K)	(Pa)	(%)	($10^4 ms^{-1}$)	($10^4 ms^{-1}$)	($10^4 ms^{-1}$)
Kametami(9)	0.1	1473	60	45	$\frac{4.9}{A/V}$	$\frac{4.6}{A/V}$	$\frac{4.0}{A/V}$
Kametami	0.1	1473	60	71	$\frac{3.1}{A/V}$	$\frac{0.0}{A/V}$	$\frac{1.0}{A/V}$
Kametami*	4.0	1473	60	45	$\frac{0.6 \text{ to } 5}{A/V}$	$\frac{0.8 \text{ to } 6}{A/V}$	$\frac{0.3 \text{ to } 3}{A/V}$
Kametami*	4.0	1473	60	62	$\frac{2.1}{A/V}$	$\frac{0.6}{A/V}$	$\frac{0.9}{A/V}$
Kametami*	4.0	1473	60	77	$\frac{1.3}{A/V}$	$\frac{0.3}{A/V}$	$\frac{0.2}{A/V}$
Player (5)	8 to 20	1423	130	46	——	0.8	——
Player	8 to 20	1523	130	46	——	0.9	——
Player	1800	1273 to 1323	40	46	——	1.0 to 2.0	——
Ayhan (62)	300	1100 to 1430	130	30	2.0	0.9	1.1
Ayhan	300	1135 to 1360	210	33	5.9	2.5	0.7
Ayhan	300	1100 to 1270	130	35	5.4	2.9	0.5
Allaire(52)	7	1523	800	33	0.5	——	0.7
Allaire	7	1403 to 1533	50 to 100	33	2.1 to 2.3	1.0 to 1.3	1.4 to 2.2
Allaire	7	1403 to 1473	70 to 100	43	1.8 to 1.9	0.8 to 1.0	0.5
Allaire	7	1448	70	54	1.2	1.0	0.4
Allaire	7	1423	130	74	2.0	0.8	——

Kametami* : Vacuum lift studies, DH process simulation
All Others: Vacuum refining of still melts

2.8 Summary

Today's copper smelting industry has several options available for the reduction of the impurities during copper matte smelting: sulphidation or chlorination in a rotary kiln, roasting of the concentrates, bleeding and processing of the smelter flue dust, basic slag fluxing and vacuum refining of copper or copper matte melts. Table 2.3 shows the superiority incumbent in vacuum refining copper matte through the simultaneous removal of bismuth, arsenic and antimony in a single process, as opposed to other methods which can only handle the removal of one or two impurities at a time. At present the kinetics of vacuum refining of copper matte remain too slow, thus methods which accelerate refining, such as LSV refining, must be investigated.

Table 2.3 : Potential Elimination of Impurities by Various Processing Options.

Element	Rotary Kiln	Roasting Concentrate	Vacuum Treatment			Basic Fluxing	Dust Bleed
			Matte	White Metal	Copper	Copper	
(Ref.)	(46)	(32,33)	(52)	(52)	(6)	(29)	(17)
Bismuth	O	n.r.	yes	yes	yes	no	yes
Arsenic	X	yes	yes	no	no	yes	no
Antimony	O	yes	yes	no	no	yes	no
Lead	O	n.r.	yes	yes	yes	yes	yes
Zinc	n.r.	n.r.	yes	yes	yes	n.r.	yes

n.r. = Not Reported, yes = Good Elimination, no = No Elimination
X = Rotary Kiln, Sulphidation Only
O = Rotary Kiln, Sulphidation and Chlorination

CHAPTER 3

The Lift-Spray Vacuum Refining Process

3.1 Description of the LSV Process

A process called "Lift-Spray Vacuum Refining" (LSV) is presently under development (27,31,49,53,56,57,71,86). The objective of this process is to provide a large liquid metal surface area for evaporation of the impurities from a melt subjected to vacuum. Figure 3.1 shows a schematic diagram of the LSV process used in the present laboratory trials.

The LSV apparatus is composed of two parts. The bottom receptacle holds a bath of impure melt, for example a liquid metal or a liquid sulphide matte. The upper portion, the separator, restrains a shower of metal or matte droplets inside the apparatus to fall back into the bath and lets the evaporated vapours flow out of the system. There is also a scavenging gas lance which injects non-condensable gases beneath the falling shower.

The LSV process is based upon the principle of the gas lift pump. A lifting gas is introduced through the bottom of the receptacle via an injector in the bottom of a hollow vertical conduit, the riser, which extends above the bath surface. The gas creates a mixture of bubbles and liquid inside the riser. The average density inside the riser is lower than the density of the liquid in the bath outside the riser. This density difference creates a pumping effect which causes

circulation of the liquid from the bath, up the riser and by overflowing, back into the bath.

As the gas bubbles travel upward in the riser, the hydrostatic pressure diminishes gradually causing their expansion. When they reach the top of the leg, they explode in the presence of the vacuum (zero pressure). This creates the desired increase in liquid surface area as a shower of finely divided droplets which accelerates the refining process. The liquid droplets fall back into the bath, keeping the top surface free of coherent slag or oxide film and providing mixing as well.

In the separator, the spray of droplets is subjected to the vacuum. There the liquid droplets disengage from the evaporating vapours. The droplets return to the bath and the vapours pass on to a condenser, not shown.

Non-condensable gas can be introduced in the system, between the bath surface and the droplet shower, if necessary, via a lance. The introduction of gas reduces the impurity partial pressures in the vicinity of the spray of droplets by dilution and helps flush the vapours out of the separator by convection, that is, it acts as a scavenger. The mixture of impurity vapours and non-condensable gases flow to the condenser where the impurity vapours condense. The non-condensable gases exit the system via the vacuum pumps.

Fig 3.1 : Schematic Diagram of Laboratory LSV Apparatus Set-Up in an Induction Furnace. Top Section Heated by Resistance Heater (49).

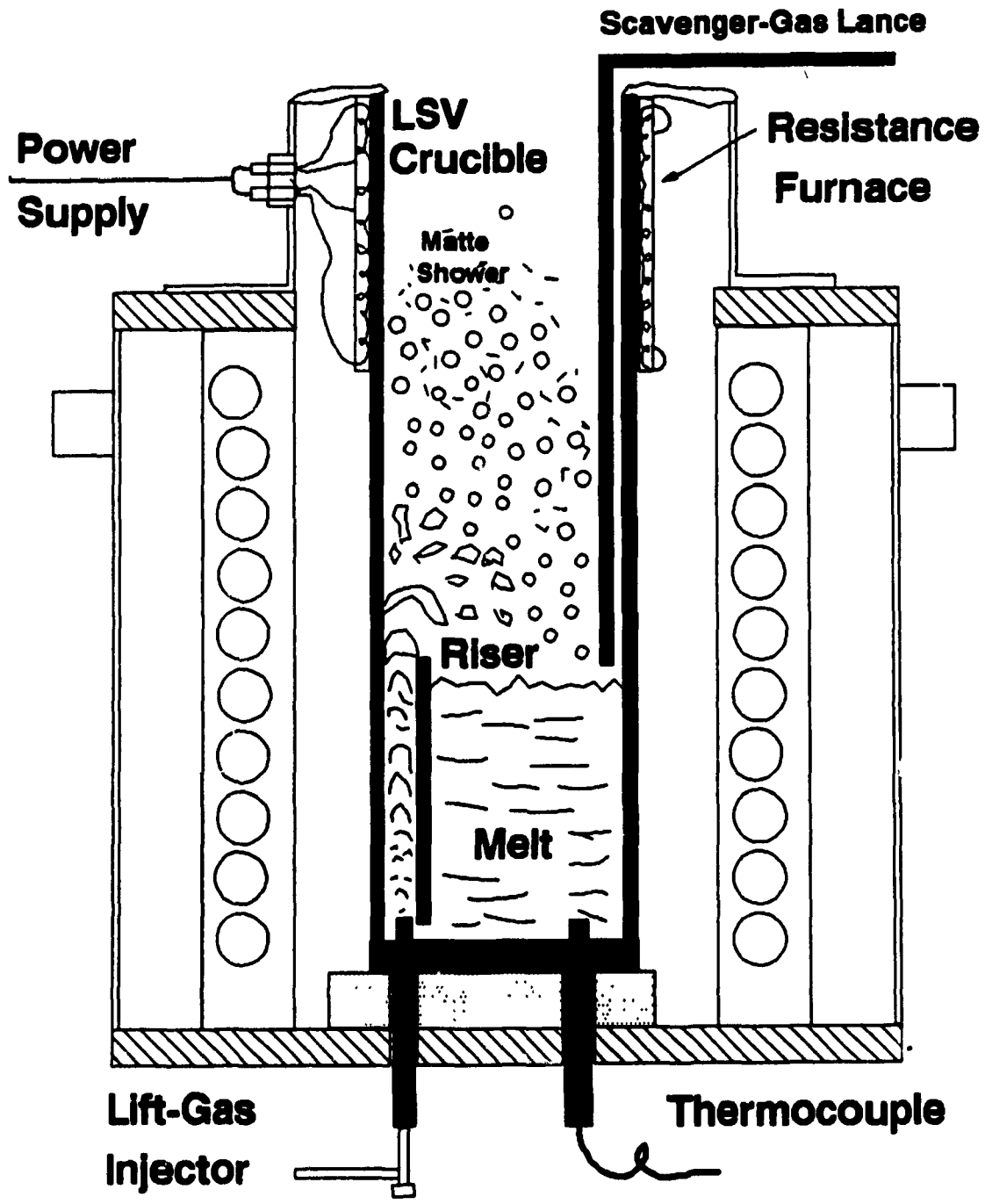

3.2 History of the LSV Process Development

The LSV process originates from a US patent awarded to Harris and Davenport (53) on the Vacuum Purification of Liquid Metal in 1982.

This patent describes the vacuum purification (not degassing) of liquid steel by subjecting it to a vacuum. In summary, the patent claims are :

1-The chamber pressure must be lower than the total equilibrium impurity pressure of the melt in order to create a bulk flow. This bulk flow permits fast removal of the impurities from the clean surface of the melt.

2-A lifting gas is provided in the melt in order to mix the liquid, create a shower of droplets and keep the liquid surface free from slag or oxide film.

3-The system provides a mean to condense the metallic vapors away from the liquid melt to prevent refluxing of the impurities in the melt.

All these conditions must be met simultaneously to accomplish maximum evaporation of the impurities. It has been claimed that the largest surface areas for evaporation are obtained by introducing the lifting gas inside a riser leg which is partially submerged in the liquid (LSV process).

The LSV process was further investigated by F. Dimayuga (27) for the rapid elimination of Mg, Sn and Pb from molten Al.

The work of Dimayuga, Figure 3.2, (56) showed that 95%, 98% and 80% of the Mg, Zn and Pb can be removed by LSV refining of molten Al. Dimayuga showed that the refining time could be reduced by an order of magnitude using LSV refining instead of still vacuum refining. Photographic studies documented that the droplets produced ranged in size from 0.2 to 1.0 cm in diameter.

Simultaneously, Pouliquen (71) was working on water the modeling of the LSV refining process. Pouliquen demonstrated that the superficial liquid velocity in the riser is linearly proportional to the superficial gas velocity, measured at midpoint along the length of the riser. It was further demonstrated that the superficial liquid velocity increased with decreasing lift ratio, see Figure 3.3. The lift ratio is equal to the fraction of the riser above the surface of the melt. The data obtained by Pouliquen made it possible to calculate the recirculation rate and the injector gas flow rate required to achieve the desired refining rate. Thus scale up to industrial size was possible.

Further work done by Harris on the removal of lead from molten tin using the LSV process (49), showed that for a specified chamber pressure and temperature of the melt there

exists a limit to the amount of refining possible. Harris introduced scavenging gas under the shower of metal droplets. The scavenging gas diluted the impurity vapours in the gas phase and permitted refining to a very low level of impurities (49,57).

The present author extended these investigations by studying the use of the LSV refining process to speed up the evaporation of Bi, As and Sb from copper matte melts. The results are presented in this thesis.

Fig. 3.2 : Ratio of Solute Concentration at Time t, Ct, to Initial Solute Concentration, C Init., in Aluminum Melts during Vacuum Treatment (Ref. 56).

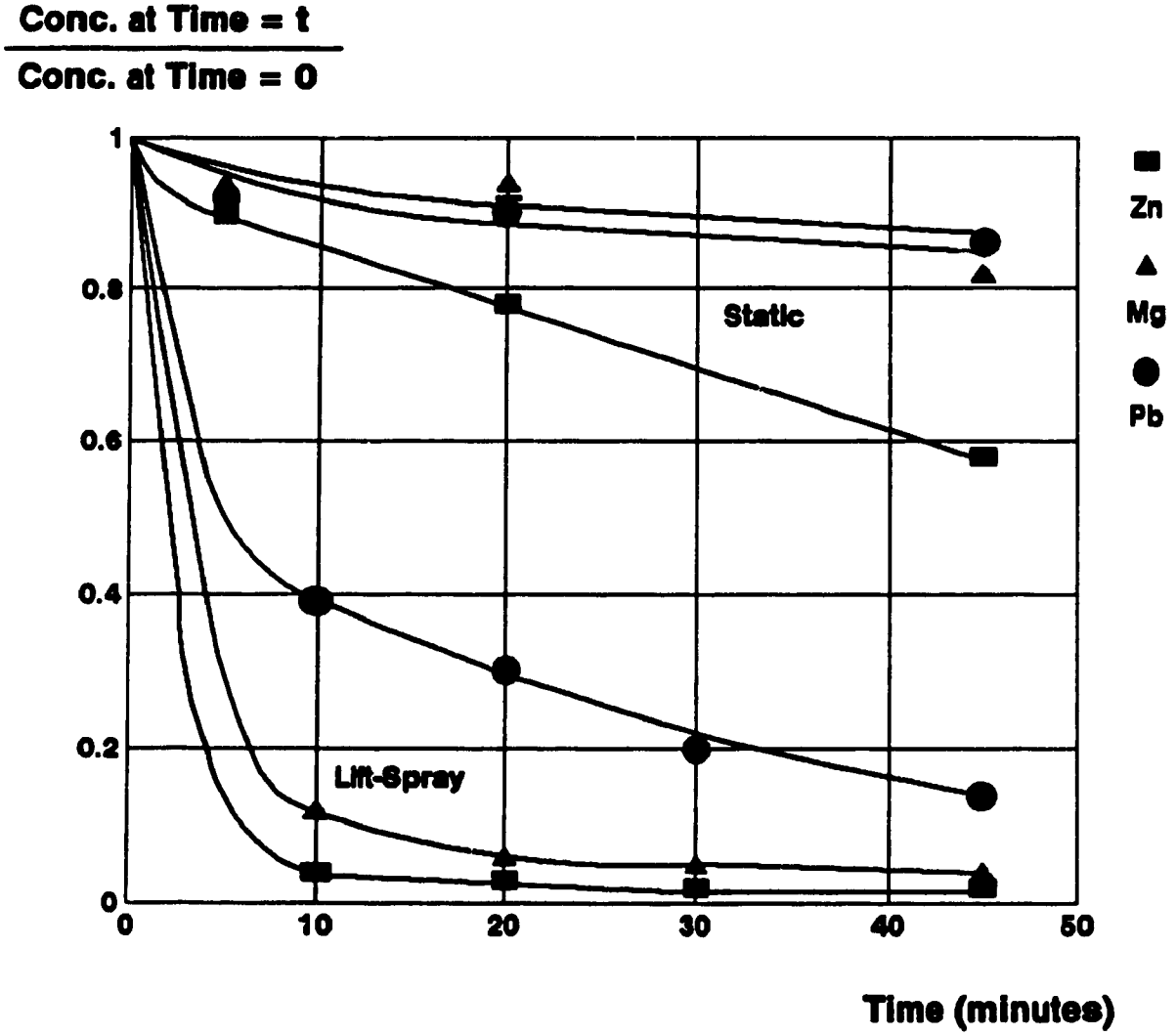

Fig. 3.3 : Effect of Lift Ratio, β, on Relationship Between Superficial Velocities of Gas, j_g, and Liquid, j_l (Ref. 71).

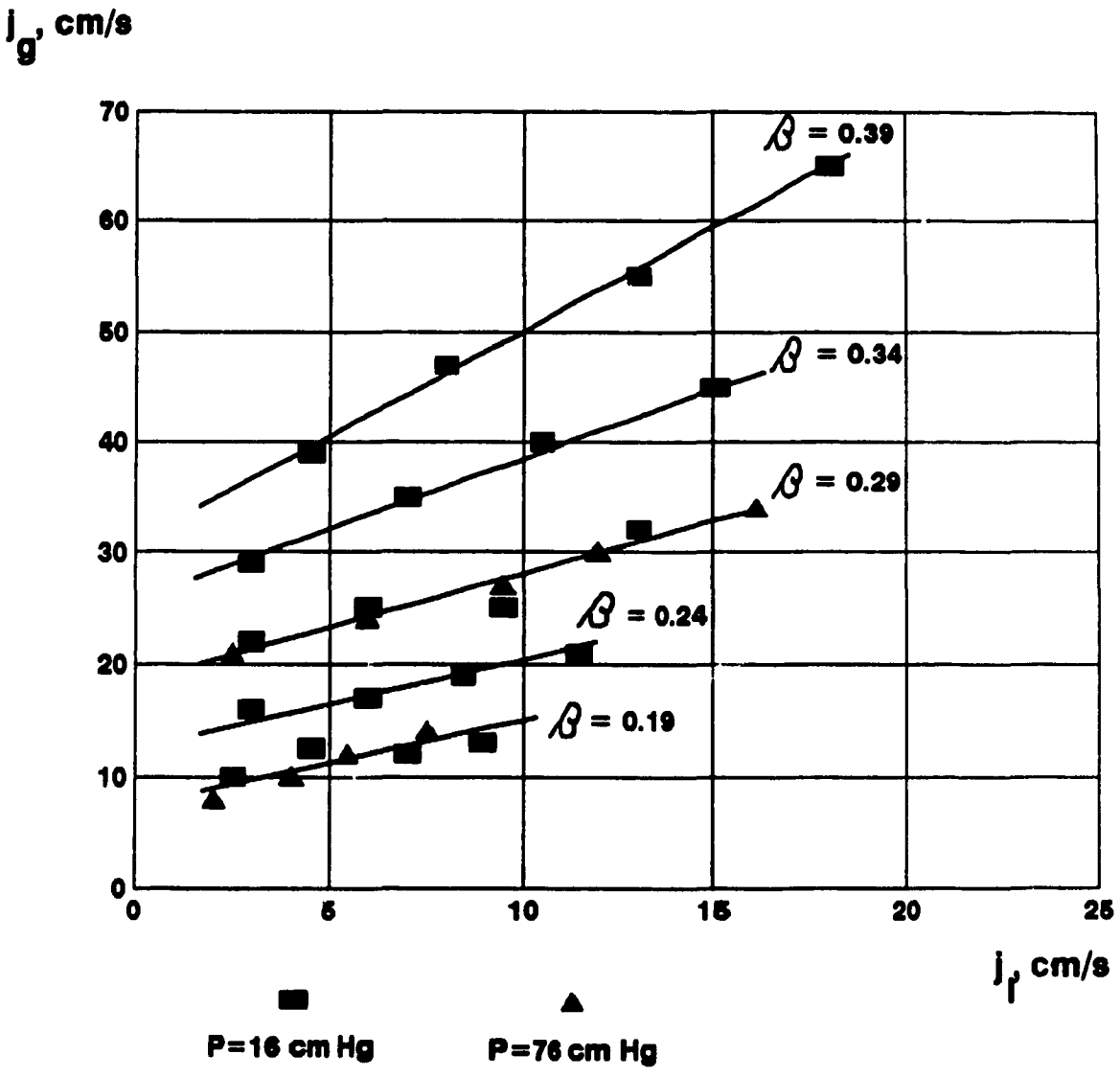

CHAPTER 4

Vacuum Purification Theory

4.1 Introduction

The process of vacuum purification can be simply conceptualized as a melt consisting of volatile solute impurities and a bulk solvent liquid subjected to a total pressure of less than one atmosphere (vacuum). The volatile impurities are removed from the melt by preferential evaporation thereby resulting in a purer bulk solvent liquid.

This chapter will describe the thermodynamics and kinetics of the vacuum refining process.

4.2 Thermodynamic Considerations

4.2.1 Volatility Coefficients

The feasibility of vacuum refining a bulk liquid of an impurity can be predicted by the volatility coefficient (ϕ_i) developed by Olette (6). The equation for ϕ_i is given below.

$$\phi_i = \frac{\gamma_i P_i^o}{P_b^o} \left[\frac{M_b}{\rho_b}\right]^{0.5} \qquad (1)$$

Where : ϕ_i = Olette's Volatility Coefficient

P_b^o = Equilibrium Vapour Pressure of bulk Species (Pa)

M_b = Molar Mass of Bulk Liquid (kg $kgmole^{-1}$)

M_i = Molar Mass of Impurity i (kg $kgmole^{-1}$)

P_i^o = Equilibrium Vapor Pressure of i over it's Pure Species (Pa)

γ_i = Activity Coefficient of i in the Melt

ρ = Density of Bulk Liquid (kg m^{-3})

Vacuum refining is possible only if the volatility coefficient, ϕ_i, is greater than one (6).

Olette's coefficient was derived for monoatomic evaporation. Harris (6) modified the criteria to obtain an expression for the volatility coefficients of polyatomic species. Harris'

modified volatility coefficient, ϕ_{i_j}, is given by Equation 2 as follows:

$$\phi_{i_j} = \left[\frac{M_b}{M_{i_j}}\right]^{0.5} \cdot \frac{(\gamma_i)^j \cdot X_i^{(j-1)} \cdot P^o_{i_j}}{P^o_b} \qquad (2)$$

Where : ϕ_{i_j} = Harris' Modified Volatility Coefficient

j = Number of Atoms in the polyatomic species

X_i = Mole fraction of i in Liquid

$P^o_{i_j}$ = Equilibrium Vapor Pressure of the pure Polyatomic Species

and all other terms were previously defined.

For vacuum refining to occur, the volatility coefficient (ϕ_{i_j}) must be larger than 1/j. By substituting unity for the value of j in Equation 2, Olette's volatility coefficient is obtained.

Equation 2 could be used to evaluate the feasibility of vacuum purifying copper matte. The equilibrium vapour pressures of many impurities such as Bi, As, Sb and Pb can easily be obtained from the literature. However, no data was available for the equilibrium vapour pressure of the bulk liquid species such as Cu_2S and FeS. This makes it impossible to calculate the volatility coefficients of the above mentioned impurities.

4.2.2 Vapour Pressure Calculations for Lead, Zinc, Bismuth, Arsenic, Antimony and Nickel

The equilibrium vapour pressures for the basic metallic vapours, the diatomic sulphide and diatomic oxide were calculated using the thermodynamic data listed in Chapter 5, Table 5.1 .

The calculated vapour pressures were used to produce a graph of the logarithm of the equilibrium vapour pressure of i, i_2, i_4, iS and iO gaseous species as a function of the logarithm of the activity of i, where i represents the metal of interest (Figures 4.1 to 4.6). Three vapour pressure curves were plotted for each of the iS and iO species at sulphur pressures of 10^{-2}, 10^{-4} and 10^{-6} atmosphere, and at oxygen pressures of 10^{-6}, 10^{-8} and 10^{-10} atmosphere, respectively.

The impurities of interest in this study of copper matte vacuum purification are Pb, Zn, Ni, Bi, As, and Sb. These impurities are very dilute in the bulk liquid and thus have activities of approximately 0.01 or less. The copper matte grade range under study is 30 to 80 % copper, hence the sulphur activity in the melt varies from 10^{-2} to 10^{-6} atmosphere. For the same copper matte range, the oxygen activity varies from 10^{-6} to 10^{-8} atmosphere. From Figures 4.1 to 4.6, it can be observed that the species with significant vapour pressures above the melt are Pb, PbS, Zn,

ZnS, NiS, Bi, BiS, As, AsS, AsO, Sb, SbS and SbO. However, Figures 4.5 and 4.6 do not take into consideration the large drop (10 to 100 times) in the activity coefficients (γ) of As and Sb when the copper matte grade increases from 70 to 80 % copper. Despite this, since all the gas species contain only one metal atom, the relative proportions of the vapour pressures of the metal, sulphide and oxide species remain unchanged. For example, the ratio of the vapour pressure of arsenic oxide over arsenic metal (AsO/As) remains constant for all arsenic activities in the melt.

Fig. 4.1: Equilibrium Vapour Pressure of Lead versus the Activity of Lead in a Melt at 1473 K.

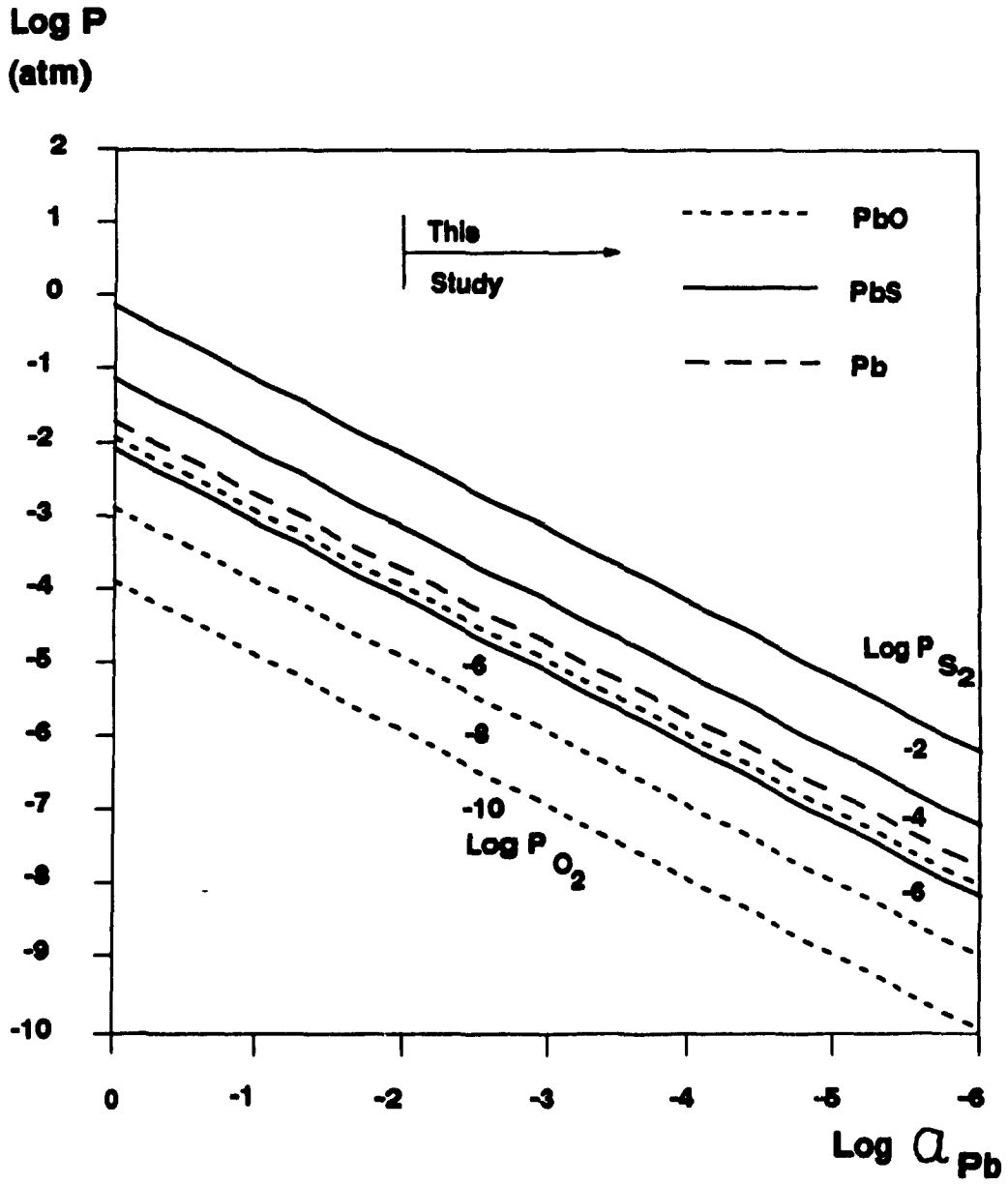

Fig. 4.2: Equilibrium Vapour Pressure of Zinc versus the Activity of Zinc in a Melt at 1473 K.

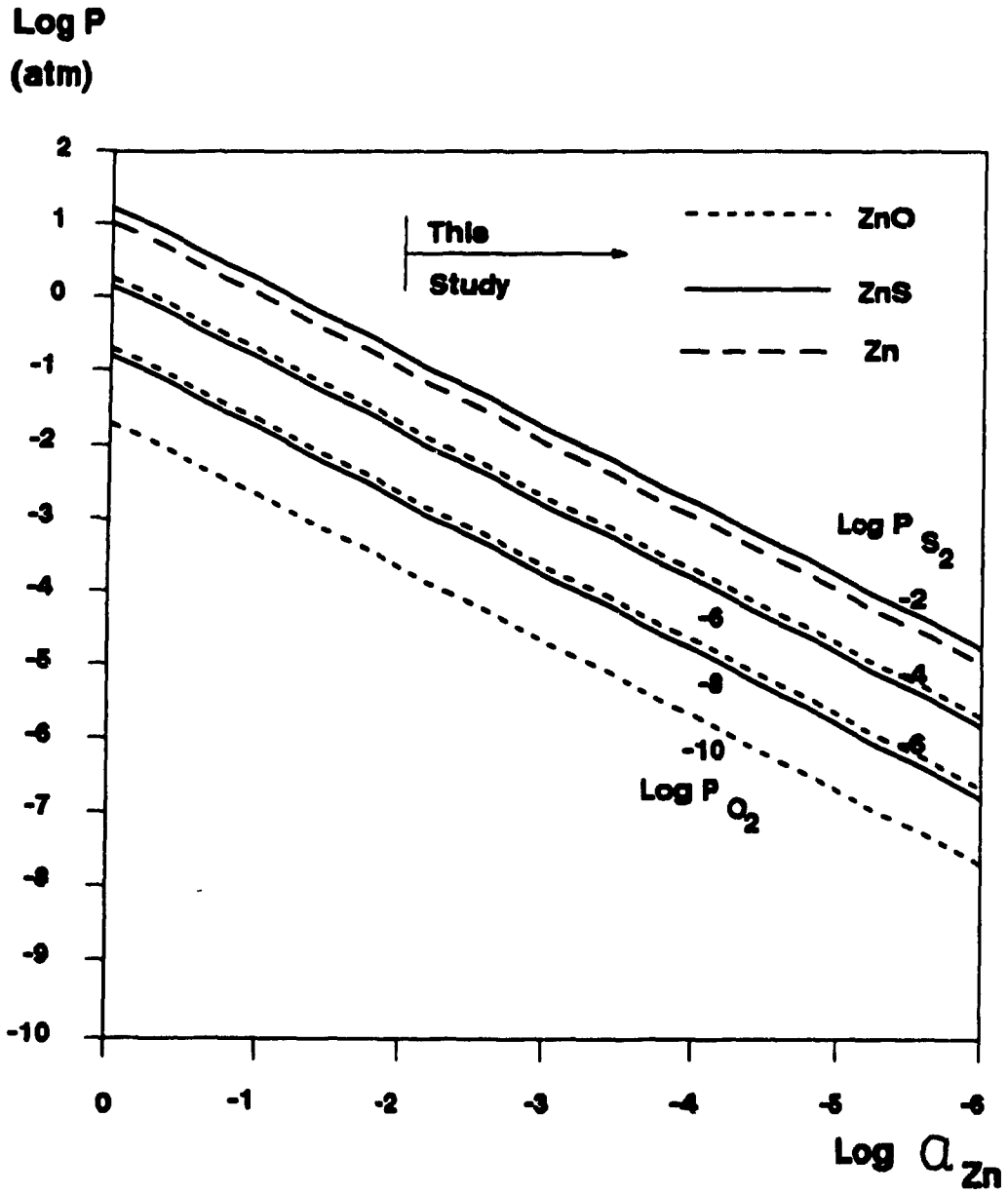

Fig. 4.3: Equilibrium Vapour Pressure of Nickel versus the Activity of Nickel in a Melt at 1473 K.

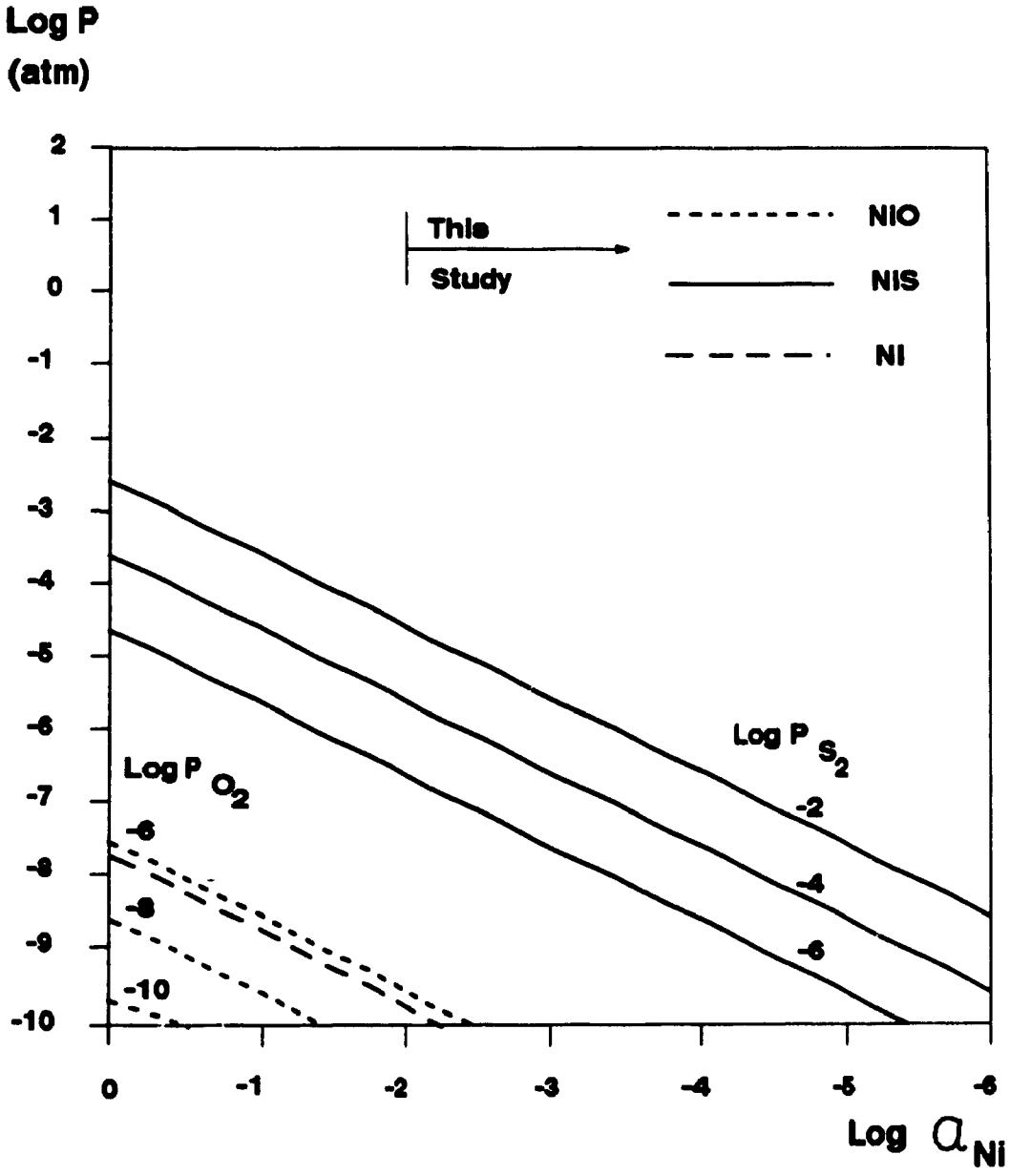

Fig. 4.4: Equilibrium Vapour Pressure of Bismuth versus the Activity of Bismuth in a Melt at 1473 K.

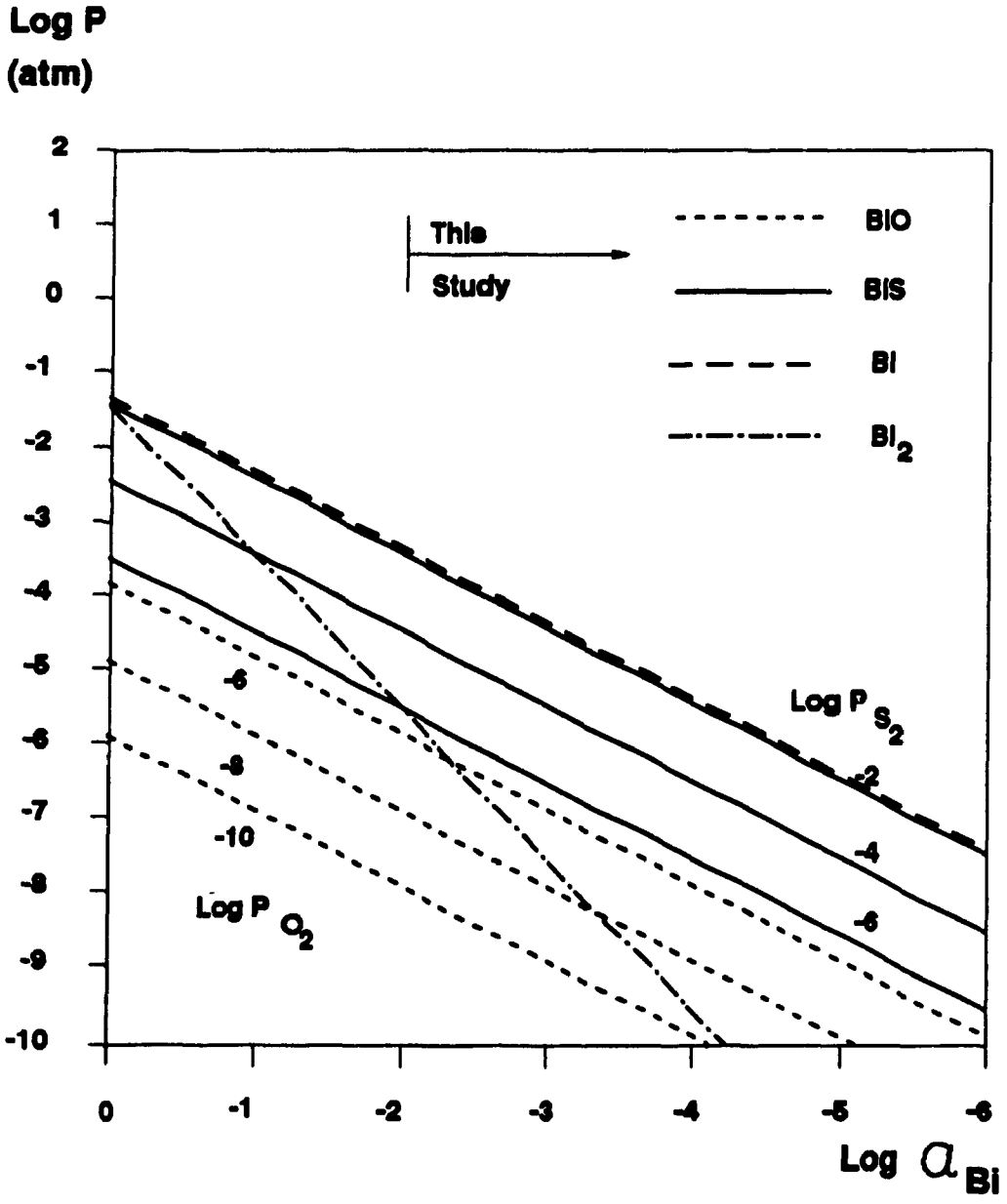

Fig. 4.5: Equilibrium Vapour Pressure of Arsenic versus the Activity of Arsenic in a Melt at 1473 K.

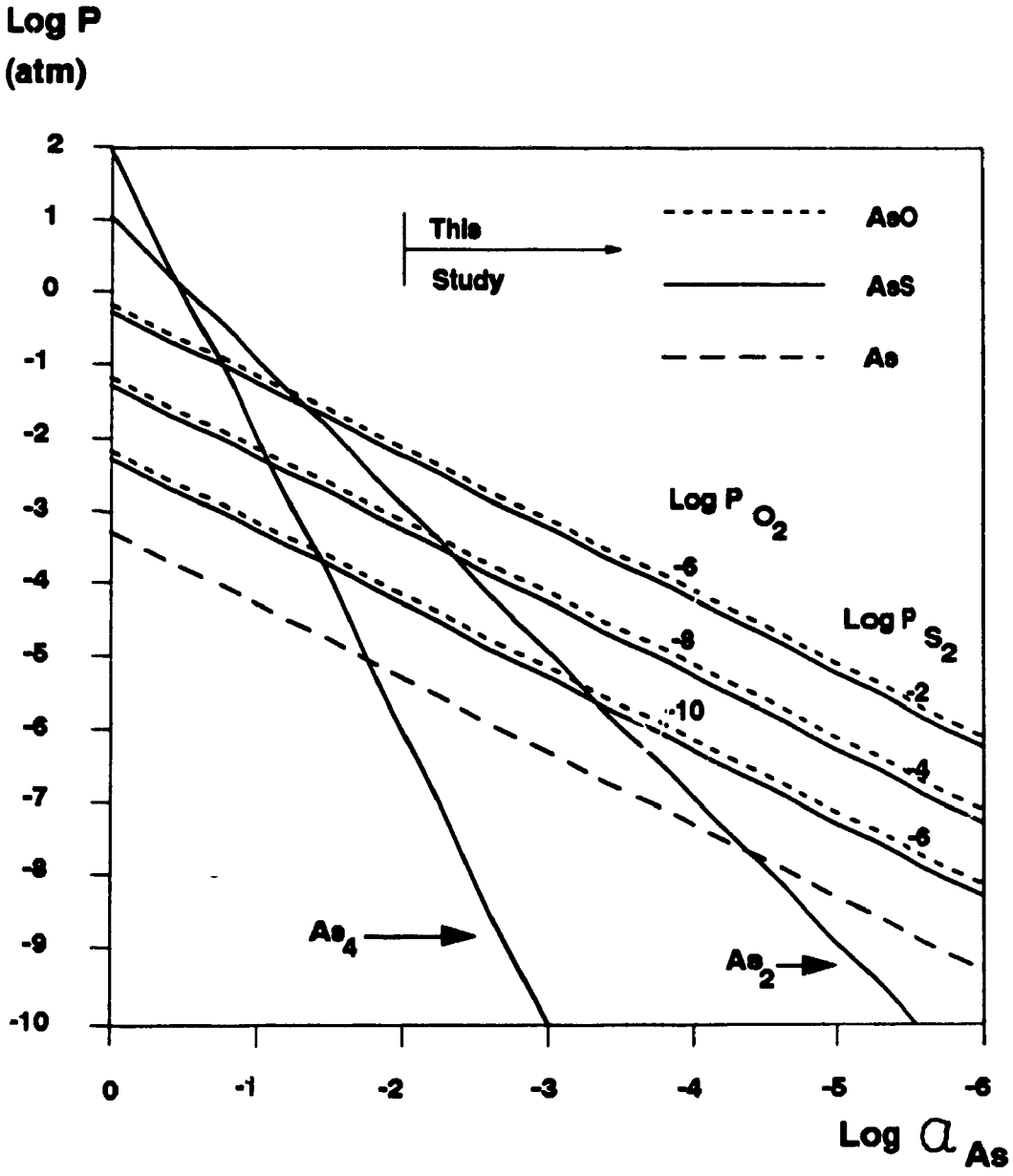

Fig. 4.6: Equilibrium Vapour Pressure of Antimony versus the Activity of Antimony in a Melt at 1473 K.

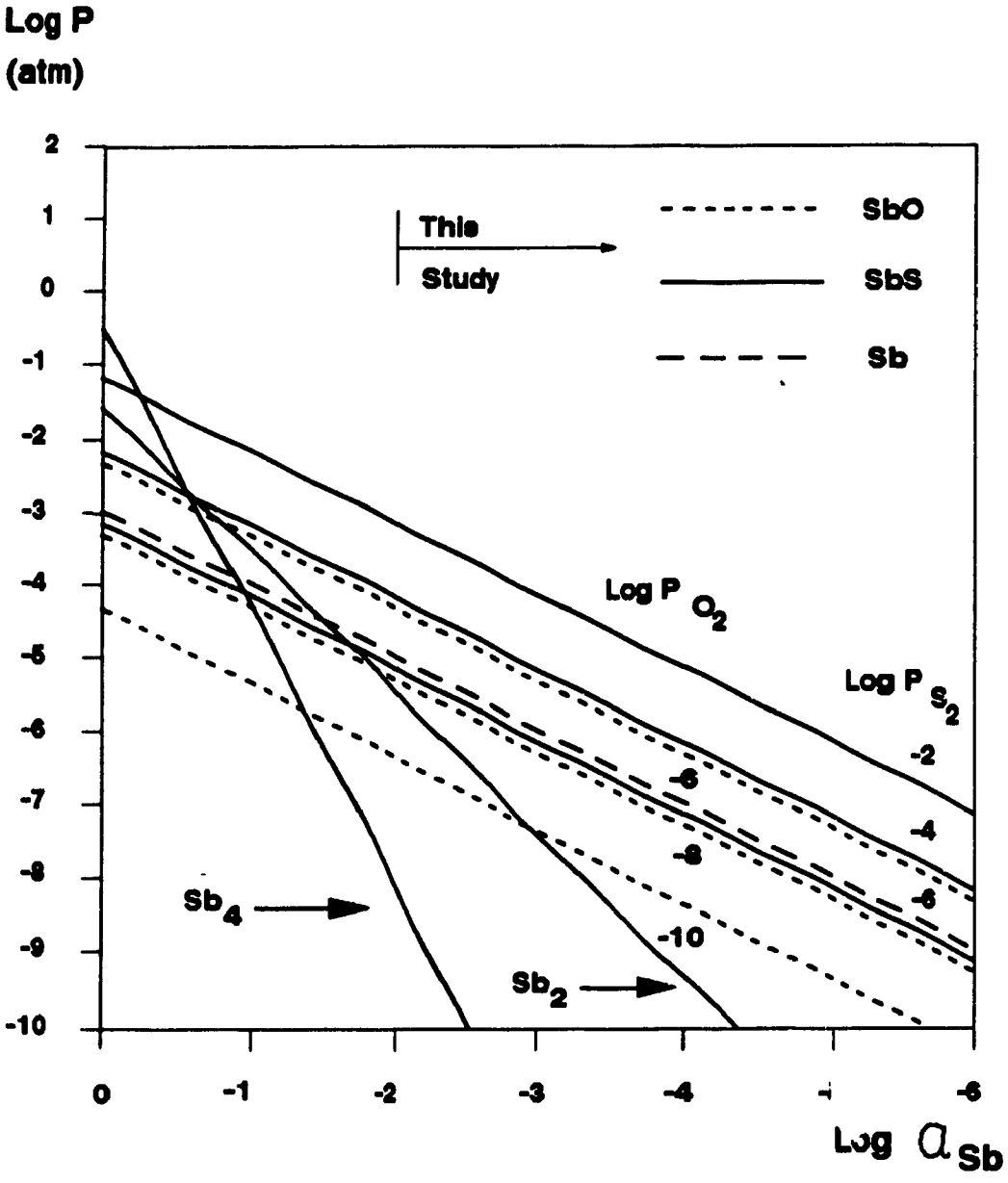

4.3 Vacuum Purification Kinetics

4.3.1 Mass Transfer Model

The model describing the kinetics of vacuum refining in terms of a multi-step process was described in detail by various authors such as Ward (20) and Ohno (83). In the present study a three step mass transfer mechanism is considered (6, 20, 27, 37, 42, 83). The three steps are:

i) Mass transfer through the liquid phase boundary layer to the liquid/vacuum interface.
ii) Evaporation of the atoms at the interface.
iii) Mass transfer through the gas phase mass transfer boundary layer away from the liquid/vacuum interface.

Any of these three steps, or combination thereof, can function as the rate limiting factor.

4.3.2 Overall Mass Transfer Coefficient for Monoatomic Impurity Evaporation

The flux of a solute (i) across one mass transfer step is proportional to the concentration drop across that step.

$$\dot{n}''_i = K_{step} \cdot \Delta N_i \tag{3}$$

This is analogous to Ohm's Law (81) where the concentration difference (ΔN_i) is viewed as the voltage drop (ΔV), the mass transfer coefficient (K) is viewed as the conductance, i.e. the reciprocal of the resistance (1/R) and the flux ($\dot{n}''_i$) is viewed as the current (I).

$$I = (1/R) \cdot \Delta V \tag{4}$$

Each of the three mass transfer steps can be written down in more detail as follows:

$$\dot{n}''_L = K_L \cdot (N_{i,b} - N_{i,LS}) \tag{5}$$

$$\dot{n}''_E = K_E \cdot \left(\frac{P_{i,LS}}{RT} - \frac{P_{i,GS}}{RT} \right) \tag{6}$$

$$\dot{n}''_G = K_G \cdot \left(\frac{P_{i,LS}}{RT} - \frac{P_{i,\infty}}{RT} \right) \tag{7}$$

Where: $\dot{n}''_L$ = Solute Flux in Liquid (kgmole $m^{-2}s^{-1}$)

K_L = Liquid Phase Mass Transfer Rate (m s^{-1})

$N_{i,b}$ = Mole Concentration of Solute i in the Bulk Liquid (kgmole m^{-3})

$\dot{n}''_E$ = Solute Evaporation Flux (kgmole $m^{-2}s^{-1}$)

$P_{i,LS}$ = Vapor Pressure of Solute on the Liquid Side of the Interface (Pa)

$P_{i,GS}$ = Vapor Pressure of Solute on the Gas Side of the Interface (Pa)

$\dot{n}''_G$ = Solute Flux in the Gas Phase (kgmole $m^{-2}s^{-1}$)

K_G = Gas Phase Mass Transport Coefficient(ms^{-1})

$P_{i,\infty}$ = Vapor Pressure of Solute in the Gas Phase (Pa)

R = Universal Gas Constant(joules $kgmole^{-1}K^{-1}$)

T = Temperature (K)

Figure 4.7 shows the diagram of the electrical circuit which expresses the three mass transfer steps. Two conditions must be met in order to interconnect the circuit. Firstly, there must be no accumulation or generation of solute between each step. Secondly, the surface area between each step must remain constant, i.e. $\dot{n}''_L = \dot{n}''_E = \dot{n}''_G$.

In order to perform calculations an interrelationship between the solute vapour pressure on the liquid side of the interface, $P_{i,LS}$, and the solute concentration on the liquid side of the interface, $N_{i,LS}$ must be established. The required relationship is obtained from the equilibrium

constant for the evaporation reaction of the impurity, $i_{(l)} = i_{(g)}$. By defining ψ_i as the equilibrium constant of the reaction the following equation can be written.

$$P_{i,LS} = \psi_i \cdot N_{i,LS} \tag{8}$$

In the case of a monoatomic gaseous specie the constant ψ_i is given by the following equation (27):

$$\psi_i = \frac{\gamma_i P_i^o M_b}{\rho_b} \tag{9}$$

Where, γ_i = Activity Coefficient of i

P_i^o = Equilibrium Vapor Pressure of pure Specie, Pa

M_b = Molar Mass of Bulk Liquid, kg $kgmole^{-1}$

ρ_b = Density of Bulk Liquid, kg m^{-3}

Through analogy from the electrical circuit performance, I=(1/R).ΔV, the result for the overall rate of impurity removal (K_{ov}) is :

$$\dot{n}_i'' = \left[\frac{1}{\left(\frac{1}{K_L}\right) + \frac{1}{\psi_i}\left(\frac{RT}{K_E} + \frac{RT}{K_G}\right)}\right]^{-1} \cdot \left(N_{i,b} - \frac{P_{i,\infty}}{\psi_i}\right) \tag{10}$$

The total resistance to the mass transfer of impurity i can thus be represented by the sum of three resistances. These

resistances originate from the mass transfer in the liquid phase, evaporation and mass transfer in the gas phase.

Fig. 4.7 : Representation of Monoatomic Vapour Transfer in Vacuum by Using an Analogy with Ohm's Law.

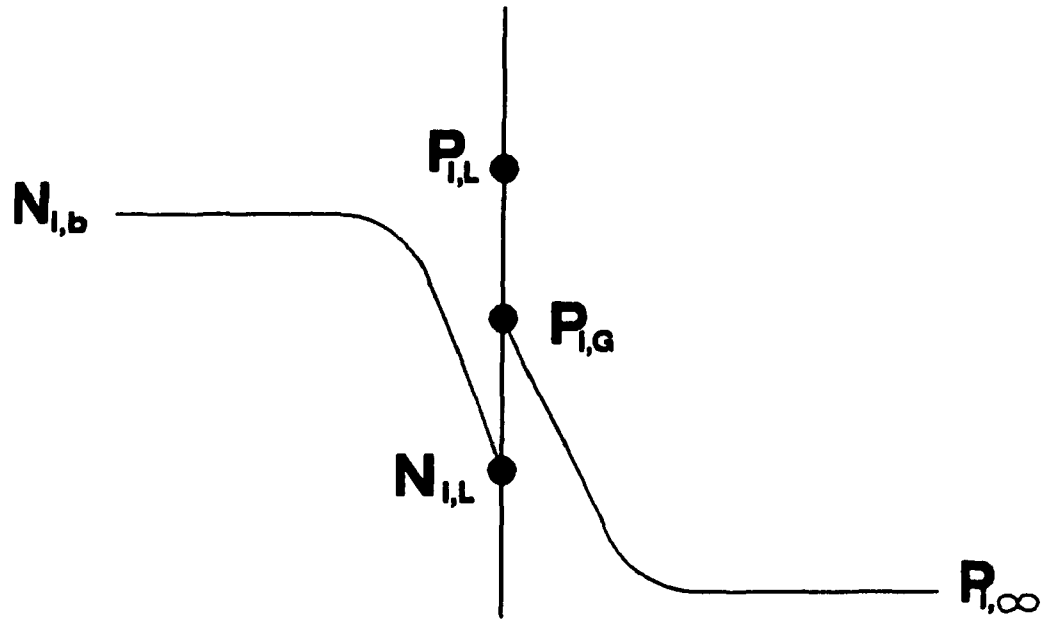

$$\dot{n}'' = K.\Delta N \longrightarrow \Delta V = R \,.\, I$$

Such that : $\dot{n}'' = I$

$\Delta N = \Delta V$

$1/K = R$

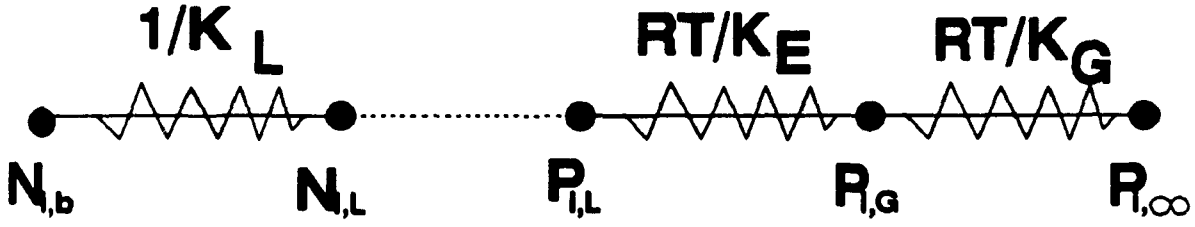

4.3.3 Mass Transfer Coefficient for Simultaneous Evaporation of Monoatomic, Diatomic Sulphide and Diatomic Oxide Vapours

Arsenic and antimony can evaporate from copper matte in the form of three different vapour species, monoatomic, diatomic sulphide and diatomic oxide vapours. Figure 4.8 represents the evaporation of such an impurity based on an analogy with Ohm's law.

In order to mathematically model this diagram, a relationship must be found between the diatomic sulphide and the diatomic oxide vapour pressures and the impurity concentration at the liquid side of the interface. This derivation was previously done by the author (52) and is rewritten here for completeness of the work.

In the case of diatomic sulphide species, the equilibrium equation between the diatomic metal vapours and the sulphur vapours can be written as follows:

$$1/2\ i_{2(g)} + 1/2\ S_{2(g)} = iS_{(g)} \qquad (11)$$

The above reaction equilibrium constant is given by:

$$K_{iS}^{eq} = P_{iS} / P_{i_2}^{0.5} \cdot P_{S_2}^{0.5} \qquad (12)$$

The equilibrium constant, K_{iS}^{eq}, is obtained from the Gibbs Energy of the reaction at the temperature specified by the relation, $\Delta G_{iS}^{o} = -RT \ln K_{iS}^{eq}$.

Rearranging Equation 12, we obtain a relationship between the diatomic sulphide pressure and the pressure of the impurity.

$$P_{iS_{(g)}} = K_{iS}^{eq} P_{i_2}^{0.5} P_{S_2}^{0.5} \qquad (13)$$

As in the case of the monoatomic metallic species, we can write:

$$\psi_{iS,L} N_{iS,L} = P_{iS_{(g)}} \qquad (14)$$

where ψ_{iS} is derived below.

Substituting Equation 14 into Equation 13, we obtain:

$$\psi_{iS,L} N_{iS,L} = K_{iS}^{eq} P_{i_2}^{0.5} P_{S_2}^{0.5} \qquad (15)$$

Taking into account that the mole fraction of the diatomic sulphide impurity in the melt is equal to the mole fraction of the monoatomic impurity in the melt, then $N_{i,L}$ is equal to $N_{iS,L}$. Furthermore, knowing that the relationship between the pressure of the solute gas and the solute properties is given by :

$$P_{i_{2(g)}} = ([\gamma_i \, N_{i,L} \, M_b] / \rho_b)^2 \, P^o_{i_{2(g)}} \qquad (16)$$

and rearranging Equation 15, we obtain the following equation for the diatomic sulphide vapour pressure: (A similar demonstration can be done for the diatomic oxide vapours).

$$\psi_{iS,L} = \frac{K^{eq}_{iS} \cdot P^{0.5}_{i_2} \cdot P^{0.5}_{S_2} \cdot M_b}{\rho_b} \qquad (17)$$

And

$$\psi_{iO,L} = \frac{K^{eq}_{iO} \cdot P^{0.5}_{i_2} \cdot P^{0.5}_{O_2} \cdot M_b}{\rho_b} \qquad (18)$$

Where, $$P_{iS,L} = \psi_{iS} \cdot N_{i,L} \qquad (19)$$

And $$P_{iO,L} = \psi_{iO} \cdot N_{i,L} \qquad (20)$$

Assuming no accumulation or generation of solute at the interface and that the surface area between each step is constant, then; $\dot{n}''_L = \dot{n}''_i + \dot{n}''_{iS} + \dot{n}''_{iO}$. The circuit can then be solved and yield Equation 21 as follows :

$$\dot{n}_i'' = \frac{N_{i.b}}{(1/K_L)} - \frac{\left[N_{i,b} + \left(\left(\frac{1}{K_L}\right)\left(\frac{P_{i,\infty}}{\left[\frac{RT}{K_{Ei}} + \frac{RT}{K_{Gi}}\right]} + \frac{P_{iS,\infty}}{\left[\frac{RT}{K_{EiS}} + \frac{RT}{K_{GiO}}\right]} + \frac{P_{iO,\infty}}{\left[\frac{RT}{K_{EiO}} + \frac{RT}{K_{GiO}}\right]}\right)\right)\right]}{\left[1 + \left(\left(\frac{1}{K_L}\right)\left(\frac{\psi_{i,\infty}}{\left[\frac{RT}{K_{Ei}} + \frac{RT}{K_{Gi}}\right]} + \frac{\psi_{iS,\infty}}{\left[\frac{RT}{K_{EiS}} + \frac{RT}{K_{GiO}}\right]} + \frac{\psi_{iO,\infty}}{\left[\frac{RT}{K_{EiO}} + \frac{RT}{K_{GiO}}\right]}\right)\right)\right]} \quad (21)$$

Since the atomic diameters of the metal, sulphide and oxide gaseous species are approximately the same, the next two assumptions are made:

Firstly $K_{Ei} \cong K_{EiS} \cong K_{EiO}$

And $K_{Gi} \cong K_{GiS} \cong K_{GiO}$

Then, defining the total pressure of metal i as the sum of the metallic, sulphide and oxide species, we obtain ;

$$P_{i,\infty}^{total} = P_{i,\infty} + P_{iS,\infty} + P_{iO,\infty}$$

Then Equation 21 reduces to:

$$\dot{n}_i'' = \left[\frac{1}{K_L} + \frac{1}{(\psi_i + \psi_{iS} + \psi_{iO})} \cdot \left(\frac{RT}{K_{E,i}} + \frac{RT}{K_{G,i}}\right)\right]^{-1} \left(N_{i,b} - \frac{P_{i,\infty}^{total}}{(\psi_i + \psi_{iS} + \psi_{iO})}\right) \quad (22)$$

As in the case of monoatomic impurity evaporation, the circuit can be represented as the sum of three resistances. However, the evaporation and gas phase mass transport resistances are reduced due to the formation of diatomic oxide and diatomic sulphide gases. The reciprocal of the sum of the three resistances is called the overall mass transport coefficient (K_{ov}).

Fig. 4.8 : Representation of Multicomponent Evaporation by Analogy with Ohm's Law.

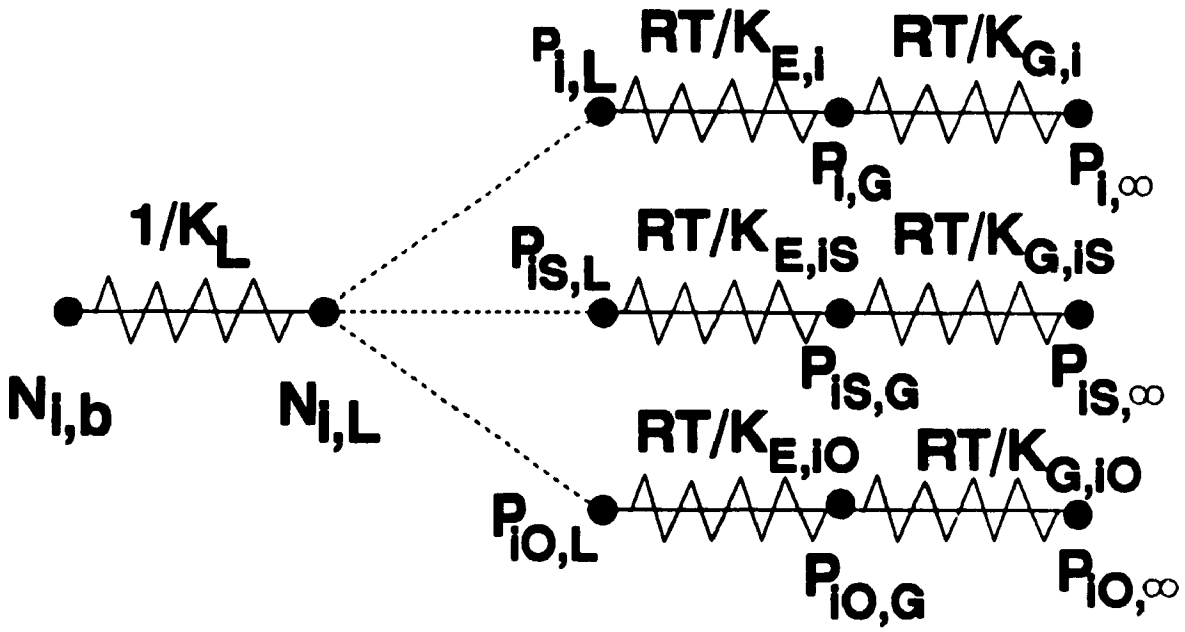

$$\dot{n}''_{i,Total} = \dot{n}''_{i} + \dot{n}''_{iS} + \dot{n}''_{iO}$$

4.3.4 Liquid Phase Mass Transfer Coefficient

The liquid phase mass transfer of the solute atom from the bulk of the melt to the liquid/gas interface can be described by the "Fluid Motion in Penetration Theory" first proposed by Higbie (18). This theory was used by Machlin (8) to describe the liquid phase mass transfer coefficient in an inductively stirred melt. The model assumes that an element of liquid is exposed to the other phase for a time, t_e, called the exposure time. Within this time, the impurity is transported to the other phase via unsteady state diffusion. Based on this model, the melt phase mass transfer coefficient is given by:

$$K_L = \left(\frac{4\ D_{i,L}}{\pi\ t_{e,L}}\right)^{0.5} \qquad (23)$$

Where : $D_{i,L}$ = Diffusion Coefficient of i in the Liquid ($m^2 S^{-1}$)

t_e = The Exposure Time of the Liquid Element to the Surface of the Liquid Phase (s).

π = 3.1416

In the case of an inductively stirred melt, the exposure time is equal to half the average distance from the center of the melt to the edge of the crucible divided by the average velocity of the melt surface; i.e., $t_e = r/2v$

Another situation where t_e can be calculated is in the case of a gas bubble rising through a liquid. Then the exposure

time of a liquid element can be estimated by;

$$t_e = d_B / v_B \qquad (24)$$

Where, d_B = Diameter of Bubble, m.

v_B = Upward Velocity of Bubble, ms^{-1}.

t_e = Exposure Time, s

It is seen that K_L can be estimated in some situations where the impurity diffusivities in the solvent are known and the hydrodynamics are simple. However in the LSV system where the droplets of liquid are projected in the vacuum space, it is impossible to get a precise value of t_e and hence an a priori estimate of K_L is inextricable.

Several values were found in the literature for the liquid phase mass transport coefficient for most liquid metal stirred systems (28). The values for K_L fluctuate between 1 and 5 X $10^{-4}ms^{-1}$. Values of overall mass transfer coefficient for still melts in vacuum, measured by the author (52), suggest that an average value of 2 X $10^{-4}ms^{-1}$ is typical of impurities such as Pb, Bi, As and Sb in copper matte melts at temperatures of approximately 1473 K.

4.3.5 Evaporation Mass Transfer Coefficient at the Interface

The evaporation of an impurity in vacuum systems can be predicted by the Hertz-Knudsen-Langmuir model (18). This model was used in several studies (6,8,27,36,39,42,52) and leads to an expression for the evaporation mass transfer coefficient of metallic species and compounds of :

$$K_E = \alpha(RT / 2 \pi M_i)^{0.5} \qquad (25)$$

where α is generally taken to be unity for metal systems.

4.3.6 Gas Phase Mass Transfer Coefficient

Two models can be used to explain and quantify the mass transfer coefficient from the interface to the bulk gas phase. One model is the Effective Film Thickness Theory and the second is the Fluid Motion in Penetration Theory which can be applied to fluids in general. The second was described in section 4.3.4 .

The Effective Film Thickness Theory was proposed by Lewis and Withman (18). In this theory it is assumed that there exists, next to the actual liquid interface, an unmixed layer or stagnant film in the gas designated as the diffusion boundary layer. This stagnant film is assumed to offer all the resistance to the mass transfer. The gas phase distanced from the interface and film is considered to be a well mixed fluid. The temperature across the stagnant layer is assumed to be constant and mass transfer occurs only by diffusion through the film, Figure 4.11 .

The following equation describes one dimensional mass transfer through the diffusion layer (δ_{eff});

$$\dot{n}''_i = K_G \, (N_{i,G} - N_{i,\infty}) \qquad (26)$$

And

$$K_G = D_{i,G} \, / \, \delta_{eff} \qquad (27)$$

This theory was shown to be accurate in cases where no natural or forced convection occurred, such as for low density gas phases in a vacuum (up to 1000 Pa) (81).

The effective film model was valid for the low pressure experimental data, <1000 Pa, obtained by Ward (20), who studied the evaporation of Mn from steel melts at a temperature of 1853 K. The gas phase mass transfer coefficient for Ward's work was calculated from the experimental refining rates according to the following equation:

$$K_G = \left(\frac{1}{K_{exp}} - \frac{RT}{\psi_i K_E} - \frac{1}{K_L} \right)^{-1} \qquad (28)$$

And $$\delta_{eff} = K_G \; / \; D_{Mn\text{-}Ar} \qquad (29)$$

The diffusion coefficient of Mn vapours into argon gas was obtained from the literature and a diffusion length of roughly 10^{-2} m was estimated, Equation 29, for gas phase mass transport over the pressure range from 10 to 100,000 Pa, see Figure 4.12.

The Fluid Motion in Penetration model which can also be used to describe the gas phase mass transfer coefficient was proposed by Higbie (18). It is used when natural or forced convection occurs. This model predicts that the gas phase mass transfer coefficient is proportional to the square root

of the diffusion coefficient.

$$K_g = 2(D_{i,G} / \pi \cdot t_e)^{0.5} \qquad (30)$$

Where: $D_{i,G}$ = Diffusion Coefficient of i in the Gas Phase.
t_e = Exposure Time of Gas Element at Interface.

The values of the gas phase mass transfer data from Ward (20) were observed to be proportional to the inverse of the square root of the chamber pressure for total pressures from 1000 to 100,000 Pa (81), see Figure 4.13. Thus, for dense gases where convection is important, the penetration theory is preferable.

Experimentally (18), the mass transport coefficient is seen to be proportional to D^n, where n varies from 0.5 to 1.0 depending on the circumstances or condition of the experiments .

In the LSV process, the evaporation surface area is composed of the surface of the melt and the surface of droplets generated in the spray. An alternative method to calculate the gas phase mass transfer coefficient around the droplets was to use the Ranz-Marshall correlation (84). This correlation was derived for spherical drops in an isothermal system and the correlation is given in terms of dimensionless numbers as follows:

$$Sh = 2 + 0.6\ (Re^{0.5} .\ Sc^{0.333}) \qquad (31)$$

Where: Sh = Sherwood Number

Re = Reynolds Number

Sc = Schmidt Number

In the LSV system, where the chamber pressure is less then 10^3 Pa, and the gas flow rate is low, the Reynolds number was calculated to be less than 0.1, such that the Sherwood number is approximately equal to 2, thus:

$$K_G = 2\ .\ D_{i,G} / l_c \qquad (32)$$

where: l_c = Diameter of the Droplet, m.

A value of the maximum droplet size for freely falling drops can be obtained from the following equation (85):

$$d_{max.} = 4\ .\ (\sigma / (g\ .\ \Delta\rho))^{0.5} \qquad (33)$$

where: σ = Surface Tension, kg s^{-2}.

$\Delta\rho$= Density Difference between the Liquid and Gas Phase, kg m^{-3}.

g = Gravitational Acceleration, m s^{-2}

Using typical data for water, aluminum, copper and iron

(Table 4.1) in Equation 28, the maximum droplet diameters of 0.011, 0.024, 0.016 and 0.020 m were calculated for each set of values, respectively.

Table 4.1 : Kinematic Viscosity for Water and Other Molten Metals of Interest (86).

	Temp. (^{o}C)	η X 0.001 (kg $m^{-1}s^{-1}$)	ρ (kg m^{-3})	ν ($m^{2}s^{-1}$)	σ (kg s^{-2})
H_2O	20	1.0	1000	1.0	0.072
Al	720	1.6	2410	0.7	0.85
Cu	1200	4.2	7940	0.5	1.29
Fe	1550	7.2	7200	1.0	1.79

Fig. 4.9 : Schematic Diagram of the Fluid Motion in Penetration Theory (18).

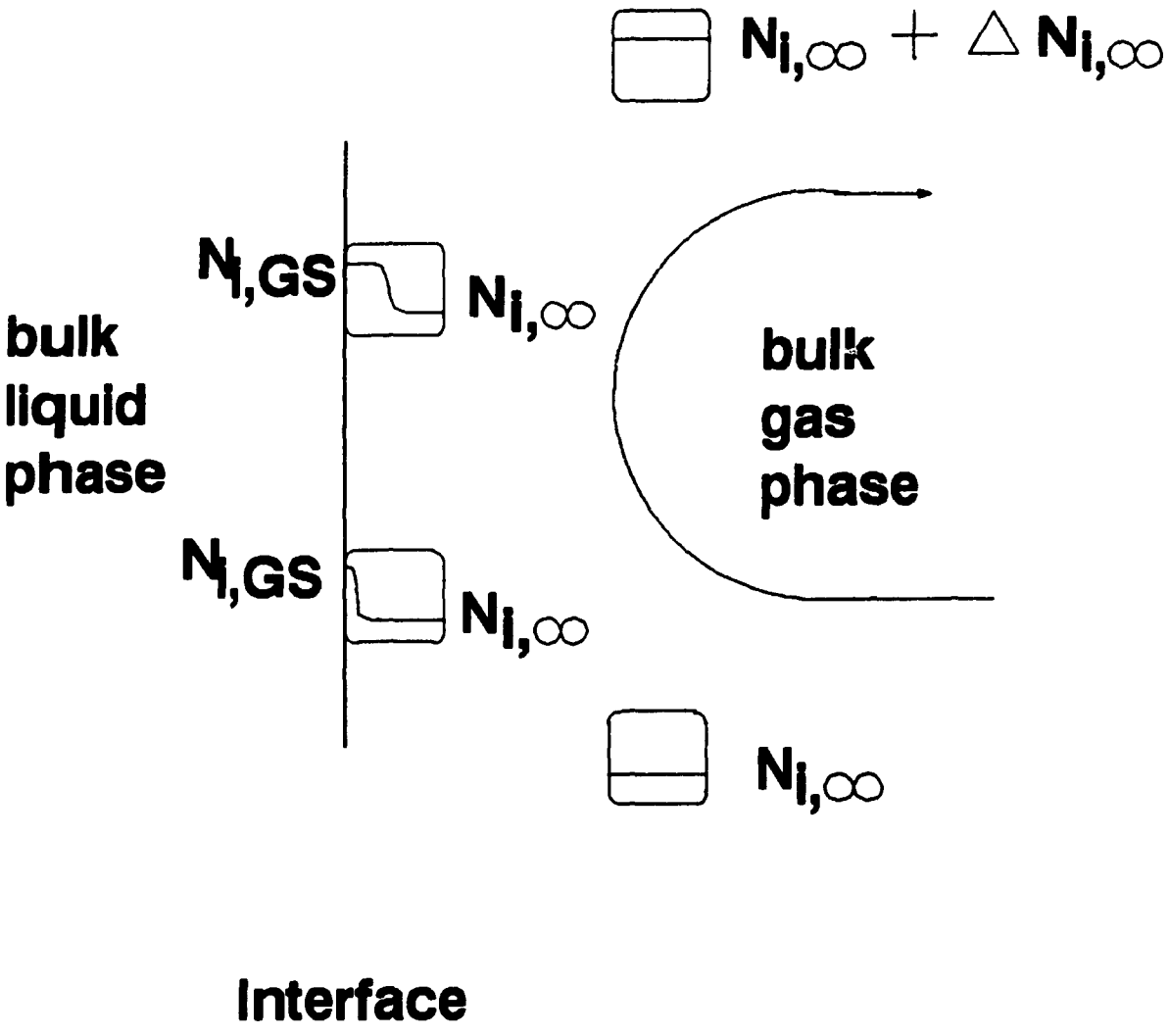

Fig. 4.10 : Schematic of Elements of Liquid or Gas Passing Over the Surface of a Spherical Bubble or Droplet (27).

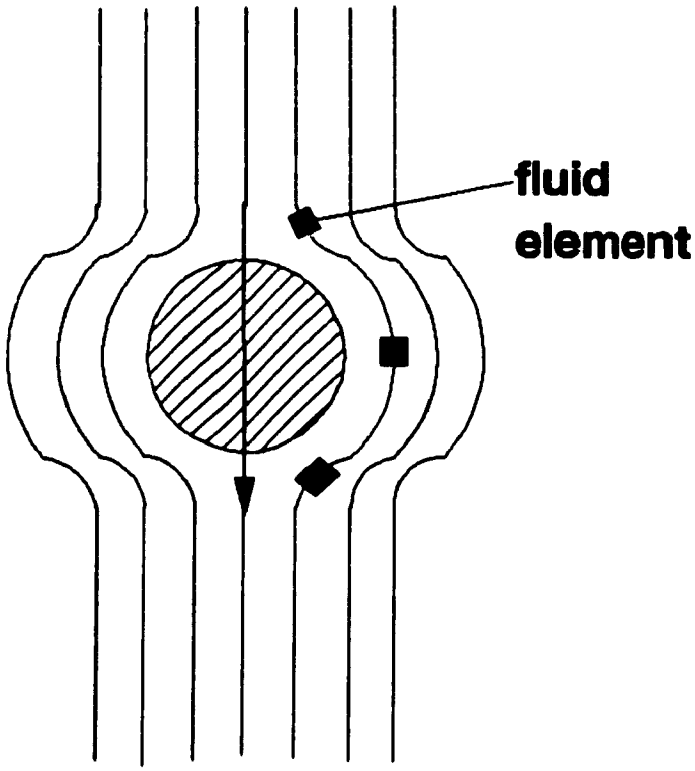

Fig. 4.11: Schematic Diagram of Film Theory (18).

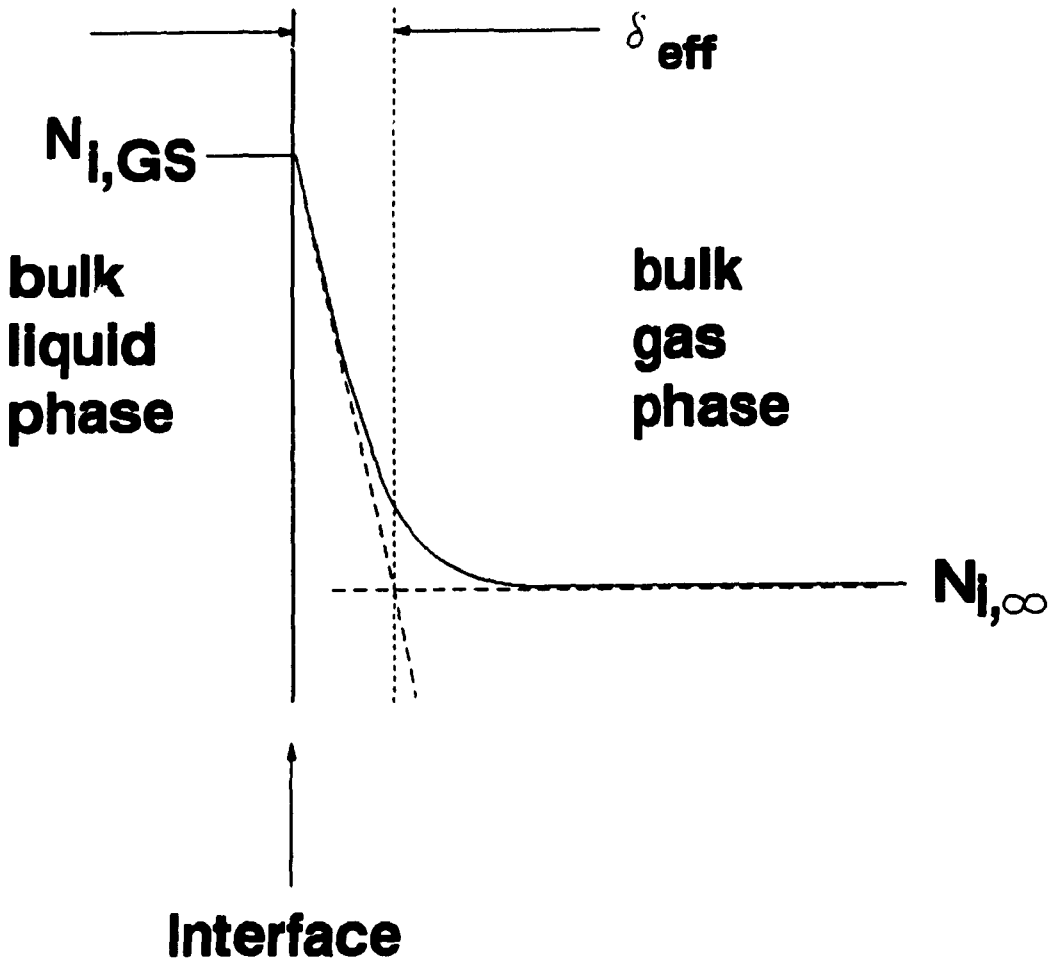

Fig. 4.12: Diffusion Path Length versus Chamber Pressure Calculated from Ward's Work (20).

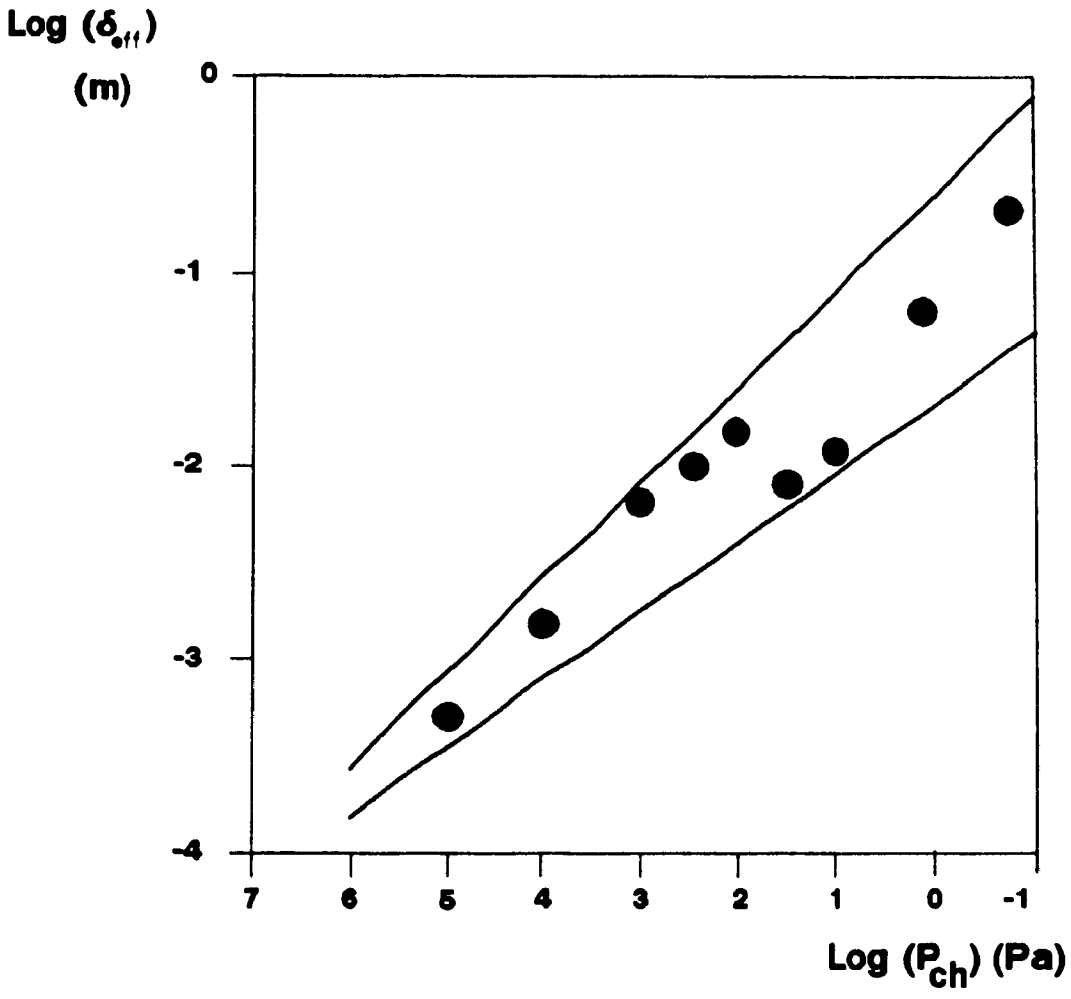

Fig. 4.13 : Logarithm of the Gas Phase Mass Transfer Coefficient versus the Logarithm of the Inverse of the Chamber Pressure from Ward's Experimental Work (20).

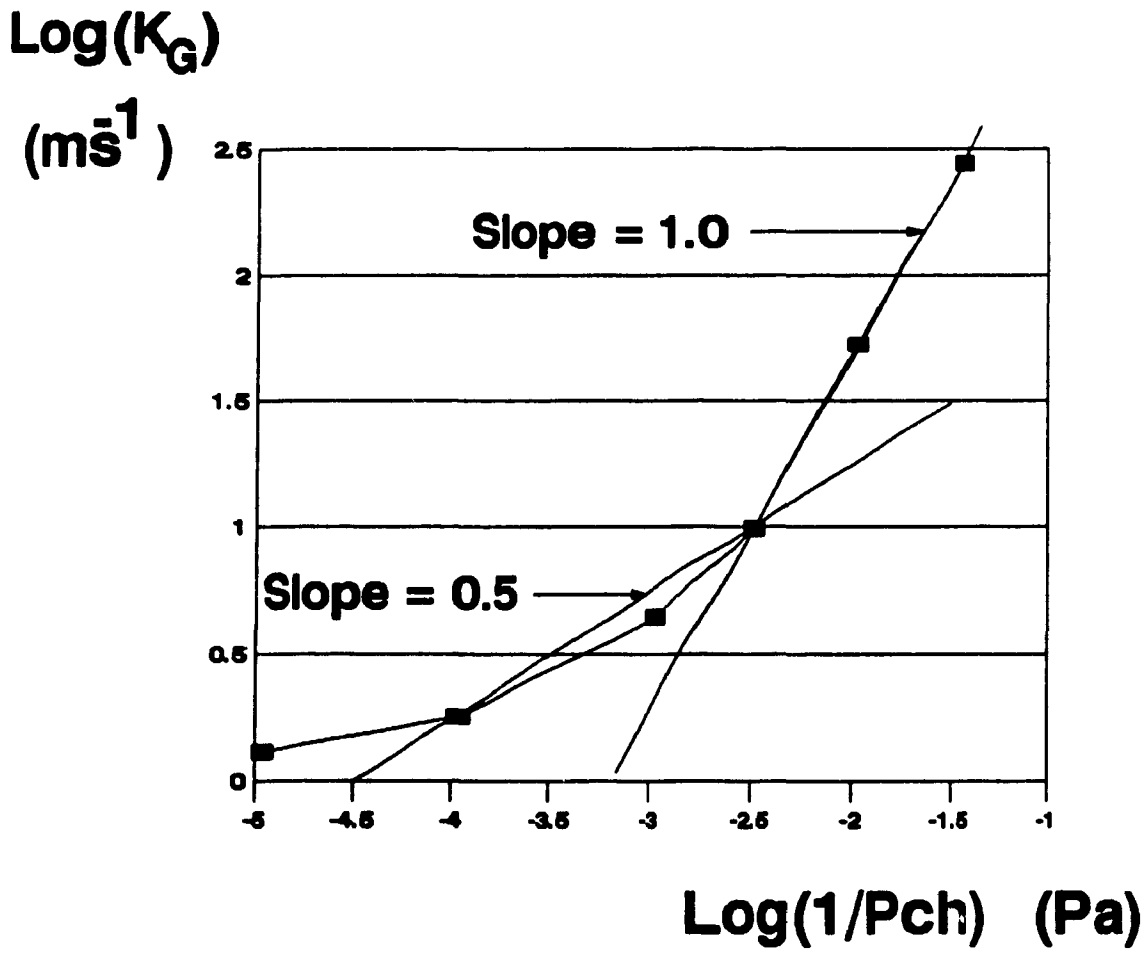

At Pch = 100,000 Pa, Log(1/Pch) = -5.0

At Pch = 1000 Pa, Log(1/Pch) = -3.0

At Pch = 10 Pa, Log(1/Pch) = -1.0

4.3.7 Operating Equations for Vacuum Refining

The mass transfer refining flux of an impurity from the bulk of the melt to the bulk gas phase can be expressed by (6);

$$\dot{n}''_i = K_{ov} \cdot (N_{i,B} - [P_{i,\infty} / \psi]) \qquad (34)$$

For a very small time interval, δ_t, one can assume steady state mass transport. Thus, the flux of the impurity leaving the melt times the surface area available for evaporation is equal to the volume of the melt (V) times the rate at which the concentration of i in the liquid is dropping, i.e.:

$$(\dot{n}''_i \cdot A)_t = -V. \left(\delta_{N_{i,b}} / \delta_t\right)_t \qquad (35)$$

By inserting the right side of Equation 34 into Equation 35 and rearranging, we obtain:

$$K_{ov} \cdot (A / V) \cdot \delta_t = -\delta_{N_{i,b}} / (N_{i,b} - P_{i,\infty} / \psi_i) \qquad (36)$$

Assuming a very low chamber pressure ($P_{i,\infty} = 0$), and a constant melt volume, we can integrate the above equation from time t = 0 to t = t and from initial concentration, $N_{Init.}$, to concentration at time t, N_t. The resulting expression for the concentration of the impurity in the melt as a function of time is:

$$-K_{ov}\left(\frac{A}{V}\right).\ t = \ln\left[\frac{N_t}{N_{Init.}}\right] \qquad (37)$$

Thus, vacuum refining under low pressure conditions follows first order kinetics.

However, the assumption of $P_{i,\infty} = 0$ is often not realistic, especially for chamber pressures in the range of 100 to 1000 Pa. Assuming that the gas phase behaves as an ideal gas and is isothermal, the pressure of the solute species is equal to its mole fraction times the chamber pressure (49, 57). The mole fraction, X_i, of the impurity in the bulk gas phase is equal to the flux of the evaporating impurity species divided by the total flux of all the gases flowing out of the system. This total flux includes all other evaporating impurities as well as the flux of inert gases (F) introduced in the system. That is:

$$P_{i,\infty} = \left(\frac{n_i'' \cdot A}{\sum n_i'' \cdot A + F}\right) \cdot P_{ch} \qquad (38)$$

By introducing Equation 38 into Equation 36, it is not possible to solve the equation analytically, thus a numerical technique must be used.

The use of a numerical technique enabled further sophistication of the model and the volume of the melt was also expressed as a function of time. This is given by the

following equation:

$$V_{b,t} = V_{b,0} - \int_0^t \sum \dot{n}_i'' \cdot A \cdot M_i \cdot \delta_t / \rho_b \qquad (39)$$

Where: $V_{b,t}$ = Volume of Melt at Time t.

$V_{b,0}$ = Initial Melt Volume.

ρ_b = Average Melt Density.

And all other terms have been previously defined.

CHAPTER 5

Mathematical Modeling of Vacuum Purification of Copper Matte

5.1 Introduction

This chapter describes the mathematical modeling of vacuum refining copper matte to remove Pb, Zn, Ni, Bi, As and Sb. The chapter is divided into two parts. Firstly, a computer model is used to calculate the maximum theoretical overall refining rate coefficient. This coefficient is calculated from equations given in Chapter 4. More precisely, the effect of temperature, chamber pressure, copper matte grade, sulphur and oxygen activity are studied.

In the second part of this chapter, the LSV process is simulated on the computer using a numerical calculation technique. This program was written by Frank Buijsen, an exchange student from the Netherlands. The program is listed in Appendix IV. It incorporates operating parameters such as lifting gas flow rate, surface area available for evaporation, chamber pressure and the evaporating species pressure in the gas phase.

5.2 Thermodynamic Data

The theoretical overall evaporation coefficients are based on kinetic equations. However, thermodynamic data is required to calculate the vapour pressures of the evaporating species in the form of monoatomic, diatomic sulphide and diatomic oxide vapours. The thermodynamic data is presented in the following tables.

From Table 5.1, it can be seen that the vapour pressures of all species are a function of temperature. Thus, the overall refining rate coefficient will be temperature dependent when it is controlled by a temperature dependent transport process.

Table 5.2 shows the activity coefficients for Pb, Bi, As and Sb from four different authors. In all the cases, it is observed that the activity coefficient is a function of matte grade. A large drop in the activity coefficient (γ) was observed as the percent copper in the matte approached 80. This indicates that the evaporation and gas phase mass transport resistance will increase with matte grade due to their dependence on ψ (see Section 4.3). Thus, the overall refining rate coefficient will depend on the matte grade used.

Table 5.3 shows the calculated variations of sulphur and oxygen activity with matte grade as well as the oxygen

activity variation with total chamber pressure. These variables will also be considered during the overall refining rate coefficient calculations.

Table 5.1 : Gibbs Energy of Formation (kJ/kgmole) for various Reactions as a Function of Temperature (K), Using the Relationship; $\Delta G^{o} = A. + B.T.\log(T) + C.T$.

Reaction	A	B	C
Pb = Pb	193961	18.86	-158.54
Zn = Zn	126754	24.03	-181.13
Bi = Bi	190523	0.00	-100.30
As = As	276640	0.00	-111.23
Sb = Sb	257332	28.91	-205.02
$Pb + 0.5\ S_2 = PbS$	62185	0.00	-56.49
$Zn + 0.5\ S_2 = ZnS$	-6319	0.00	-37.17
$Bi + 0.5\ S_2 = BiS$	97945	0.00	-54.96
$As + 0.5\ S_2 = AsS$	127070	0.00	-64.73
$Sb + 0.5\ S_2 = SbS$	158706	28.91	-157.22
$Pb + 0.5\ O_2 = PbO$	6566	0.00	30.59
$Zn + 0.5\ O_2 = ZnO$	-174154	0.00	55.88
$Bi + 0.5\ O_2 = BiO$	103213	0.00	-54.79
$As + 0.5\ O_2 = AsO$	6000	0.00	-65.17
$Sb + 0.5\ O_2 = SbO$	40034	28.91	-159.35

All reactions are in the form : (l) = (g)
or (l) + (g) = (g)

Table 5.2 : Activity Coefficients of Impurities in Copper Matte for various Matte Grades from Various Authors.

a) Yasawa and Itagaki

Matte Grade (%Cu)	γ_{Pb}	γ_{Bi}	γ_{As}	γ_{Sb}	Ref.
50	10	16	5.0	10	30
60	10	16	4.5	8.9	30
70	10	13	2.0	7.9	30
80	3.0	5.0	0.04	0.16	30

b) Roine

Matte Grade (%Cu)	γ_{Pb}	γ_{Bi}	γ_{As}	γ_{Sb}	Ref.
35	1	13	30	56	44
65	4	40	10	40	44
80	26.1	42.5	0.049	0.34	44

c) Nagamori and Chaubal

Matte Grade (%Cu)	γ_{Pb}	γ_{Bi}	γ_{As}	γ_{Sb}	Ref.
35	--	--	11.6	64.4	47
65	--	--	5.2	50.3	47
80	--	--	4.6	36.3	47

d) Lau, Lamoreaux and Hildenbrand

Matte Grade (%Cu)	γ_{Pb}	γ_{Di}	γ_{As}	γ_{Sb}	Ref.
35	--	--	0.7	--	87

e) Values Used for the Computer Simulation

Matte Grade (%Cu)	γ_{Pb}	γ_{Bi}	γ_{As}	γ_{Sb}	Ref.
35	1	13	4	10	--
65	4	10	10	8	--
80	26.1	3	0.049	0.34	--

The activity coefficient were chosen to reflect best the experimental results.

Table 5.3 : Variation of the Sulphur and Oxygen Activity for various Matte Grade and Chamber Pressure.

Chamber Pressure		10 Pa	100 Pa	1000 Pa
Matte Grade (%Cu)	P_{S_2}	P_{O_2}	P_{O_2}	P_{O_2}
35	10^{-2}	10^{-11}	10^{-10}	10^{-9}
65	10^{-4}	10^{-10}	10^{-9}	10^{-8}
80	10^{-6}	10^{-9}	10^{-8}	10^{-7}

Note: The oxygen activity was calculated using the equilibrium constant of the equation $SO_2 = 1/2\ S_2 + O_2$, the equilibrium sulphur activity above the melt from the literature and assuming that the SO_2 pressure is equal to the chamber pressure.

5.3 Mathematical Modeling of the Overall Mass Transfer Coefficient

5.3.1 Mathematical Model Equations

The overall mass transfer coefficient, assuming that K_E and K_G are the same for all vapour species of the same impurity, is given by Equation 22, in Chapter 4,i.e.:

$$K_{ov} = \left[\left(\frac{1}{K_L}\right) + \left(\frac{1}{\psi_i + \psi_{iS} + \psi_{iO}} \cdot \left(\frac{RT}{K_{E,i}} + \frac{RT}{K_{G,i}}\right)\right)\right]^{-1} \quad (22)$$

All terms of Equation 22 were previously defined.

The overall mass transfer coefficient is a combination of the liquid, evaporation and gas phase mass transfer coefficients.

Liquid Phase Mass Transfer Coefficient

As explained in Chapter 4, it is difficult to obtain values of exposure time for the liquid phase. Thus, a theoretical calculation of K_L is impossible for the LSV system. However, a value of 2×10^{-4} ms^{-1} is a reasonable estimate when compared to vacuum refining rates experimentally measured for copper matte melts (52).

Evaporation Mass Transfer Coefficient

In this model it is assumed that the evaporation mass transport coefficient is constant for all three vapours from the same impurity, that is $K_{E,i} \cong K_{E.iS} \cong K_{E,iO}$. The equation for K_E can be obtained from Chapter 4, Equation 25.

$$K_E = (RT / 2\pi M_i)^{0.5} \qquad (25)$$

Gas Phase Mass Transfer Coefficient

The gas phase mass transfer coefficient is given by Equation 27, Chapter 4.

$$K_G = D_i / \delta_{eff} \qquad (27)$$

This expression is simple and valid for chamber pressures up to 1000 pascal. A value for the effective film thickness was calculated to be 0.02 m from Ward's work (20) using the method described in Chapter 4. The value for the diffusion coefficient of the impurity vapours in air at low pressure was estimated to obey the following equation (52):

$$D_{i,Air} = 4.4 \times 10^{-5} T^{1.75} / P \qquad (40)$$

Where, $D_{i,Air}$ = Diffusion Coefficient, $(m^2 s^{-1})$

T = Temperature, (K)

P = Pressure. (Pa)

5.3.2 Results of the Computer Simulation

Having defined all the thermodynamic and mass transfer data, the overall mass transfer rate coefficient can now be calculated. The program requires the following input data:

i) Activity coefficient of the impurities
ii) Percent Copper in the Melt
iii) Temperature of the Melt
iv) Chamber Pressure
v) Sulphur Activity in the Melt
vi) Oxygen Activity in the Melt

The program was used to estimate the overall mass transfer rate coefficients of Pb, Zn, Ni, Bi, As and Sb versus the following parameters: matte grade, chamber pressure and temperature of the melt.

In all, 54 simulations were run. The low oxygen activity represents the situation where graphite crucibles were used. The reaction between the graphite and the oxygen in the matte leads to very low oxygen activity in the melt. The results of these simulations are summarized in Figures 5.1 to 5.6.

Figure 5.1 shows the effect of matte grade (1473 K, 100 Pa) on the elimination of Pb, Bi, As and Sb. The results for Zn elimination were omitted since the model predicted rates of

evaporation of 2 X 10^{-4} ms^{-1} through out the 54 simulations due to the very high Zn vapour pressure. Hence zinc is always liquid phase controlled over the range of matte grade, temperature and chamber pressure studied. One can see on Figure 5.1 that the rate of Pb elimination is mostly liquid phase controlled (> 1.5 X 10^{-4} ms^{-1}) over the whole range of matte grade. In the case of Bi, the removal rate is mainly liquid phase controlled up to 70 % Cu and then decreases to a mixture of liquid and gas phase control at 80 % Cu (≈ 1 X 10^{-4} ms^{-1}).

The arsenic removal rate increases from 1 to 1.6 X 10^{-4} ms^{-1} as the matte grade is increased from 30 to 65 % Cu. This is due to increases in both the arsenic activity coefficient and the oxygen activity which result in an increased AsO pressure and faster refining rates. However, the overall refining rate drops sharply from 70 to 80 % Cu in the matte due to a very large drop in the activity coefficient of arsenic.

The Sb removal rate is always gas phase controlled at 100 pascal chamber pressure over the range of matte grade studied. The Sb refining rate drops from 0.5 X $10^{-4}ms^{-1}$ to less than 0.1 X $10^{-4}ms^{-1}$ as the matte grade increases from 70 to 80 % Cu. As in the case with As, this is due to a drop in the activity coefficient of Sb as the percent copper increased from 70 to 80 percent.

Figure 5.2 depicts the effect of temperature on the removal rates of Pb, Bi, As and Sb. It can be seen that as the temperature increases, the rate of Pb and Bi removal increases because of the higher vapour pressures of the diatomic sulphide and monoatomic metal gaseous species. In the cases involving As and Sb, where the vapours are mainly monoatomic oxide, this trend is not as pronounced.

In Figure 5.3, the removal rates of Pb and Bi in 35 and 65 % Cu matte are shown as a function of chamber pressure. The refining rates decrease as pressure increases. The rate changes from liquid phase control at 10 pascal to gas phase control at 1000 pascal chamber pressure.

Figure 5.4 shows the removal rates versus pressure of As and Sb in both alumina and graphite crucibles for 35 % Cu matte. One observes firstly, that the refining rates decrease with increasing chamber pressure. Secondly, the refining rates found in alumina crucibles are significantly faster than in the graphite crucibles due to the production of AsO and SbO vapours in these crucibles. These same trends are observed in Figure 5.5 where the matte grade is 65 % copper in the simulation. The effect of simulating very low oxygen activity (graphite crucibles) upon the Pb and Bi evaporation rates is very small since their diatomic sulphide and monoatomic vapour pressures are an order of magnitude higher than the pressure of the diatomic oxide. This is the reason why low

oxygen activity curves for lead and bismuth were not plotted on Figure 5.3.

Figure 5.6 shows the overall refining rate coefficients of As and Sb at 80 % Cu matte grade in alumina and graphite crucibles. Even though the rates are very low and gas phase controlled, one can still observe the decrease in rates from alumina to graphite crucibles. Again it is observed that the refining rate decreases with increasing vapour pressure of the chamber.

Fig. 5.1: Overall Evaporation Rate Coefficients versus the Percent Copper in the Matte, 1473 K, 100 Pa, Alumina Crucibles.

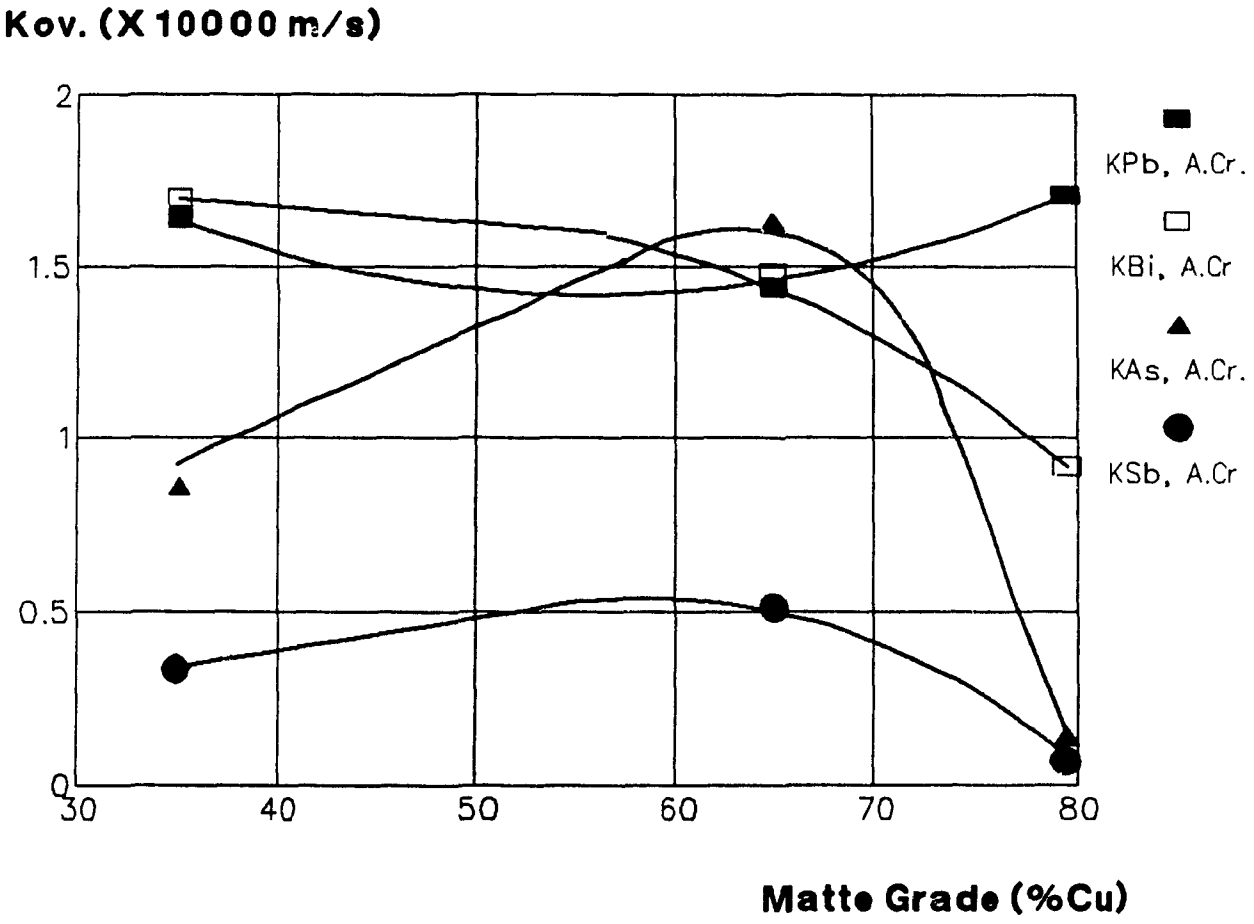

Fig. 5.2 : Overall Evaporation Rate Coefficients vs the Temperature, 100 Pa, 65 % Cu, Alumina Crucibles.

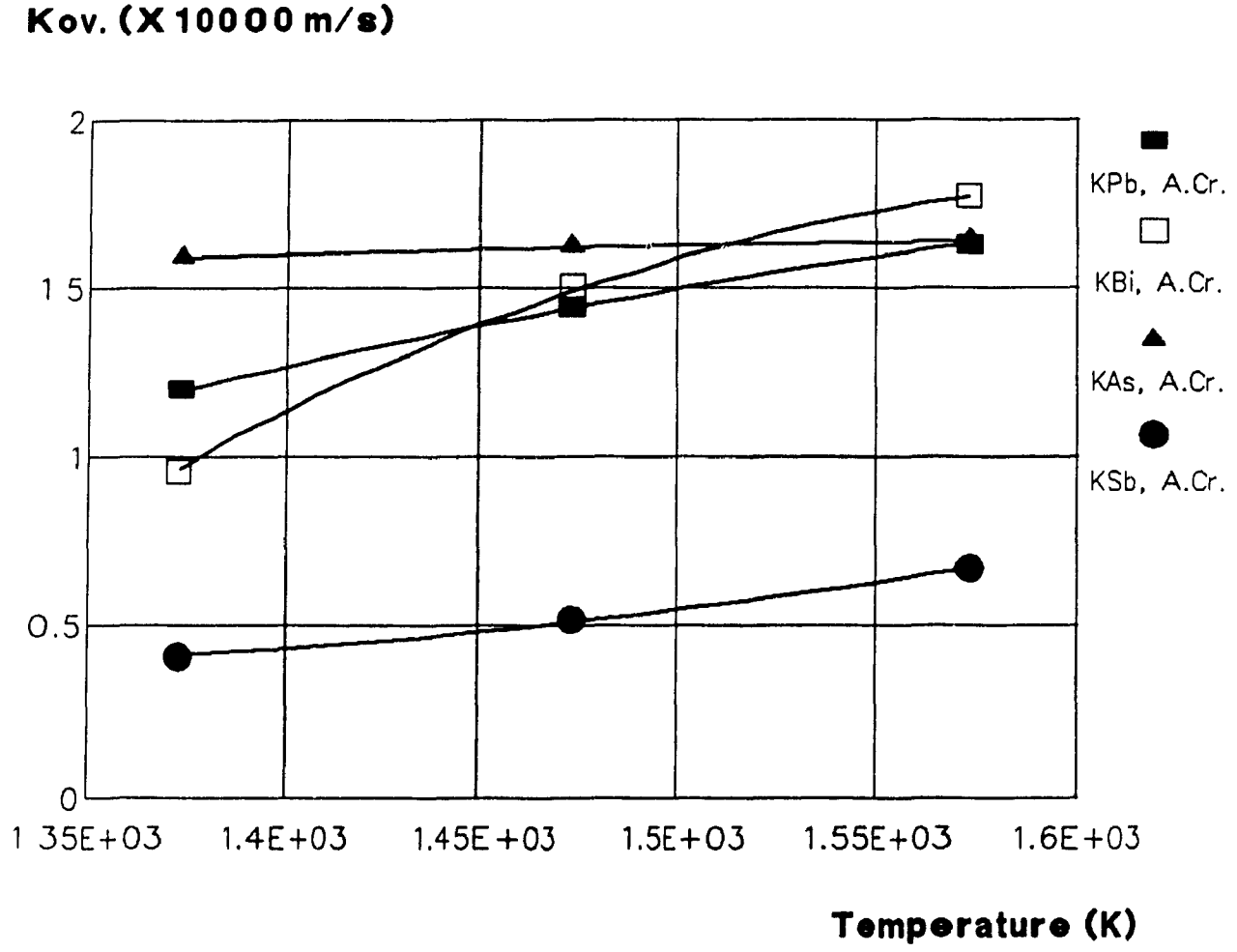

Fig. 5.3: Overall Evaporation Rate Coefficients versus the Chamber Pressure, 1473 K, 35 and 65 % Cu.

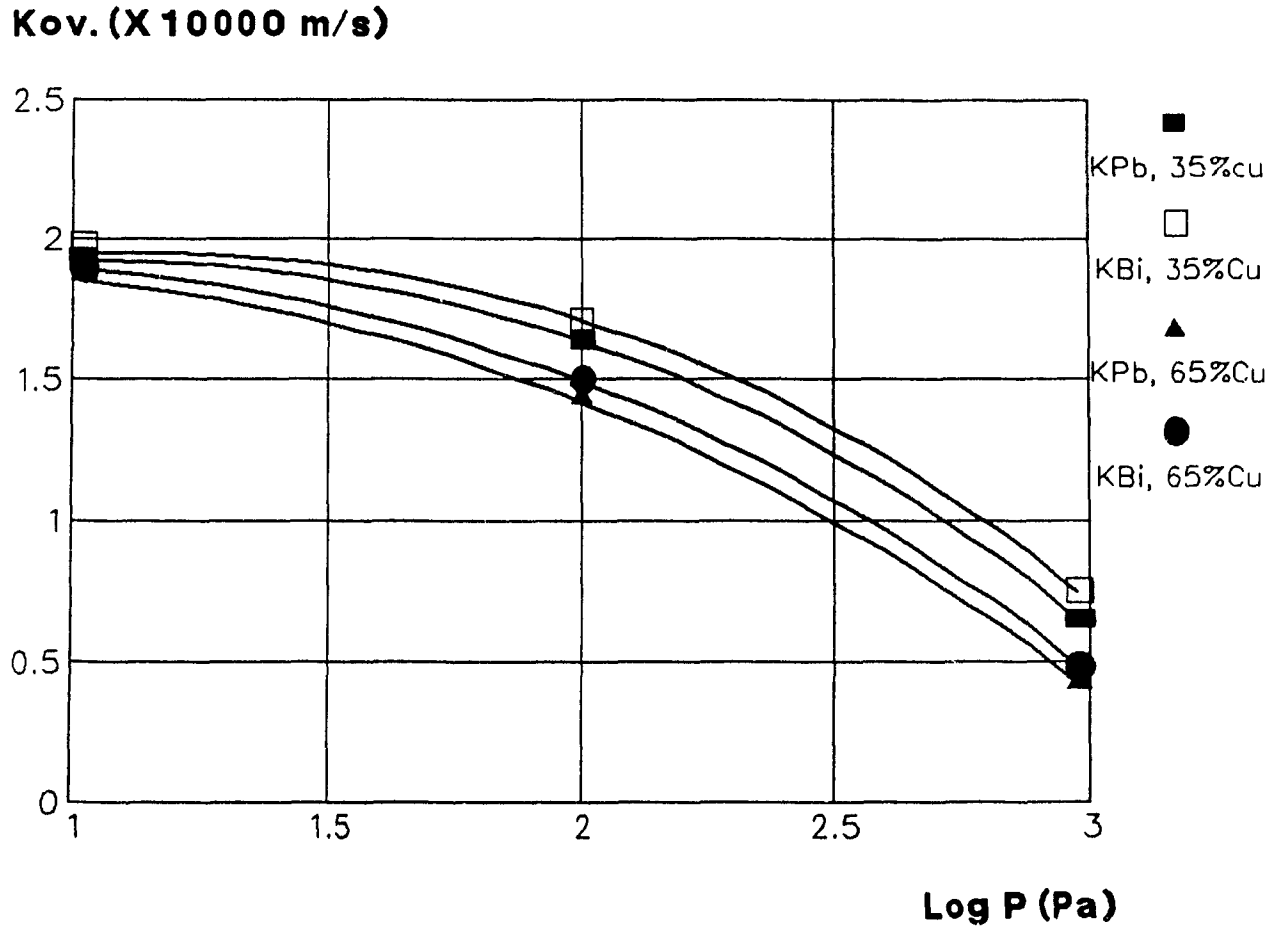

Fig. 5.4 : Overall Evaporation Rate Coefficients versus the Chamber Pressure, 1473 K, 35 % Cu, Alumina or Graphite Crucibles.

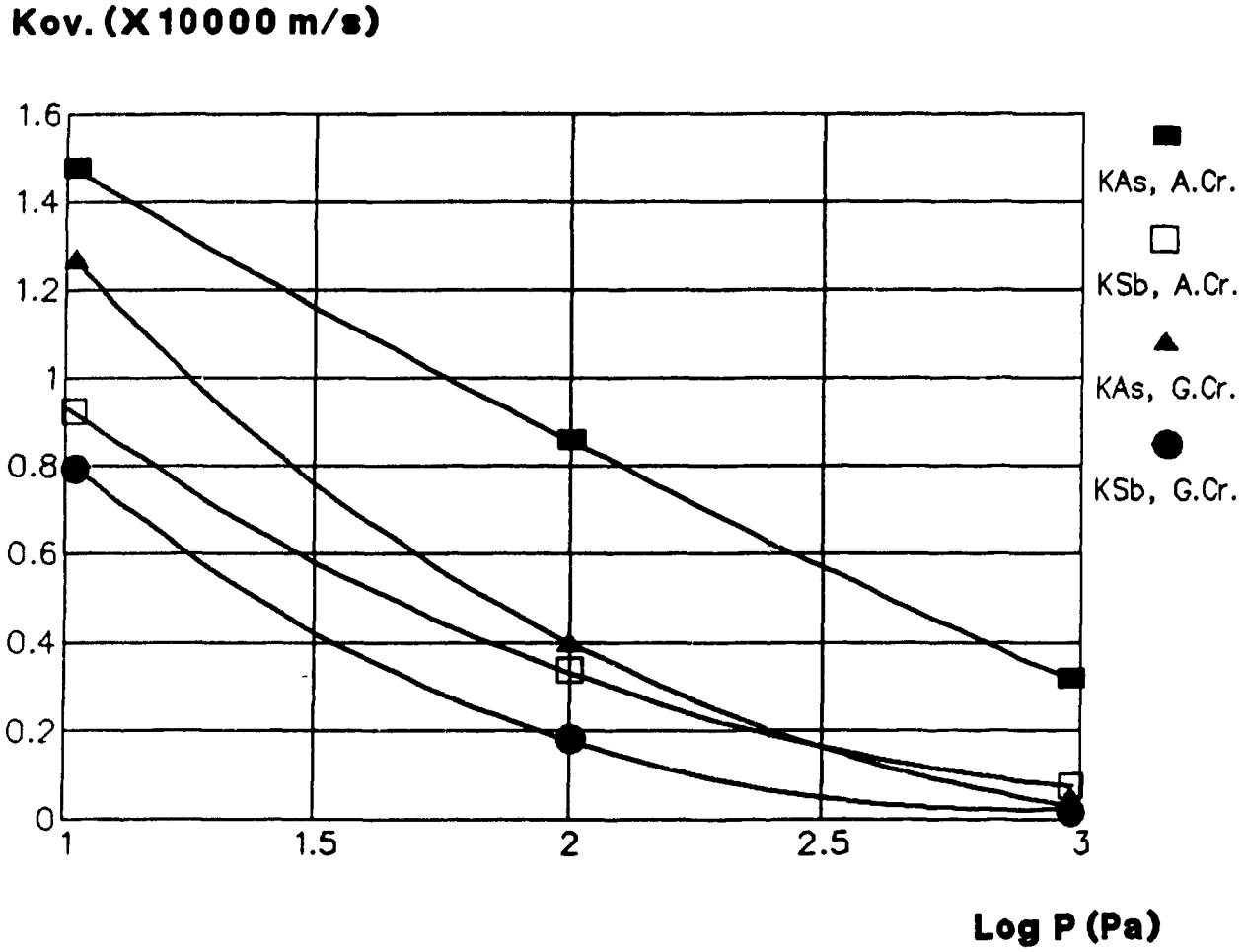

Fig. 5.5 : Overall Evaporation Rate Coefficients versus the Chamber Pressure, 1473 K, 65 % Cu, Alumina or Graphite Crucibles.

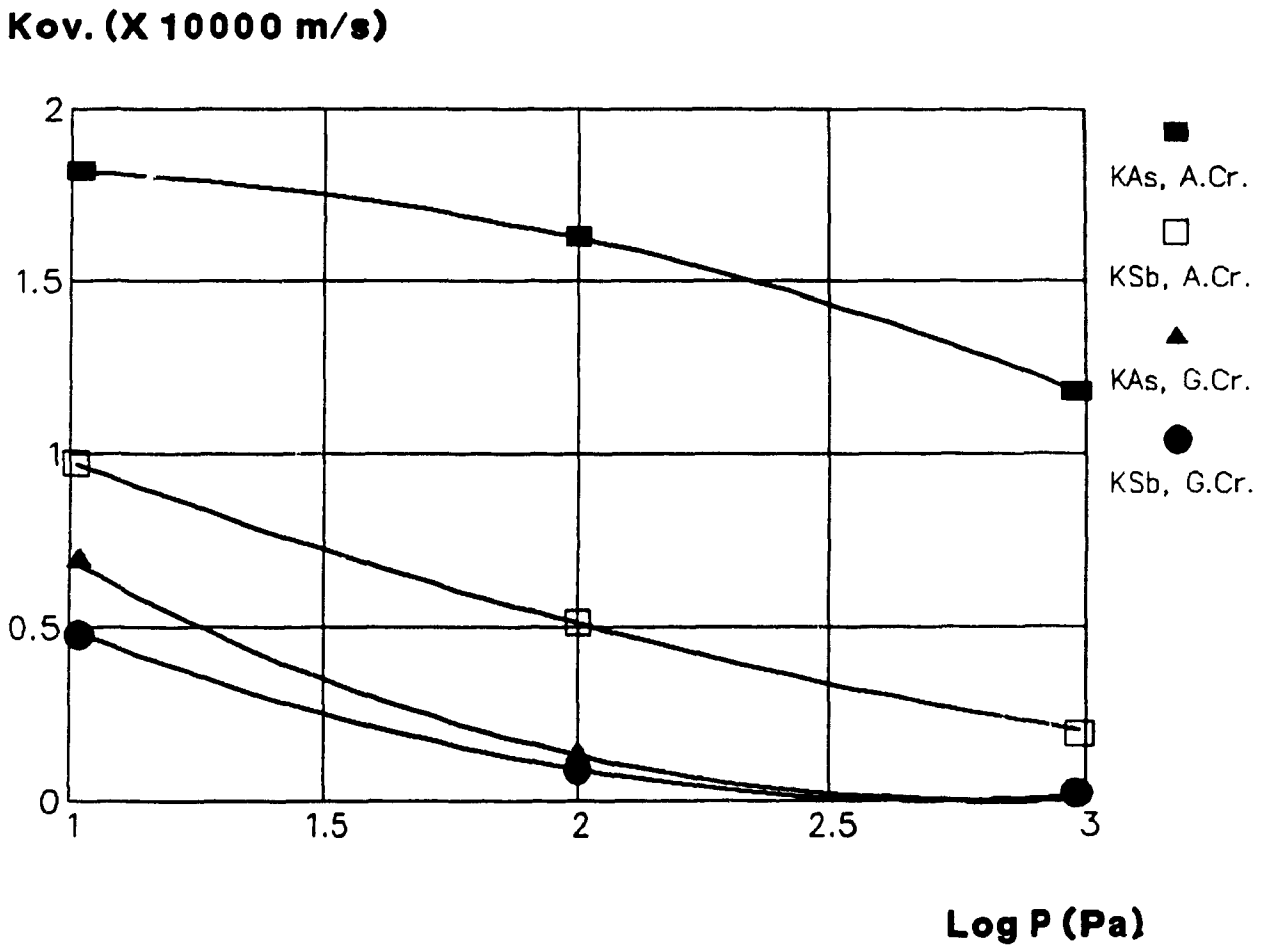

Fig. 5.6 : Overall Evaporation Rate Coefficients versus the Chamber Pressure, 1473 K, 80 % Cu, Alumina or Graphite Crucibles.

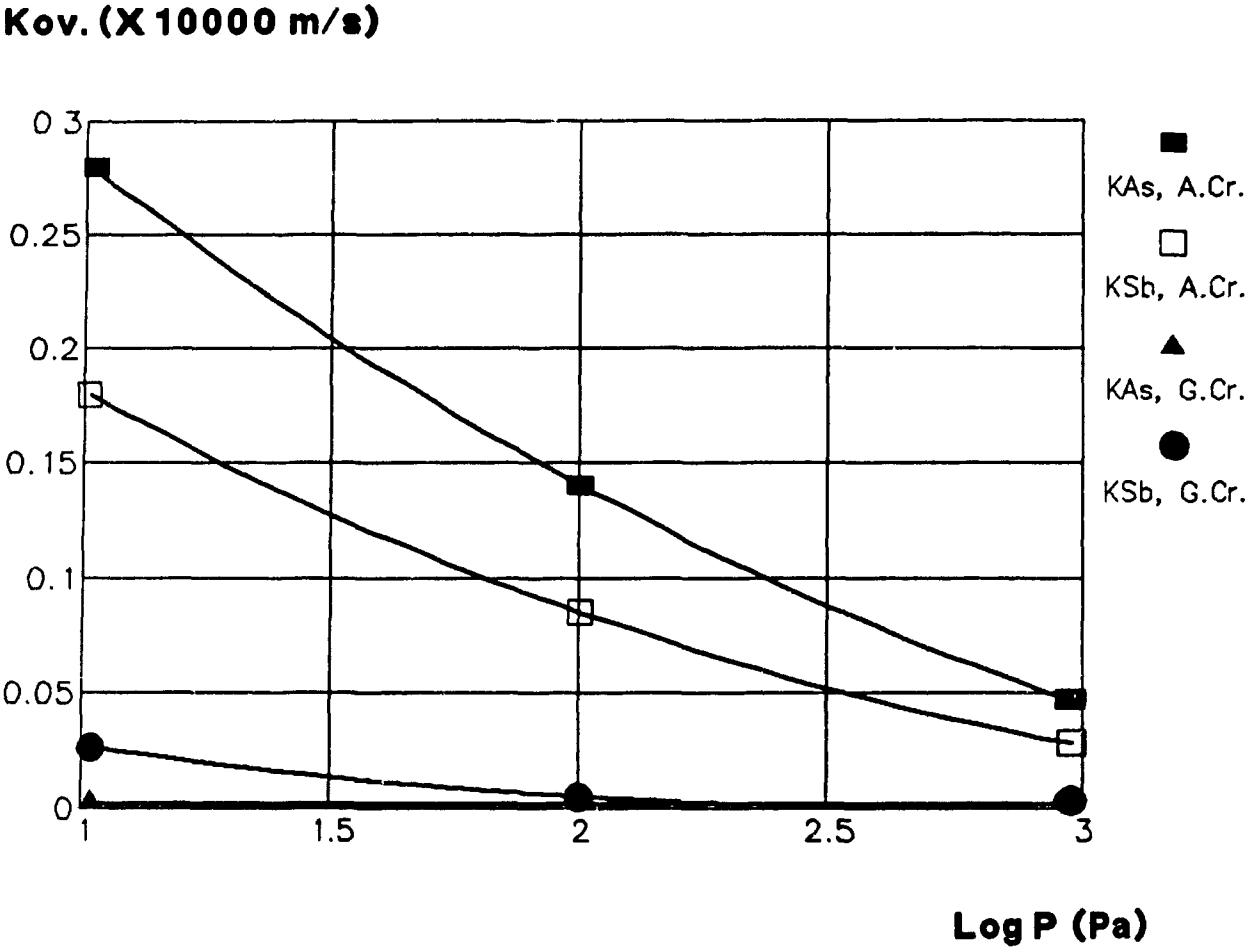

5.4 Modeling of the LSV Refining Process

5.4.1 Equations and Assumptions

A computer program was written to simulate the LSV refining process (Appendix II). The simulation uses the Equations described in Chapter 4, more precisely Equations 5, 6, 7, 20, 22, 38 and 39. The program works as follows. Firstly, the chamber pressure is assumed to be negligible. The concentration of each impurity in the liquid can be evaluated at the interface by assuming that the mass transport flux of the impurity in the liquid is equal to the sum of the monoatomic, diatomic sulphide and diatomic oxide flux in the gas phase.

The interface concentration of the impurity can then be used to calculate the flux of all the gaseous species and thus arrive at an approximation of the vapour pressures of each species in the bulk gas phase using Equation 38. Using these vapour pressures, new impurity concentrations can be calculated at the interface. These calculations are repeated until the fluxes converge to a constant value.

Then, assuming that for a very small time interval the flux is constant, a new bulk liquid concentration can be calculated for the time t + Δt. Using Equation 39, a new melt volume can be calculated for time t + Δt. With the new bulk

liquid concentrations, new interface concentrations and impurity flux can be calculated. This process is repeated until the final refining time has been reached. This is similar to performing a graphical integration of Equation 36.

5.4.2 Results of the LSV Computer Simulations

The LSV computer simulation program was used to predict the concentration of Zn, Pb, Bi, As and Sb versus time for typical experimental conditions used in the laboratory. The simulation was used assuming the same oxygen activity as in the alumina apparatus and a copper matte grade of 65 % Cu.

Two levels of lifting gas and chamber pressure were selected as can be seen in Table 5.4, below.

Table 5.4: Summary of the Variables Studied in the Computer Simulation.

Simulation #	Matte Grade (% Cu)	Chamber Pres. (Pa)	Lifting Gas (Nml/s)
1	65	100	0
2	65	100	30
3	65	600	0
4	65	600	30

When no lifting gas was used, the simulation results were identical to a still vacuum refining experiment. When lifting gas was used (30 Nml/s), the surface area available for evaporation was increased by the presence of the spray. In the present calculations, the surface area of the spray (0.02 m^2) was taken from the analysis of the present experiments,

see Table 8.5 in Section 8.3.2 .

Figure 5.7 shows the logarithm of the bulk concentration at time, t, divided by the initial concentration for zinc against the refining time. There is little difference between the concentration profiles of zinc at chamber pressures of 600 and 100 pascal. Thus, it can be deduced that the zinc gas phase resistance is minimal and is not predominating as was shown in the previous section. The effect of a lifting gas flow rate of 30 Nml/s is observed by an increase in the slope of the line of 2.3 times (the refining rate is thus 2.3 times faster). The increase in the refining rate simulates the shower of droplets produced in the LSV process.

The logarithm of the lead concentration versus time is plotted on Figure 5.8. It can be observed that the line for 100 Pa chamber pressure and 30 Nml/s of lifting gas is not straight but curves slightly. This is due to the fact that the pressure of the impurities in the bulk gas phase is affecting the rate of evaporation, i.e., the concentration difference ($N_{Pb,b} - P_{Pb,\infty}/\Psi$) tends towards zero when the lead concentration gets smaller. In the case of copper matte refining, this effect is insignificant due to the large number of gaseous species evaporating simultaneously. The gases dilute one another keeping their pressures low. Scavenging gas can further be used to dilute the impurity vapours and reduce the effect of the chamber pressure.

The above result does not change the fact that evaporation is a first order kinetic reaction. However, the logarithm of $((N_{i,b} - P_{i,\infty})_t / (N_{i,b} - P_{i,\infty})_{t=0}$ vs time should be plotted to generate a straight line. Since, the lead pressure in the bulk gas phase is difficult to evaluate, only the logarithm of $((N_{i,b})_t / (N_{i,b})_{t=0})$ vs time is plotted when experiments are performed.

On Figure 5.8 it can be observed that when the chamber pressure is raised from 100 to 600 pascal (with or without lifting gas) the lead refining rate decreases by 2.5 times. This demonstrates that the gas phase mass transport resistance plays an important role in determining the refining rate of lead for pressures higher than 100 pascal.

Figures 5.9, 5.10 and 5.11 show the plots of Bi, As and Sb concentration versus time. Both bismuth and arsenic are observed to behave similarly to lead. Antimony however, shows a much slower rate of removal than the other four impurities under all operating conditions. At a 100 pascal chamber pressure, antimony gas phase mass transfer resistance is much more significant as compared to the other four impurities.

Table 5.5 : Summary of the Predicted Percent Impurity Removal after 40 Minutes of Refining for a Matte Grade of 65 Percent Copper with an Alumina Interior.

Case #	Pres. (Pa)	Lift.Gas (ml/s)	Zn (%)	Pb (%)	Bi (%)	As (%)	Sb (%)
1	100	0	82.0	72.0	73.6	73.6	33.0
2	100	30	94.8	94.1	95.5	96.4	59.3
3	600	0	82.0	42.0	48.7	67.1	18.1
4	600	30	98.2	69.4	78.9	93.0	35.6

Table 5.5 summarizes the percentage of impurity removal expected after 40 minutes of refining in an alumina lined apparatus (oxygen activity 10^{-9}atm). It depicts the percent removal range from highest to lowest in the following order; Zn, As, Bi, Pb and Sb. These results show the superiority of zinc as a tracer over lead in evaluating the surface areas in the LSV process. Zinc is the impurity that is least affected by the chamber pressure.

Fig. 5.7 : Zinc Concentration versus Time, for 65 % Cu, 100 and 600 Pascal Chamber Pressure.

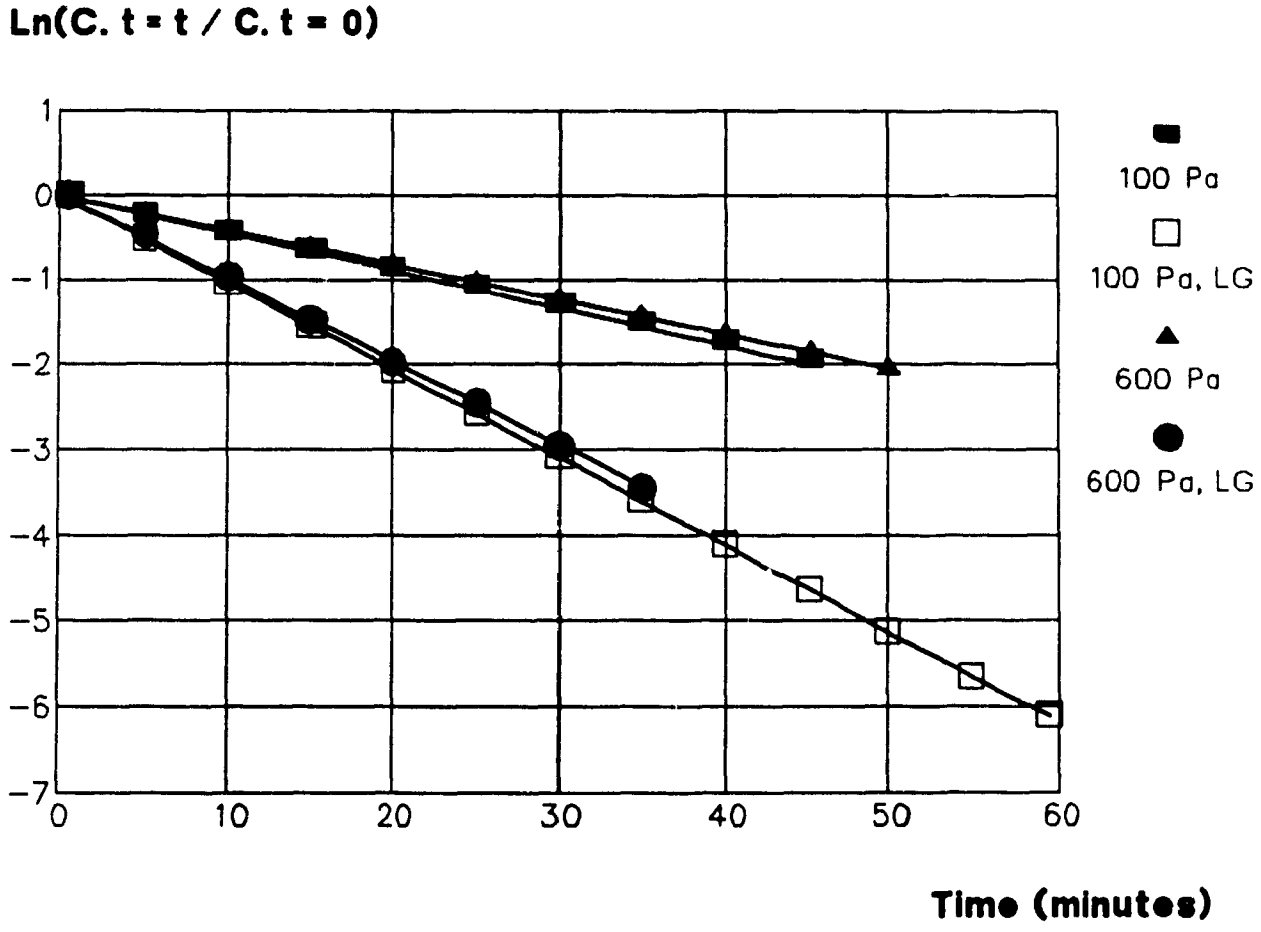

Fig. 5.8 : Lead Concentration versus Time, 1473 K, for 65 % Cu, 100 and 600 Pascal Chamber Pressure.

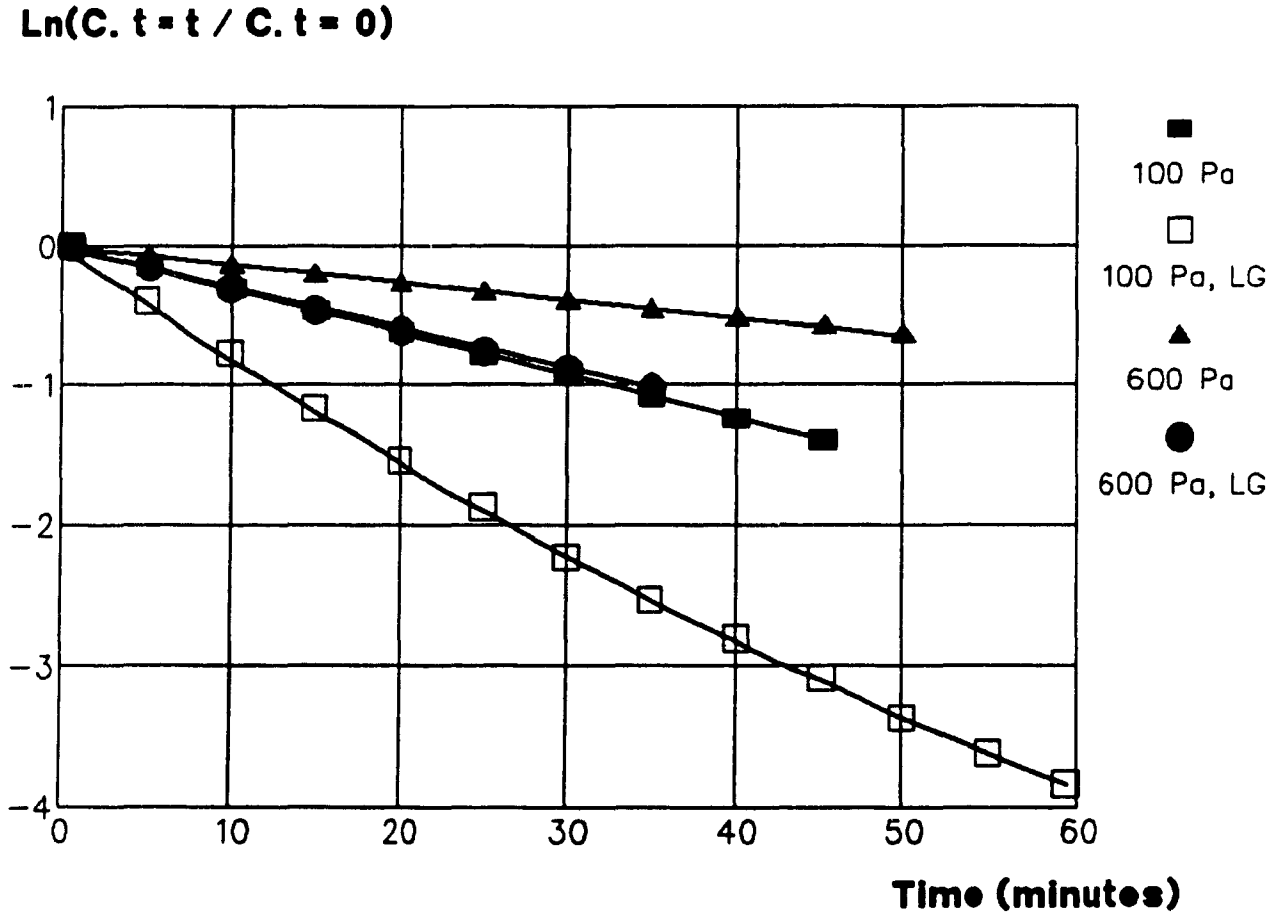

Fig. 5.9 : Bismuth Concentration versus Time, 1473 K, for 65 % Cu, 100 and 600 Pascal Chamber Pressure.

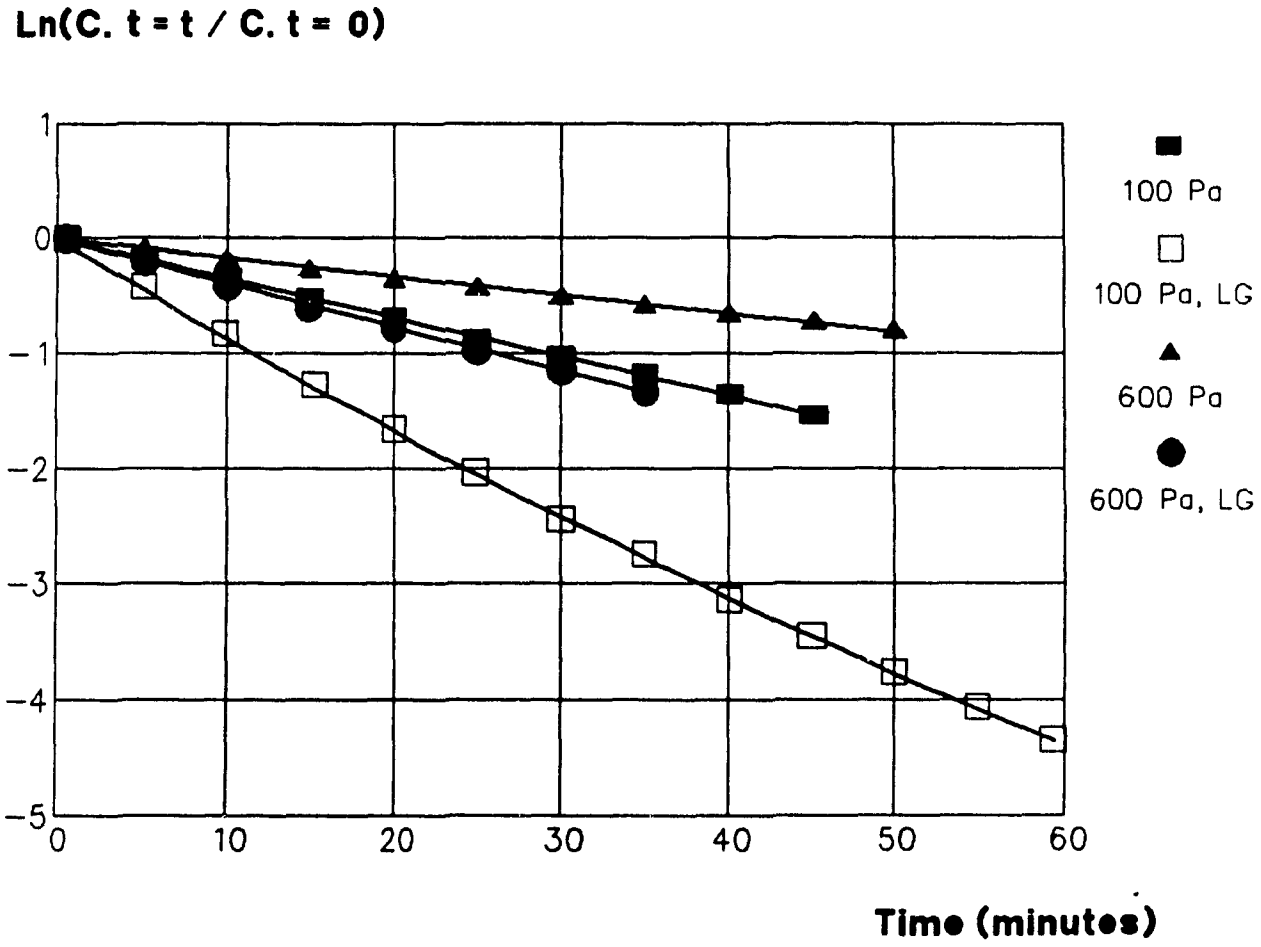

Fig. 5.10 : Arsenic Concentration versus Time, 1473 K, for 65 % Cu, 100 and 600 Pascal Chamber Pressure.

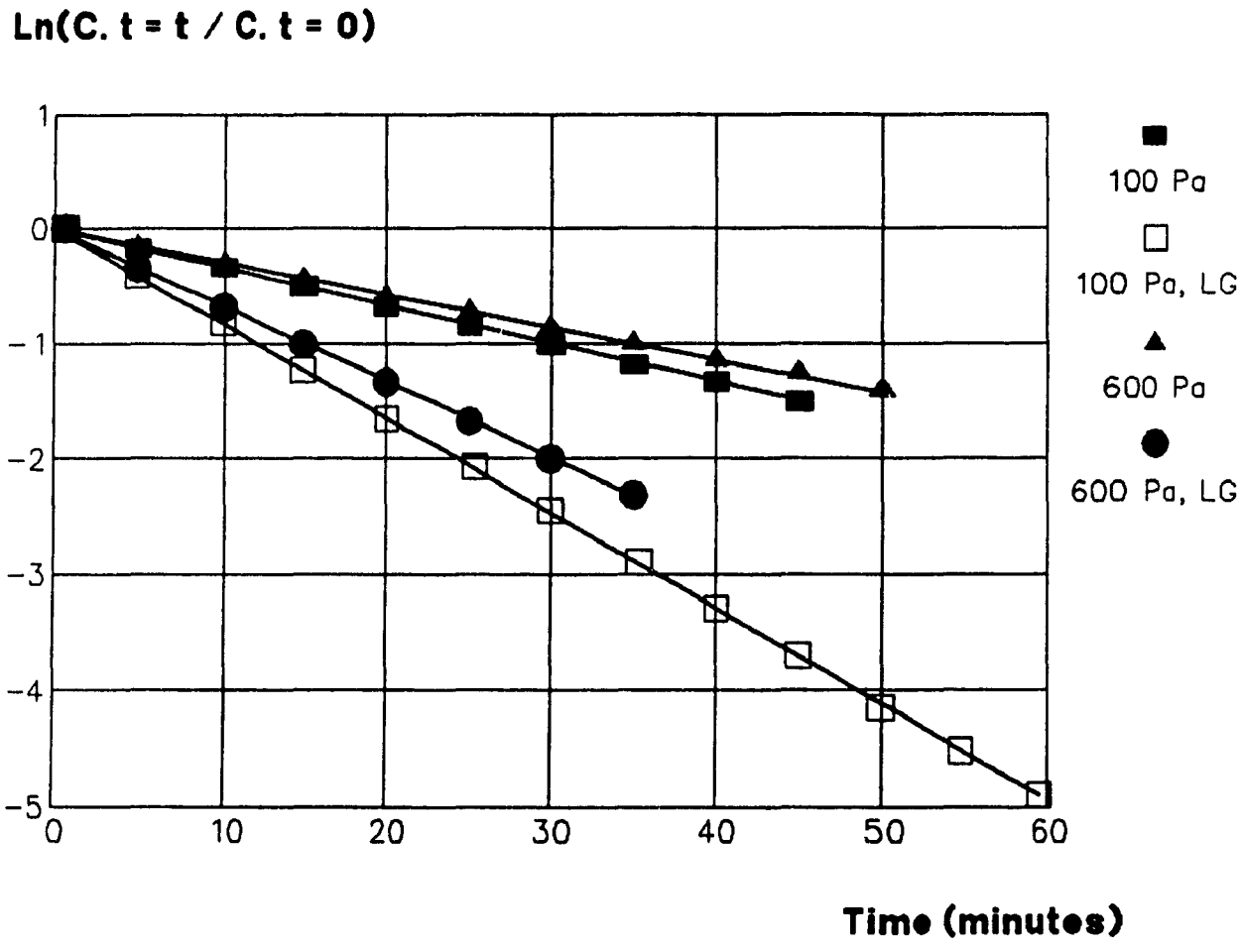

Fig. 5.11 : Antimony Concentration versus Time, 1473 K, for 65 % Cu, 100 and 600 Pascal Chamber Pressure.

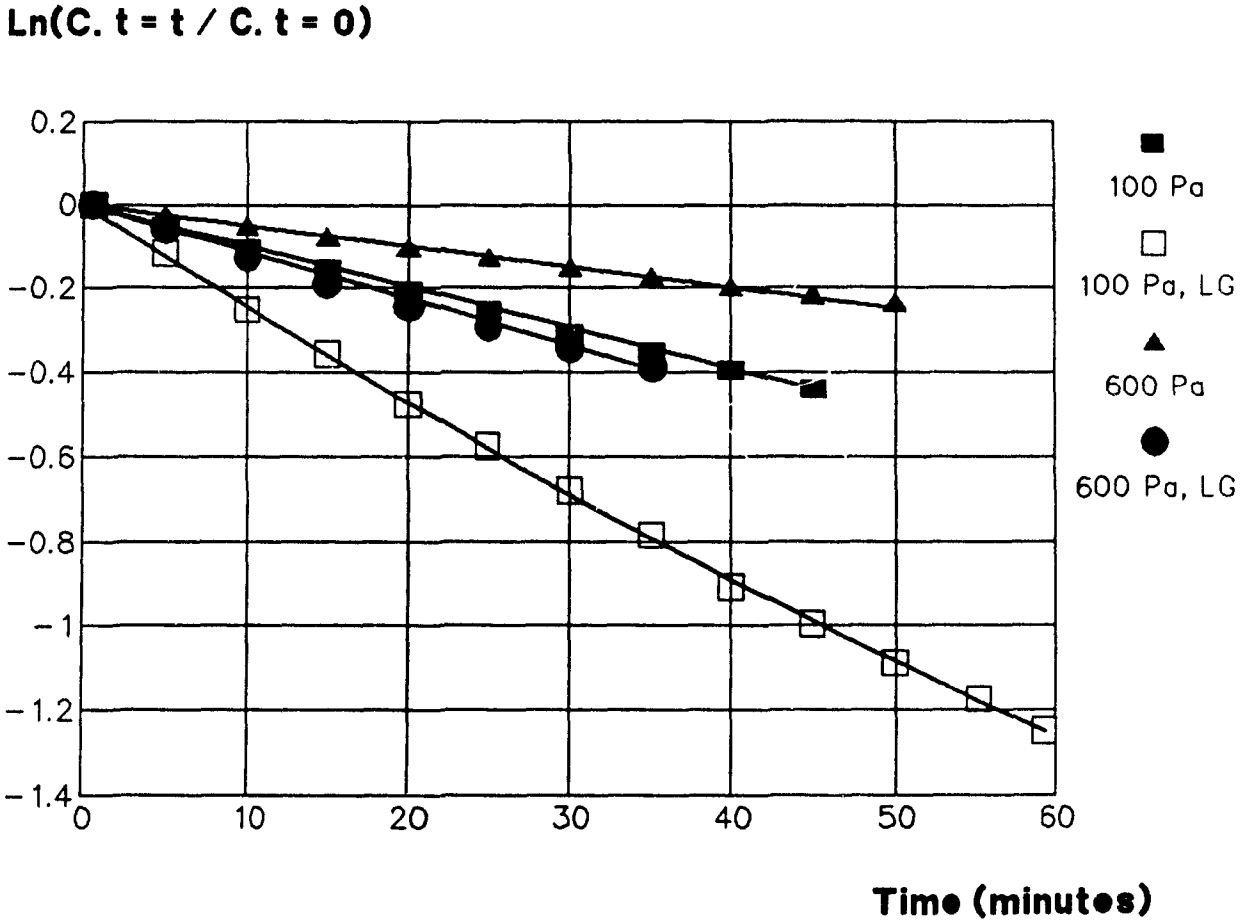

CHAPTER 6

Characterization of the Vacuum Refining Dust; Experimental and Results

6.1 Introduction

The impurity vapours produced during the vacuum refining experiments condensed in the vacuum chamber producing a very fine, black dust. The dust contained 5 to 20 % Cu, 20 to 50 % Pb, 20 to 50 % Zn and 0 to 3 % As, Bi and Sb. Furthermore, some sulphur and oxygen were present in the dust. The recovery of these valuable metals would be an added asset to the financial viability of the process. Hence, the characteristics of the dust were determined so as to comprehend the condensation process to determine a possible treatment for their recovery.

6.2 Characterization of the Dust Produced during Vacuum Refining of Copper Matte

6.2.1 Methodology

The following steps were carried out to gain understanding on the characteristics of the dust.

1- A chemical assay was performed on a bulk sample for each of the 15 vacuum refining experiments.

2- A dry screening of a bulk dust sample from LSV Experiment 6 was done to determine the particle size distribution.

3- A chemical analysis was performed on each size fraction of the dry screening test mentioned above to determine if chemical segregation occurred.

4- The dust was examined under an optical microscope to discern particle size and shape.

5- An X-Ray diffraction analysis was performed to identify the principal phases present in the dust of Experiment 6.

6- The dust particles were observed and photographed under the Scanning Electron Microscope (SEM).

7- Finally, an X-Ray Energy Dispersion Spectrum analysis was carried out on randomly selected particles.

6.2.2 Experimental

1- Chemical Analysis:

At the end of each experiment, the dust produced was collected using a brush and pan. All the walls and windows of the vacuum chamber, and the induction furnace were brushed. The dust was put in a plastic bag to be weighed and mixed. The dust was then spread out on a table where a sample was cut. The sample was labelled and sent for assaying at the Noranda Technology Center in Pointe Claire, Québec.

2- Particle Size Distribution :

A 100 gram dust sample from LSV Experiment 6 was used for a dry screening test. Screens of 28, 35, 48, 65, 100, 150, 200, 270 and 325 mesh size were used. The sample was left in the shaker for a period of 30 minutes. After, the oversize fraction on each screen was weighed as well as the -325 mesh under size. The weights were used to calculate the percent oversize fraction for each mesh size.

3- Chemical Assays versus Size Distribution :

A sample was cut from each screen fraction in Step 2 above. The samples were labelled and sent to the Noranda Technology Center for chemical assays for lead, copper, bismuth, arsenic

and antimony.

4- Optical Microscopy :

A sample of dust from Experiment 6 was taken to be examined under the optical microscope. A pinch of dust was sprinkled on a glass slide and mounted on the microscope. The maximum magnification (400X) was used to make observations.

5- X-Ray Diffraction Analysis :

The vacuum refining dust sample from Experiment 6 was mixed, a representative sample was cut and mounted for X-Ray diffraction analysis. The sample was scanned for 83 minutes on the X-Ray diffractometer. The sample was scanned from 5.0 to 100.0 degrees on steps of 0.020 degrees and a scanning time of 1.00 second. The computer data bank and programs were used to identify the main mineralogical species from the X-Ray diffraction pattern lines.

6- SEM of Vacuum Refining Dust :

Dust samples were prepared by concocting a mixture of dust and isopropyl alcohol used as a dispersant. The solid liquid mixture was placed 15 minutes in an ultrasonic bath for maximum dispersion. Immediately following the ultra sound, two drops of liquid were placed on two aluminum SEM sample

holders. After the alcohol evaporated, particles of dust remained on the holder. The surface of the samples were carbon coated for SEM microscopy. Several photographs of the dust particles were taken to evaluate their shape and size.

7- X-Ray Energy Dispersion Spectra Analysis of Dust :

The samples from step 6 were used to generate X-Ray EDS spectrum in order to identify the elements present in the discrete dust particles. Particles of various sizes and shapes were selected. The electron beam was focused at the center of the particle and the energy dispersion spectra was recorded. The computer data bank was used to help identify the peaks on the energy spectrum to identify the elements present in the particles.

6.2.3 Results

1- Chemical Analysis :

Table 6.1 shows the chemical analysis of the dust bulk sample collected in all 15 vacuum refining experiments.

As can be seen in Table 6.1, the chemical analysis of Cu, Pb, Ni, Bi, As and Sb show wide ranges. The copper ranges from 3 to 60 %, lead from 5 to 60 %, nickel from 0.2 to 0.3 %, bismuth from 0.1 to 5 %, arsenic from 0.01 to 1.5 % and antimony from 0.02 to 0.5 %.

Table 6.1 : Chemical Analysis for the Dust Bulk Samples of Experiments # 1 to 15.

Experiment #	Cu (%)	Pb (%)	Bi (%)	As (%)	Sb (%)	Ni (%)
GL1	10.5	22.6	0.91	0.090	0.26	---
GL2	5.52	55.4	0.43	0.30	0.42	---
GL3	9.64	28.3	0.37	0.12	0.33	---
GL4	5.93	60.4	0.12	0.43	0.45	---
GL5	25.3	30.1	0.12	0.23	0.066	---
GL6	15.8	35.7	0.12	0.36	0.17	---
GL7	3.63	33.9	0.45	0.10	0.12	---
GL8	60.4	12.4	0.10	0.016	0.027	---
GL9	54.7	15.4	0.41	0.018	0.027	---
AL10	10.1	16.4	1.07	1.42	0.42	0.32
AL11	17.4	13.6	0.65	0.76	0.13	0.33
AL12	22.8	36.2	0.98	0.66	0.18	0.27
AL13	16.9	6.8	1.68	0.76	0.092	0.33
AS14	45.0	4.59	1.48	0.56	0.029	0.13
AS15	23.4	23.5	5.54	1.28	0.14	0.21

Legend : A = Alumina Crucible

G = Graphite Crucible

L = Lift-Spray Vacuum Refining Experiment

S = Still Vacuum Refining Experiment

2- Particle Size Distribution :

Table 6.2 shows the percent under size versus the particle size. Figure 6.1 shows the cumulative weight percent under size versus the particle diameter. It can be observed that the 50 % passing size (d_{50}) is approximately 80 μm . It must be noted, that at less than 200 mesh, the dust agglomerated preventing all of it from passing through the screen. Thus, the 50 % passing size is probably a high estimate.

Table 6.2 : Weight of Each Size Fraction versus the Screen Size in Mesh.

Mesh Size	Equivalent Size (μm)	Weight (gr.)	Size Fraction (%)	Cum. Und. Fraction (%)
+28	550	9.01	9.16	90.84
+35	425	4.44	4.51	86.33
+48	332	5.28	5.37	80.96
+65	230	5.69	5.78	75.18
+100	150	7.80	7.93	67.25
+150	106	7.52	7.64	59.61
+200	75	10.16	10.33	49.28
+270	58	24.21	24.61	24.67
+325	49	11.81	12.01	12.66
-325	-49	12.45	12.66	
Total		98.37	100.0	

Cum. Und. = Cumulative Undersize

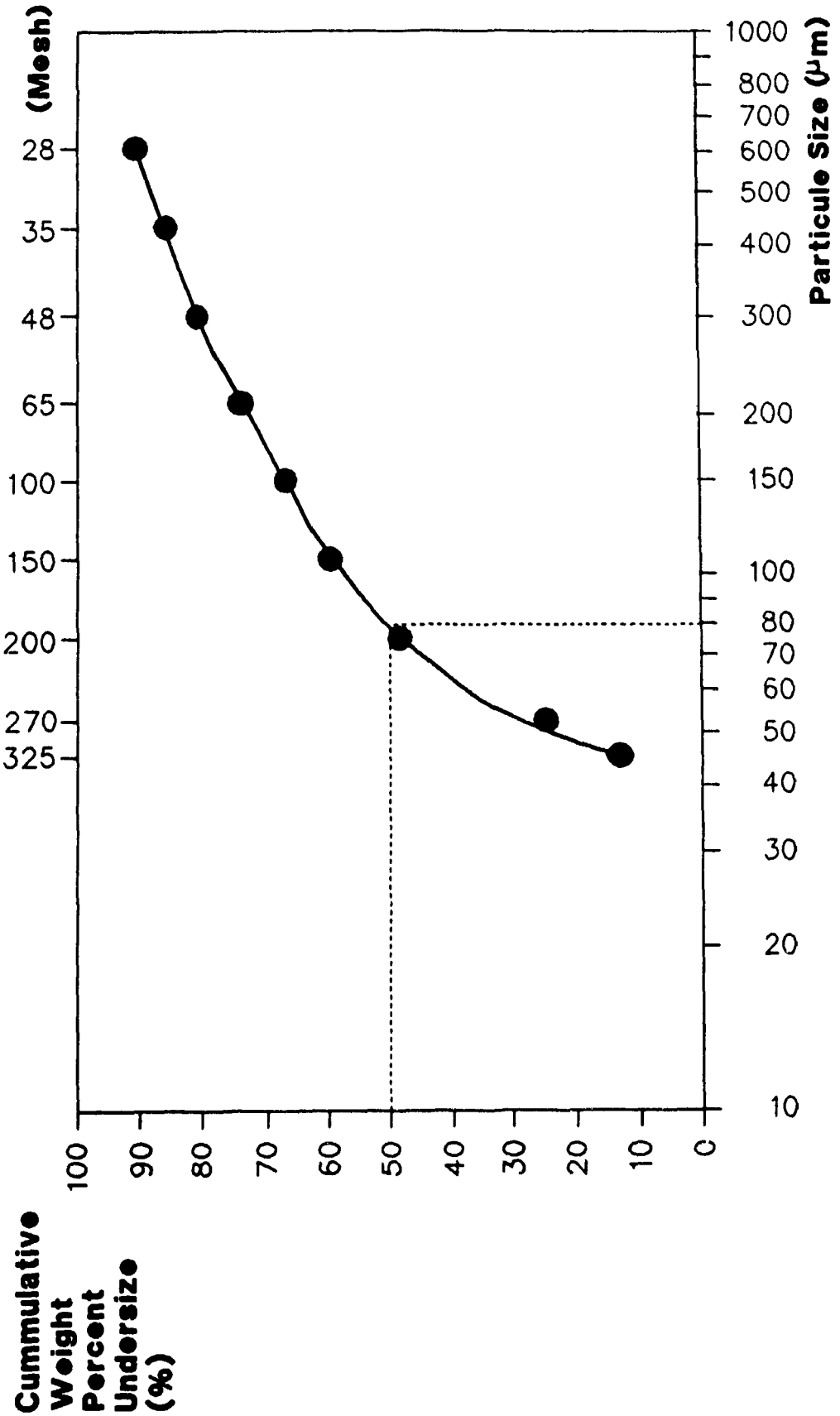

Fig. 6.1 : Dry Screen Analysis of the Dust from Experiment 6.

3- Chemical Assay versus Size Distribution :

Table 6.3 gives the chemical analysis of each size fraction of the dry screening test. These analysis were used to plot Figures 6.2 and 6.3.

Table 6.3 : Chemical Analysis of the Dust Fractions of the Dry Screening Test of Experiment 6 Dust.

Mesh Size	Weight (gr.)	Cu (%)	Pb (%)	Bi (%)	As (%)	Sb (%)
+28	9.01	43.8	9.84	0.033	0.14	0.027
+48	9.72	43.5	9.09	0.033	0.092	0.027
+100	13.49	16.2	22.9	0.065	0.23	0.041
+200	17.68	3.07	47.3	0.13	0.40	0.29
+270	24.21	1.91	52.2	0.50	0.15	0.26
+325	11.81	0.82	57.2	0.54	0.19	0.29
-325	12.45	1.48	51.6	0.62	0.25	0.26

Fig. 6.2 : Copper and Lead Analysis versus Size Fraction of the Dust from Experiment 6.

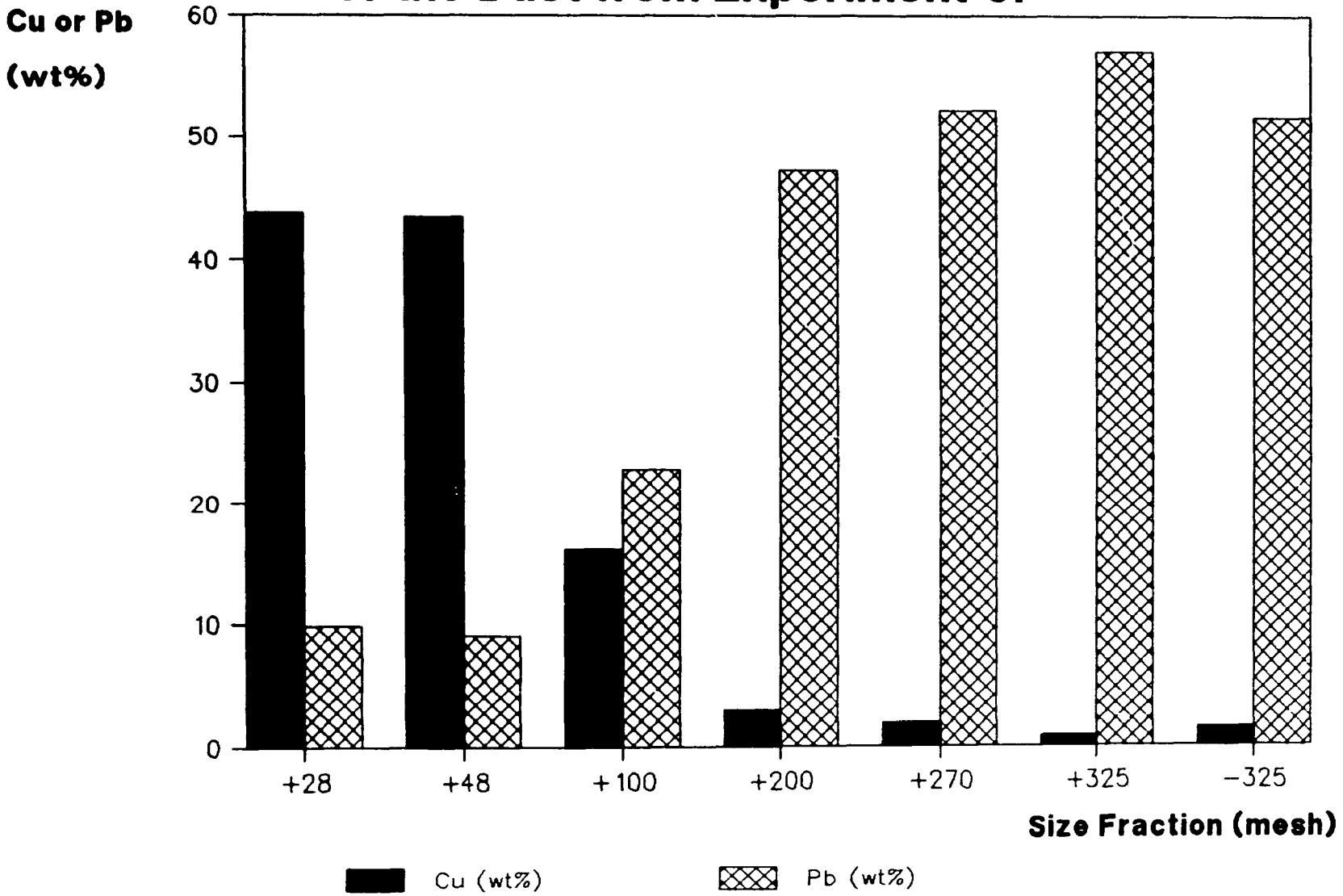

Fig. 6.3 : Arsenic, Bimuth and Antimony Analysis versus Size Fraction of the Dust from Experiment 6.

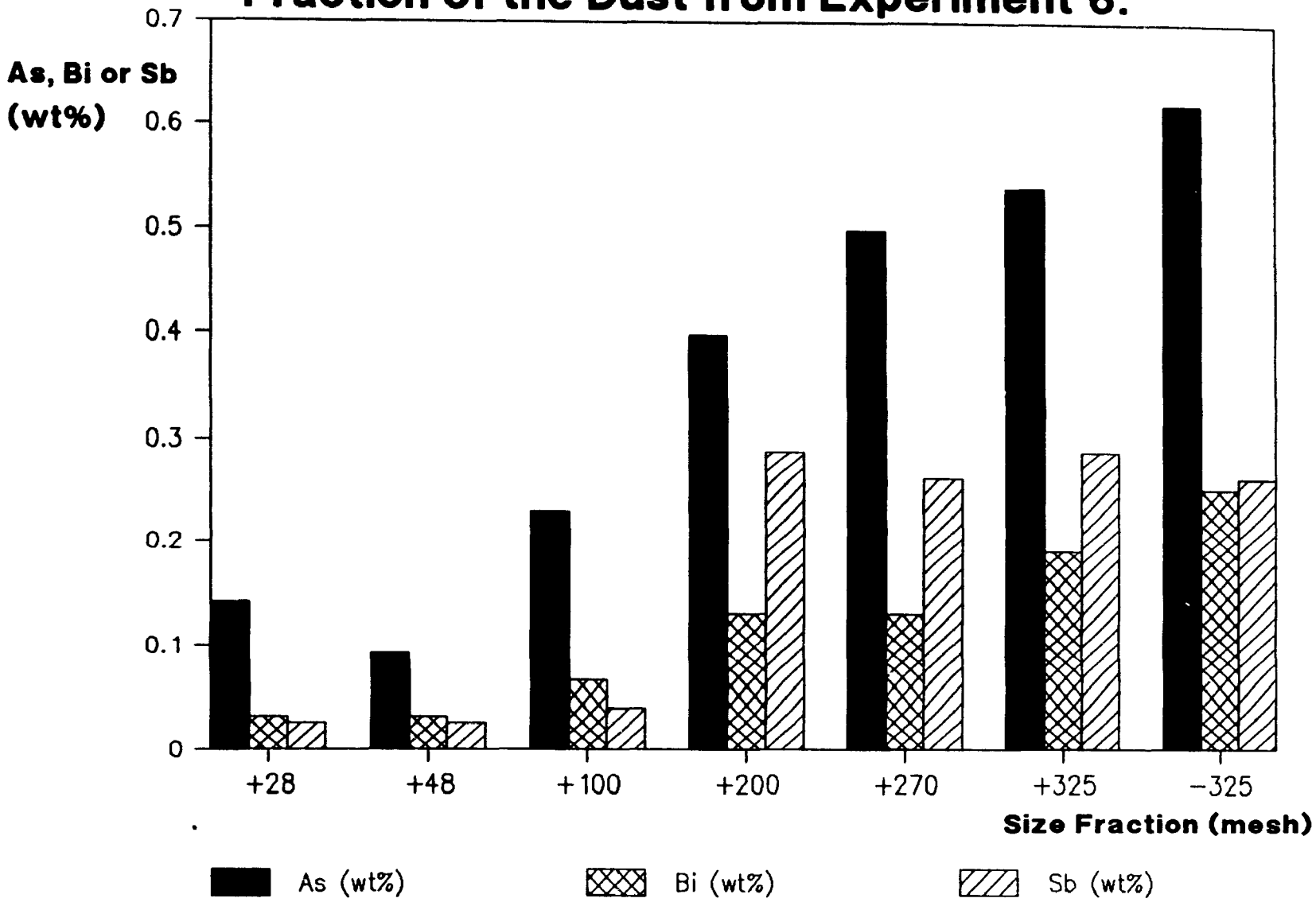

4- Optical Microscopy :

No observations were possible using the optical microscope because the dust particles were too small to be properly evaluated for their size and shape.

5- X-Ray Diffraction Analysis :

Using the computer data bank and the search program, three phases were positively identified, namely PbS, ZnS and Pb. The mineralogical form of Bi, As and Sb could not be identified due to an insufficient concentration level in the dust. Figure 6.4 shows the diffraction pattern of the dust as well as those of PbS, ZnS and Pb.

Figure 6.4: X-Ray Diffraction Pattern of the Vacuum Refining Dust as well as those of Synthetic Galena (PbS), Wurtzite (ZnS) and Metallic Lead (Pb).

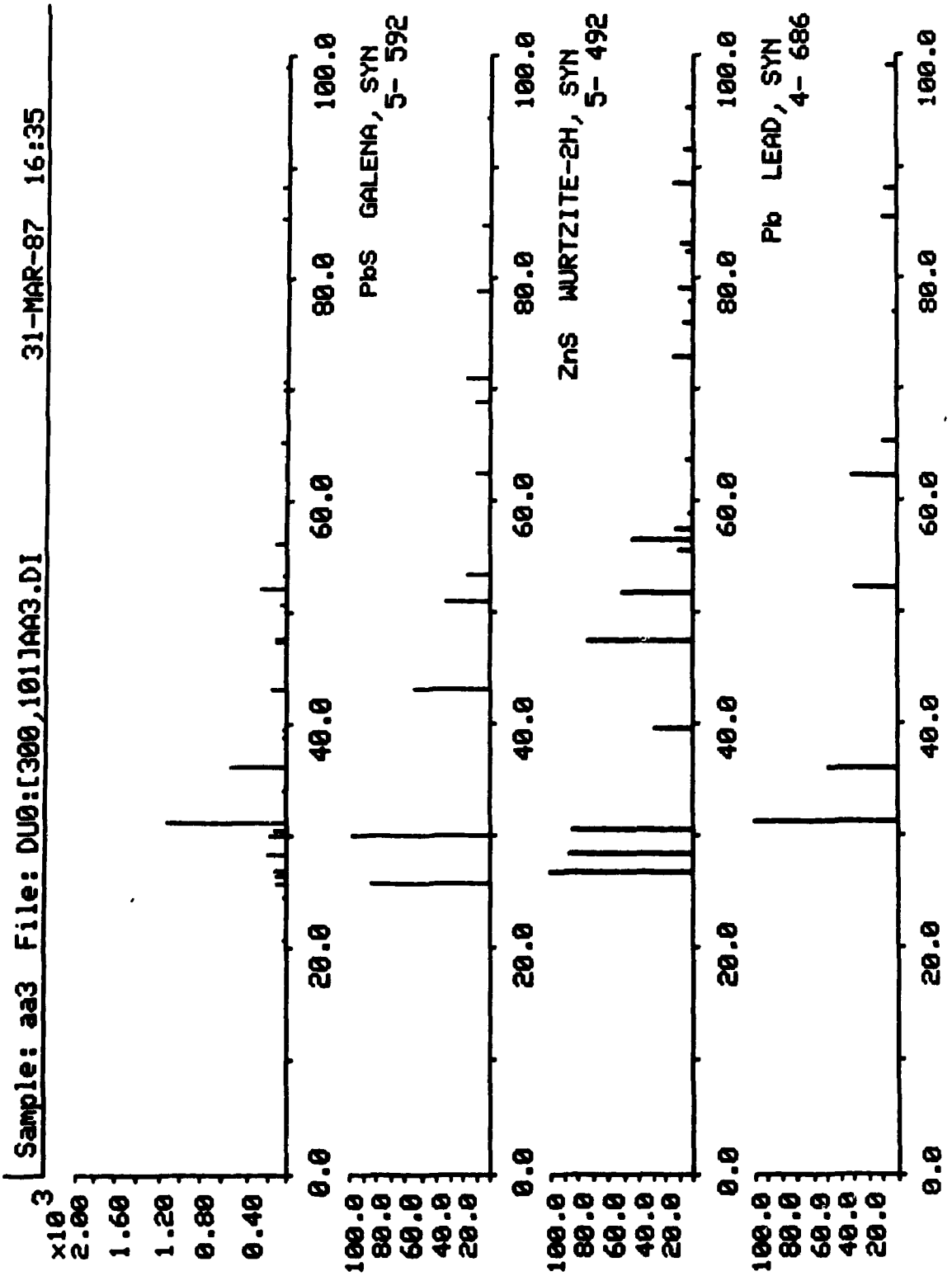

6- Scanning Electron Microscopy :

The scanning electron microscope enabled one to observe that the dust particles were grouped in clusters ranging from a few to several hundred particles. The particle size ranged from 0.1 to 10 microns. The shape of the small particles were very irregular. The larger particles were spherical in shape as seen by Figure 6.5 A and B.

Figure 6.5: Photographs of Vacuum Refining Dust Using a Scanning Electron Microscope (SEM).

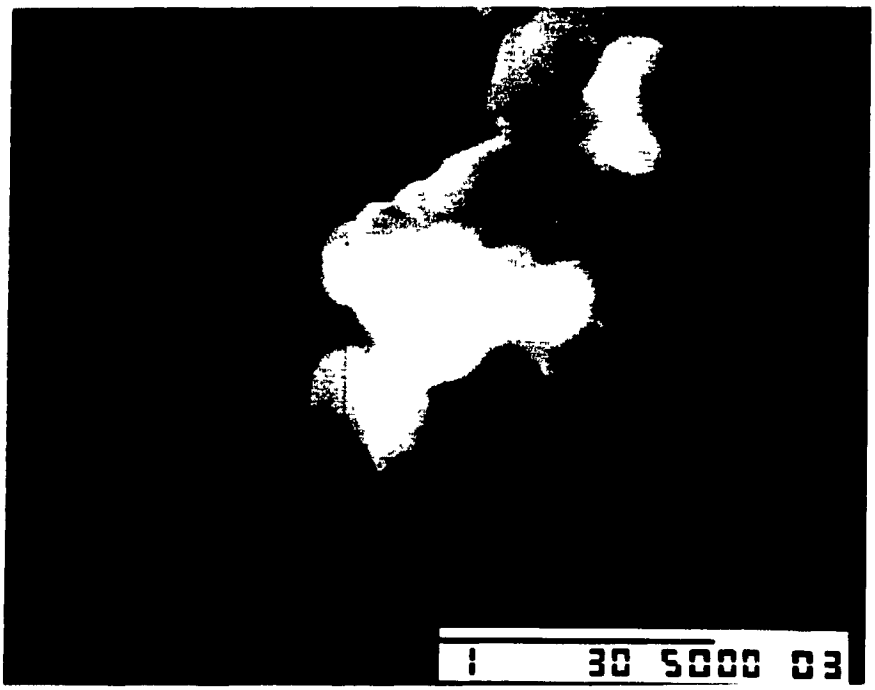

Photo A: Submicron Particles of Irregular Shape.

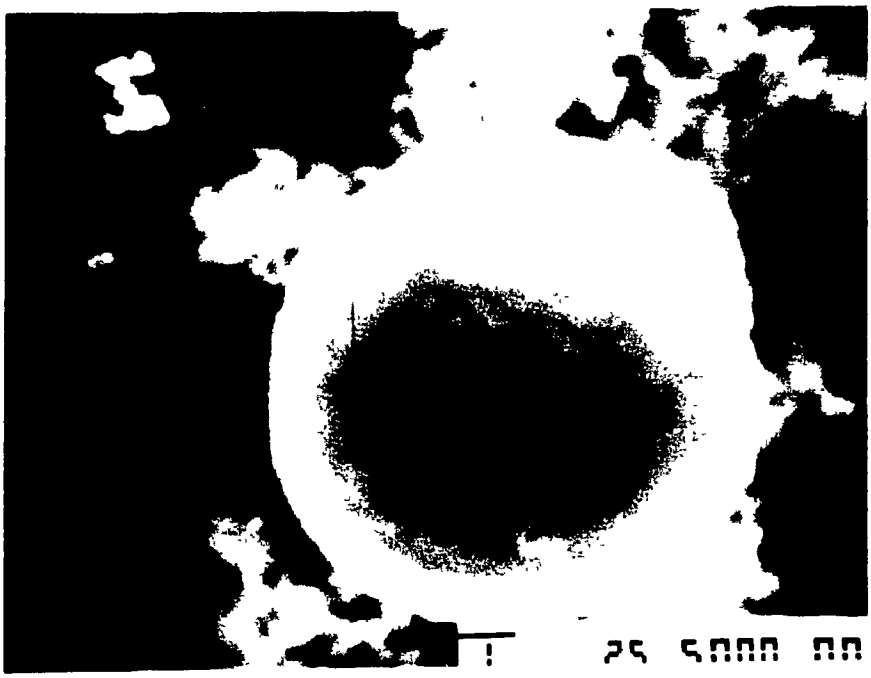

Photo B: Large (≅ 10 μm) Particle Almost Perfectly Spherical.

7- X-Ray E.D.S. Analysis :

Figures 6.6 A and B show an X-Ray E.D.S. taken at two different sites of a cluster of particles. At location A, the X-Ray beam was focused to an area of irregular small particles. At that location large Pb and Zn peaks were recorded on the spectra. The Al peak can be accredited to the aluminum composition of the sample holder. At location B, the beam was focused toward the center of a large spherical particle. At that location only one large peak of lead was detected.

Figure 6.6: X-Ray Emission Spectra of Vacuum Refining Dust.

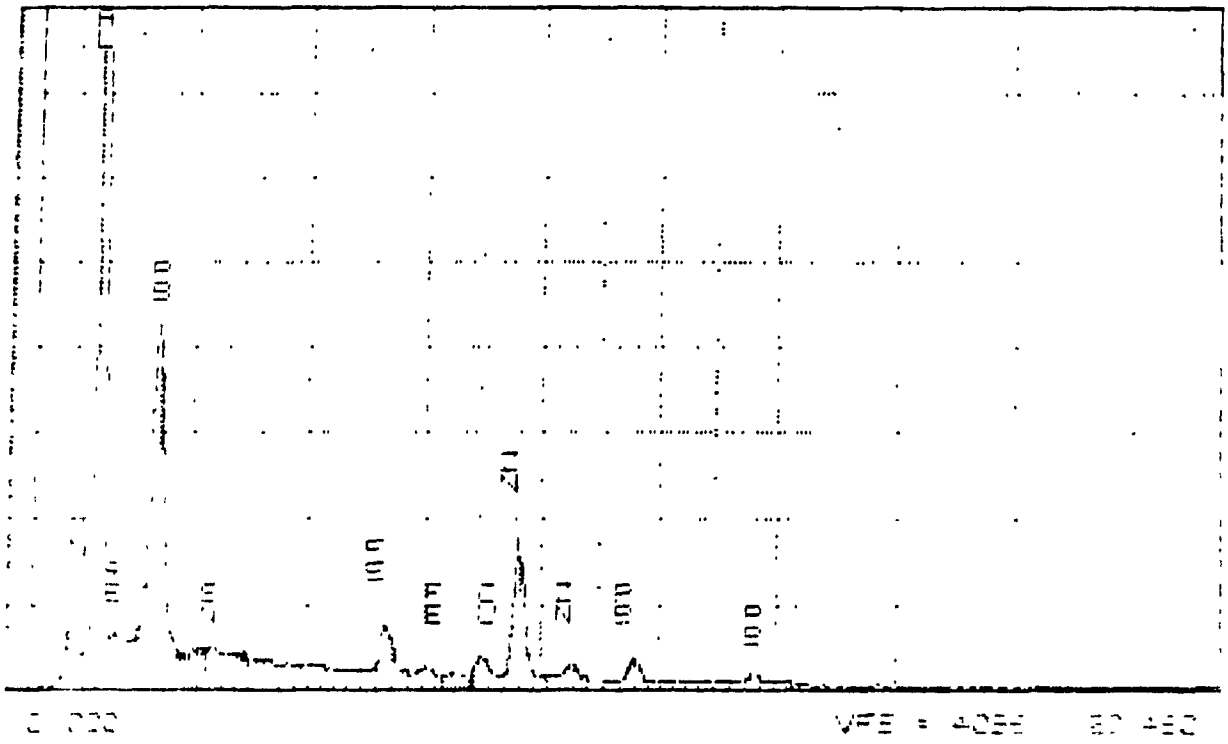

Spectra A: Scanning Electron Beam Focused on an Area of Small Irregular Shaped Particles.

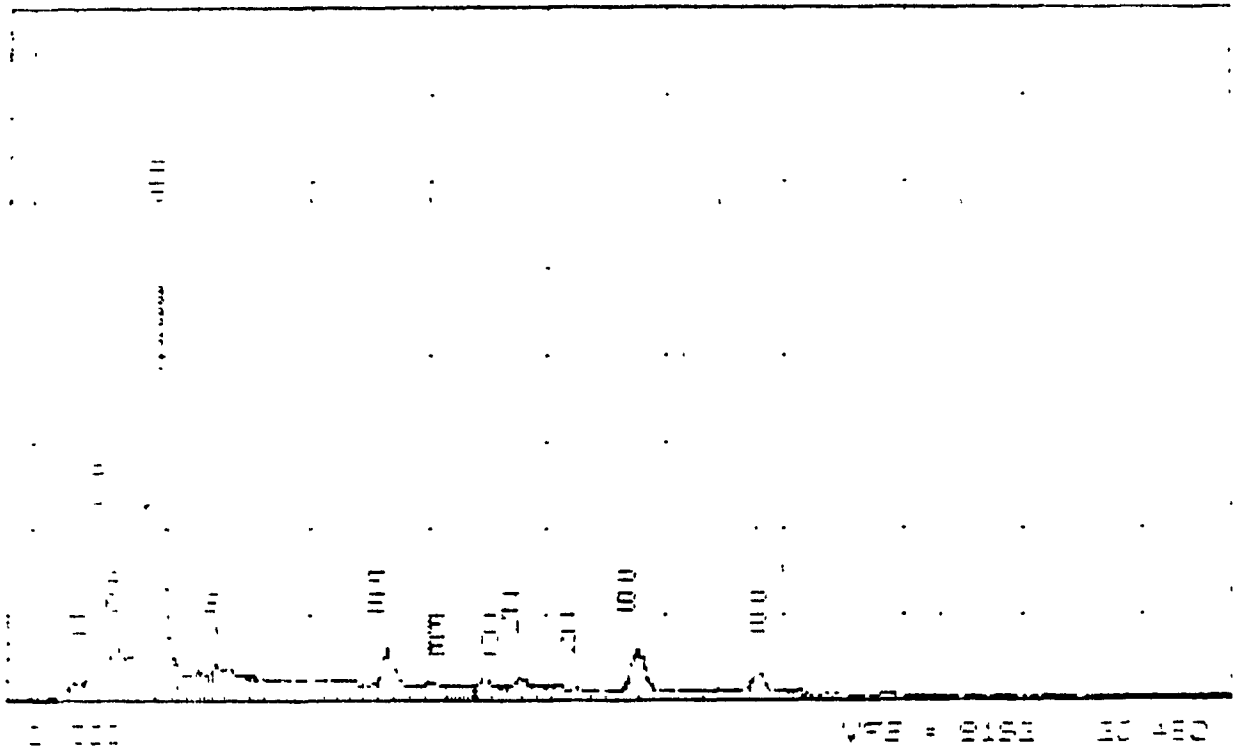

Spectra B: Scanning Electron Beam Focused at the Center of a Large Spherical Particle.

6.3 Selective Condensation of the Vapours Produced during LSV Refining of Copper Matte

6.3.1 Objective

The objective of these experiments was to demonstrate that a mixture of vapours produced during vacuum refining of copper matte can be condensed selectively into separate metal fractions. The idea originated from a Russian thesis abstract (Chem. Abst. 90:125066r) which stated that pure ZnS condensed separately from a mixture of PbS and ZnS vapours onto condensers at temperatures varying between 800 and 1050 degrees Celsius. At temperatures below 800 degrees, it was stated that PbS containing one percent ZnS condensed. The pressure range during those experiments varied from 500 to 10,000 pascal. The vapour source was copper matte vacuum refining dust heated to 1150 degrees Celsius.

6.3.2 Experimental Procedure

The experimental variables under study were as follows. The pressure ranged between 30 to 1000 pascal. The temperature of the condenser ranged from 700 to 925 degrees Celsius. The source of vapour was a mixture of vacuum refining dust collected from several copper matte vacuum refining experiments. The dust was heated to 1200 degrees Celsius. Five experiments were carried out. Experiments 1, 2, 3, 4 and 5 represents points A, B, C, D and E on Figure 6.7.

The schematic diagram of the apparatus used for these experiments can be seen in Figure 6.8. The apparatus was machined from solid pieces of graphite electrode. The apparatus consisted of a 0.90 m high graphite tube with an internal diameter of 0.23 m. The lower section of the apparatus was heated by an induction furnace. A type K thermocouple was placed inside the source of vapours, from the bottom of the graphite crucible. The upper section of the apparatus (the Condenser) was kept at the desired temperature using a 8 kW resistance heater connected to a variable voltage power source.

Figure 6.9 shows an enlargement of the condenser section of the apparatus. Three type K thermocouples were placed at different locations in the upper section of graphite. The temperature of the condenser was monitored precisely

throughout the experiment.

Fig. 6.7 : Equilibrium Vapour Pressure of Lead, Lead Sulphide and Zinc Sulphide versus the Temperature (K).

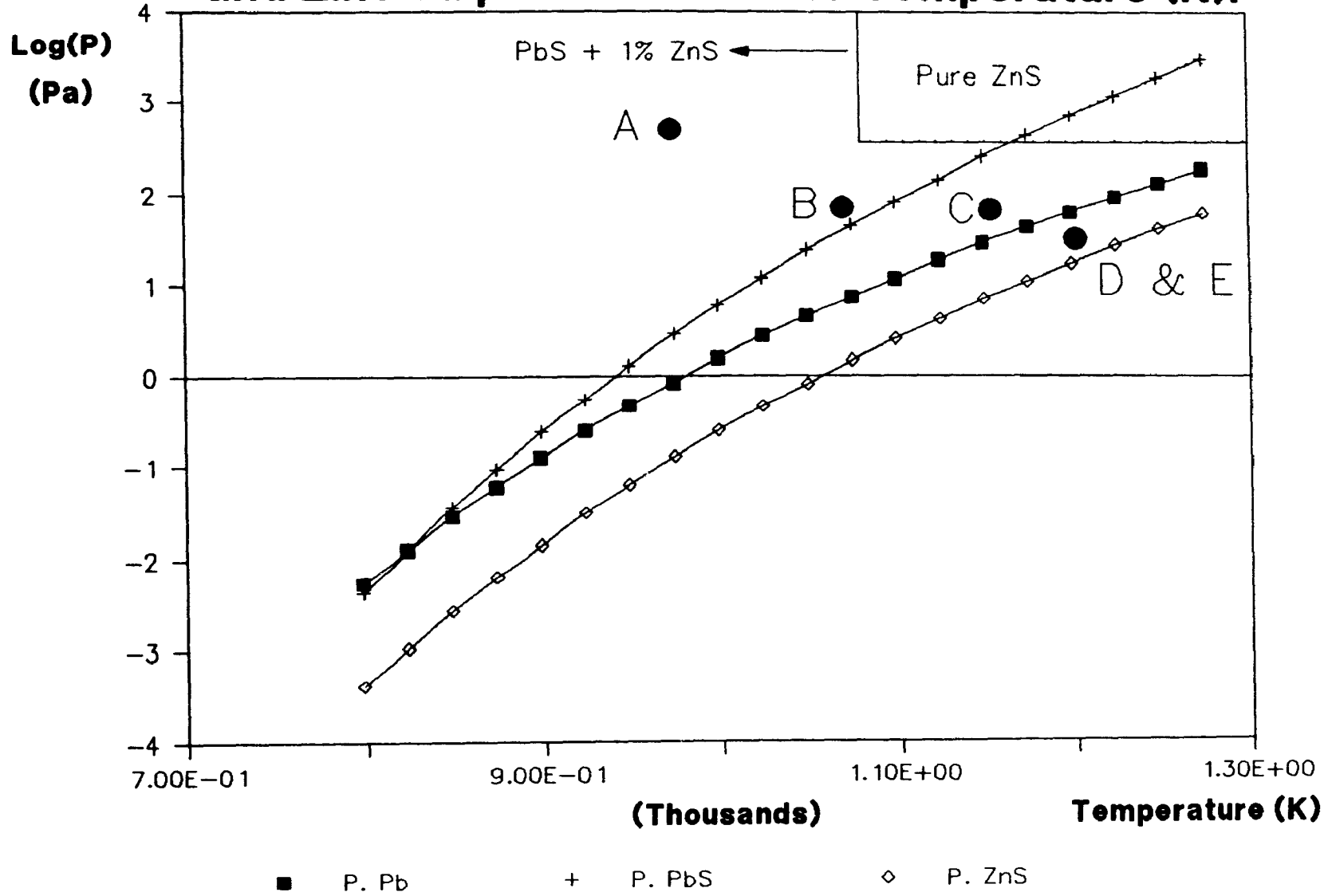

Fig. 6.8: Schematic Diagram of Selective Condensation Apparatus.

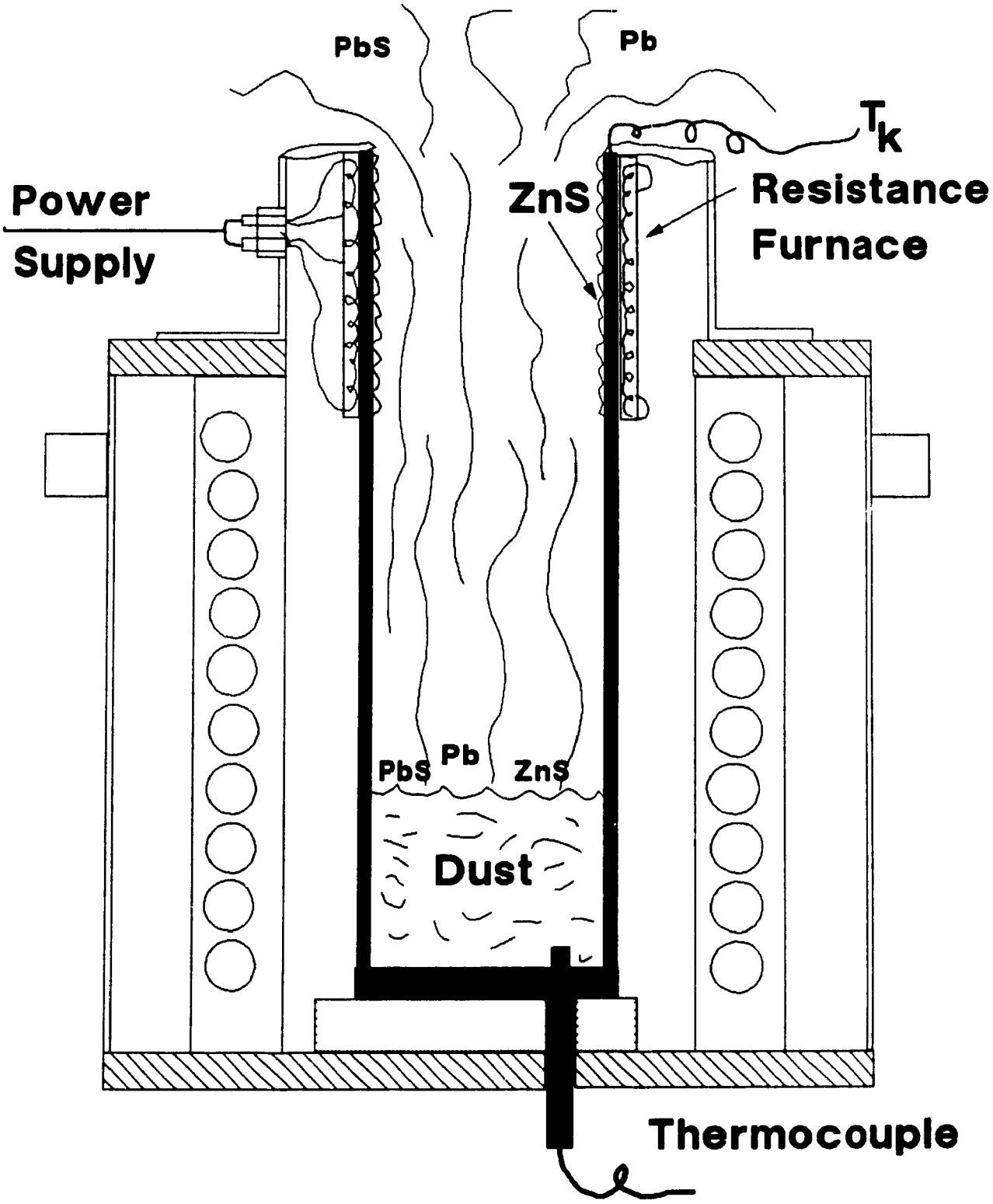

Fig. 6.9 : Schematic Diagram of the Upper Section of the Selective Condensation Apparatus.

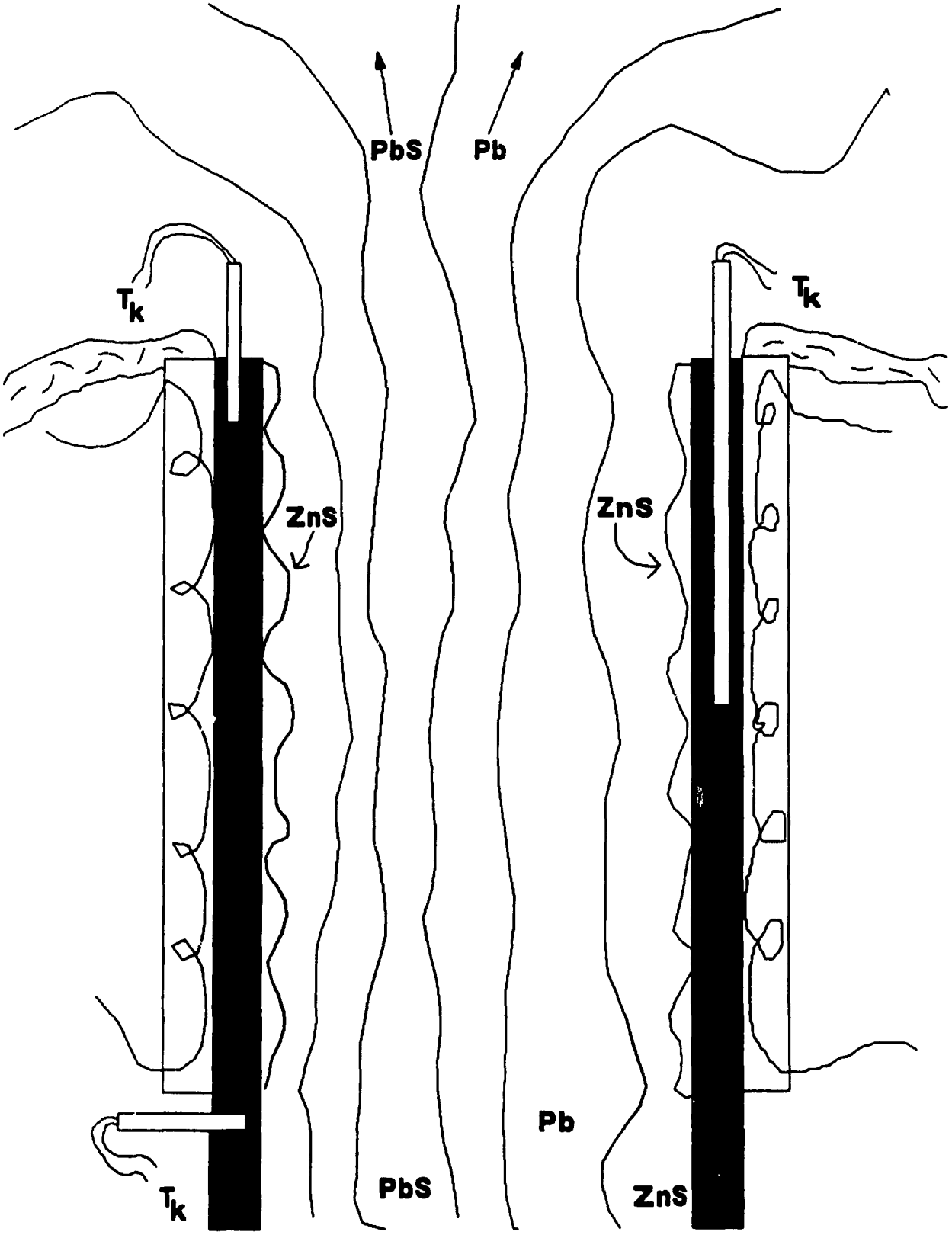

The experimental procedure was as follows:

1- An 8 kg mixture of vacuum refining dust was placed in the apparatus.

2- The vacuum chamber was evacuated and then filled with nitrogen gas.

3- The condenser section and the vapour source were heated to the desired experimental temperatures.

4- The vacuum chamber pressure was lowered to the preselected value.

5- The temperature was monitored for the next 20 minutes. The power input to the induction furnace and condenser were controlled to keep the temperatures constant.

6- After 20 minutes, all power was shut off and the vacuum chamber was flooded with nitrogen gas. The apparatus was cooled under inert atmosphere to prevent oxidation of the dust.

7- After cooling, dust samples were collected from the condenser and the vacuum chamber.

8- The dust collected from the condenser and the walls of the vacuum chamber was mixed together and put back into the apparatus for the next experiment (Note : 0.5 kg of sulphur was added while mixing the dust for Experiments B and C).

9- The dust samples were sent to the Noranda Technology Center to be analyzed for Pb, Zn, Bi, As, Sb and S.

6.3.3 Results

The results of the Selective Condensation Experiments are presented in Table 6.4. This table gives the location at which the sample was taken, the temperature of the condenser and the chemical assays of the sample.

Table 6.4 : Results of Selective Condensation Experiments: Chemical Analysis.

Exp. #	Location	T (K)	P (Pa)	Pb (%)	Zn (%)	Bi (%)	As (%)	Sb (%)	S (%)
A	Condenser	973	1000	52.7	19.0	0.55	0.42	0.31	7.58
A	Chamber	---	1000	42.4	17.0	0.50	0.31	0.26	8.77
B	Condenser	1073	100	53.8	20.5	0.43	0.12	0.35	13.6
B	Chamber	---	100	50.0	13.0	0.39	0.48	0.34	17.3
C	Condenser	1143	100	11.6	39.4	.082	<	0.12	23.7
C	Cond. Cr.	1300	100	0.49	53.6	<	<	<	29.9
C	Chamber	---	100	45.2	12.9	0.34	0.19	0.31	19.7
D	Condenser	1173	40	10.8	27.7	0.13	<	0.10	21.6
D	Chamber	---	40	32.7	14.8	0.23	.097	0.21	12.0
E	Condenser	1203	40	1.01	49.1	.022	<	<	26.2
E	Chamber	---	40	32.0	15.1	0.22	.081	0.19	15.9

Lower detection limit : Bi = 0.018
As = 0.064
Sb = 0.021

Bi, As or Sb = < = Not detected by assaying method

Cond. Cr. = Condenser Crusty Material

CHAPTER 7

LSV Refining; Experimental and Results

7.1 Objective of the LSV Refining Experimental Program

The objective of the experimental program was to explore the feasibility of Lift-Spray vacuum refining copper matte. The removal rates of several impurities, namely lead, bismuth, arsenic, antimony, selenium and nickel, were measured during the experiments.

The experimental program was divided into two parts. In the first part, a graphite apparatus was used to keep the oxygen level dissolved in the melt at a minimum. In the second part, an alumina lined apparatus was used for the experiments to keep the oxygen activity in the melt at a maximum.

7.2 Variables Influencing the Rate of Evaporation

Several variables affected the rate of evaporation of the impurities from copper matte in the LSV process. The following is a list of the most important ones:

1) The Temperature of the Melt
2) The Chamber Pressure
3) The Concentration of Copper in the Melt
4) The Oxygen Activity in the Melt
5) The Area to Volume Ratio of the Melt
6) The Scavenging Gas Flow Rate
7) The Initial Concentration of the Impurities
8) The Presence of Slag on the Surface of the Melt
9) The Stirring Condition in the Liquid

Of the above variables, 1) to 6) were controlled during the experiments, while 7), 8) and 9) were not. However, the levels or conditions of variables 7), 8) and 9) were noted and taken into consideration when calculating the overall refining rates or during the interpretation of the results.

7.2.1 Temperature of the Melt

The temperature range of the experiments went from 1473 to 1573 K. These represent typical limits for industrial liquid copper matte temperatures. Ideally the temperature was set at 1523 K and was held constant throughout the experiment by manually adjusting the power input to the induction furnace. The temperature readings employed a platinum-rhodium thermocouple (Type R) in a graphite probe inserted in the melt. When a thermocouple failed, an optical pyrometer was used to monitor the melt temperature and hold it constant. The optical pyrometer was calibrated at the beginning of each experiment against the thermocouple readings and was used as a backup in case of thermocouple failure.

7.2.2 Chamber Pressure

The chamber pressure range investigated was from 10 to 600 pascal. The chamber pressure was measured using a tilting type McCloud gauge. Typically, the chamber pressure was set at 10, 100 or 600 pascal by partially opening the vacuum valves to the pumps. Once the desired pressure was obtained, the pressure was held constant throughout the experiment.

7.2.3 Copper Content of the Melt

Changes in the composition of the melt affect the rate of evaporation of the impurities via the changes in activity coefficients of the impurities, and the changes in the sulphur and oxygen activities.

Copper matte can be thought of as a mixture of Cu_2S and FeS molecules. Thus, the chemical composition of the melt can be described by the percent copper in the matte (matte grade) since it is directly related to the relative proportions of Cu_2S and FeS present in the liquid. The matte grade range under study was between 30% to 80% copper.

The matte grade was varied by using three different charge materials; they were: reverberatory furnace matte (35% Cu), Noranda reactor matte (65% Cu) and copper converting matte (80% Cu). All the copper matte was provided by the Noranda Horne Smelter.

7.2.4 Oxygen Activity in the Melt

In copper matte, the sulphur activity is directly related to the amount of FeS present in the solution and thus the matte grade. The oxygen activity however, is determined by the equilibrium: $0.5\ S_2 + O_2 = SO_2$, and thus is a function of the SO_2 pressure in the system. In industrial practice the SO_2 pressure is typically 20,000 pascal (i.e., 1/5 atm). Under vacuum, the total pressure of the system is reduced to approximately 10 to 600 pascal. It was observed that as the pressure was lowered, the melt boiled due to the evolution of sulphur dioxide gas. Assuming that the sulphur and oxygen were at equilibrium with the pressure in the vacuum chamber (SO_2 pressure), the dissolved oxygen levels and oxygen activities were calculated to be 10 to 1000 times lower as compared to industrial smelting practices.

The oxygen content was further reduced by the use of a graphite crucible. In a graphite crucible, the dissolved oxygen reacted with the crucible to form carbon dioxide. The net result was that the oxygen activities were approximately six orders of magnitude lower than they would have been in alumina-silica crucibles. In this study, both types of crucibles were used such that a comparison could be made on the effect of the dissolved oxygen content on the rate of evaporation of the impurities.

7.2.5 Area to Volume Ratio of the Melt

The aim of the LSV process is to create a large surface area to volume ratio for the melt during vacuum treatment. The surface area available for evaporation is composed of two components, namely, the area of the bath and the area of the suspended droplets in the spray. The bath surface area is fixed by the size and geometry of the system. However, the spray surface area can be adjusted by altering the amount of lifting gas injected at the bottom of the riser leg. Both the diameter and total length of the leg were kept constant in the present study to facilitate the analysis of the results. Other factors such as the lift ratio and the nozzle submergence affected the surface area produced in the spray. These were not controlled and resulted in the scattering of the data.

7.2.6 Scavenging Gas Flow Rate

An inert gas introduced in a vacuum system can increase evaporation rates by diluting the vapours of the impurities in the gas phase, see Reference 49. However, this was not attempted in the present experiment. Furthermore, it is believed that the small amount of lifting gas that was introduced did not have an impact on the results.

7.2.7 Impurity Concentration

The impurity levels found in the copper matte received from the smelter were unadulterated for most of the experiments. Only small amounts of As, Bi and Sb were added in Experiment 10, 11, 12 and 13 to improve Bi, As and Sb determination by using higher concentrations.

7.2.8 Slag on the Surface of the Melt

The maximum rates of refining were attained when the surface of the melt was free of slag. During matte melt down, some entrained slag surfaced to form a layer covering the surface. However, in the LSV process, fresh matte is pumped from the bottom of the crucible and ejected to the spray. This provided a clean surface for evaporation, stirred the bath surface thus, preventing the formation of a coherent slag layer at the surface.

7.2.9 Stirring Conditions in the Liquid

The LSV process provides good stirring of the liquid bath. However, it was not possible to quantify that variable. The stirring or melt recirculation rate was determined by the experimental operating conditions such as the pumping rate in the riser leg and natural convection.

7.3 Experimental Set-Up

7.3.1 Apparatus Construction

The LSV process is undergoing development. Thus, the apparatus was designed and built from scratch in the laboratory. A total of five vacuum apparatus were machined from solid graphite electrodes. Two were made entirely from graphite electrodes and three had an alumina castable cement or ramming mix lining and internals mounted inside a graphite suceptor. The schematic drawings of the two most advanced prototypes built can be found in Figures 7.1 and 7.2.

The apparatus in Figure 7.1 measures 0.90 meters in height and 0.21 meters in diameter. It was machined using three sections of graphite electrodes bonded together with ceramic cement. The bottom two sections were heated in the induction furnace and the top section was heated by an eight kW resistance furnace connected to a variable voltage power supply. The liquid matte and spray occupied the bottom two sections. Gas was introduced into the lifting leg through a graphite injector. Scavenging gas could have been added into the top two sections through a lance. The capacity of the apparatus was approximately 35 to 40 kg of liquid matte. A second prototype was also built with a smaller capacity of approximately 20 to 22 kg.

Figure 7.2 shows the LSV prototype with an alumina interior.

Fig 7.1 : Schematic Diagram of Laboratory Graphite LSV Apparatus Set-Up in an Induction Furnace. Top Section Heated by Resistance Heater.

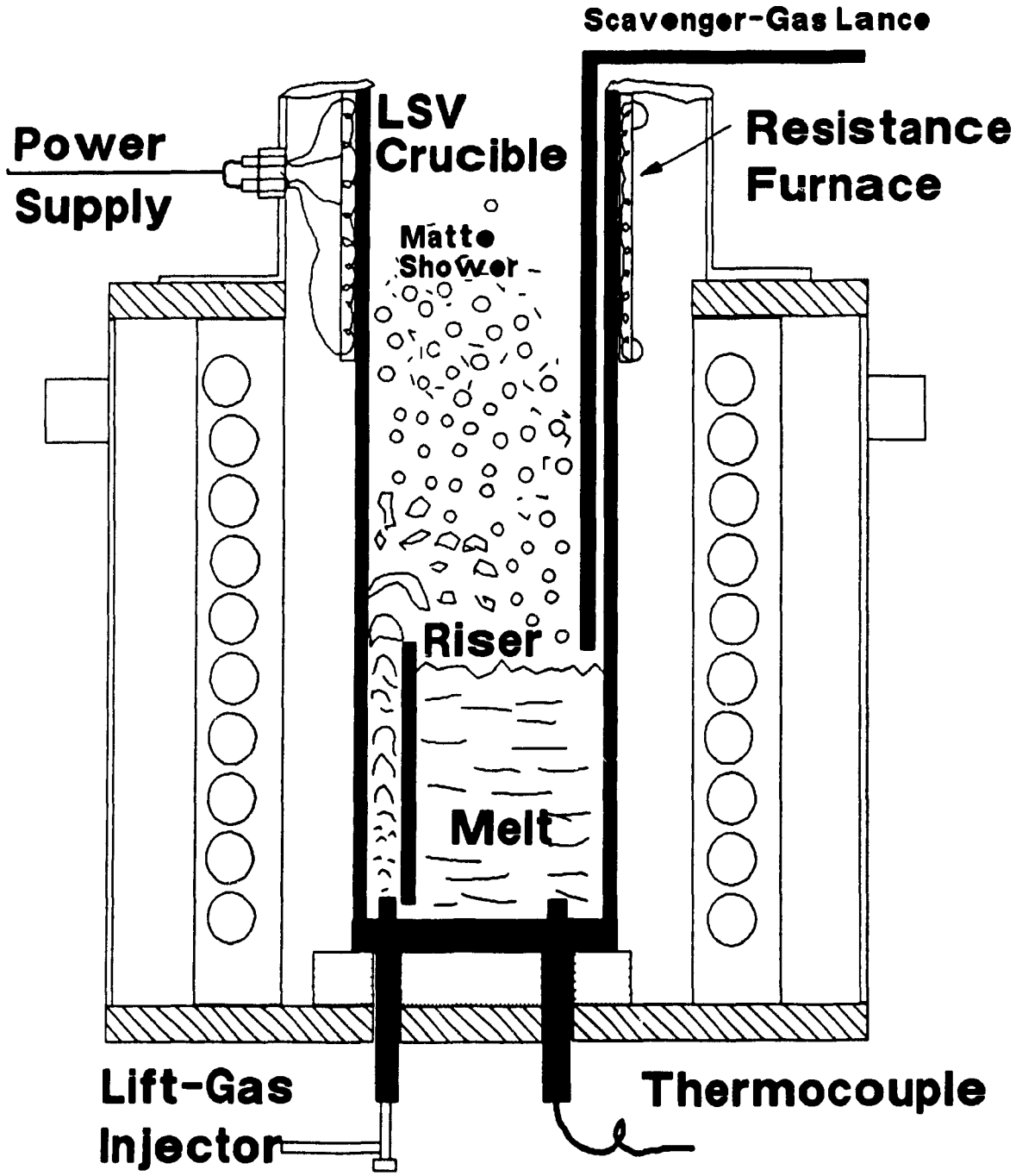

Fig 7.2 : Schematic Diagram of Laboratory Alumina LSV Apparatus Set-Up in an Induction Furnace. Top Section Heated by Resistance Heater.

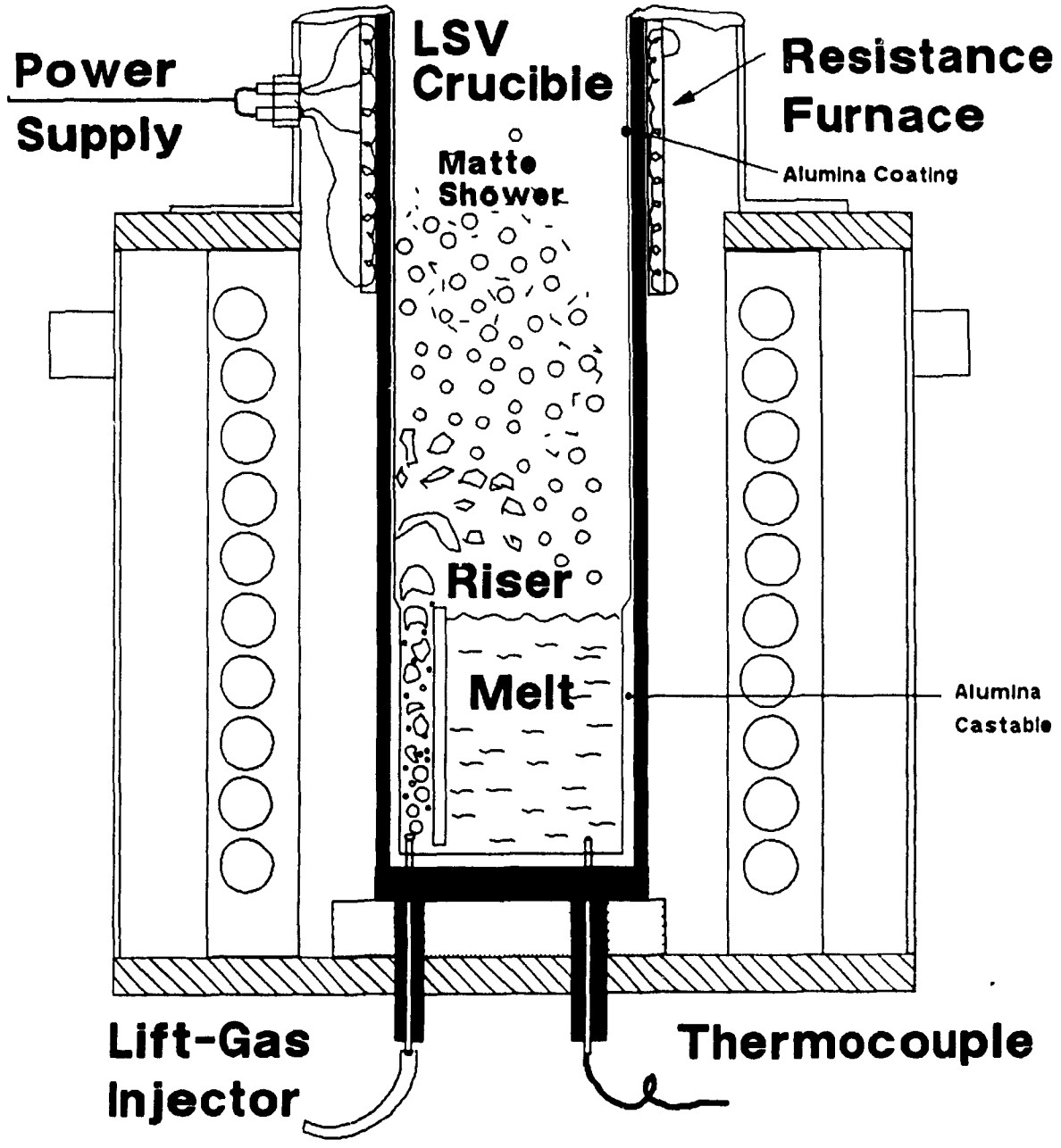

The apparatus consisted of a graphite suceptor 0.9 meters in height and 0.21 meters in internal diameter. The alumina riser leg and melt holding crucible of approximately 1.5 cm thick walls was cast inside this suceptor. This resulted in a melt capacity of approximately 25 kg of matte in the bottom section. Tungsten wires were imbedded in the alumina cement to prevent breaking of the riser leg due to thermal shock. The temperature probe was built from a graphite holder and a mulite tube running through the graphite, see Figure 7.3. The mulite tube was held in place with ceramic cement to prevent matte leaks. The injector was built from a graphite holder and an alumina tube, see Figure 7.4.

Table 7.1 gives the capacity and the dimensions of the LSV apparatus used for these experiments. Table 7.2 shows the steps to be followed and the time requirements to build an LSV apparatus, prepare the furnace and run one experiment. Due to the complexity of the experimental set up, it took a minimum of 2.5 weeks to complete the experiment, from the beginning of the fabrication to the actual run. If no break downs or leaks occurred, only phase III had to be repeated over for each experiment. Thus, a minimum of three days per experiment was required once the initial fabrication and set up was performed.

Fig. 7.3 : Schematic Diagram of Thermocouple Probe.

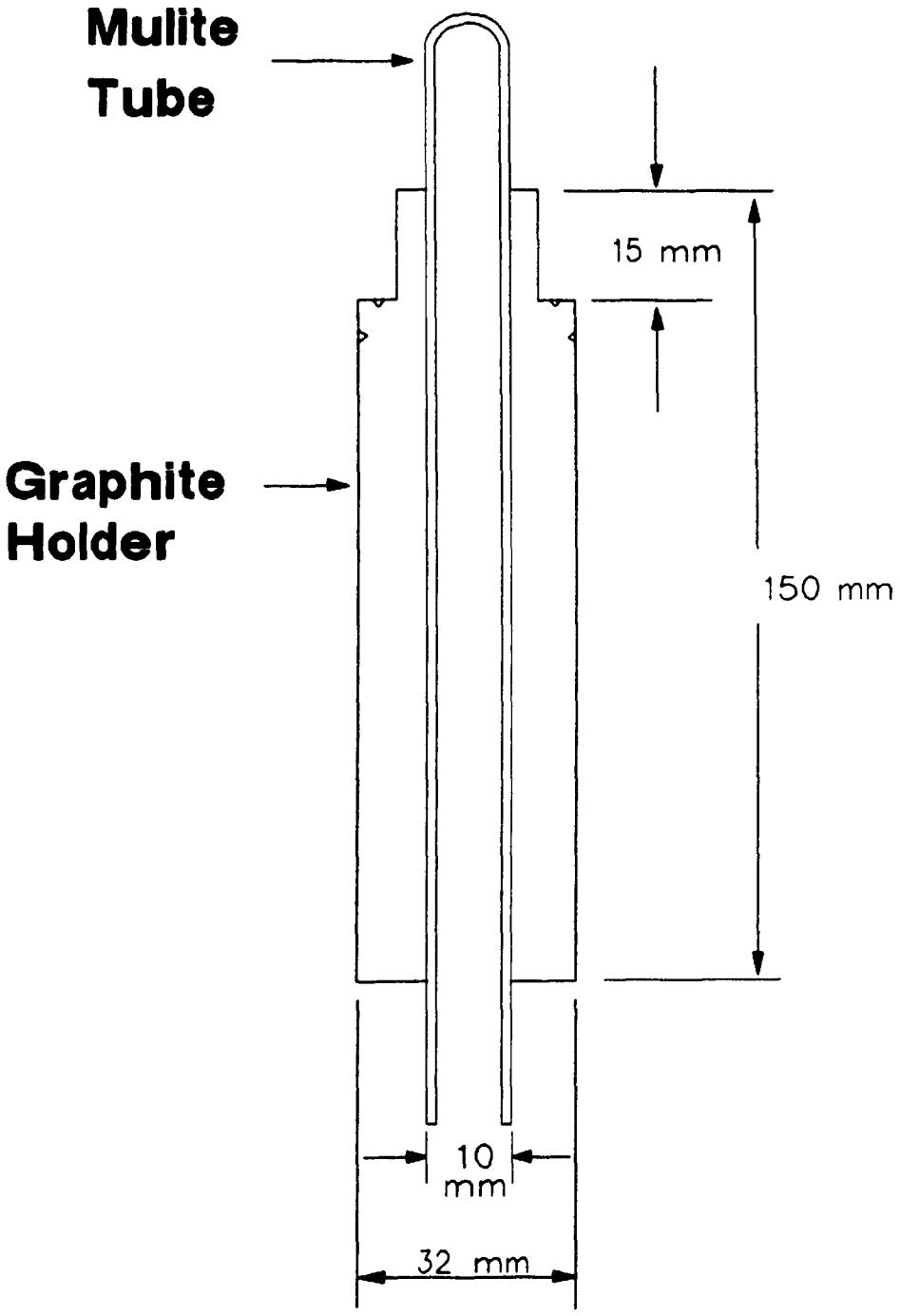

Fig. 7.4 : Schematic Diagram of Alumina Injector.

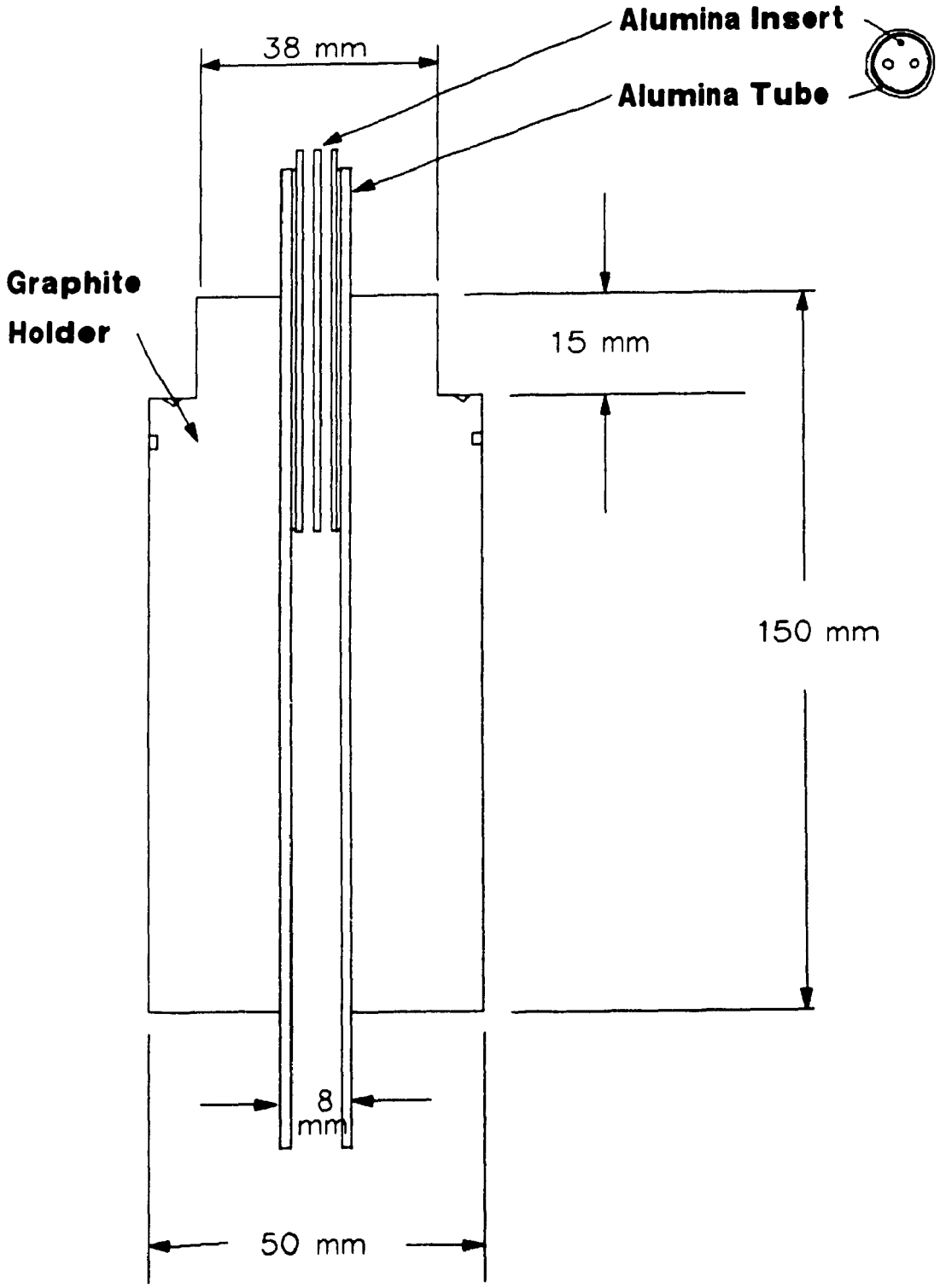

During the course of this study, many problems were encountered. Phase II and repairs were repeated five times. In addition, five separate apparatus were built requiring the repetition of all three phases of construction.

Table 7.1 : Dimensions and Capacities of Graphite and Alumina LSV Refining Apparatus.

type	Melt Section		Spray Section		Total Height (m)	Melt Capacity (kg)
	Height (m)	Dia. (m)	Height (m)	Dia. (m)		
Gr.A. A	0.28	0.21	0.56	0.21	0.90	35 to 40
Gr.A. B	0.28	0.15	0.56	0.21	0.90	20 to 22
Al.A.	0.28	0.17	0.56	0.21	0.90	25 to 27

For all three apparatu Riser Internal Diameter = 0.05m

Riser Height = 0.26m

Gr.A. A : Graphite Apparatus, Prototype # A

Gr.A. B : Graphite Apparatus, Prototype # B

Al.A : Alumina Apparatus

Table 7.2: Time Scale for Apparatus Construction, Preparation and Experiment Run.

Phase I : Apparatus Construction		
a)	Machining of Graphite LSV Apparatus and Base (Cut, Machine, Face and Drill Electrodes)	2 Days
b)	Machining of Temperature Probe and Gas Injector	1 Day
c)	Gluing of Apparatus Sections, Temperature Probe and Gas Injector	1 Day
For alumina interior apparatus only:		
d)	Construction of Aluminum Molds to Cast the Alumina Interior	1 Day
e)	Casting of the Alumina interior and Leave to Dry	1 Day
	Total :	6 Days
Phase II : Assembly of Apparatus in the Vacuum Chamber		
a)	Removal of the Induction Furnace from the Chamber, Clean, Empty and Prepare Base	1 Day
b)	Mounting of the Apparatus Inside the Vacuum Furnace, Cementing and Packing Sand	1 Day
c)	Reassembling the Induction Furnace Inside the Chamber, Connecting and Checking all Hoses	1 Day
	Total :	3 Days

Phase III : Preparation and Experimental Run

a)	Cleaning of all Vacuum Seals, Preparation of Thermocouples, Connections, Preparation of Sample Cups and Bags, Test of Vacuum, Etc.,	1 Day
b)	Run Experiment, Let Apparatus Cool Down	1 Day
c)	Open Furnace, Collect Dust, Clean Chamber, etc.,	1 Day
	Total :	3 Days
	Grand Total :	12 Days

7.3.2 Equipment Used and Accuracy

Vacuum Chamber and Induction Furnace

The experiments were conducted in a Deltec cylindrical vacuum chamber of 1.5 m in diameter and 1.8 m in length. The pumping outlet was located in the rear wall of the furnace. The location of the outlet was of no importance to the impurity removal since the chamber was water cooled and the impurity vapours condensed on the walls. The chamber had several vacuum tight windows which allowed for observations and the taking of photographs during the experiments. A vacuum lock on top of the chamber enabled sample taking without disruption of the vacuum. Connections were also provided for thermocouples and pressure gauges attachments.

A Tocco 3000 Hertz, 100 kW furnace was mounted inside the chamber. The furnace could be tilted, via a hydraulic system, to pour the matte at the end of each experiment. The induction furnace power supply was assembled by Bradley Controls Limited.

The pumping was done via a two stage system consisting of a "Stokes" mechanical pump (0.142 m^3s^{-1} nominal capacity) connected in series to a "Roots" blower (0.614 m^3s^{-1} nominal capacity) to obtain lower pressure levels.

Fig. 7.5 : Schematic Diagram of Upper Section of LSV Alumina Apparatus.

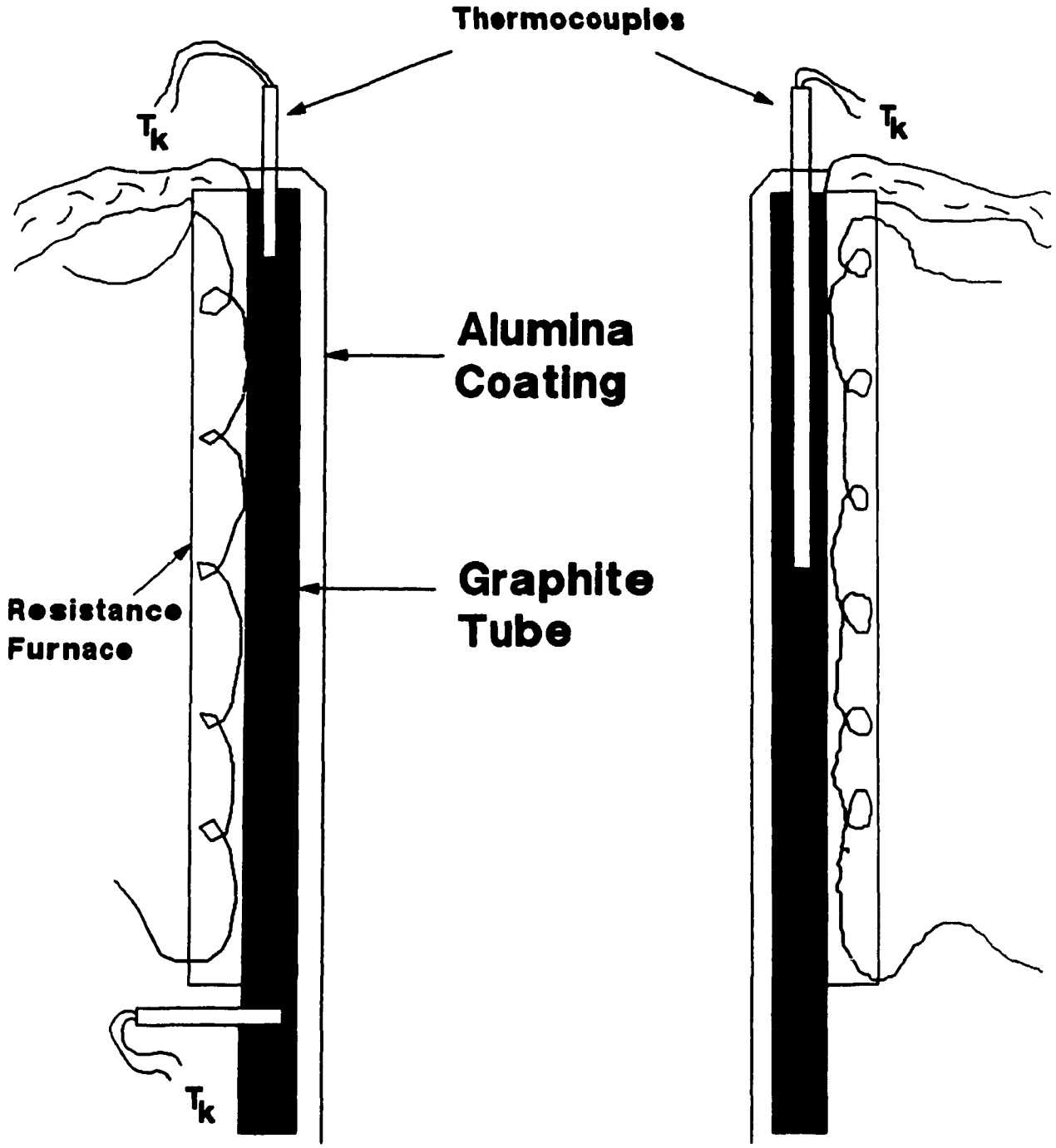

Apparatus Set-Up

The apparatus was mounted according to Figure 7.1 and 7.2 . The apparatus was supported on two refractory bricks placed at the bottom of the furnace. Care was taken not to hit and break the injector and thermocouple probe. Quartz sand was used as packing material to hold the apparatus in place. The resistance heater was placed around the upper section of the apparatus and secured using three large stainless steel hose clamps. The electric connections were made and more packing sand was placed. High temperature cement was used to cover the sand and build a pouring spout.

Temperature Measurement

The melt temperature was measured using a type R platinum-rhodium thermocouple protected by a graphite probe or by a mulite sheath, Figure 7.3 . The thermocouple probe penetrated 0.025 m into the melt and was located at the bottom of the crucible. The probe was held in place by "Aremco 503" ceramic cement. The seal was excellent and no leaks occurred due to cement failure.

The temperature was read directly in degrees celsius on an Omega or Analogic type R digital thermometer. The accuracy of the temperature readings (claimed by the manufacturer) varied plus or minus 1 degree celsius.

An optical pyrometer was used as a back up to measure the temperature of the melt in case the thermocoupl failed. The pyrometer was calibrated against the thermocouple at the beginning of the experiment. The pyrometer was a disappearing hot filament type with an accuracy of plus or minus 25 K at best. Once the filament temperature was adjusted at the beginning of the experiment, it was not changed so as to keep the melt temperature constant. If the thermocouple failed, the pyrometer was used as a reference to keep the melt temperature constant by adjusting the power to the induction furnace.

The temperature of the upper section of the apparatus was measured using three type K Chromel-Alumel thermocouples. The location of the thermocouples is seen on Figure 7.5 . The objective of all fifteen experiments was to keep the temperature of thermocouple 1 and 2 around 1273 K so as to prevent the condensation of the volatilized impurities on the walls and the freezing of copper matte droplets from the spray.

Pressure Measurements

Three instruments were available to read the pressure. One was a mercury manometer which gave an approximate reading of the pressure inside the chamber (range, 0 to 101,000 pascal). The other was a capsule dial gauge which had a range of 0 to 2500 pascals with an accuracy of plus or minus 100 pascal.

The other was a tilting type Mccloud gauge which had a range of 0 to 665 pascal (0 to 5 mm Hg) with the smallest measurable pressure of 0.5 pascal. The accuracy of the Mccloud gauge was plus or minus 3 % of the scale reading, as quoted by the distributor.

Sampling of the Melt

Mild steel sample cups were machined to obtain 10 gram minimum samples, Figure 7.6 . The sample cups had interior dimensions of 2.5 cm diameter and 1.0 cm depth. Six cups were machined and engraved # 1 to #6. The cups were reused for many experiments since solidified copper matte did not adhere to the steel.

Oxygen Activity Measurements

The oxygen activity of the liquid matte was measured by Temp-Q-Tips probes (Ni/NiO reference) from Leeds and Northrup Co. The oxygen probes were connected to an Omega 2 channel chart recorder with an accuracy of plus or minus 0.5% . One channel of the chart recorder was connected to the type S (platinum-rhodium) dip tip thermocouple of the probe and the other was connected to the Ni/NiO cell of the probe.

The oxygen potential was related to the measured Emf using the following equation:

Fig. 7.6 : Mild Steel Sample Cup.

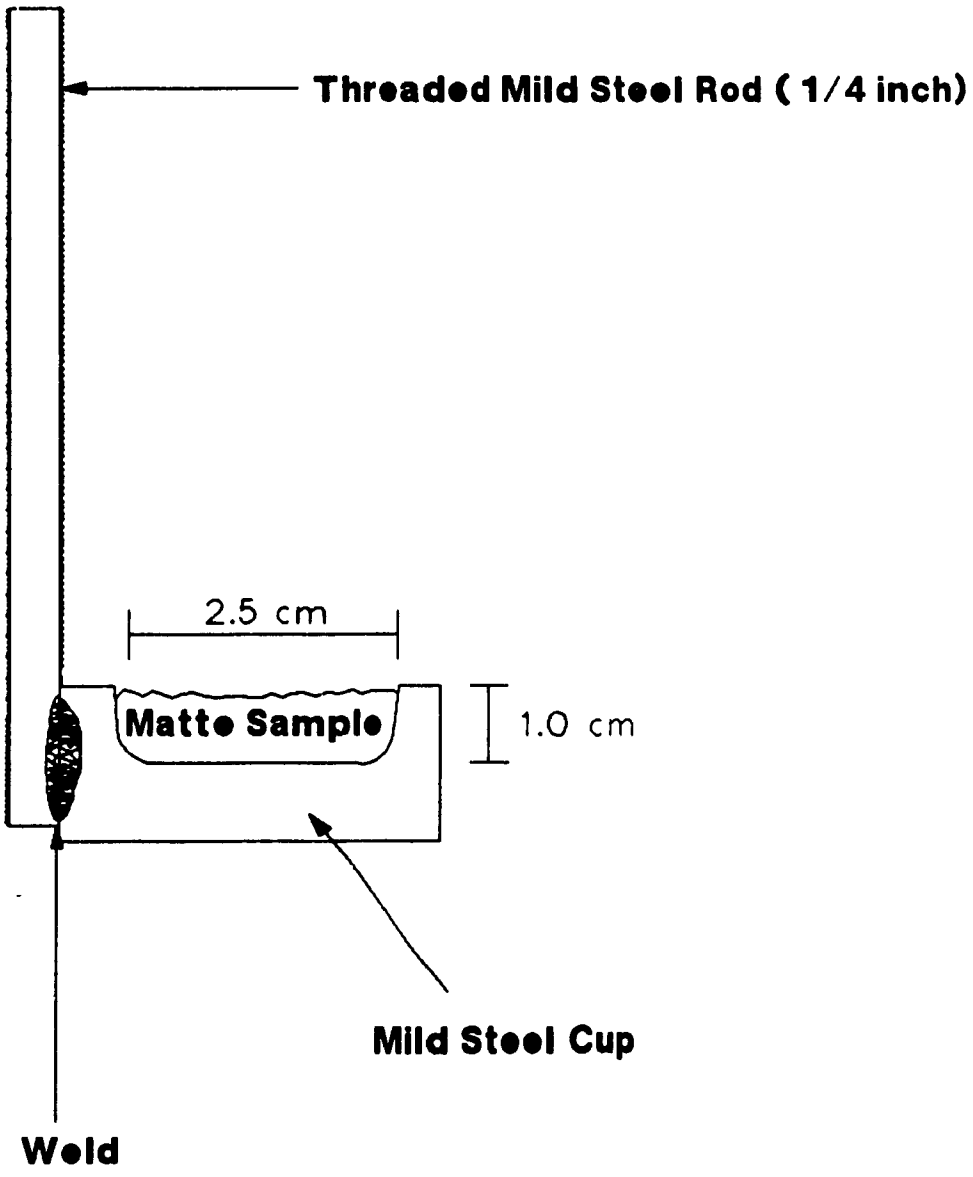

$$Emf = E_c + E^o + \frac{-RT}{ZF} \left[1/P_{O_2}^{0.5} \right] \quad (41)$$

$$\text{where: } E^o = \frac{-\Delta G_{(NiO)}}{ZF} \quad (42)$$

and E_c is the contact voltage produced by the two electrodes in contact with the copper matte melt.

Calibration curves were not available from the supplier for copper matte melts. Thus, the method of approximation described below was adopted. The initial oxygen activities were assumed to be 10^{-8} and 10^{-7} atmosphere for reverberatory and Noranda reactor matte, respectively based on the literature (11). By knowing the starting oxygen activity before the chamber was under vacuum and the melt temperature, the contact Emf (E_c) in Equation 41 was calculated. Assuming E_c was constant, an approximate oxygen pressure was calculated for Emf measurements taken during the experiments.

7.4 Experimental Procedure

7.4.1 Copper Matte Preparation

The reverberatory furnace matte, Noranda reactor matte and converter white metal were provided by Noranda Inc., Horne smelter. The matte received had pieces ranging from 1.0 to 15.0 cm. The matte was crushed to minus 0.5 cm and thoroughly mixed. This was done to facilitate manipulation, weighing and homogenization of the chemical composition.

7.4.2 Chemical Composition of the Melt

The copper matte grade under study ranged from 35 to 80 % copper. The matte composition was varied by selecting either reverberatory furnace matte (35% Cu), Noranda reactor matte (65% Cu) or white metal (80% Cu). The matte was weighed before being charged into the apparatus to document the initial weight (accuracy $\pm$0.05 kg). If any matte additions were required after melting, they were also carefully weighed.

7.4.3 Charge Melting

Before melting started, the vacuum chamber was evacuated to verify that no air infiltration occurred. The pressure was then increased to approximately 20,000 pascal (150mm Hg). The lifting gas (nitrogen) flow rate was adjusted to the preselected value and then the furnace power was turned on. The maximum power used was 40 kw to avoid damaging the thermocouples. The resistance furnace, on the top part of the apparatus was also turned on. Once the melt temperature was attained and the resistive heater temperature reached 1273 K, a sample was taken and labelled as the initial condition. Typical initial impurity concentrations ranged from 1.5 to 3.0 % lead, 0.01 to 0.03 % bismuth, 0.02 to 0.09 % arsenic and 0.01 to 0.04 % antimony.

7.4.4 Pump Down

After taking the initial sample, the auxiliary vacuum valve was opened and depressurization started. The chronometer was started as well. At pressures below 5000 pascal , very violent bubbling occurred due to SO_2 or CO_2 evolution from the melt. The melt was closely observed during that time. The extent to which the vacuum valve was open was adjusted to minimize matte losses due to excessive splashing. After the bubbling diminished (15 to 30 minutes later and chamber pressure less than 500 pascal), the main vacuum valve was opened if necessary and the pressure was set to the preselected value. By opening and closing the vacuum valves, the chamber pressure could be controlled.

7.4.5 Temperature Control

The temperature of the melt was kept constant by varying the power input to the induction furnace. Usually a power of 25 kW was required during depressurization due to the high heat losses during the SO_2 or CO_2 boil. After depressurization, the power was decreased and 10 to 15 kW was sufficient to keep the temperature constant at plus or minus 25 K.

7.4.6 Sampling of the Melt

During an experiment, a maximum of six samples were taken. The matte sampling was carried out as follows:

Sample 1: At time t = 0, Once the selected melt temperature was reached, before depressurization.

Sample 2: After the SO_2 boil, t = 15 to 20 minutes.

Sample 3-5: Every 15 to 20 minutes, as required.

Sample 6: At the end of the experiment.

The time at which the samples were taken was documented in the experiment log book at plus or minus 30 seconds. The samples were catalogued and sent to the Noranda Technology Center for assaying.

7.4.7 Oxygen Activity Measurements

Oxygen activity measurements were taken only in Experiments 13, 14 and 15. To take oxygen measurements, the vacuum had to be broken. This meant that measurements were taken at the beginning and at the end of the experiments. In Experiments 14 and 15, an oxygen measurement was also taken after the SO_2 boil. The time during which the vacuum was disrupted was measured and taken into consideration for the concentration versus time curves of Experiments 14 and 15 in Section 7.5 .

7.4.8 Termination of Experiments

After the last sample, the power to the furnace and resistance heater was turned off. The apparatus was tilted and the matte was poured into a steel mold. During the cooling of the apparatus, the lifting gas was left on (3 to 4 hours). This prevented the blocking of the injector by residual freezing matte. The apparatus was left to cool overnight before the vacuum was broken. The matte ingot was then retrieved and weighed to record the final weight.

7.4.9 Dust Sampling

The next day, after removing the matte ingot, the dust was swept off the walls and collected. The dust was well mixed and an 8 mesh screening was done to remove the matte which had splashed out of the bath. The dust was spread on a table and a 50 gram sample was cut to be sent for assaying. The vacuum chamber was cleaned using a vacuum cleaner. Preparation for a new experiment could then be started.

A mention must be made here regarding safety precautions that must be taken during the clean up of the vacuum chamber. The dust contains high levels of lead, arsenic, cadmium, etc. Hence, a dust mask must be worn at all times during clean up, or other work done in the vacuum chamber. Furthermore, it is advisable to wash hands and shower to avoid lead and cadmium poisoning through the ingestion of the dust (i.e., eating your lunch with dirty hands).

7.5 Tabulation and Presentation of the Experimental Results

This section of Chapter 7 presents the results of all the experiments in tabular and graphical form. For each experiment, one table will be provided as well as the corresponding graphs of the logarithm of the concentration of lead, bismuth, arsenic and antimony versus the time.

Table 7.4: Results of Experiment 1, Concentration of Pb, Bi, As, Sb, and Se versus Time in a **Graphite Apparatus.**

Time (s)	Temp. (K)	Press. (Pa)	Pb (%)	Bi (%)	As (%)	Sb (%)	Se (%)
0	1473	19950	4.64	0.084	0.029	0.045	0.0047
600	(pyro.)	3990	3.52	0.045	0.027	0.039	0.0070
1200		1330	1.30	0.013	0.025	0.037	0.017

Notes : Matte Grade : 35.8 % Cu

Lifting Gas : 130 Nml/s Scavenging Gas : 30 Nml/s

Matte Weight: Start 30.5 kg, End 22.6 kg

Dust and Splashing Weight : 6.04 kg

(pyro.) : Temperature measured with the pyrometer.

Table 7.5: Results of Experiment 2, Concentration of Pb, Bi, As, Sb, and Se versus Time in a Graphite Apparatus.

Time (s)	Temp. (K)	Press. (Pa)	Pb (%)	Bi (%)	As (%)	Sb (%)	Se (%)
0	1423	19950	4.05	0.015	0.032	0.054	0.029
150	1403	7980					
240	1373	3990					
450	1373	3000					
600	1383	2600	3.96	0.017	0.030	0.056	0.039
900		2400					
1200	1523	2200	3.40	0.012	0.030	0.046	0.025
1440	(Pyro.)	2000					
1800		1000					
2100							
2220			1.14	0.0063	0.026	0.041	0.032
2400		300					
2580		80					
2700		66					
2820		240					
3000		53	0.29	0.0043	0.023	0.033	0.040
3060		53					
3240		130					
3420		40					
3660		66					
3900		40	0.24	0.0038	0.022	0.033	0.061

Notes : Matte Grade : 65.3 % Cu

Lifting Gas : 39.0 Nml/s Scavenging Gas : 50 Nml/s

Matte Weight : Start 39.0 kg, End 33.2 kg

Dust and Splash Weight :

At time equal 50 minutes, good spray observed.

Some dust falls from the roof to the bath, refluxing.

Table 7.6: Results of Experiment 3, Concentration of Pb, Bi, As, Sb, and Se versus Time in a **Graphite Apparatus.**

Time (s)	Temp. (K)	Press. (Pa)	Pb (%)	Bi (%)	As (%)	Sb (%)	Se (%)
0	1473	21280	3.61	0.062	0.028	0.037	0.015
120	1459	13300					
240	1473	6650					
360	1473	5320					
420	1473	3990					
600			3.56	0.042	0.040	0.045	----
720	1473	3330					
840	(Pyro.)	3330					
960		2100					
1080		1500					
1200		1500	3.34	0.041	0.031	0.041	----
1320		1300					
1500		1000					
1860		700	0.99	0.011	0.022	0.028	<0.0047
2100		100					
2250		100					
2460		100	0.49	0.0090	0.021	0.027	<0.0047
3900		100	0.054	0.0062	0.016	0.024	0.0047

Notes : **Matte Grade : 35.0 % Cu**

Lifting Gas : 30 Nml/s Scavenging Gas : 50 Nml/s

Matte Weight : Start 34.0 kg, End 26.1 kg

Dust and Splashing Weight : 6.1 kg

Table 7.7: Results of Experiment 4, Concentration of Pb, Bi, As, Sb, and Ni versus Time in a **Graphite Apparatus.**

Time (s)	Temp. (K)	Press. (Pa)	Pb (%)	Bi (%)	As (%)	Sb (%)	Ni (%)
0	Approx.	2260	4.75	0.012	0.041	0.060	0.41
300	1523	1330					
1800	No	1330					
2700	Measure	1330	5.13	0.013	0.051	0.055	0.43
3000		930					
3120		2020					
3300		1520					
3600		1210					
3900		808	3.85	0.0038	0.045	0.063	0.45
4200		505					
4500		93					
4800		27					
5100		13					
5400		13	0.23	0.0035	0.020	0.051	0.49
5700		27					
6000		13					
6300		27	0.10	0.0040	0.011	0.033	0.47

Notes : **Matte Grade : 63.4 % Cu**

Lifting Gas : 13 Nml/s

Matte Weight : Start 21.1 kg, End 9.9 kg

Dust and Splashing Weight : 10.5 kg

At 50 minutes, the matte froze on the top of the apparatus. At 65 minutes, the main vacuum valve was opened. At 75 minutes, the melt was white hot. At 90 minutes the spray was very small and there was not enough matte.

Table 7.8: Results of Experiment 5, Concentration of Pb, Bi, As, Sb, Se and Ag versus Time in a Graphite Apparatus.

Time (s)	Temp. (K)	Press. (Pa)	Pb (%)	Bi (%)	As (%)	Sb (%)	Se (%)	Ag (%)
0	1473	19950	4.47	0.014	0.033	0.053	0.078	0.24
300	1523	7980						
600	1510	2400						
900	1503	1200						
1200	1503	900	3.82	0.0090	0.028	0.044	0.080	0.26
1500	1503	600						
1800	1473	200						
2100	1503	100						
2400	1533	27	0.34	0.0061	0.011	0.030	0.074	0.28
2700	1549	13						
3000	1533	20						
3600	1523	13	0.24	0.0076	0.0093	0.021	0.070	0.28
3900	1515	5						
4200	1533	13						
4500	1535	13						
4800	1536	13	0.022	0.0030	0.0071	0.019	0.070	0.29
5100	1533	13						
5400	1528	27						
5700	1523	5						
6000	1515	5	0.34	<0.0030	0.0079	0.022	0.073	0.29

Notes : Matte Grade : 60.3 % Cu

Matte Weight : Start 18.8 kg, End 11.8 kg

Dust and Splashing Weight : 5.8 kg

Lifting Gas : 8.5 Nml/s

Spray Quality : At 0 minutes, filled to rim.

At 50 minutes, good spray.

At 100 minutes, poor spray.

Table 7.9: Results of Experiment 6, Concentration of Pb, Bi, As, Sb, and Se versus Time in a **Graphite Apparatus.**

Time (s)	Temp. (K)	Press. (Pa)	Pb (%)	Bi (%)	As (%)	Sb (%)	Se (%)
0	1523	13300	3.67	0.015	0.033	0.053	0.059
120	(pyro.)	9310					
300		5320					
600		2000					
900		1300					
1080		900					
1200		800					
1380		400					
1500		200					
1560		80					
1800		80	0.88	0.0053	0.016	0.032	0.055
1920		13					
2220		13					
2400		13					
2700		33	0.20	0.0053	0.0093	0.026	0.053
3180		27					
3600		27	0.15	0.0053	0.0076	0.019	0.054
5400		27	0.028	0.0068	0.0075	0.020	0.052

Notes : Matte Grade : 62.9 % Cu

Matte Weight : Start 20.6 kg End 18.4 kg

Dust Weight : 1.6 kg

Lifting Gas : 8.5 Nml/s

At 32 minutes, poor spray due to a big skull

Table 7.10: Results of Experiment 7, Concentration of Pb, Bi, As, Sb, and Se versus Time in a **Graphite Apparatus.**

Time (s)	Temp. (K)	Press. (Pa)	Pb (%)	Bi (%)	As (%)	Sb (%)	Se (%)
0	1523	19950	3.07	0.048	0.0097	0.041	----
300	1523	6650					
600		3990					
900	1523	3990	2052	0.020	0.010	0.042	----
1200	(pyro.)	1500					
1320		1000					
1500		500					
1800		300	1.28	0.0061	0.0089	0.028	----
2100		67					
2400		40					
2700		27	0.24	0.0045	0.0048	0.024	----
3000		13					
3600		13	0.023	0.0030	0.0043	0.021	----
3900		13					
4200		10					
4500		10					
4700		10					
5000		10					
5400		10	0.033	0.0030	0.0040	0.012	----

Notes : Matte Grade : 40.2 % Cu

Lifting Gas : 7.0 Nml/s

Matte Weight : Start 21.3 kg, End 17.6 kg

Dust and Splashing Weight : 2.7 kg

At 15 minutes, crucible filled to rim, very good spray.

At 30 minutes, no skull forming.

At 40 minutes, very good spray.

Table 7.11: Results of Experiment 8, Concentration of Pb, Bi, As, Sb, and Se versus Time in a **Graphite Apparatus.**

Time (s)	Temp. (K)	Press. (Pa)	Pb (%)	Bi (%)	As (%)	Sb (%)	Se (%)
0	1523	19950	1.00	0.0056	0.013	0.019	----
120	(pyro.)	10640					
300		4660					
600		2000					
900		1500	0.64	0.0056	0.013	0.019	----
1200		1000					
1320		500					
1500		319					
1800		130	0.53	0.0048	0.011	0.017	----
1920		27					
2100		13					
2400		13					
2700		10	0.22	0.0024	0.0085	0.023	----
3300		10					
3600		10	0.070	0.0020	0.015	0.025	----
4500		10	0.046	0.0016	0.010	0.015	----

Notes : **Matte Grade : 78.3 %**

Lifting Gas : 8.6 Nml/s

Matte Weight : Start 22.7 kg, End 21.0 kg

Dust and Splashing Weight : 1.1 kg

At 0 minutes, the crucible was filled to the rim, some slag was present on the melt surface (very viscous).

At 25 minutes, good spray.

Table 7.12: Results of Experiment 9, Concentration of Pb, Bi, As, Sb, and Se versus Time in a **Graphite Apparatus.**

Time (s)	Temp. (K)	Press. (Pa)	Pb (%)	Bi (%)	As (%)	Sb (%)	Se (%)
0	1523	13300	0.69	0.0052	0.011	0.017	----
300	1543	6650					
600	1543	1500					
900	1543	700	0.61	0.0060	0.012	0.018	----
1020	1541	300					
1200	1540	120					
1500	1535	67					
1620	1536	13					
1800	1536		0.19	0.0036	0.012	0.020	----
2100	1538	27					
2400	1533	10					
2700	1533	27	0.084	0.0028	0.016	0.026	----
3000	1527	10					
3300	1528	10					
3600	1533	10	0.037	<0.0016	0.0085	0.017	----
4500	1531	10	0.017	0.0020	0.0090	0.015	----

Notes : Matte Grade : 77.6 % Cu

Lifting Gas : 8.0 Nml/s

Matte Weight : Start 22.7 kg End 21.6 kg

Dust and Splashing Weight : 0.4 kg

Good spray throughout the experiment.

Table 7.13: Results of Experiment 10, Concentration of Pb, Bi, As, Sb, and Ni versus Time in an **Alumina Apparatus.**

Time (s)	Temp. (K)	Press. (Pa)	Pb (%)	Bi (%)	As (%)	Sb (%)	Ni (%)
0	1423	6644	1.83	0.12	0.19	0.078	0.75
150		1010					
300		404					
600		202	1.12	0.019	0.012	0.043	0.76
900		133					
1200		32					
1500		32					
1800	1448	133	0.22	0.0069	<0.005	0.028	0.82
2100	1473	133					
2400		133					
2700	1473	133	0.052	0.0038	<0.005	0.022	0.80

Notes : Matte Grade : 36.6 % Cu

Lifting Gas : 16 Nml/s

Matte Weight : Start 20.3 kg, End 16.7 kg

Dust and Splashing Weight : 2.8 kg

At 0 minutes, the riser broke, the lifting gas flow rate fluctuated, the spray looked OK without riser.

At 45 minutes, the gas nozzle blocked, the experiment was stopped.

Table 7.14: Results of Experiment 11, Concentration of Pb, Bi, As, Sb, and Ni versus Time in an **Alumina Apparatus.**

Time (s)	Temp. (K)	Press. (Pa)	Pb (%)	Bi (%)	As (%)	Sb (%)	Ni (%)
0	1453	19930	1.41	0.12	0.13	0.051	0.62
150	1459	6640					
300	1470	2020					
450	1475	1110					
600	1472	707					
660			1.29	0.079	0.050	0.044	0.59
750	1480	707					
900	1493	505					
1050	1494	505					
1200	1493	133					
1500	1482	93	0.37	0.11	0.049	0.032	0.66
1800	1491	120					
2100	1498	78					
2400	1498	78	0.062	0.0083	<0.005	0.041	0.70
2700	1499	93					
3000	1490	66					
3300	1483	78	0.094	0.0082	<0.005	0.041	0.71
3600	1473	93	0.062	0.0058	<0.005	0.042	0.72

Notes : **Matte Grade : 34.8 % Cu**

Lifting Gas : 16 Nml/s

Matte Weight : Start 23.9 kg End 18.2 kg

Dust and Splashing Weight : 3.5 kg

At 0 minutes, the crucible was filled to the rim. At 17.5 minutes, a very violent spray was seen. At 30 minutes, very good spray. At 45 minutes, good spray. At 60 minutes, satisfactory spray. Some slag was on the surface of the melt.

Table 7.15: Results of Experiment 12, Concentration of Pb, Bi, As, Sb, and Ni versus Time in an Alumina Apparatus.

Time (s)	Temp. (K)	Press. (Pa)	Pb (%)	Bi (%)	As (%)	Sb (%)	Ni (%)
0	1493	19930	4.42	0.15	0.12	0.089	0.70
150	1493	3990					
300	1515	1919					
450	1404	1616					
600	1481	505					
750	1469	159	2.91	0.024	0.081	0.093	0.70
900	1477	133					
1050	1464	93					
1200	1469	93					
1500	1487	106	1.62	0.0087	0.067	0.054	0.69
1800	1484	80					
2100	1513	93					
2400	1507	80	0.58	0.0061	0.035	0.047	0.69
2700	1503	80					
3000	1491	80	0.35	0.0052	0.029	0.041	0.70
3300	1489	80					
3600	1486	60					
3900	1482	66	0.21	0.0051	0.020	0.040	0.70

Notes : Matte Grade : 61.0 % Cu

Lifting Gas : 16 Nml/s

Matte Weight : Start 27.5 kg End 18.9 kg

Dust and Splashing Weight : 7.4 kg

At 12.5 minutes, very good spray.

At 40 minutes, good spray.

At 65 minutes, poor spray.

Table 7.16: Results of Experiment **13**, Concentration of Pb, Bi, As, Sb, and Ni versus Time in an **Alumina Apparatus**.

Time (s)	Temp. (K)	Press. (Pa)	Pb (%)	Bi (%)	As (%)	Sb (%)	Ni (%)
0	1473	19930	1.30	0.21	0.010	0.020	0.54
150	(pyro.)	3990					
300		2020					
450		1515					
600		984					
750		438	1.24	0.14	0.036	0.029	0.55
900		452					
1050		558					
1200		584					
1500		638					
1800		664	1.36	0.15	0.041	0.038	0.56
2100		638					
2400		585					
2700		638	1.22	0.081	0.025	0.031	0.54
3000		664					
3300		584					
3600		584	1.14	0.039	0.0094	0.034	0.58
3900		611					
4200		611					
4500		611	1.06	0.028	0.025	0.032	0.57

Notes : Matte Grade : 29.8 % Cu

Lifting Gas : 12 Nml/s

Matte Weight : Start 25.0 kg End 17.5 kg

Dust and Splashing Weight : 1.0 kg

At 50 minutes, good spray.

At 75 minutes, poor spray.

Oxygen was measured at the beginning and end of the experiment.

Table 7.17: Results of Experiment **14**, Concentration of Pb, Bi, As, Sb, and Ni versus Time in an **Alumina Apparatus.**

Time (s)	Temp. (K)	Press. (Pa)	Pb (%)	Bi (%)	As (%)	Sb (%)	Ni (%)
0	1364	101100	1.05	0.32	0.27	0.038	0.18
150	1368	9300					
300	1451	3990					
450	1523	2323					
600		1919					
750	1473	1515					
900	(pyro,)	505	0.83	0.15	0.28	0.037	0.18
1050		101100					
1200		101100					
1500		664					
1800		531					
2100		598					
2400		478	0.71	0.11	0.25	0.031	0.15
2700		584					
3000		664					
3600		531	0.77	0.10	0.31	0.039	0.15

Notes : **Matte Grade : 60.0 % Cu**

lifting Gas : 0 nml/s

Matte Weight : Start 15.0 kg End 12.7 kg

Dust and Splashing Weight : 0.6 kg

From 15 to 22.5 minutes, the vacuum was broken to take an oxygen measurement. There is bubbling at the thermocouple probe. Slag is observed on the surface, 1/2 covered.

Table 7.18: Results of Experiment 15, Concentration of Pb, Bi, As, Sb, and Ni versus Time in an **Alumina Apparatus.**

Time (s)	Temp. (K)	Press. (Pa)	Pb (%)	Bi (%)	As (%)	Sb (%)	Ni (%)
0	1373	101100	3.62	0.86	0.24	0.068	0.54
150		19930					
300	1547	5320					
450		1919					
600		598					
750	1473	664					
900		101100					
1050			3.65	0.65	0.25	0.073	0.55
1200		664					
1500	1613	585					
1800	1613	585					
2100	1608	425					
2400	1610	638					
2700	1608	558					
3000	1604	664					
3300	1603	584					
3600		101100	2.84	0.26	0.24	0.068	0.57
4200	1571	13					
4800	1586	13					
5400	1597	27	0.21	0.0097	0.13	0.069	0.60
6000	1596	13					
6600	1592	27					
7200	1589	27	0.32	0.0037	0.14	0.067	0.60
8100	1583	13					
9000	1576	13	0.30	0.0025	0.11	0.044	0.61

Notes : Matte Grade : 59.6 % Cu

Lifting Gas : 0 Nml/s

Matte Weight : Start 15.0 Kg End 11.1 kg

Dust and Splashing Weight : 2.7 kg

Break vacuum for oxygen from 900 to 1080 s, 3600 to 3720 s and 7200 to 7380 s.

Fig. 7.7: Lead Concentration vs Time, Experiment #1

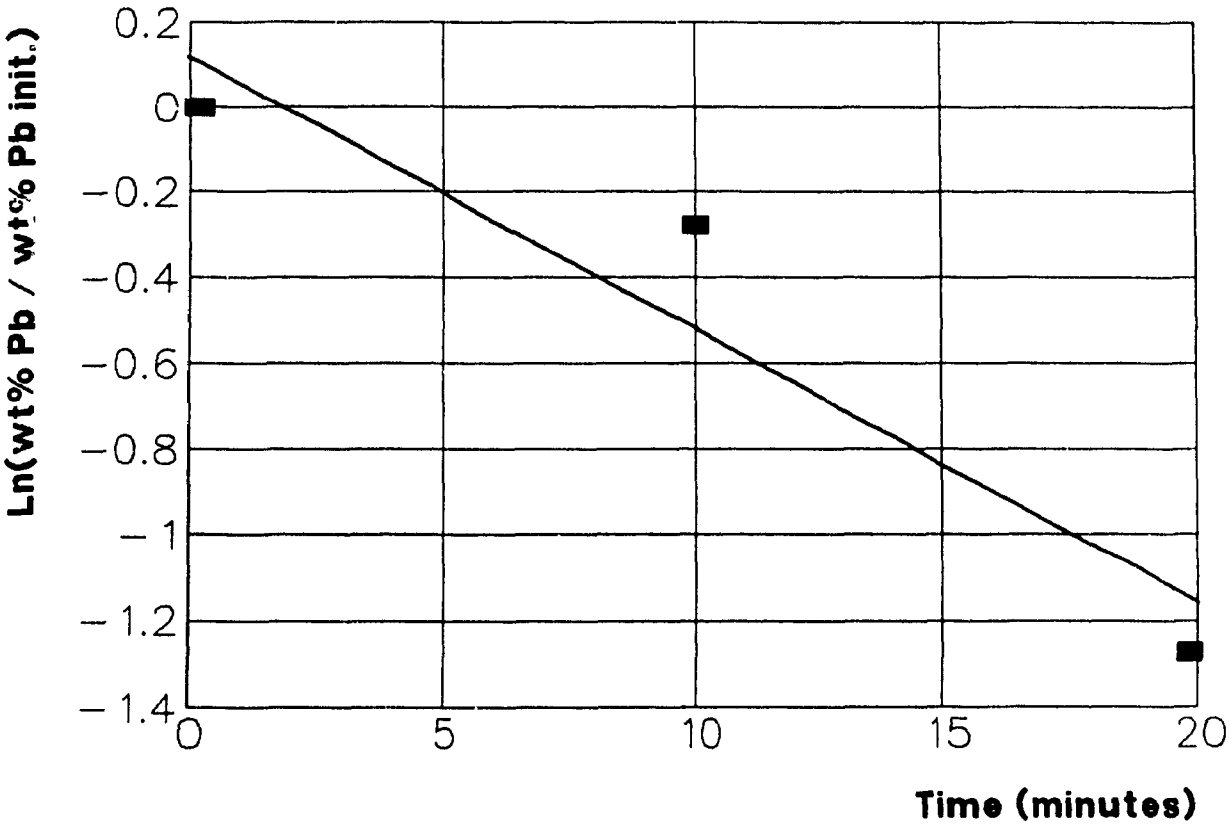

$y = -0.06362x + 0.1199$

$R^2 = 0.90$

Fig. 7.8 : Bismuth Concentration vs Time, Experiment # 1

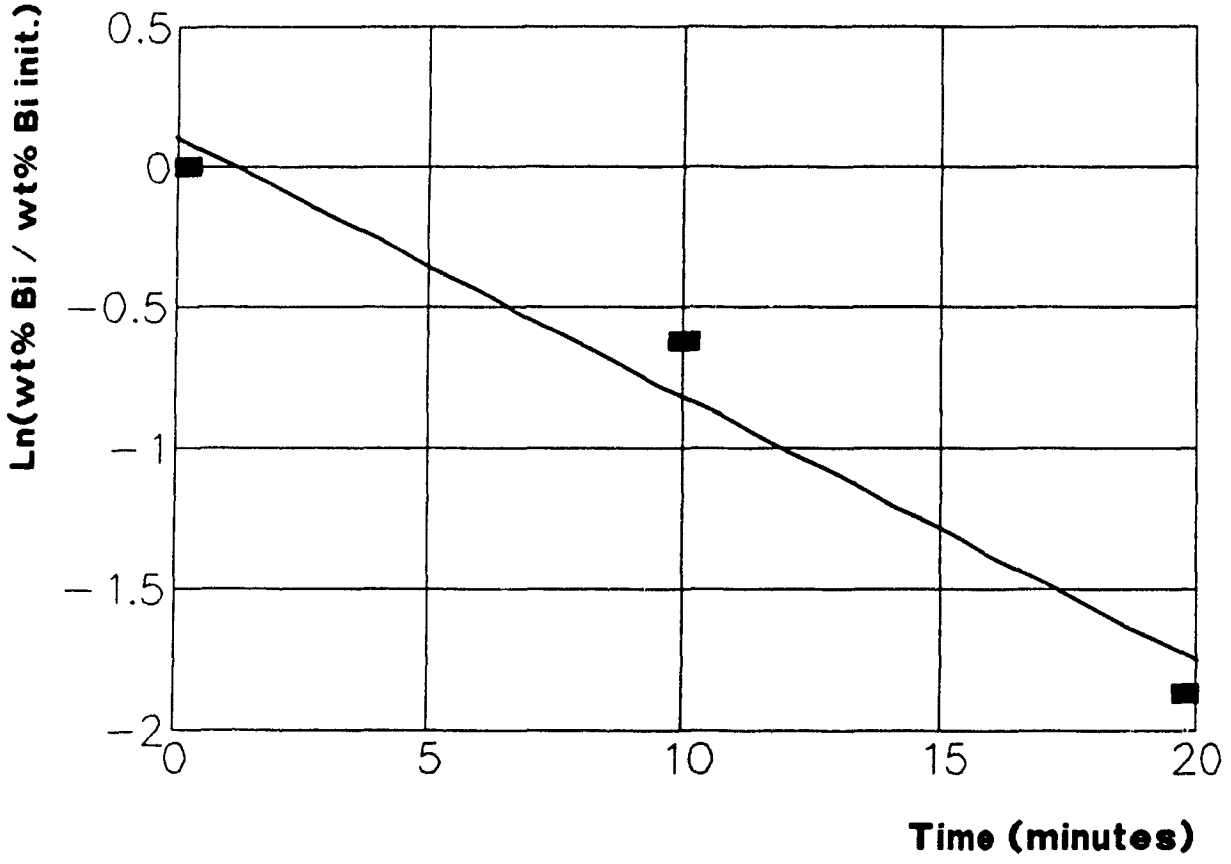

$y = -0.09329\,x + 0.1029$

$R^2 = 0.96$

Fig. 7.9 : Arsenic Concentration vs Time, Experiment #1

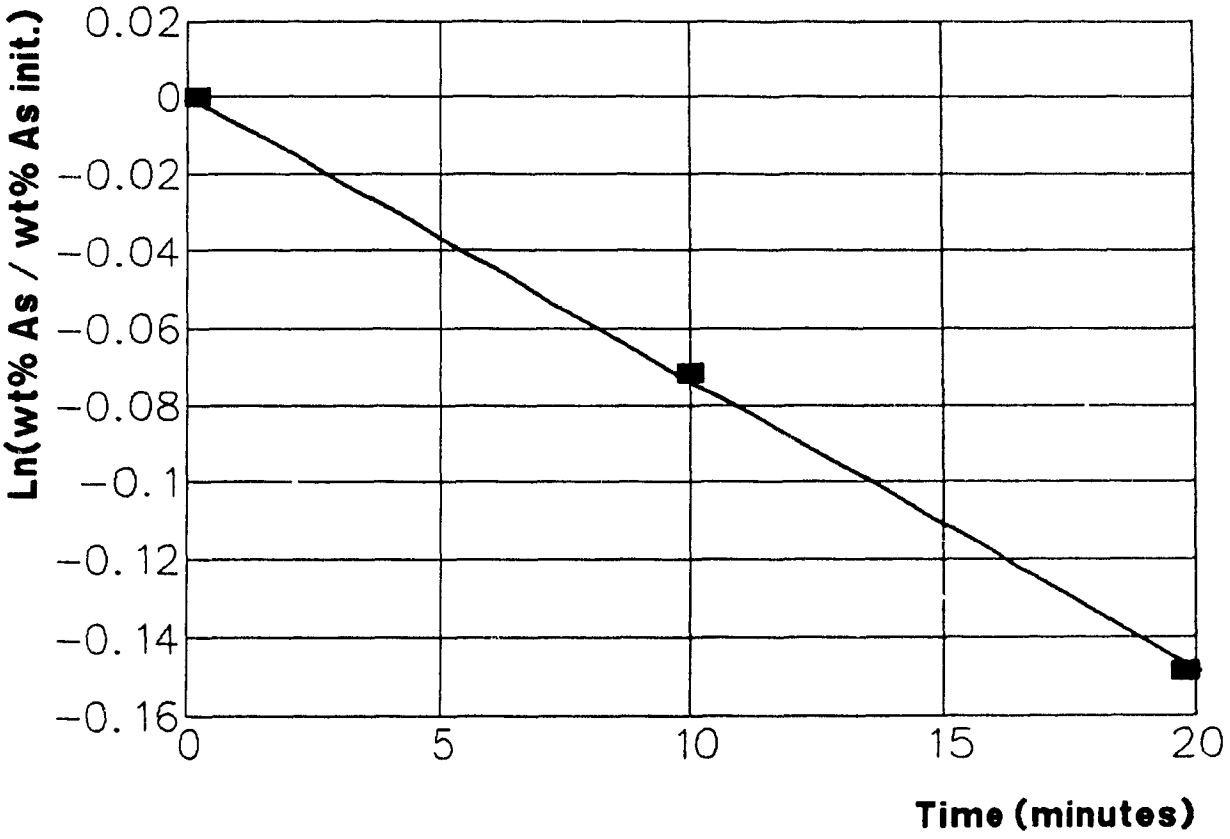

$y = -0.00742x + 0.000917$

$R^2 = 1.0$

Fig.7.10:Antimony Concentration vs Time Experiment #1

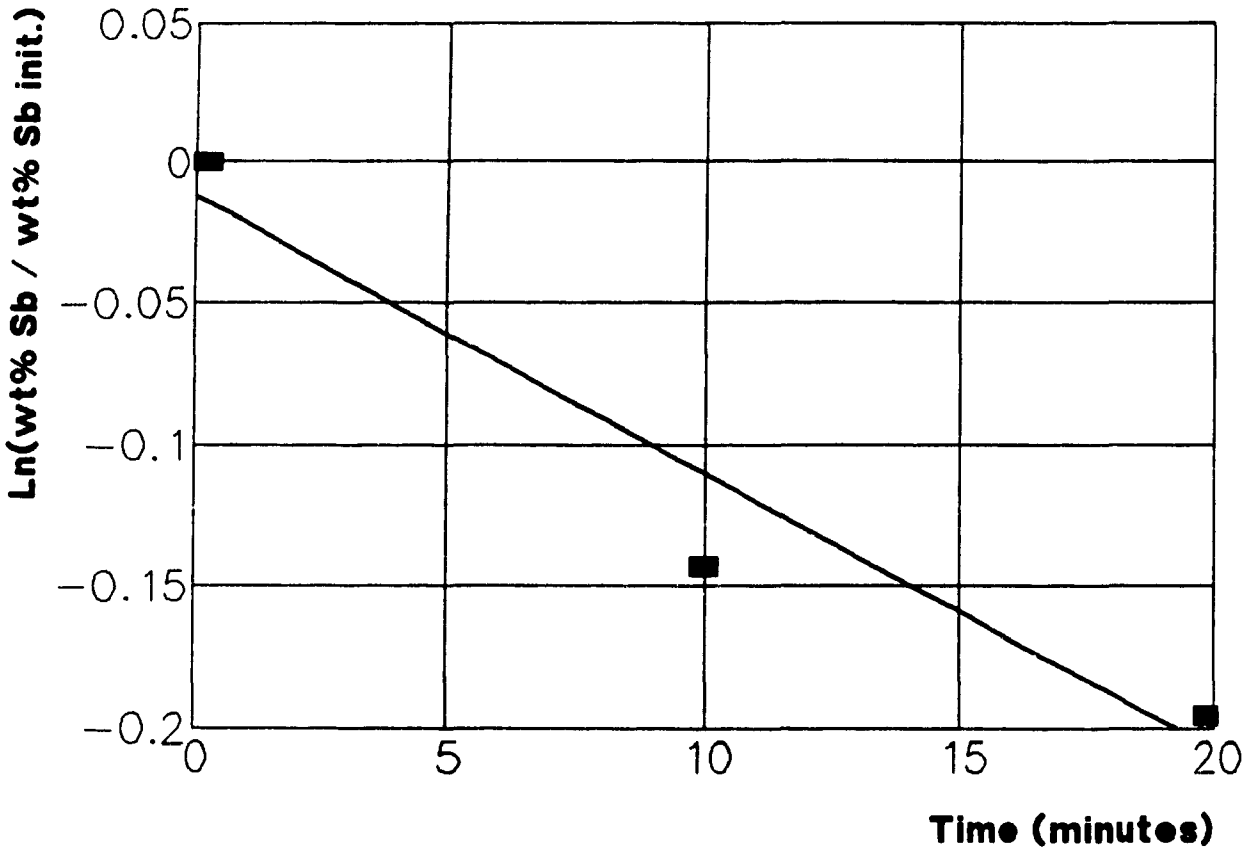

$y = -0.00979\,x - 0.1508$

$R^2 = 0.93$

Fig. 7.11 : Lead Concentration vs Time, Experiment #2

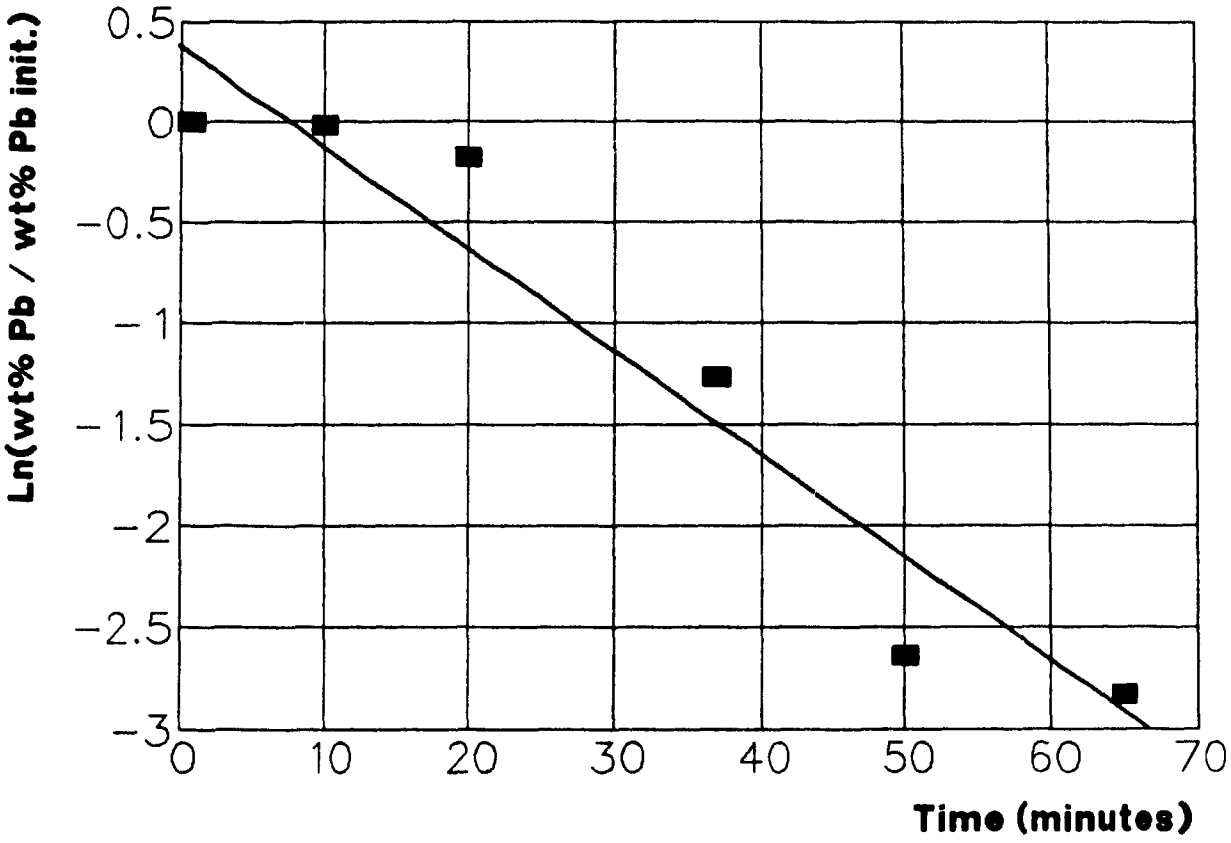

$y = -0.05076x + 0.3851$

$R^2 = 0.92$

Fig. 7.12 : Bismuth Concentration vs Time, Experiment #2

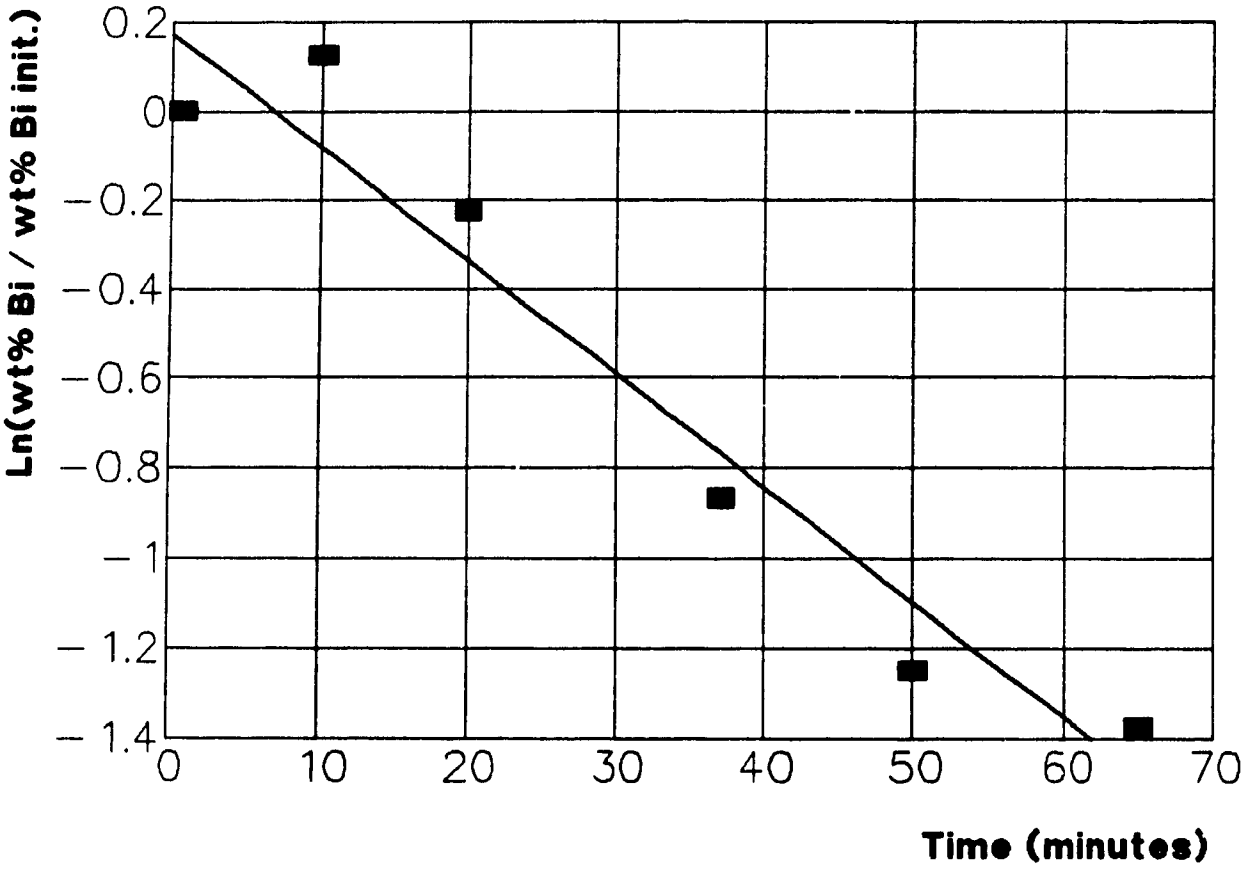

$y = -0.02544x + 0.1738$

$R^2 = 0.94$

Fig. 7.13 : Arsenic Concentration vs Time, Experiment #2

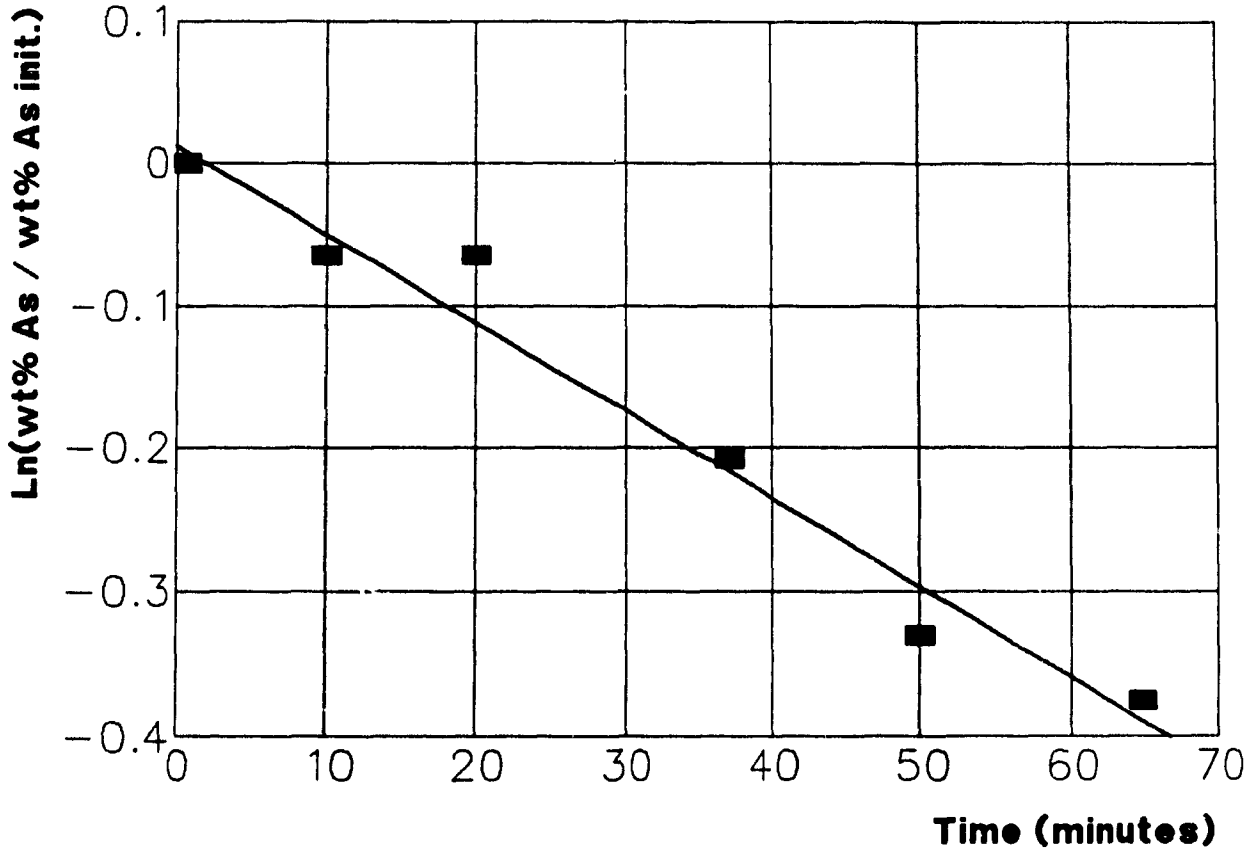

$y = -0.00615x + 0.01283$

$R^2 = 0.97$

Fig. 7.14 : Antimony Concentration vs Time Experiment #2

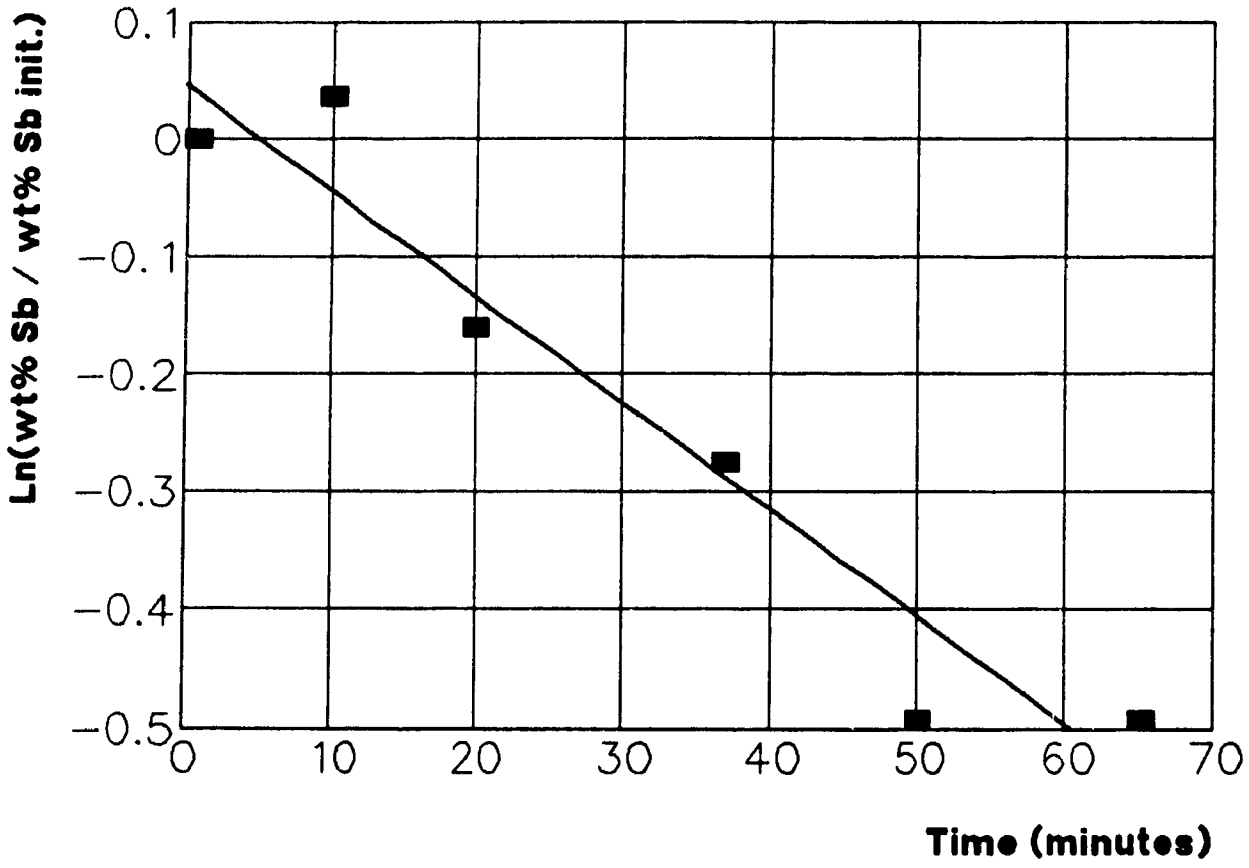

$y = -0.00901x + 0.04244$

$R^2 = 0.93$

Fig. 7.15 : Lead Concentration vs Time, Experiment #3

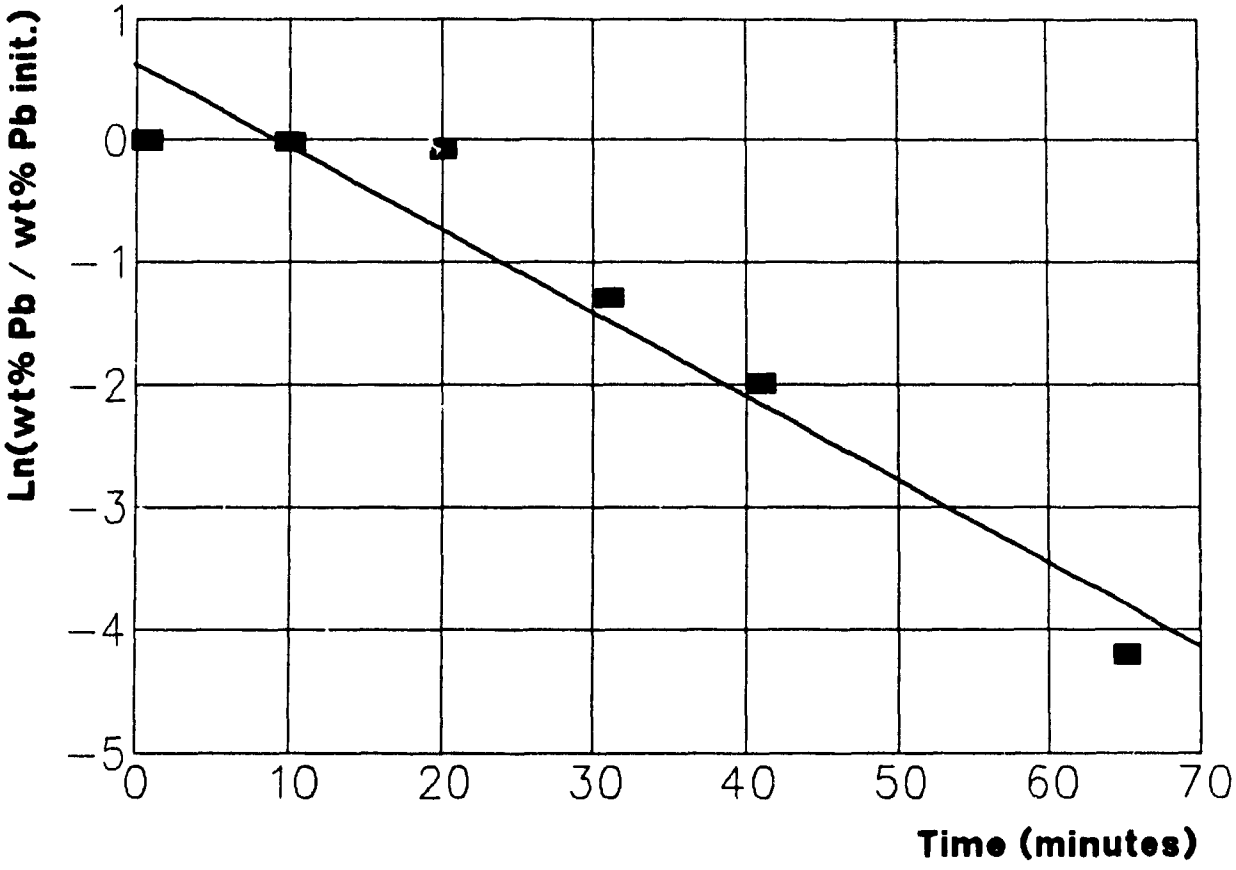

$y = -0.06831\,x + 0.6372$

$R^2 = 0.92$

Fig. 7.16 : Bismuth Concentration vs Time, Experiment #3

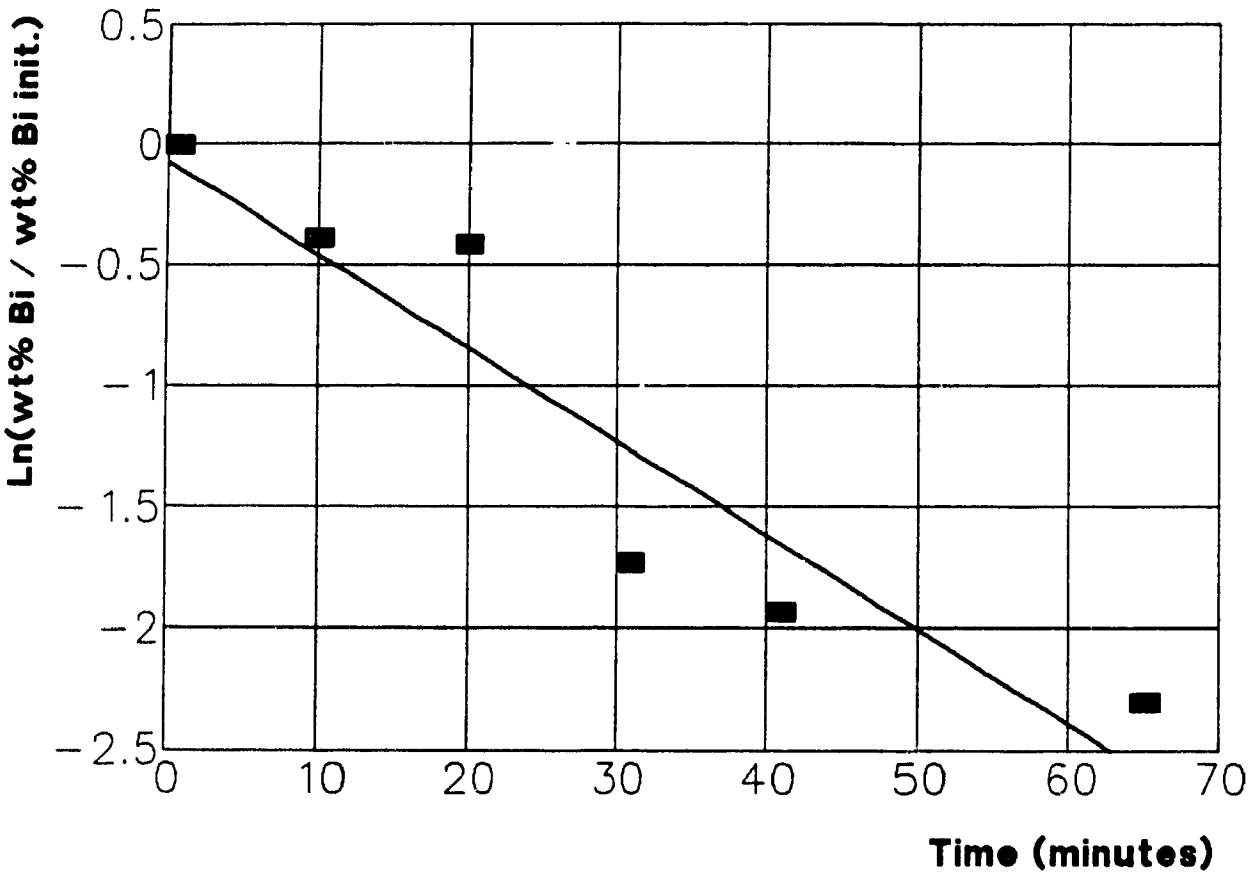

$y = -0.03909\,x - 0.03944$

$R^2 = 0.88$

Fig. 7.17 : Arsenic Concentration vs Time, Experiment #3

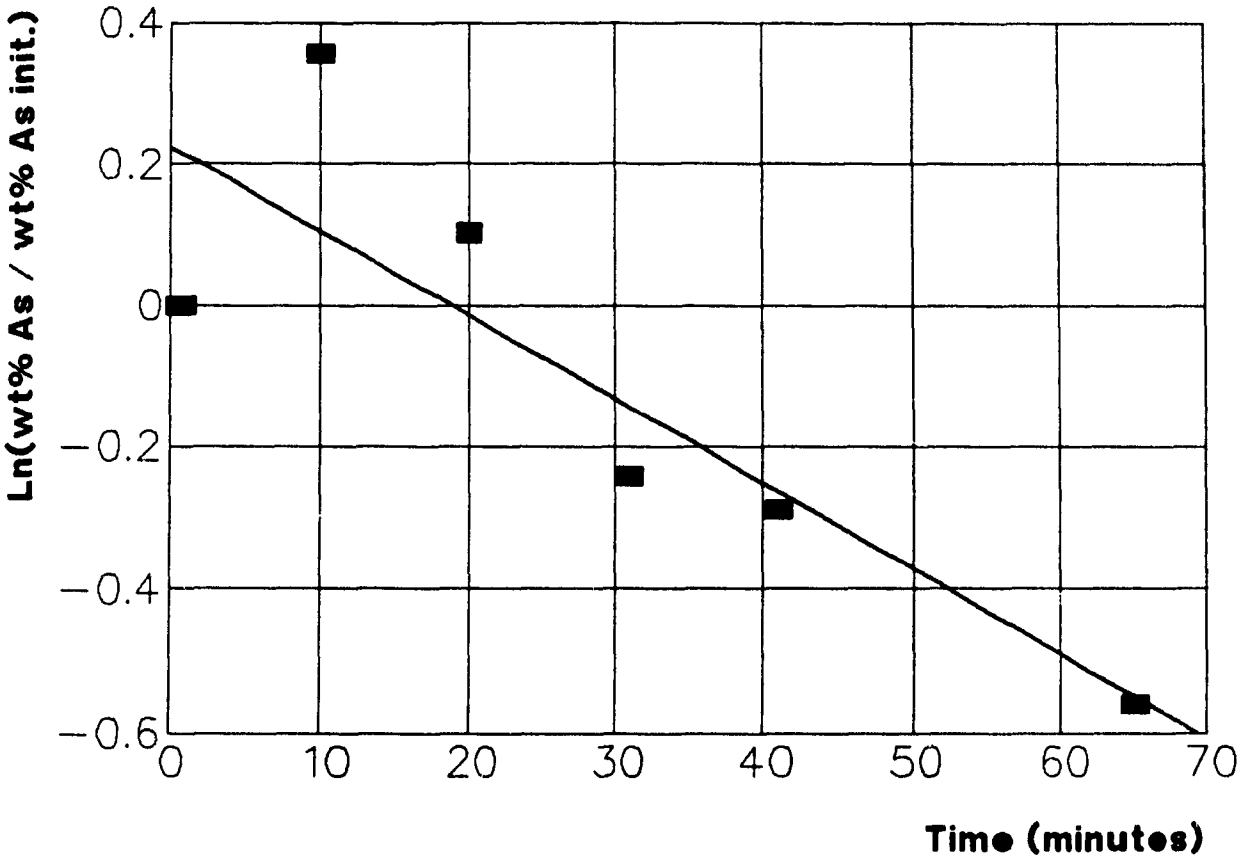

$y = -0.01196\,x + 0.2278$

$R^2 = 0.74$

Fig. 7.18 : Antimony Concentration vs Time

Experiment #3

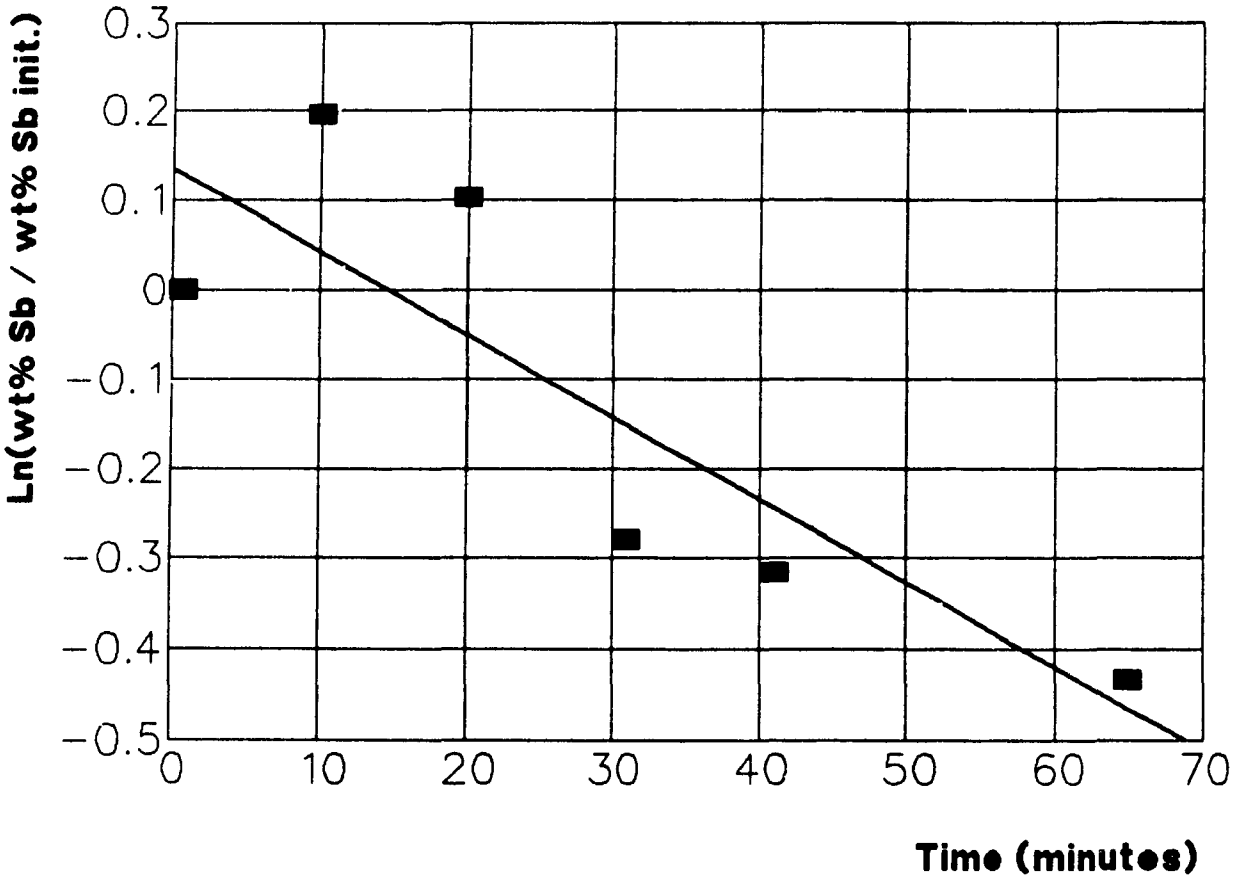

$y = -0.00935x + 0.1388$

$R^2 = 0.73$

Fig. 7.19 : Lead Concentration vs Time, Experiment #4

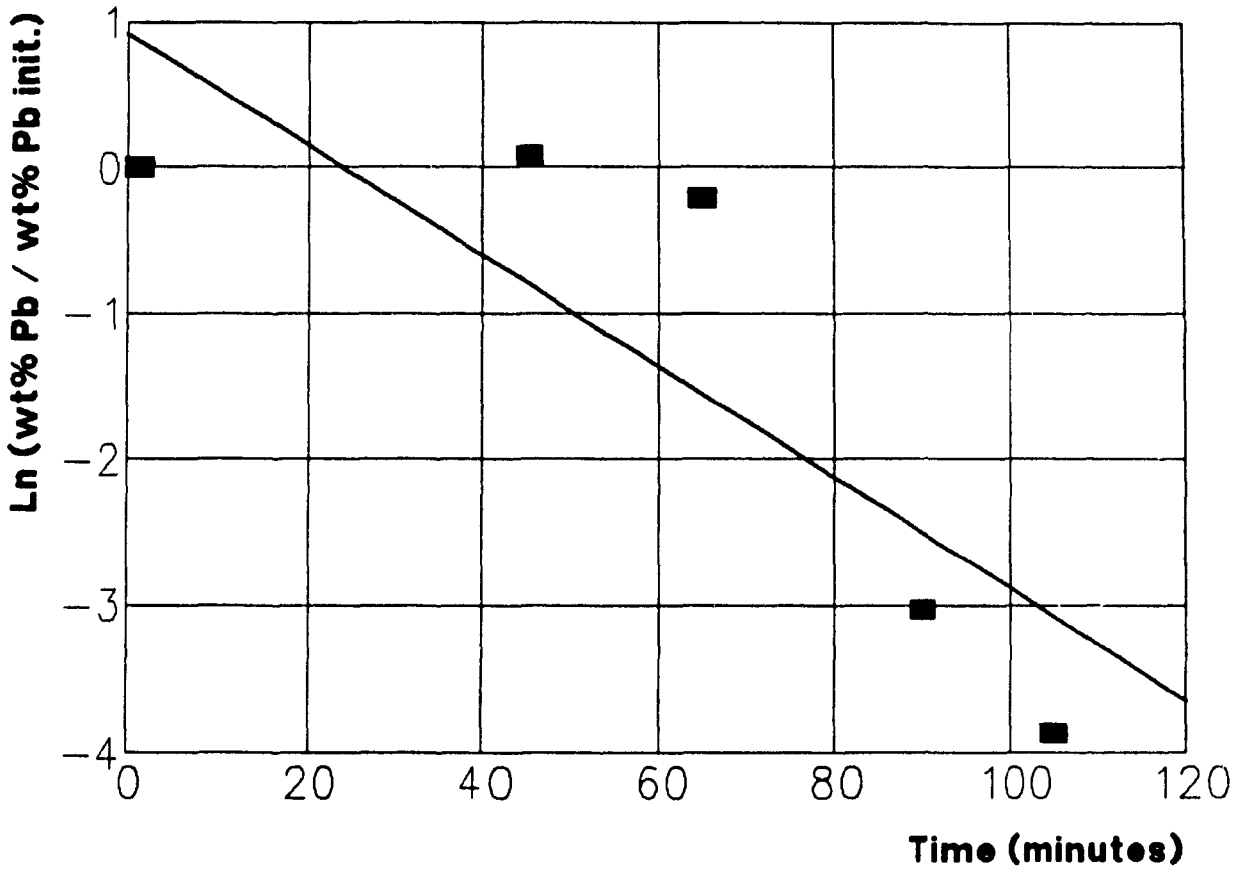

$y = -0.03837 x + 0.9361$

$R^2 = 0.70$

Fig. 7.20 : Bismuth Concentration vs Time, Experiment #4

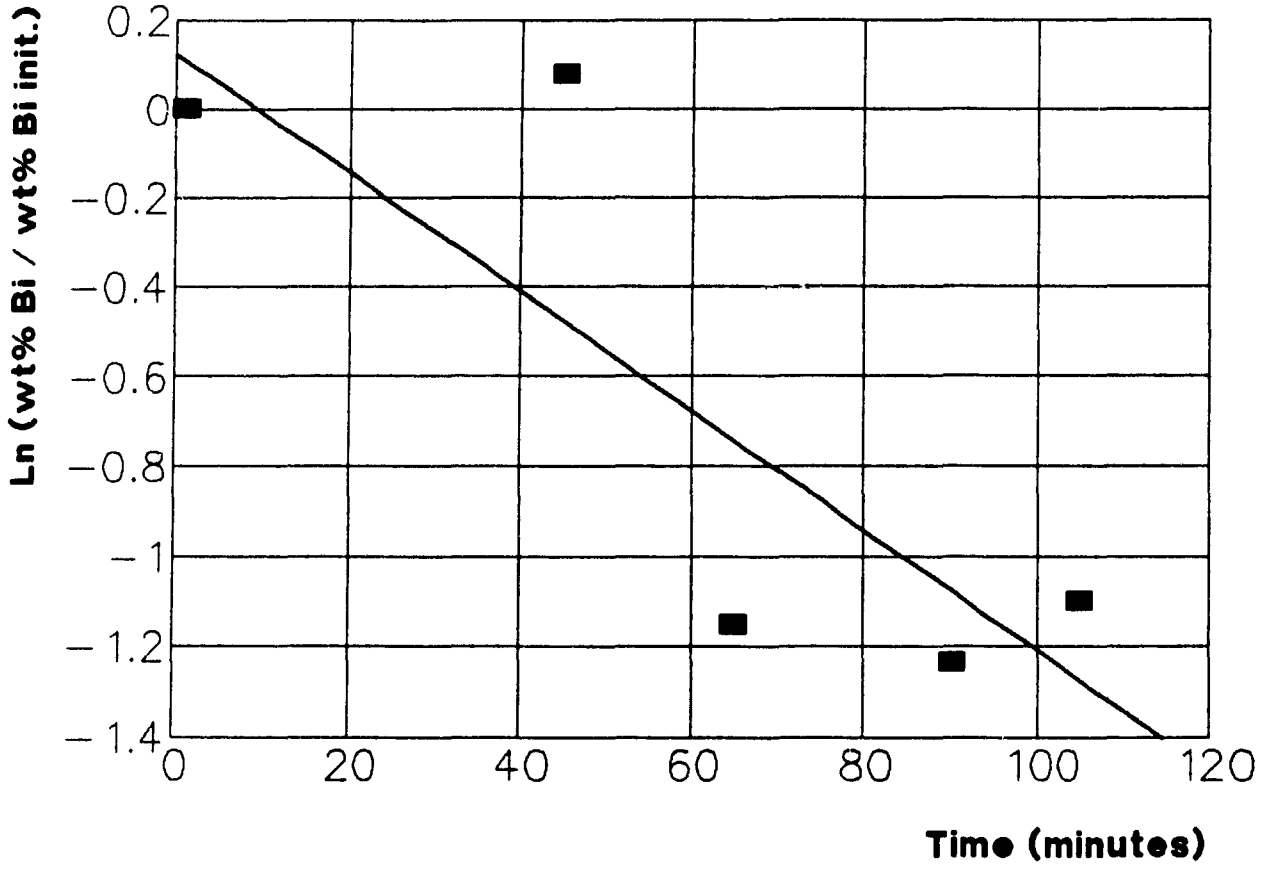

$y = -0.01329x + 0.1304$

$R^2 = 0.69$

Fig. 7.21 : Arsenic Concentration vs Time, Experiment #4

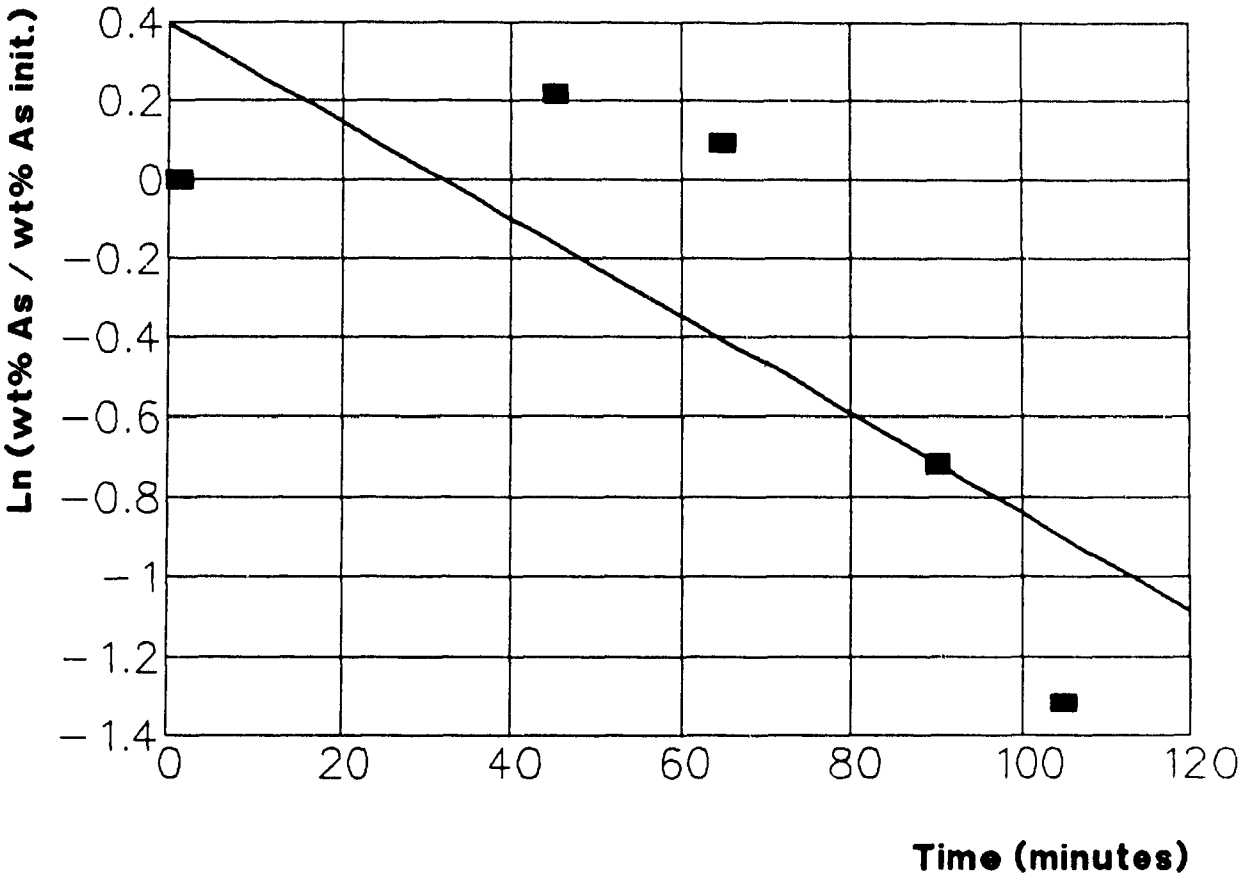

$y = -0.01209x + 0.3929$

$R^2 = 0.59$

Fig. 7.22 : Antimony Concentration vs Time

Experiment #4

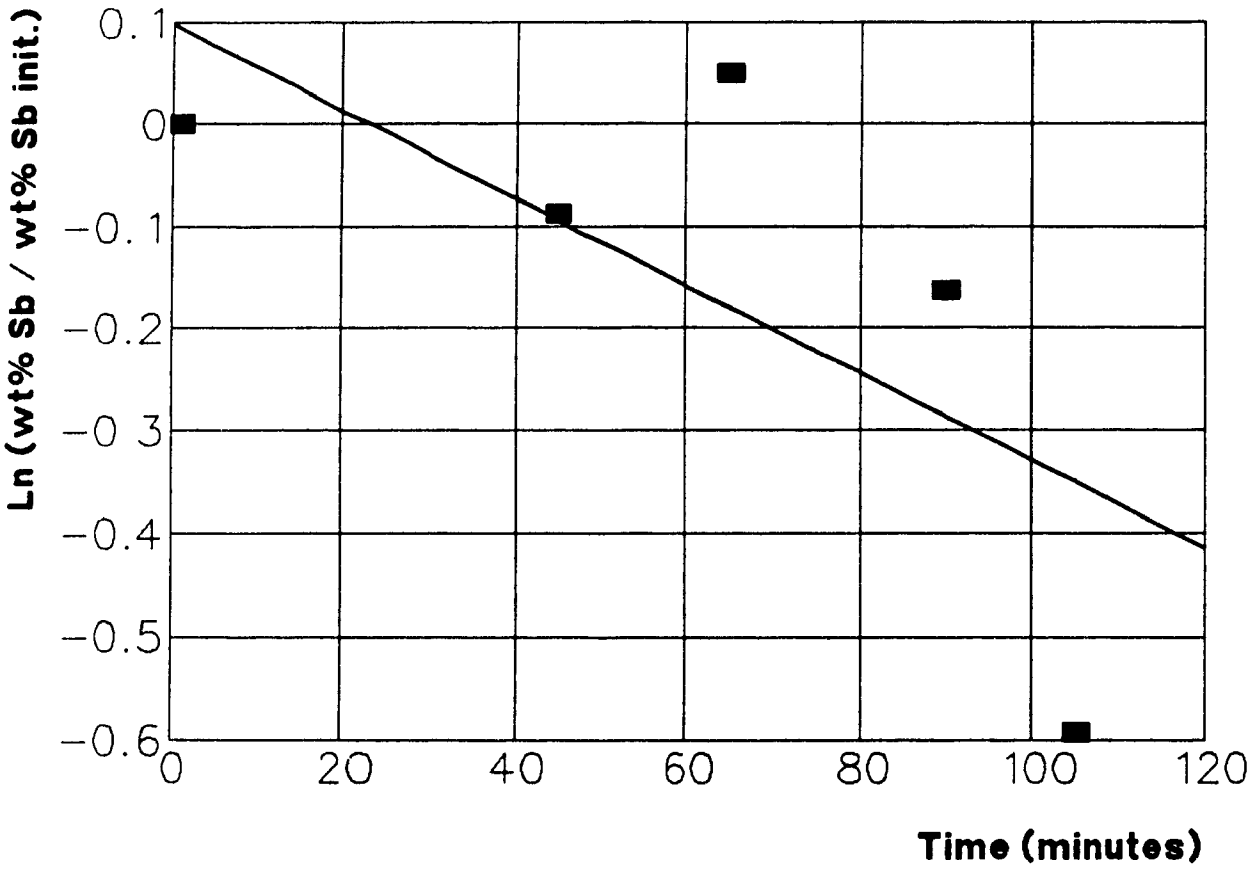

$y = -0.00435x + 0.1055$

$R^2 = 0.48$

Fig. 7.23 : Lead Concentration vs Time, Experiment #5

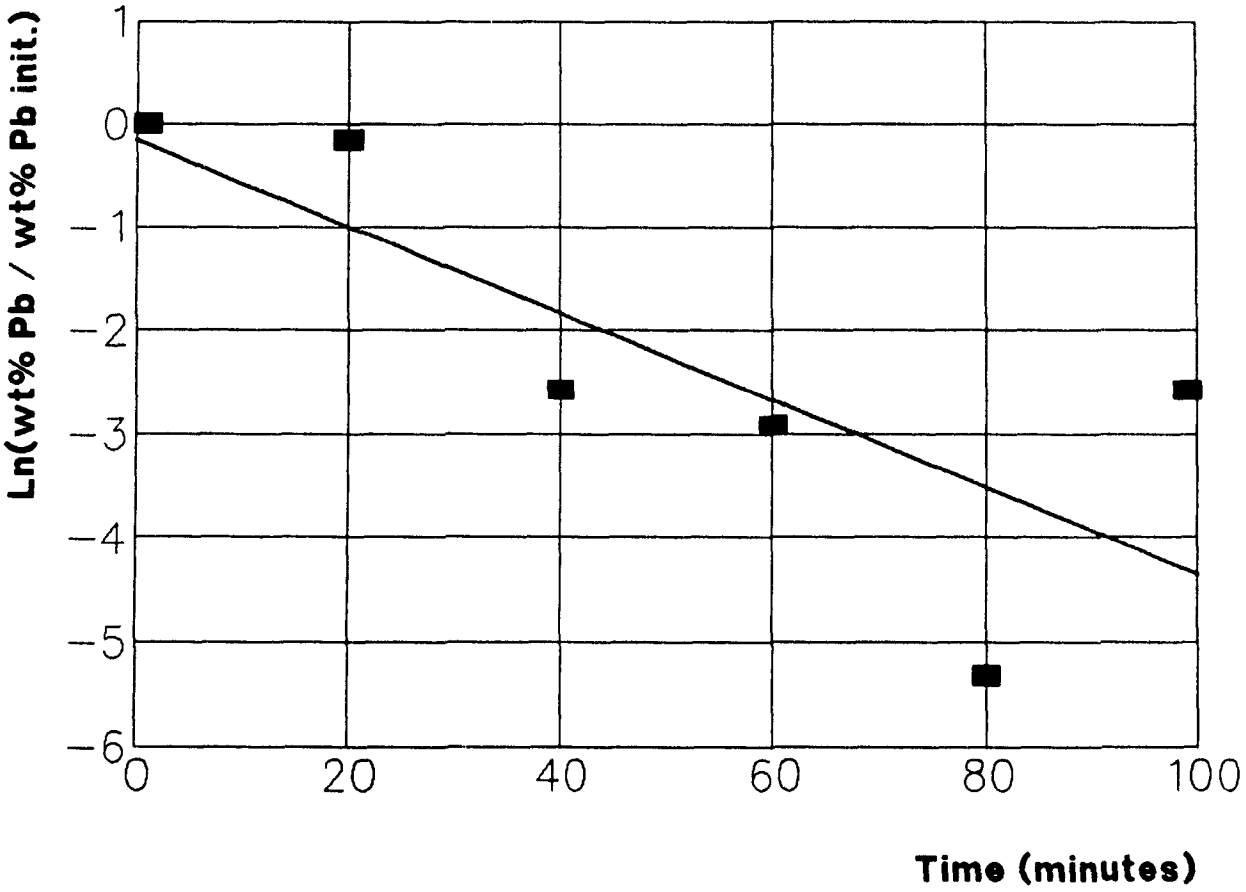

$y = -0.041x - 0.2080$

$R^2 = 0.60$

Fig. 7.24 : Bismuth Concentration vs Time, Experiment #5

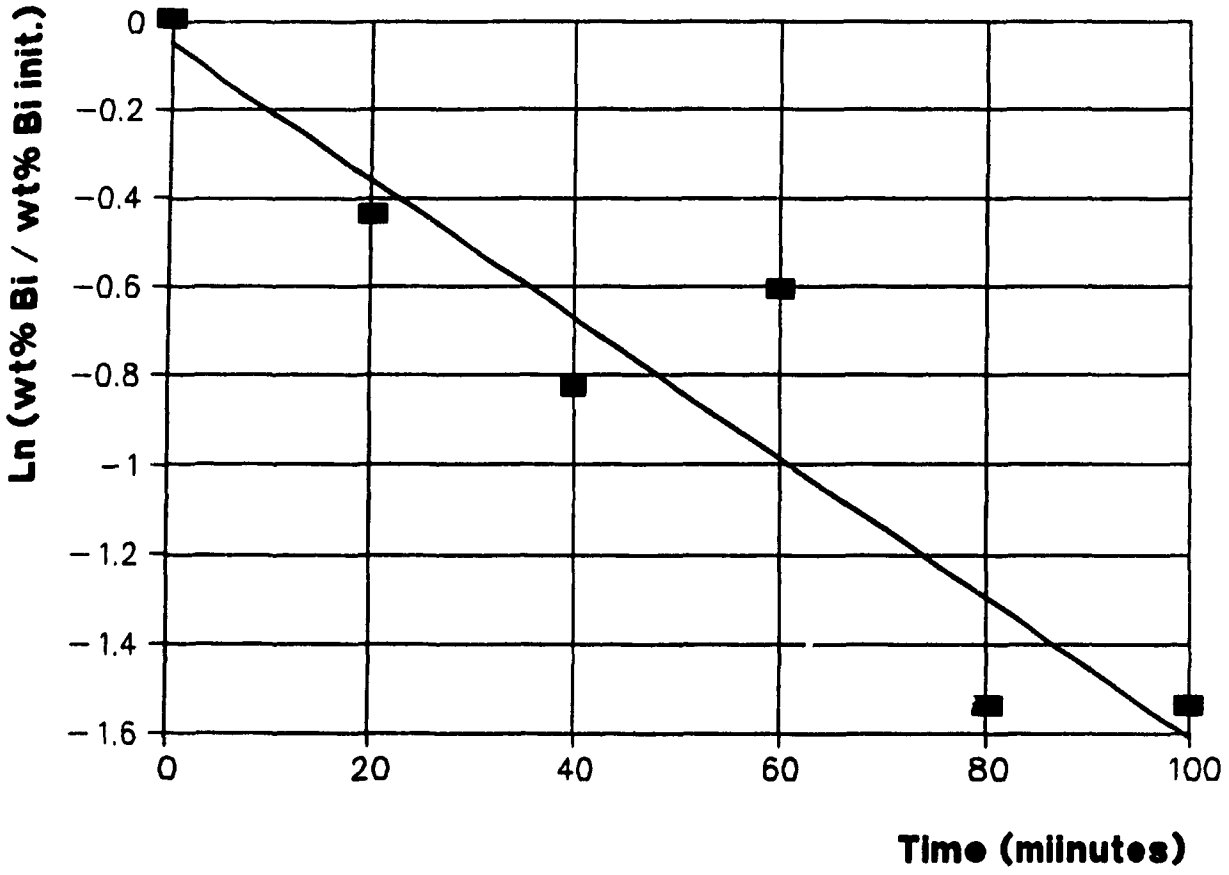

$y = -0.0154x - 0.05753$

$R^2 = 0.87$

Fig. 7.25 : Arsenic Concentration vs Time, Experiment #5

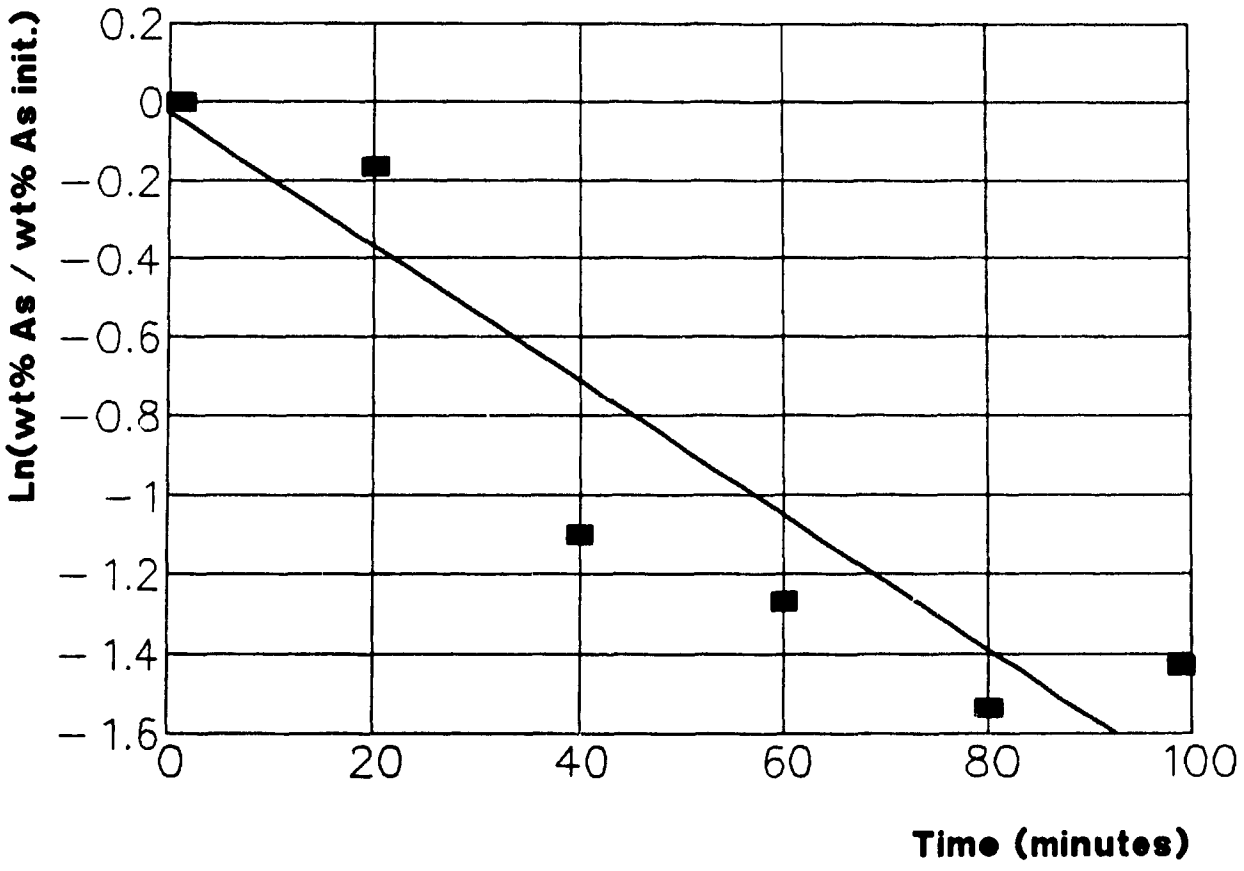

$y = -0.01633x - 0.09931$

$R^2 = 0.85$

Fig. 7.26 : Antimony Concentration vs Time

Experiment #5

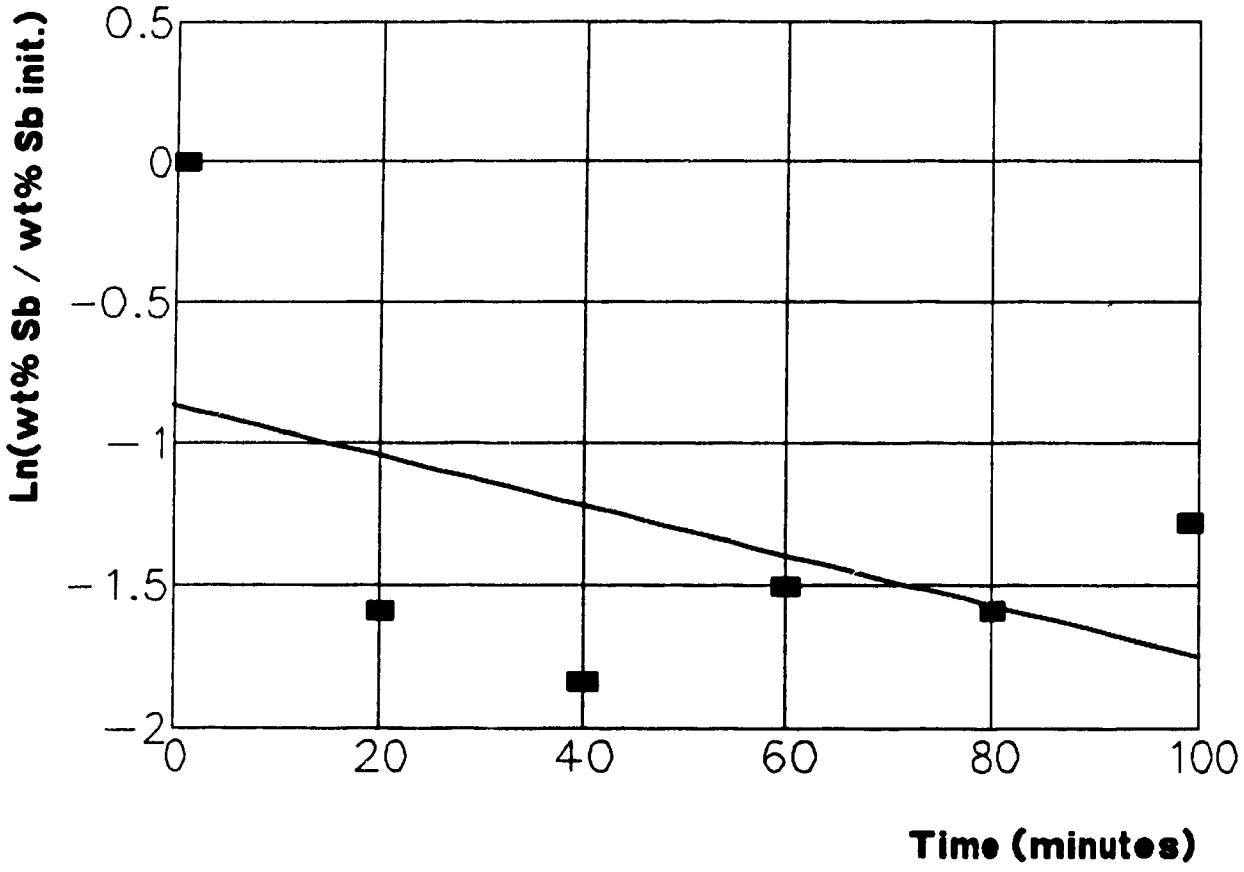

$y = -0.00867x - 0.8671$

$R^2 = 0.24$

Fig. 7.27 : Lead Concentration vs Time, Experiment #6

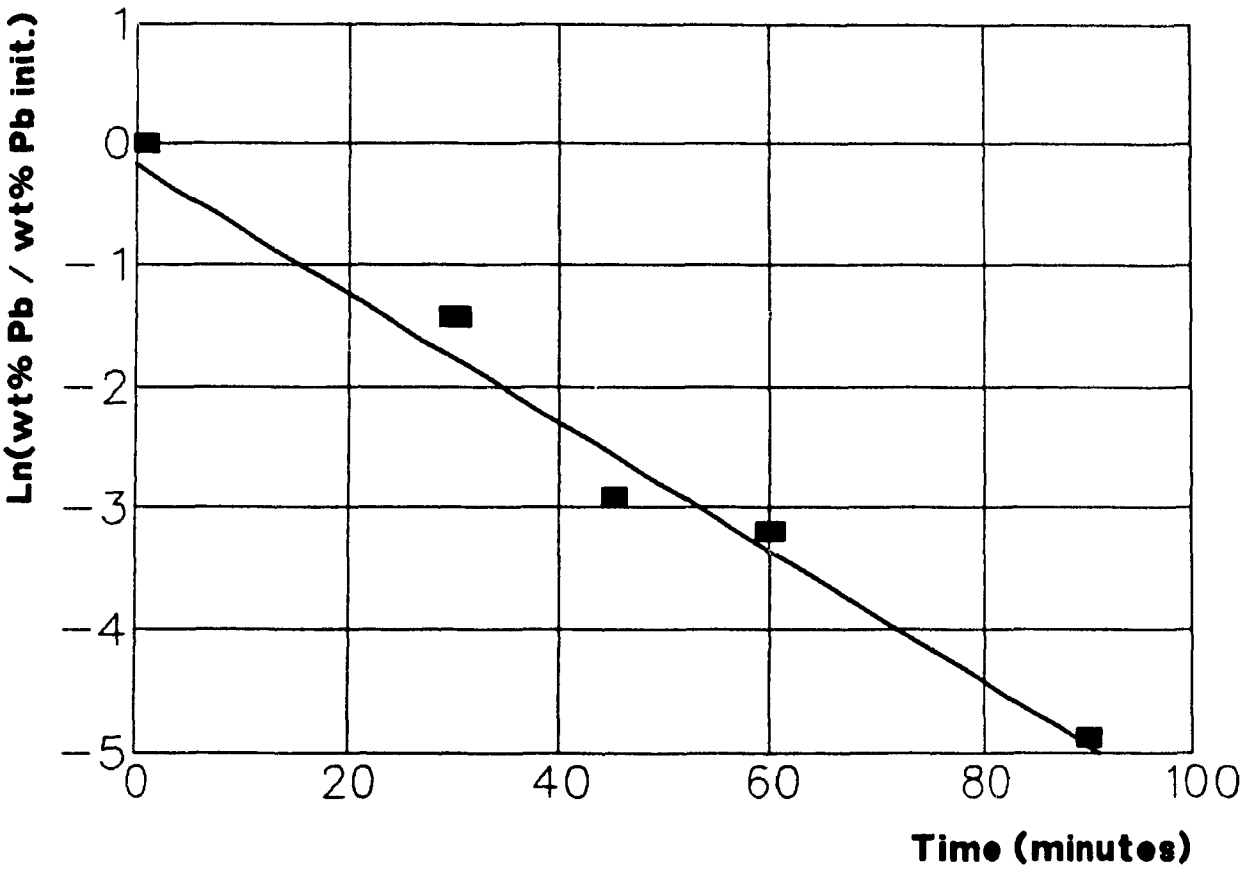

$y = -0.0547 x - 0.02266$

$R^2 = 0.98$

Fig. 7.28 : Bismuth Concentration vs Time, Experiment #6

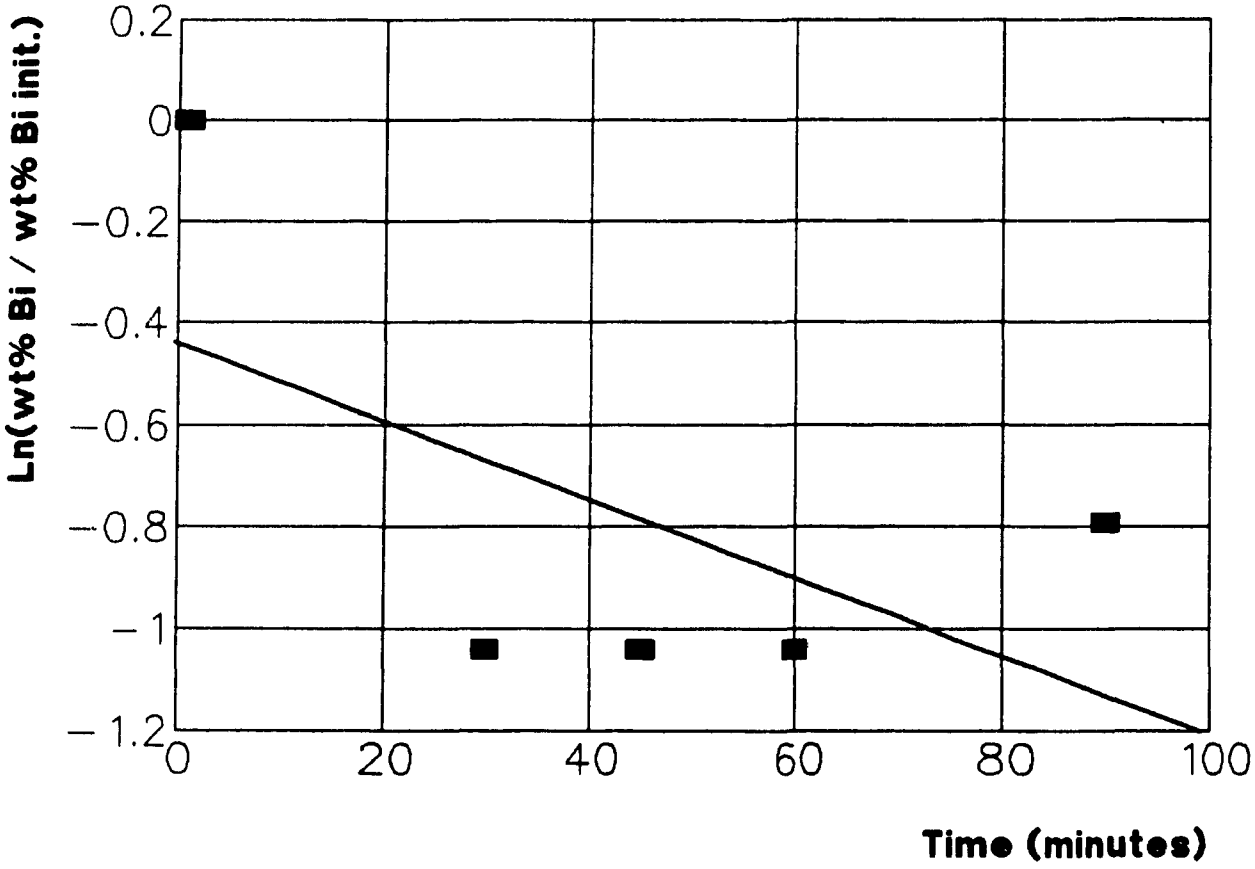

$y = -0.00791x - 0.4264$

$R^2 = 0.35$

Fig. 7.29 : Arsenic Concentration vs Time, Experiment #6

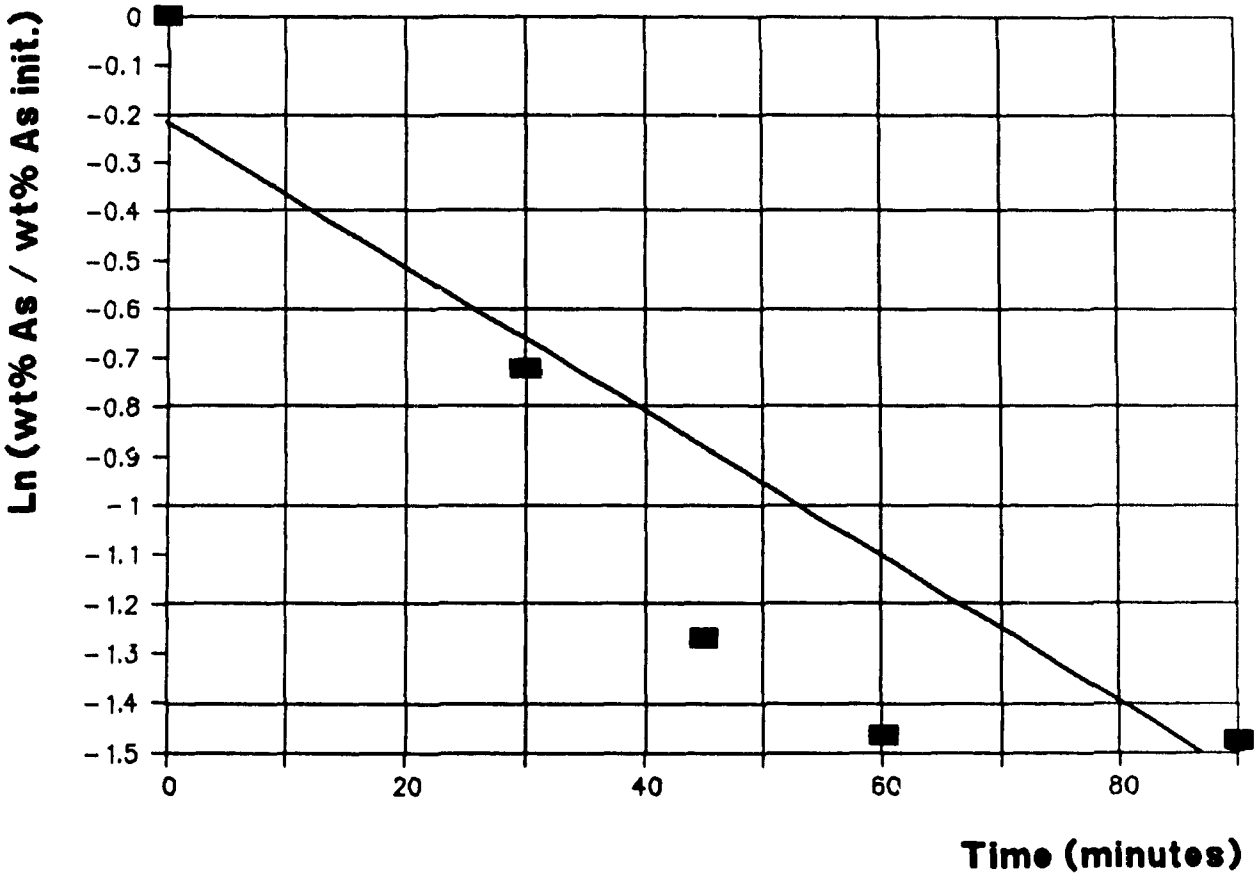

$y = -0.0173x - 0.2097$

$R^2 = 0.84$

Fig. 7.30 : Antimony Concentration vs time

Experiment #6

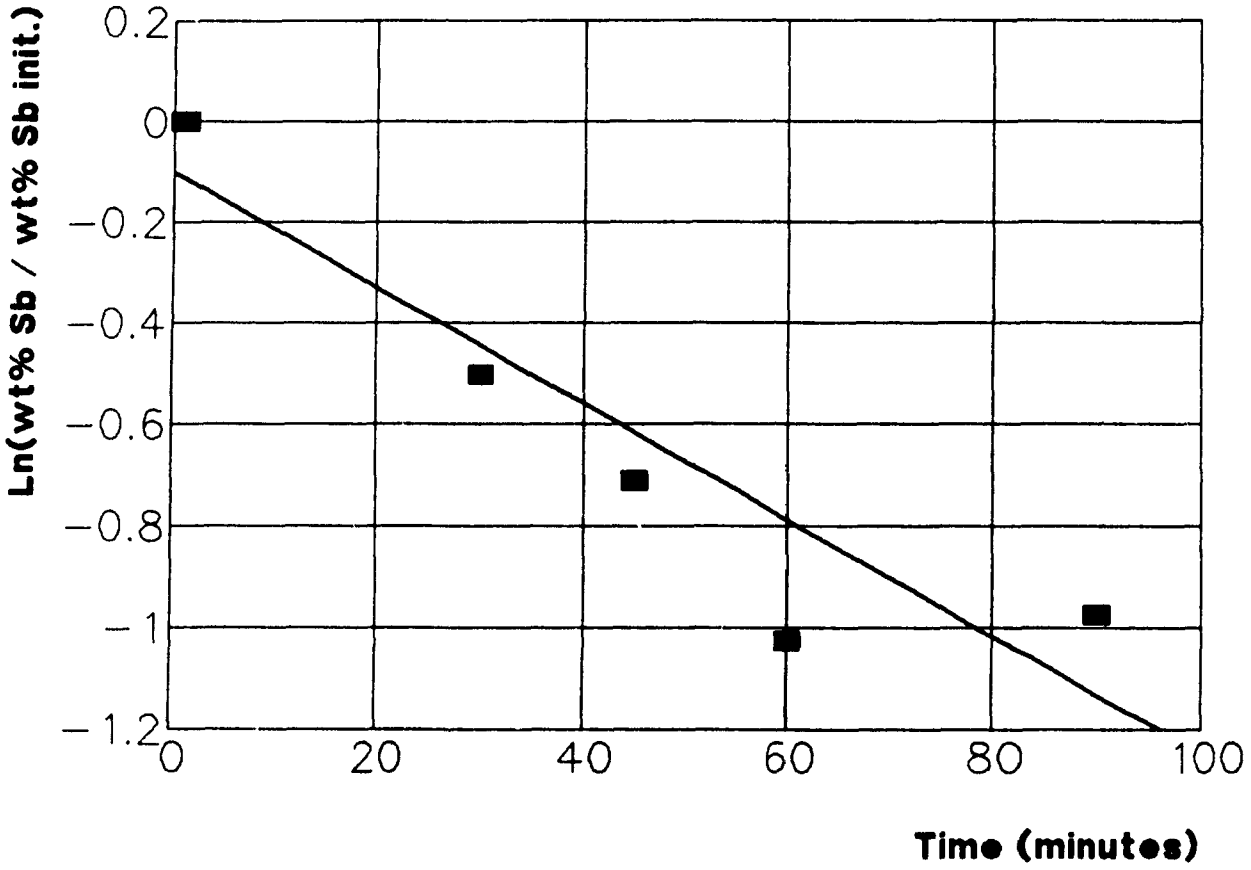

$y = -0.01148\,x - 0.1267$

$R^2 = 0.86$

Fig. 7.31 : Lead Concentration vs Time, Experiment #7

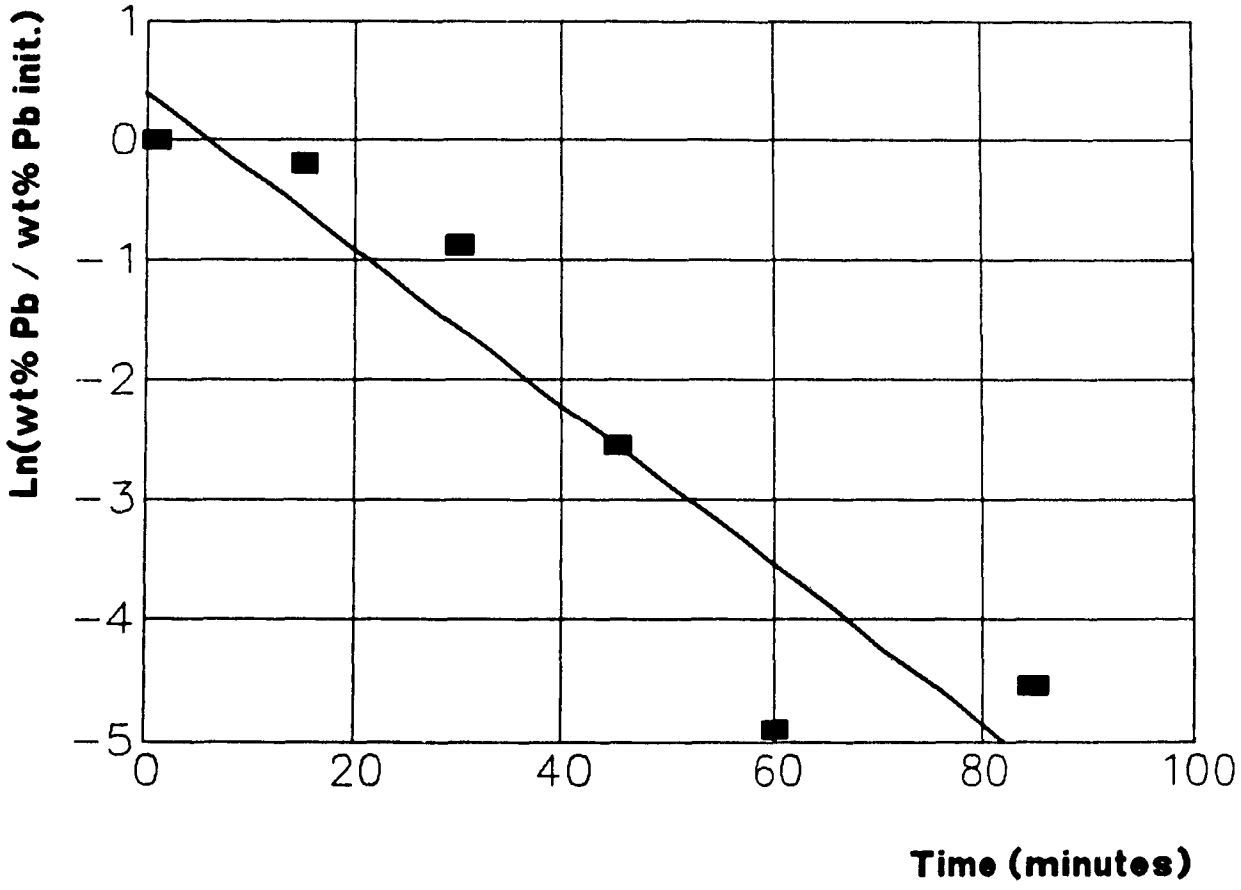

$y = -0.06535\,x + 0.3851$

$R^2 = 0.87$

Fig. 7.32 : Bismuth Concentration vs Time, Experiment #7

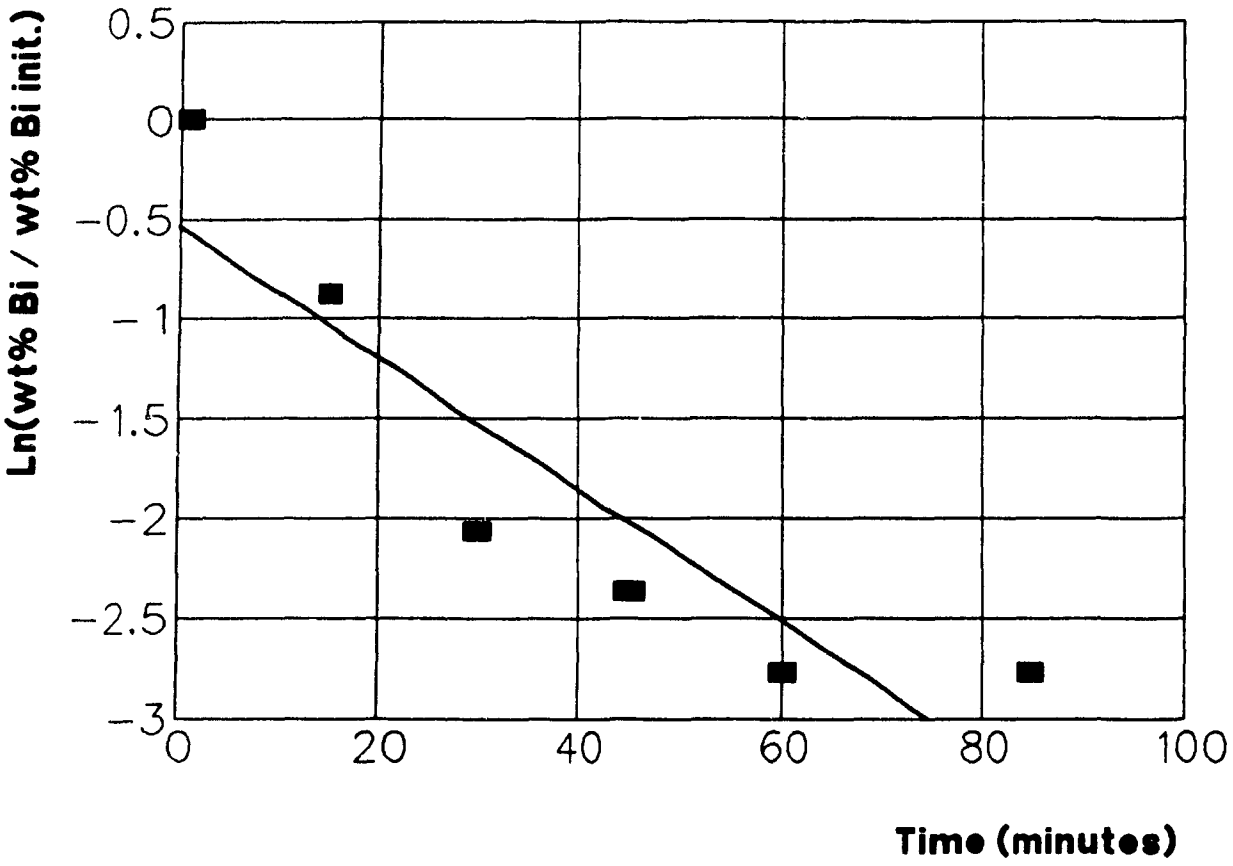

$y = -0.03324 - 0.5066$

$R^2 = 0.83$

Fig. 7.33 : Arsenic Concentration vs Time, Experiment #7

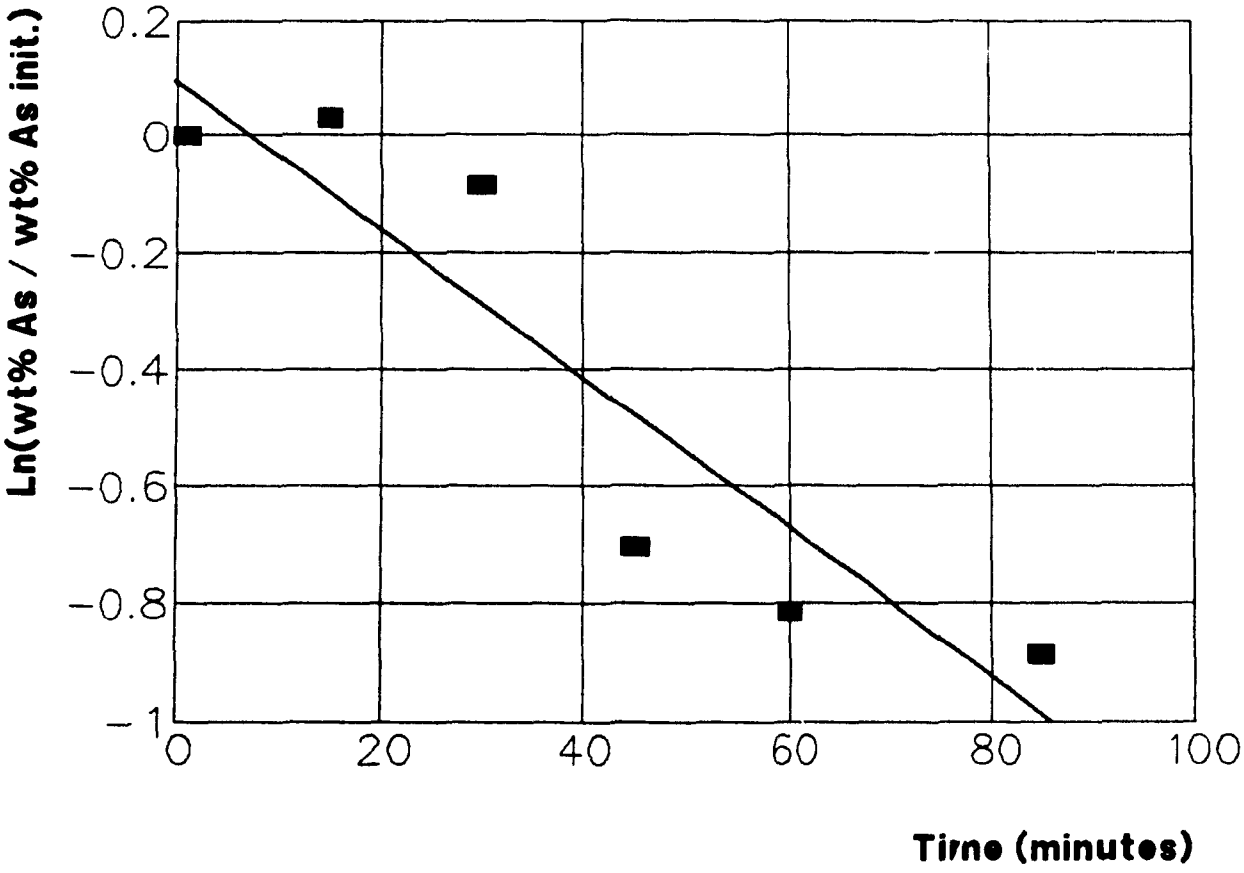

$y = -0.01291x + 0.09596$

$R^2 = 0.84$

Fig. 7.34 : Antimony Concentration vs Time

Experiment #7

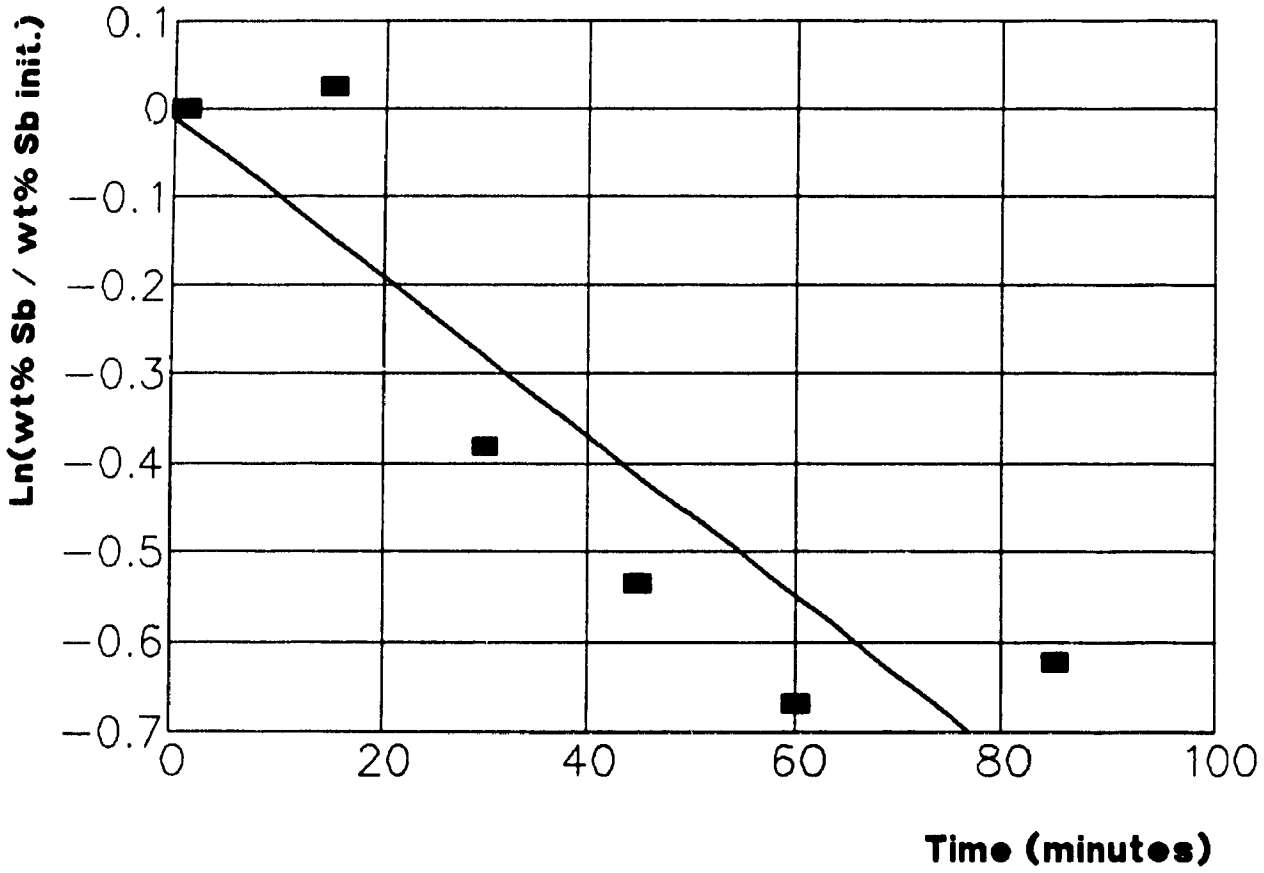

$y = -0.00895\,x - 0.01366$

$R^2 = 0.81$

Fig. 7.35 : Lead Concentration vs Time, Experiment #8

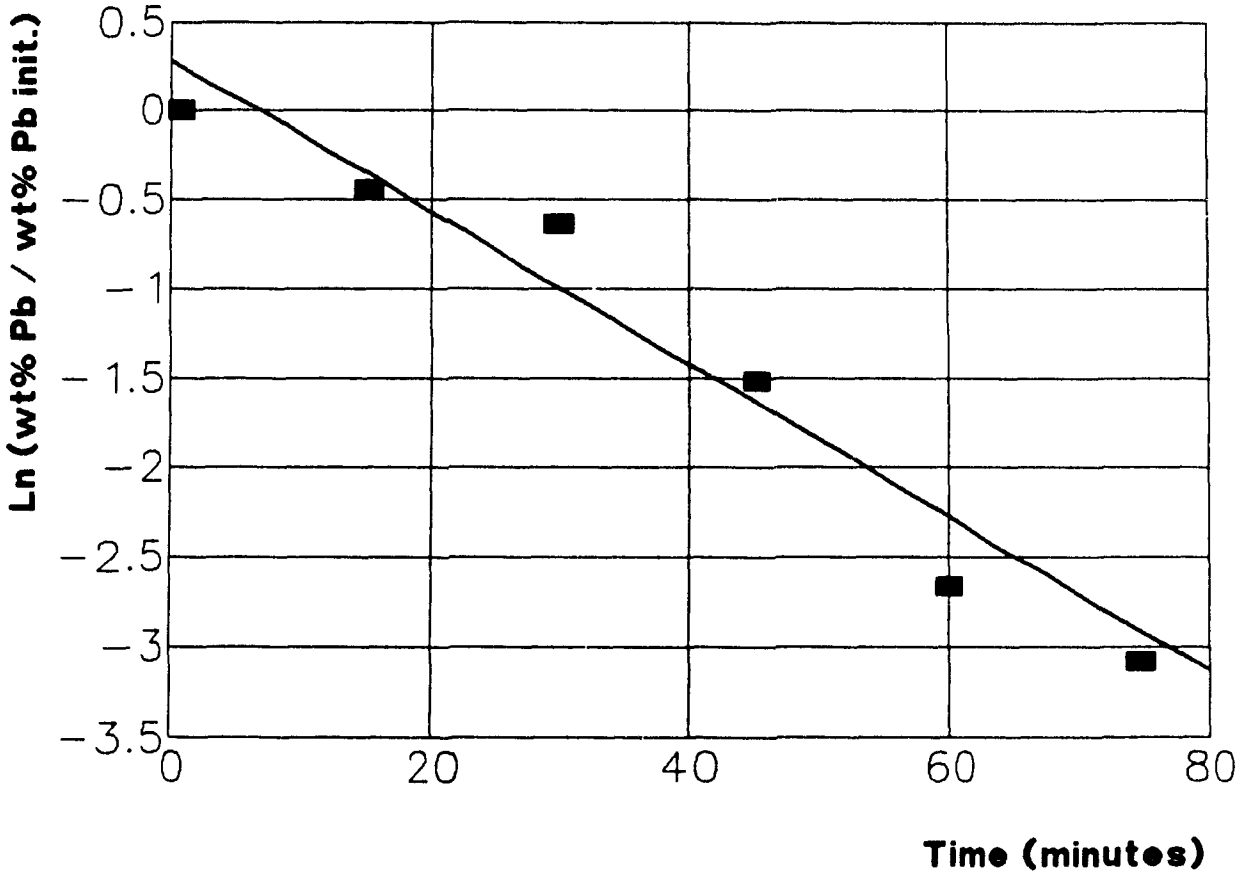

$y = -0.04365 + 0.2478$

$R^2 = 0.95$

Fig. 7.36 : Bismuth Concentration vs Time, Experiment #8

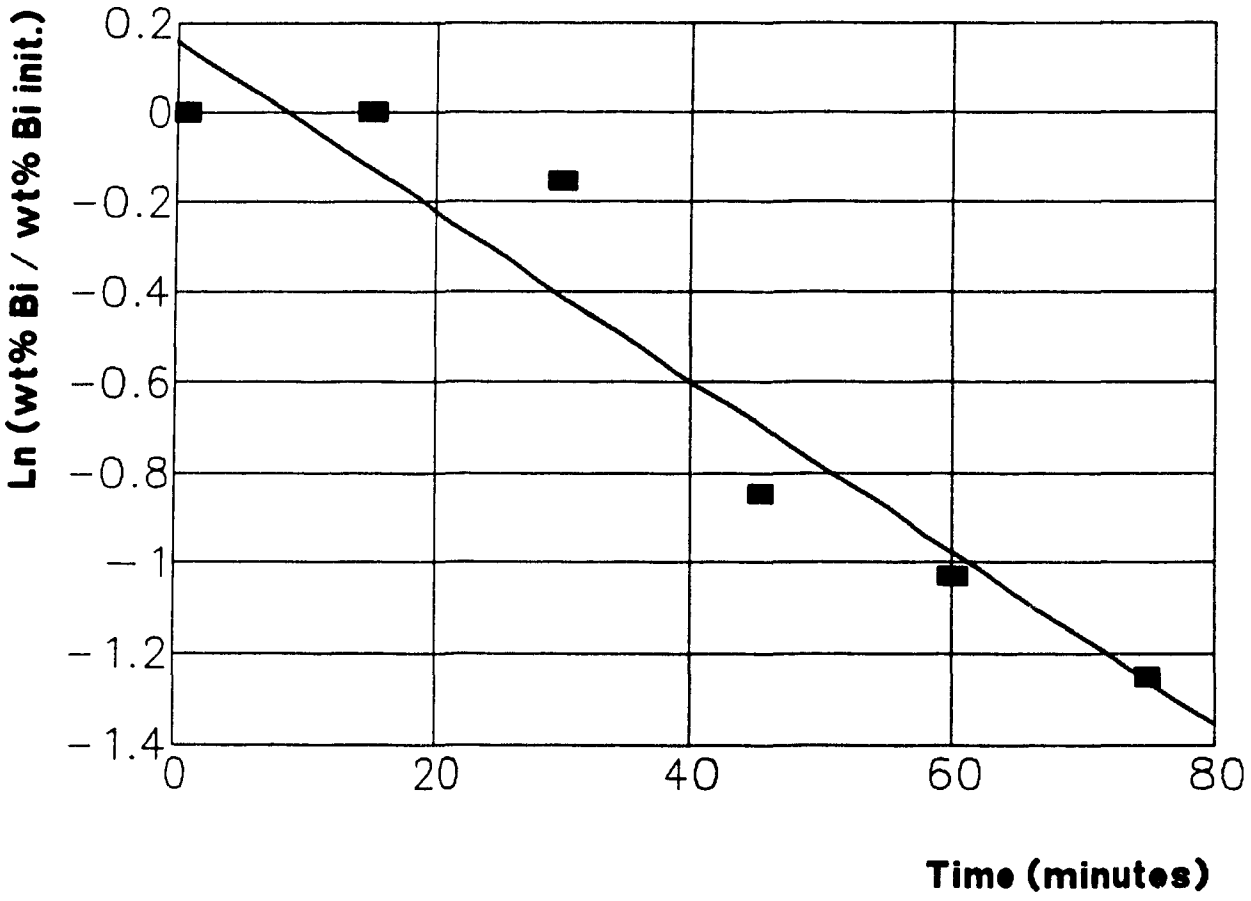

$y = -0.01913x + 0.1703$

$R^2 = 0.92$

Fig. 7.37 : Arsenic Concentration vs Time, Experiment #8

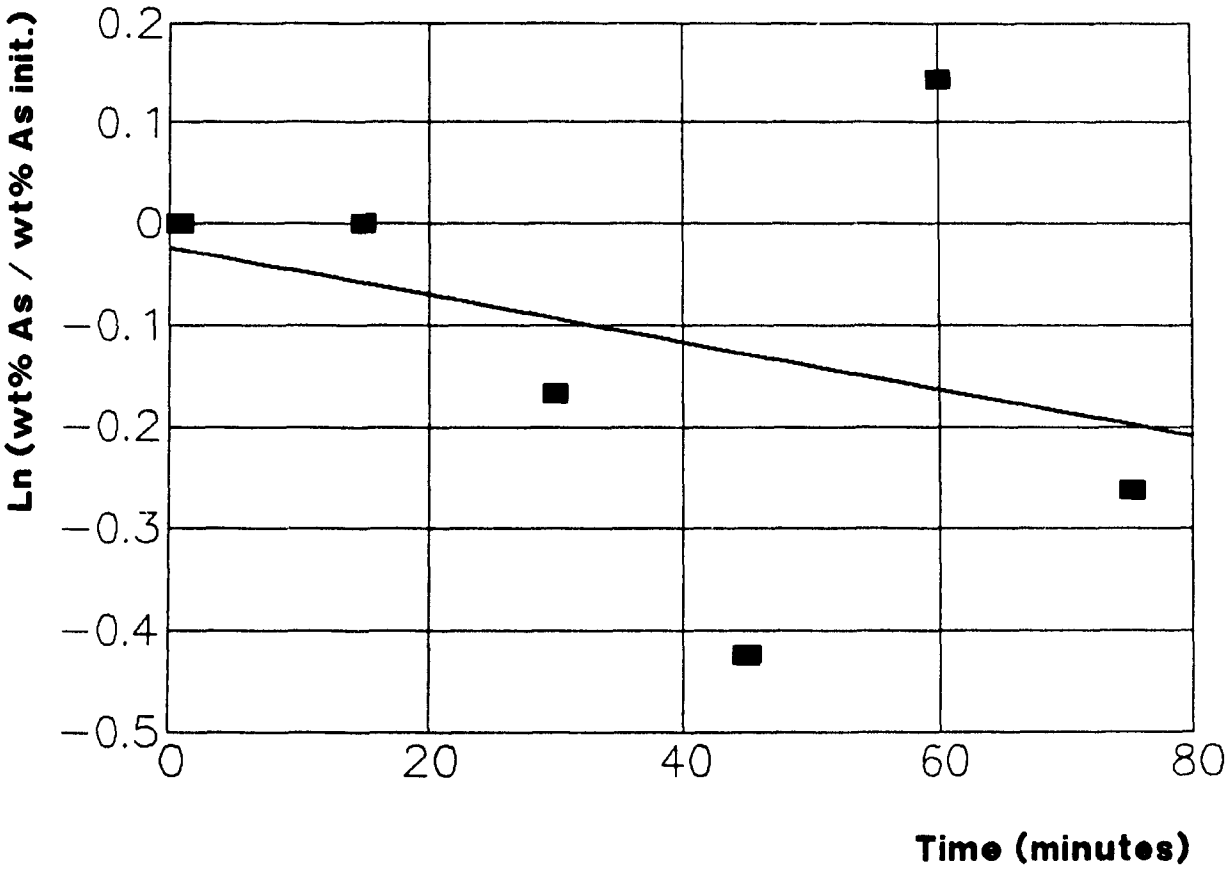

$y = -0.00217 - 0.03708$

$R^2 = 0.09$

Fig. 7.38 : Antimony Concentration vs Time Experiment #8

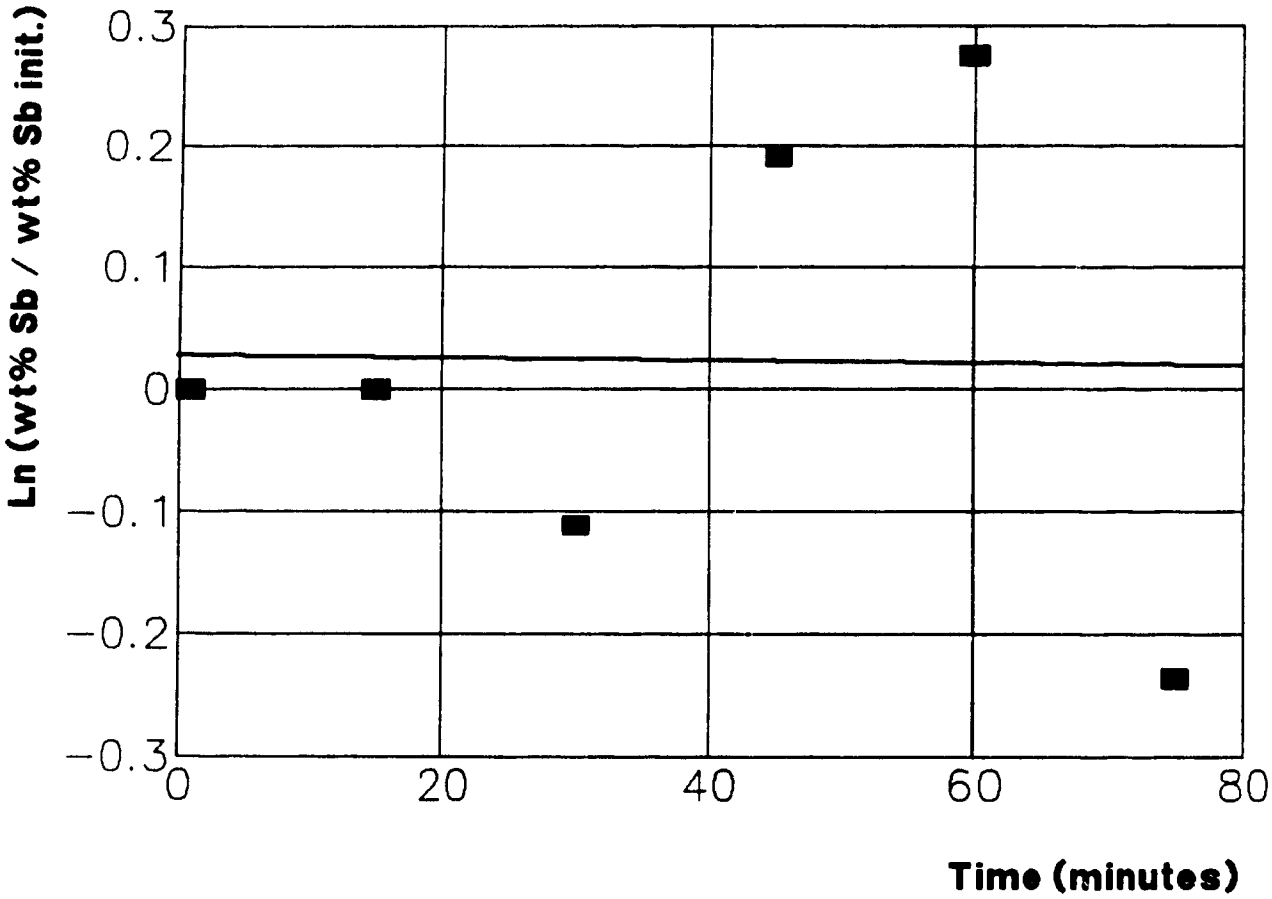

$y = -0.00011x + 0.02367$

$R^2 = 0.0003$

Fig. 7.39 : Lead Concentration vs Time, Experiment #9

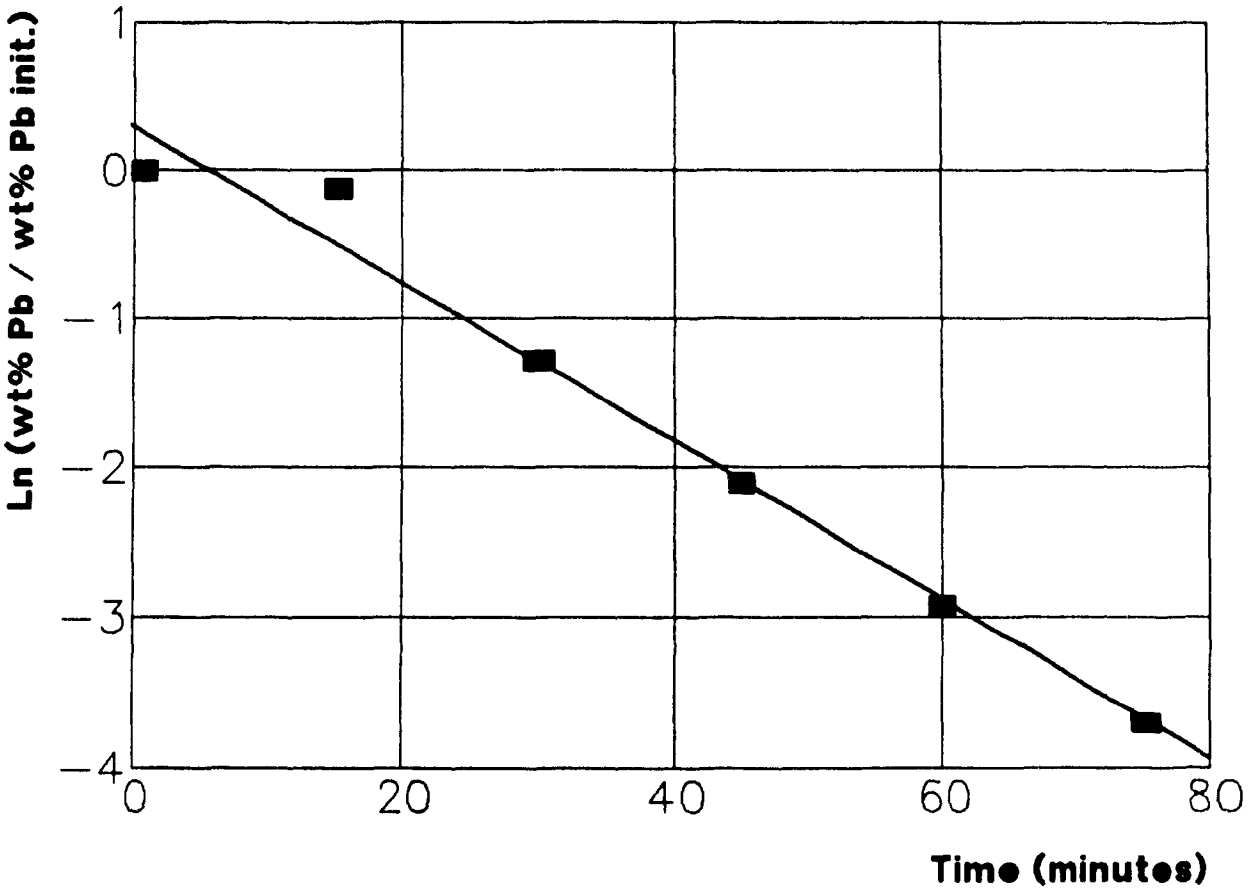

$y = -0.05284x + 0.2902$

$R^2 = 0.98$

Fig. 7.40 : Bismuth Concentration vs Time, Experiment #9

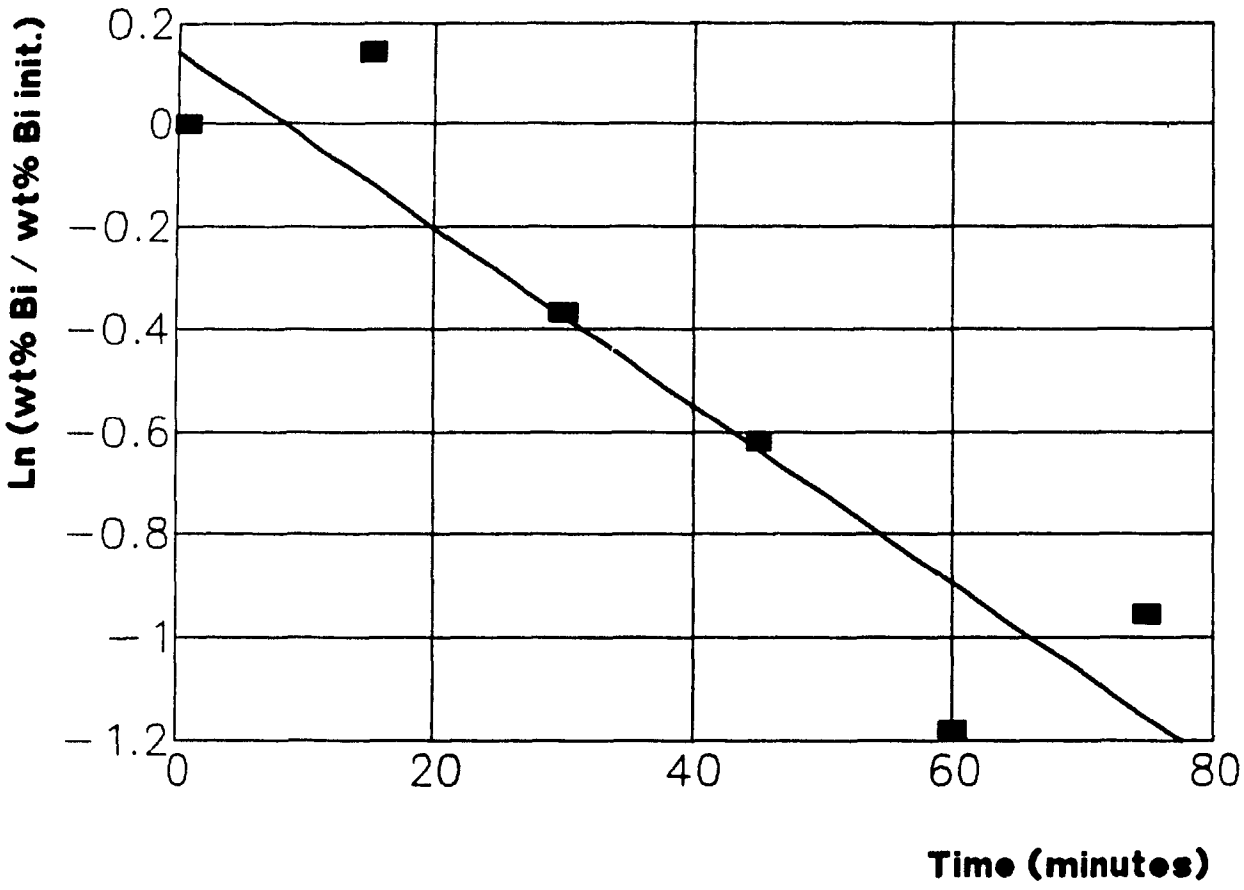

$y = -0.01713x + 0.1461$

$R^2 = 0.85$

Fig. 7.41 : Arsenic Concentration vs Time, Experiment #9

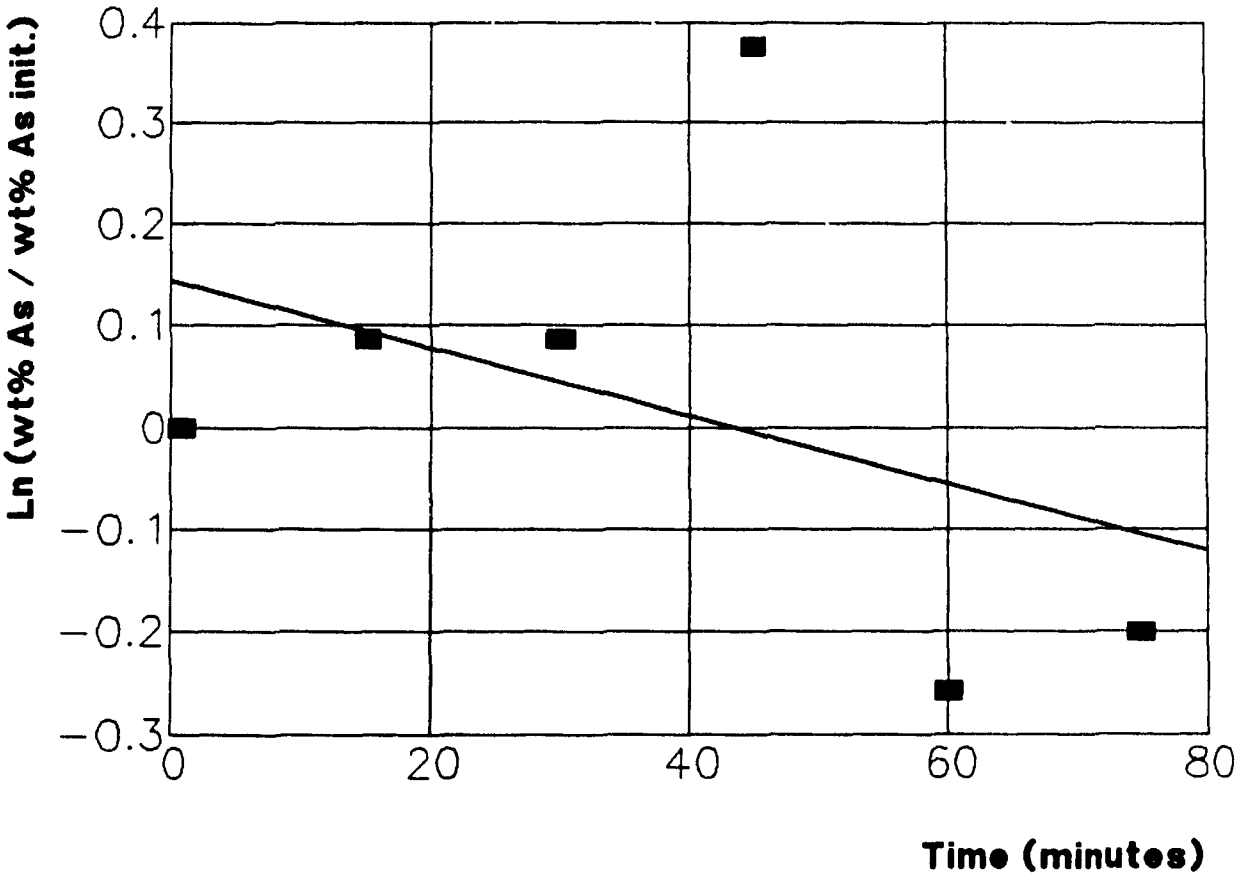

$y = -0.00333 x + 0.1401$

$R^2 = 0.17$

Fig. 7.42 : Antimony Concentration vs Time Experiment #9

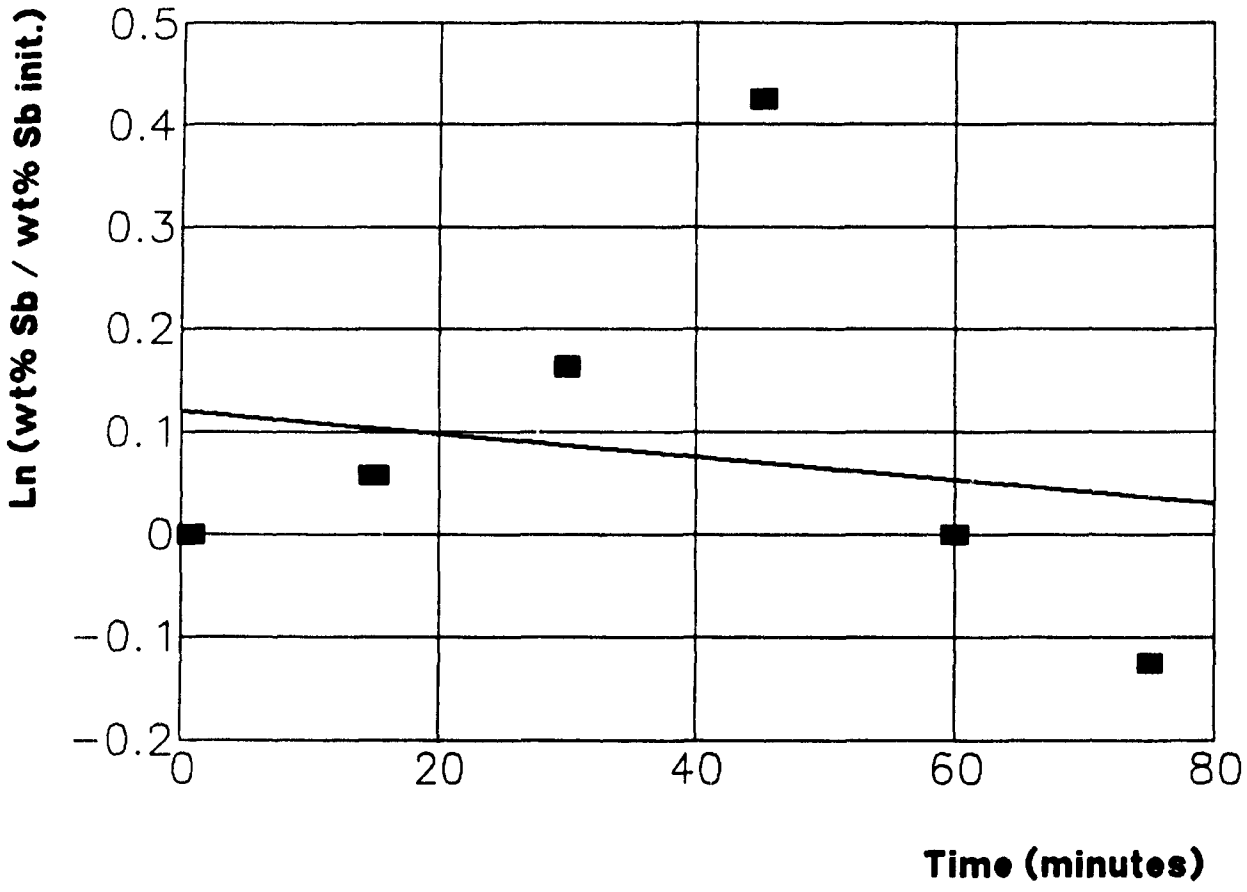

$y = -0.00102x + 0.1248$

$R^2 = 0.02$

Fig. 7.43 : Lead Concentration vs Time, Experiment #10

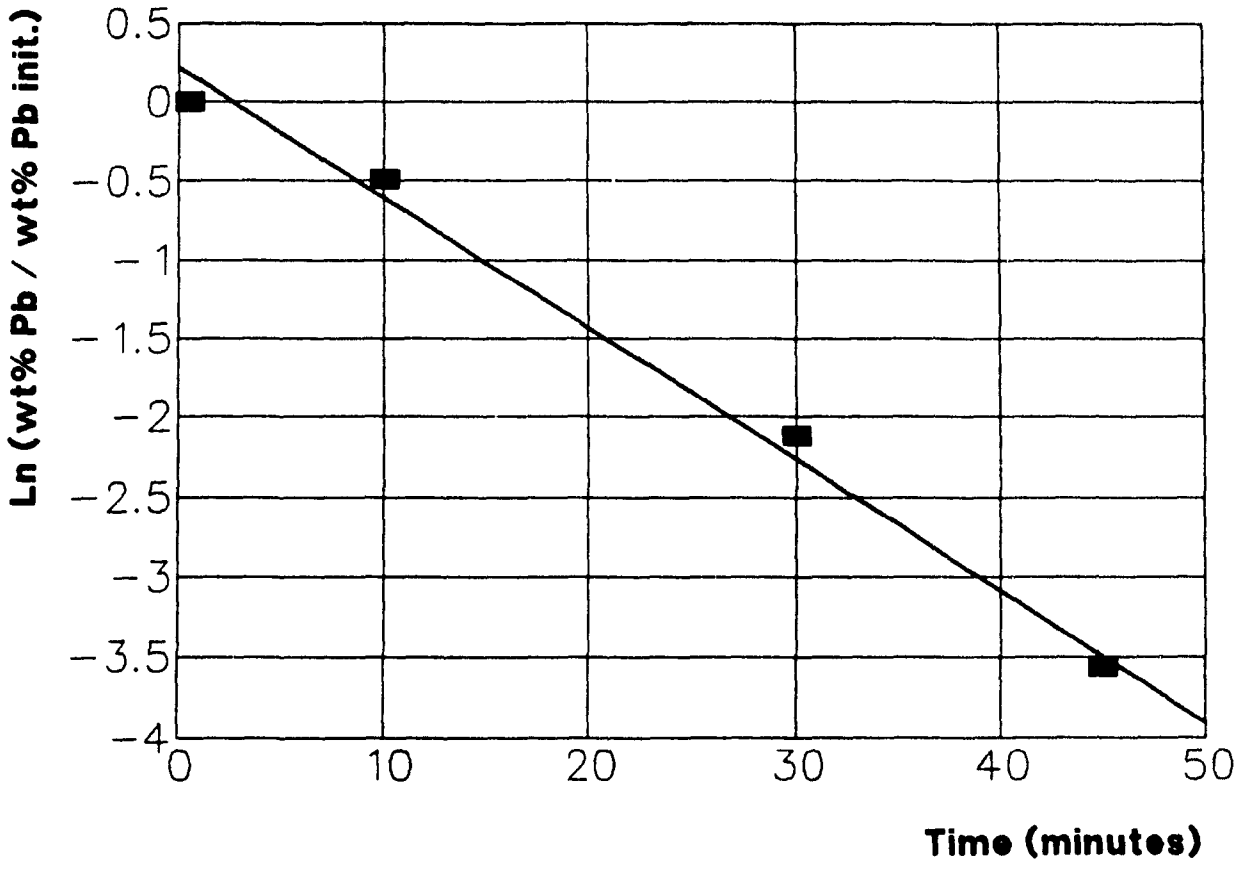

$y = -0.08007 + 0.1589$

$R^2 = 0.99$

Fig. 7.44 : Bismuth Concentration vs Time, Experiment #10

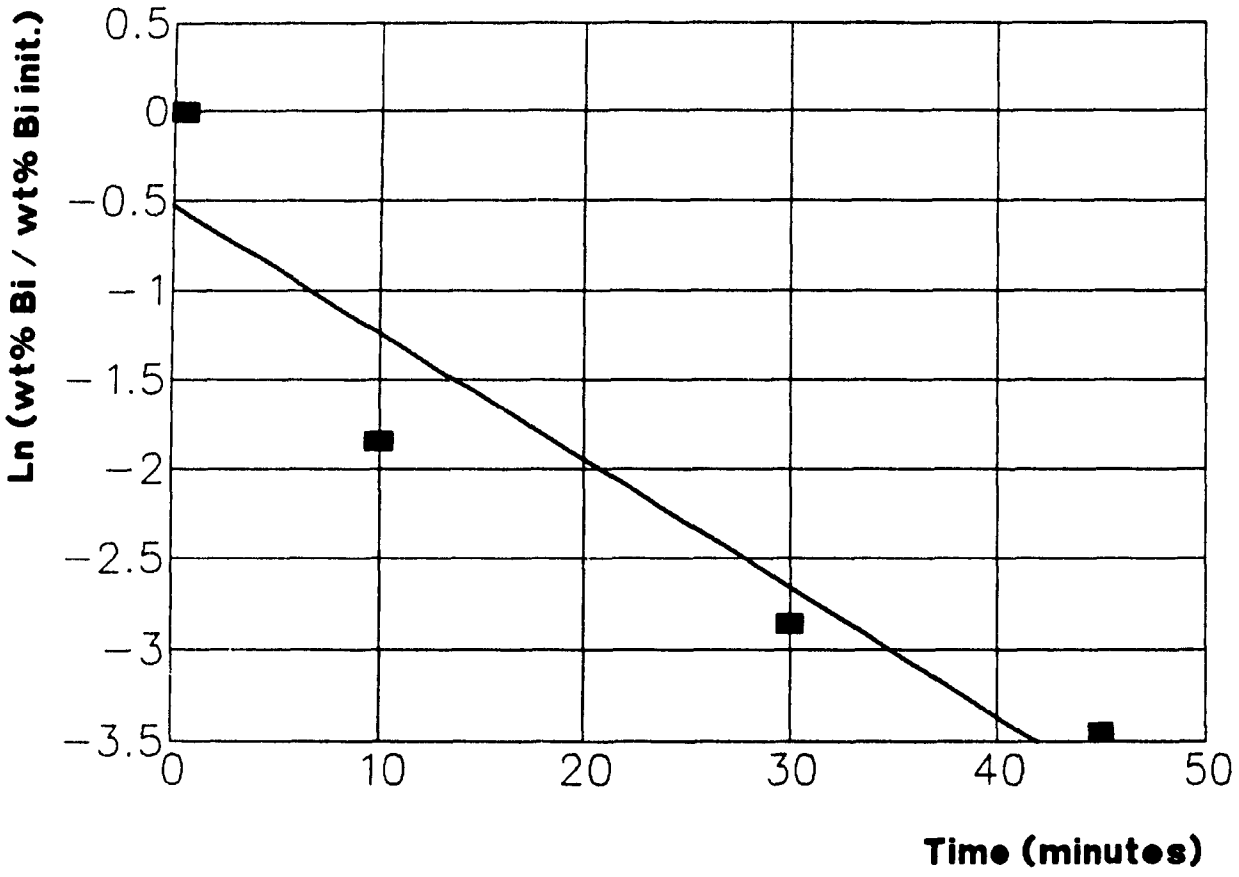

$y = -0.07077x - 0.534$

$R^2 = 0.89$

Fig. 7.45 : Arsenic Concentration vs Time, Experiment #10

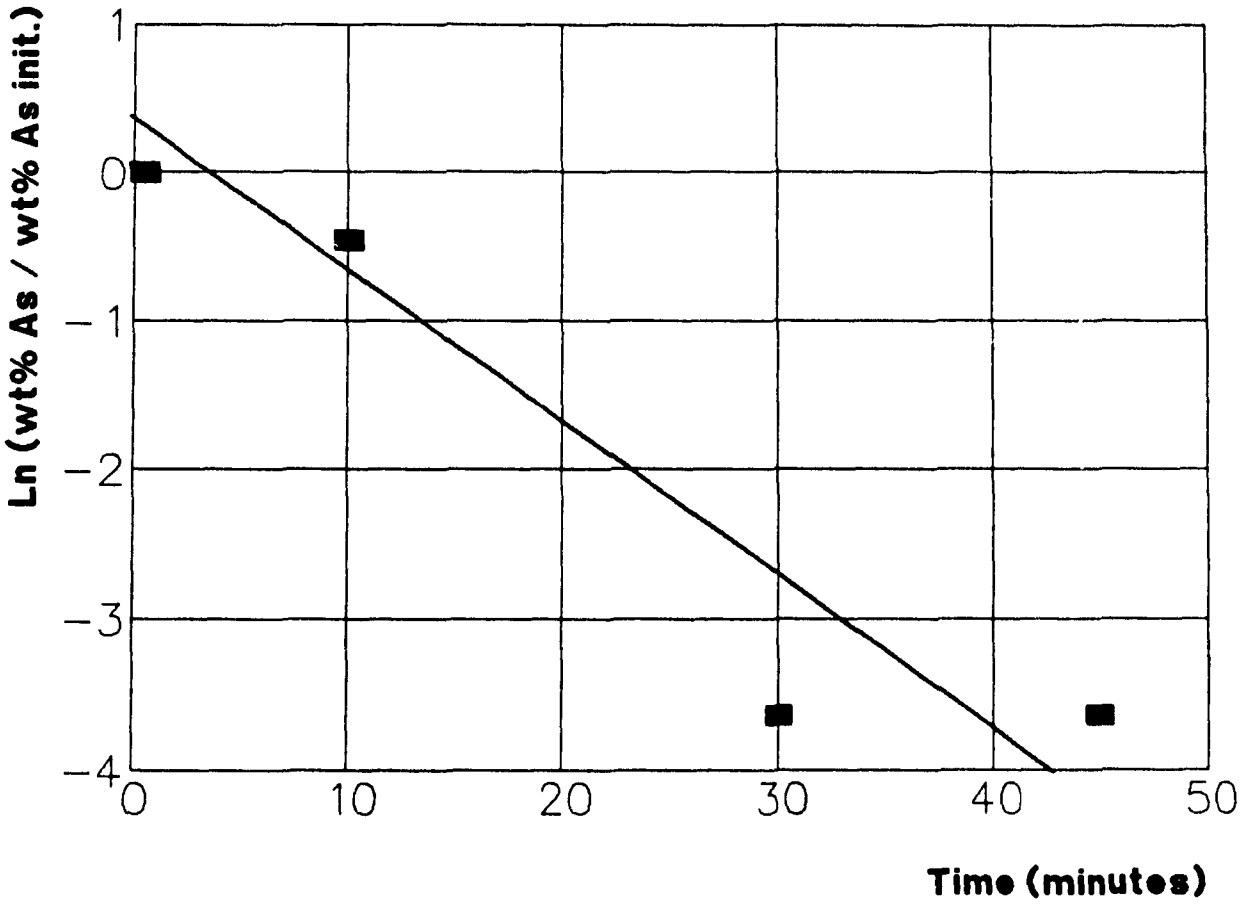

$y = -0.09276 + 0.03748$

$R^2 = 0.89$

Fig. 7.46 : Antimony Concentration vs Time

Experiment #10

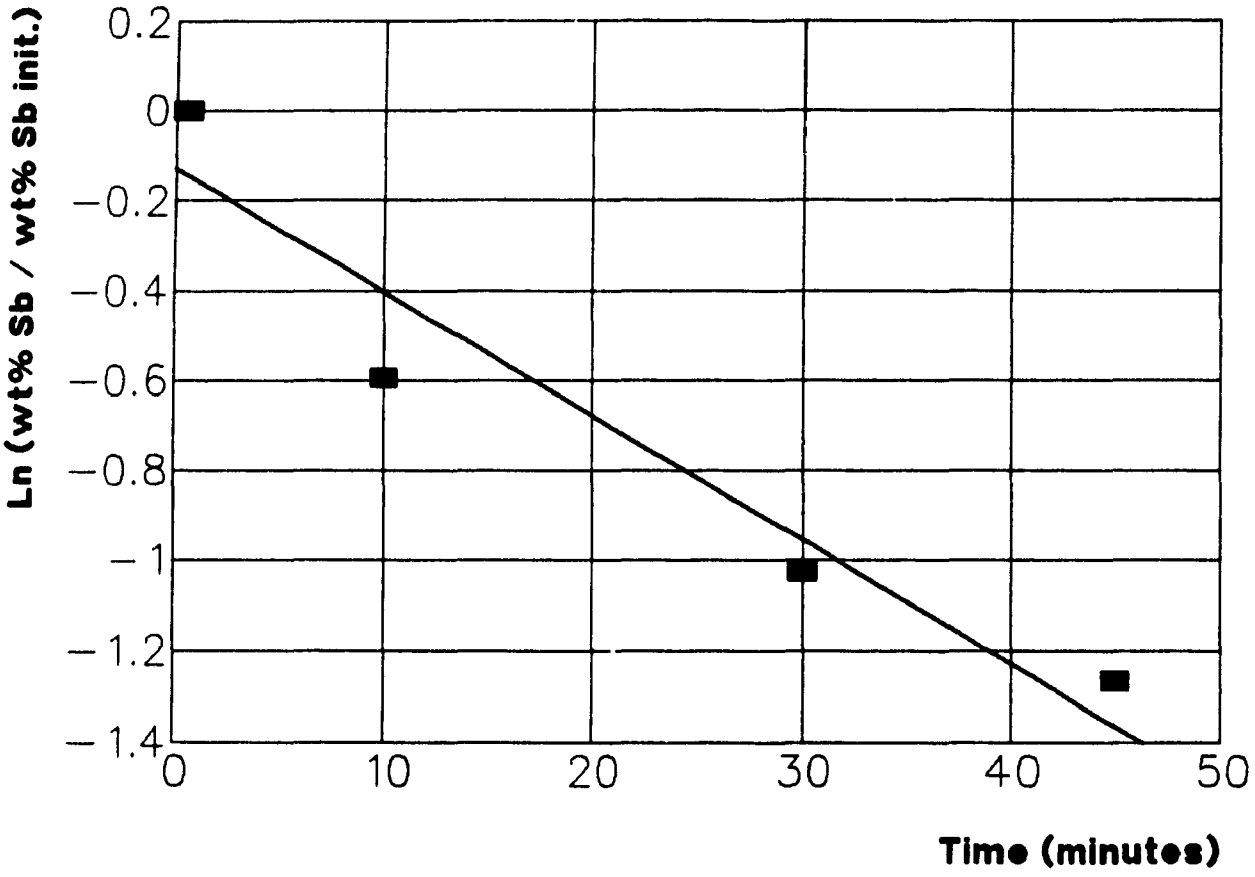

$y = -0.02652 - 0.1578$

$R^2 = 0.93$

Fig. 7.47 : Lead Concentration vs Time, Experiment #11

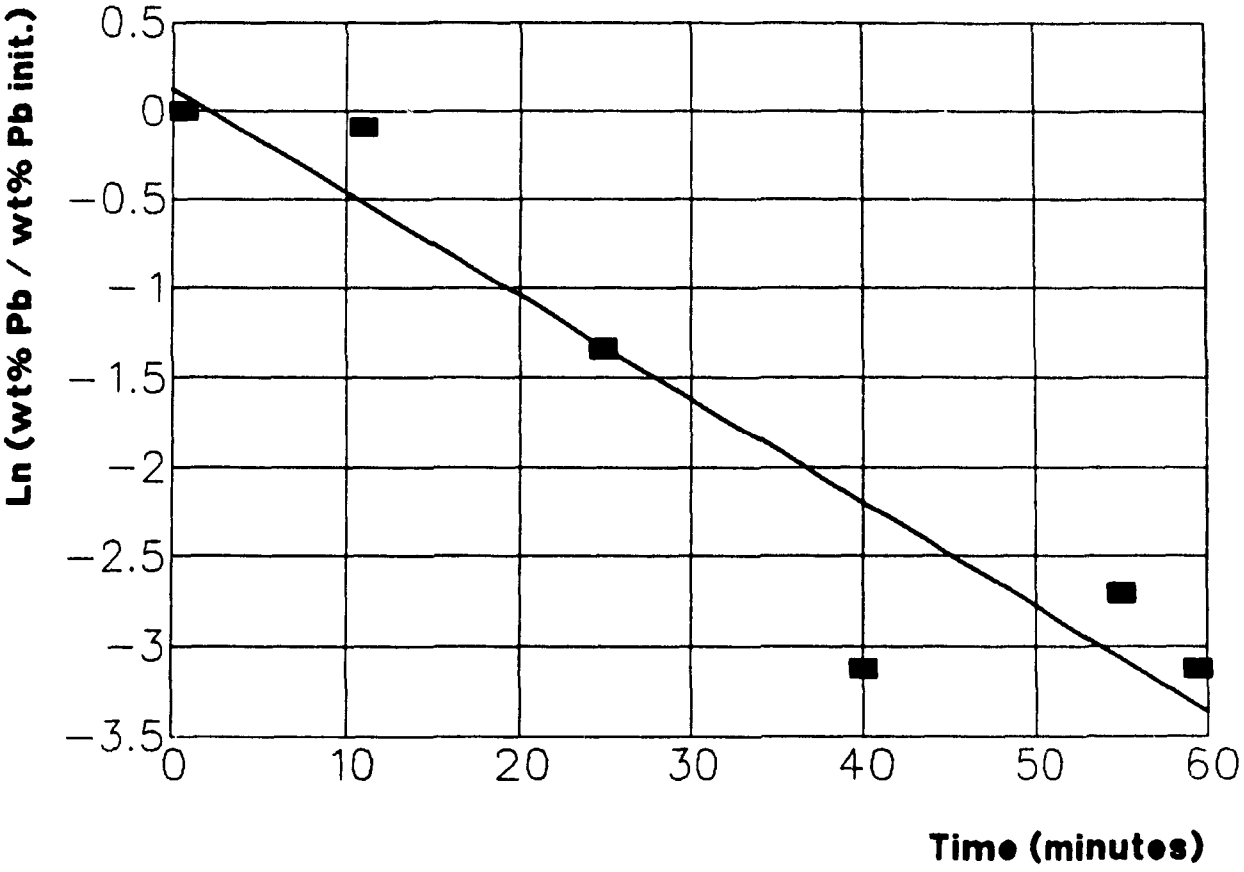

$y = -0.05717 + 0.08921$

$R^2 = 0.88$

Fig. 7.48 : Bismuth Concentration vs Time, Experiment #11

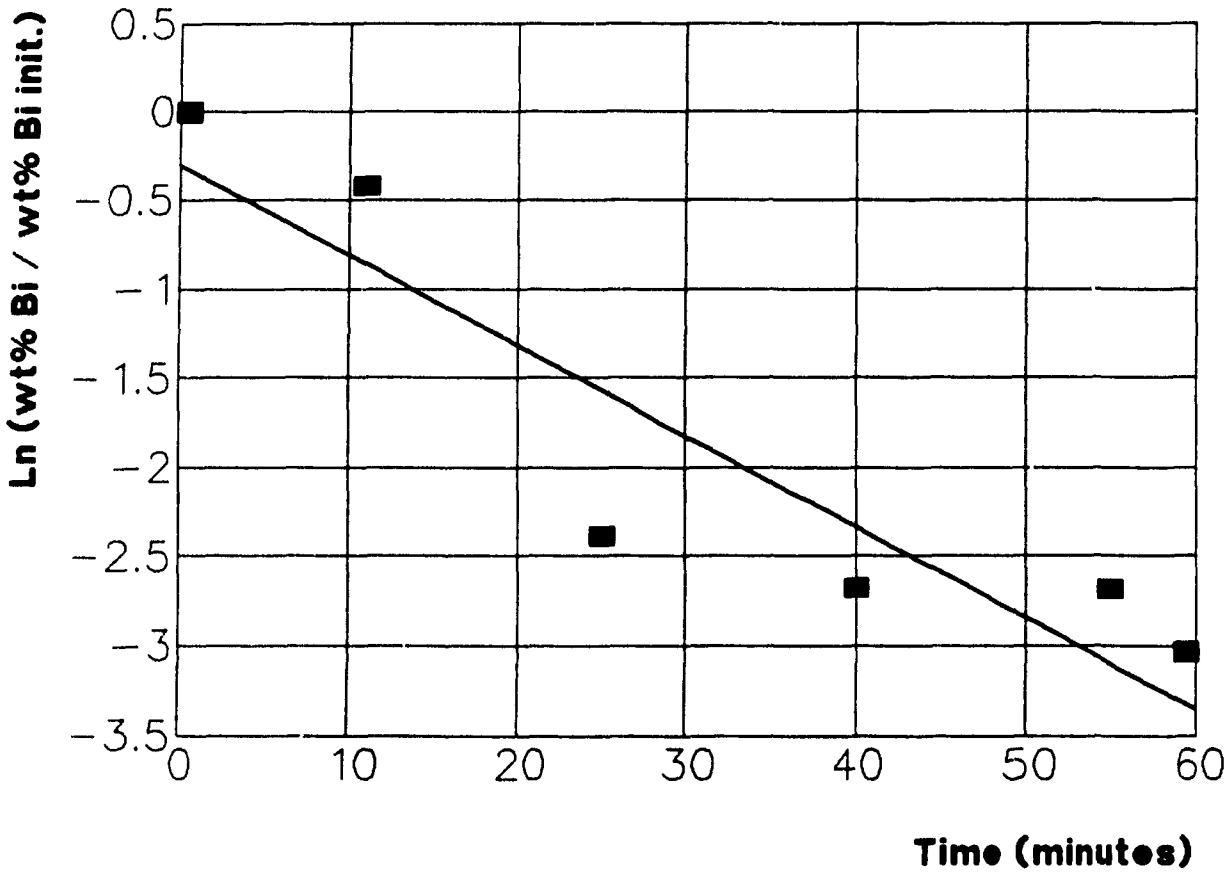

$y = -0.04991x - 0.2766$

$R^2 = 0.84$

Fig. 7.49 : Arsenic Concentration vs Time, Experiment #11

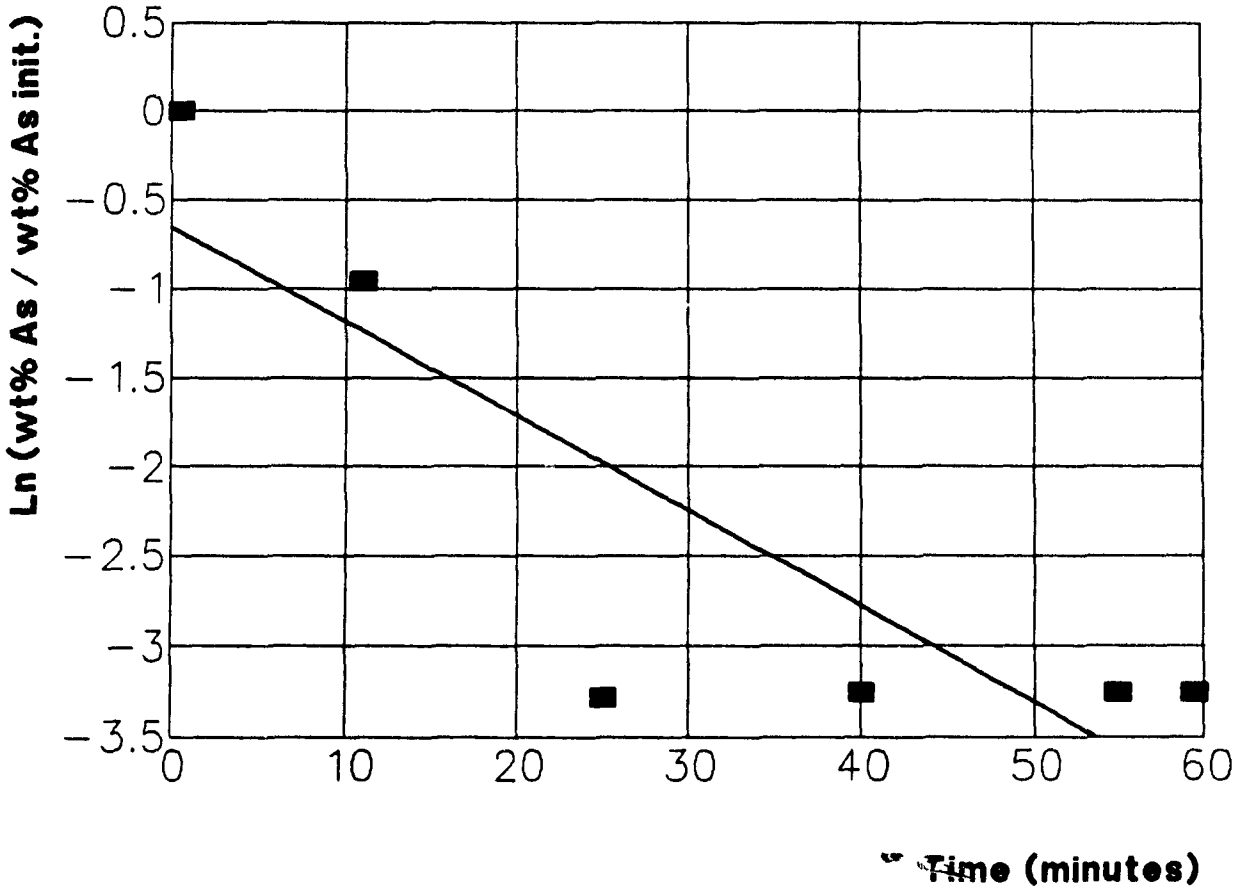

$y = -0.05242\,x - 0.6659$

$R^2 = 0.74$

Fig. 7.50 : Antimony Concentration vs Time

Experiment #11

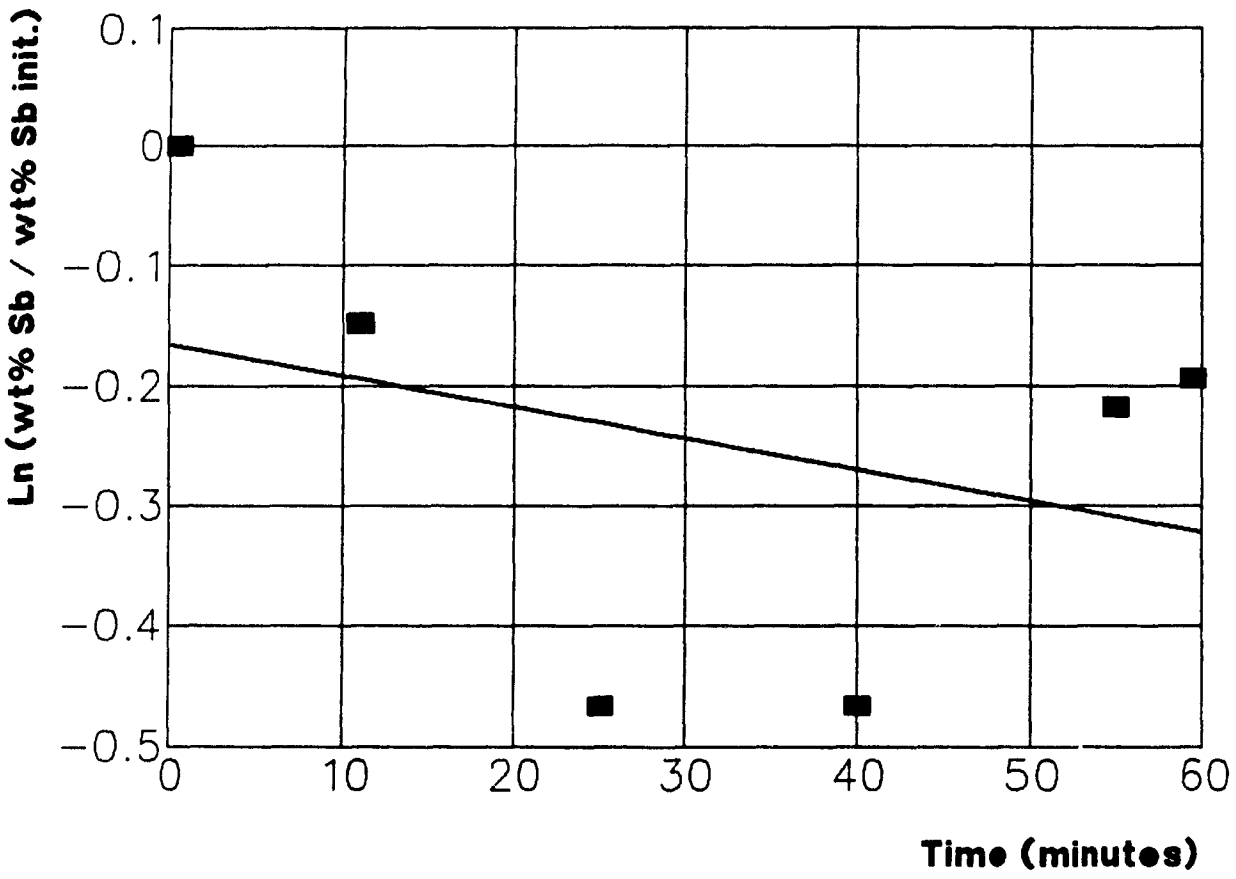

$y = -0.00279 - 0.1598$

$R^2 = 0.13$

Fig. 7.51 : Lead Concentration vs Time, Experiment #12

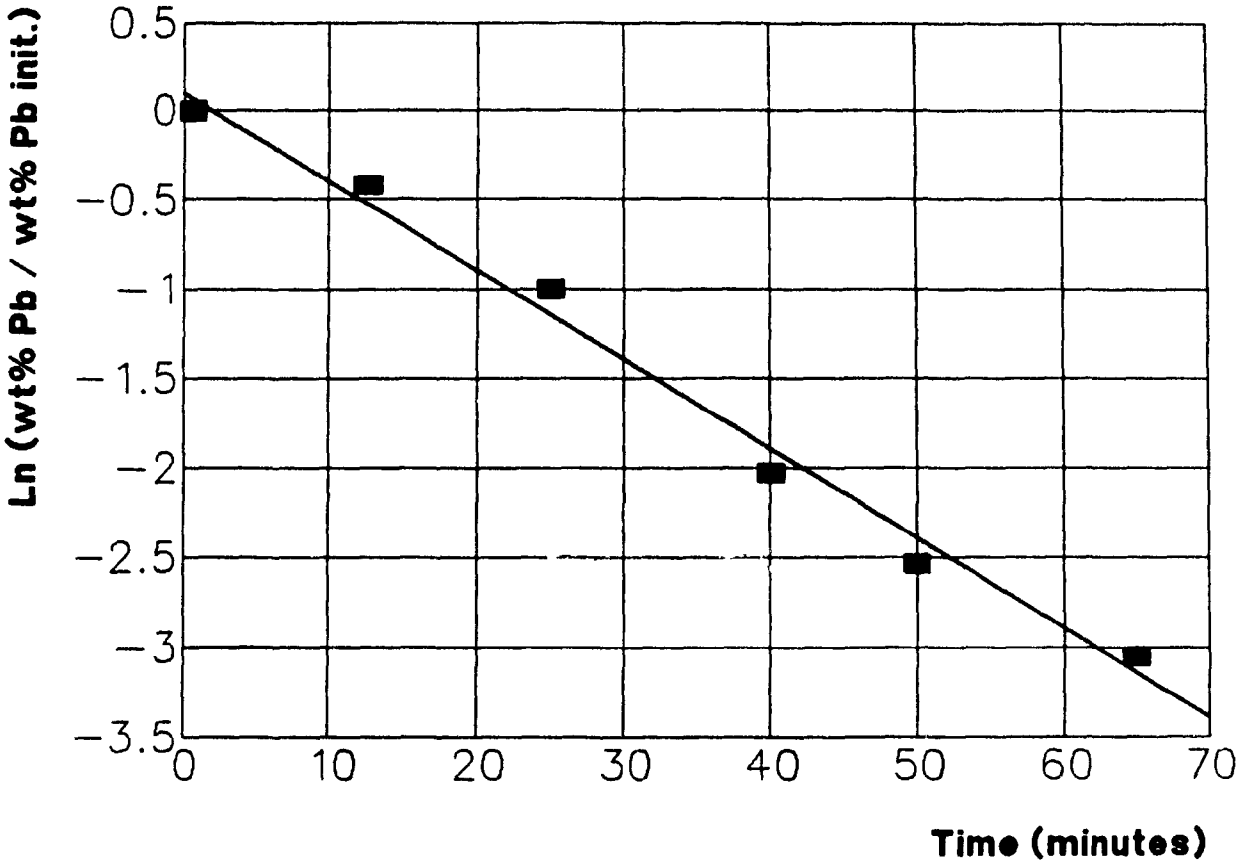

$y = -0.0500 x + 0.09826$

$R^2 = 0.99$

Fig. 7.52 : Bismuth Concentration vs Time, Experiment #12

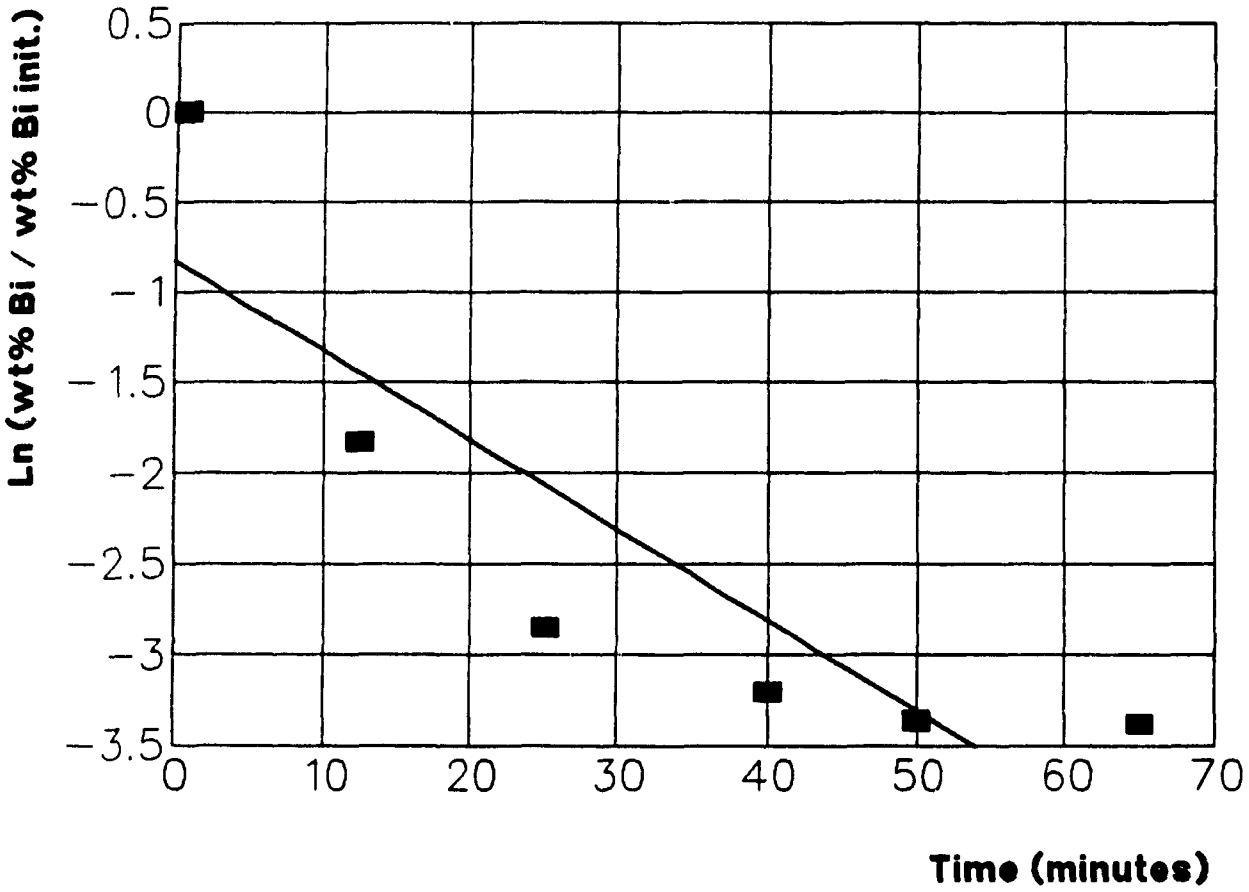

$y = -0.04806 x - 0.8956$

$R^2 = 0.77$

Fig. 7.53 : Arsenic Concentration vs Time, Experiment #12

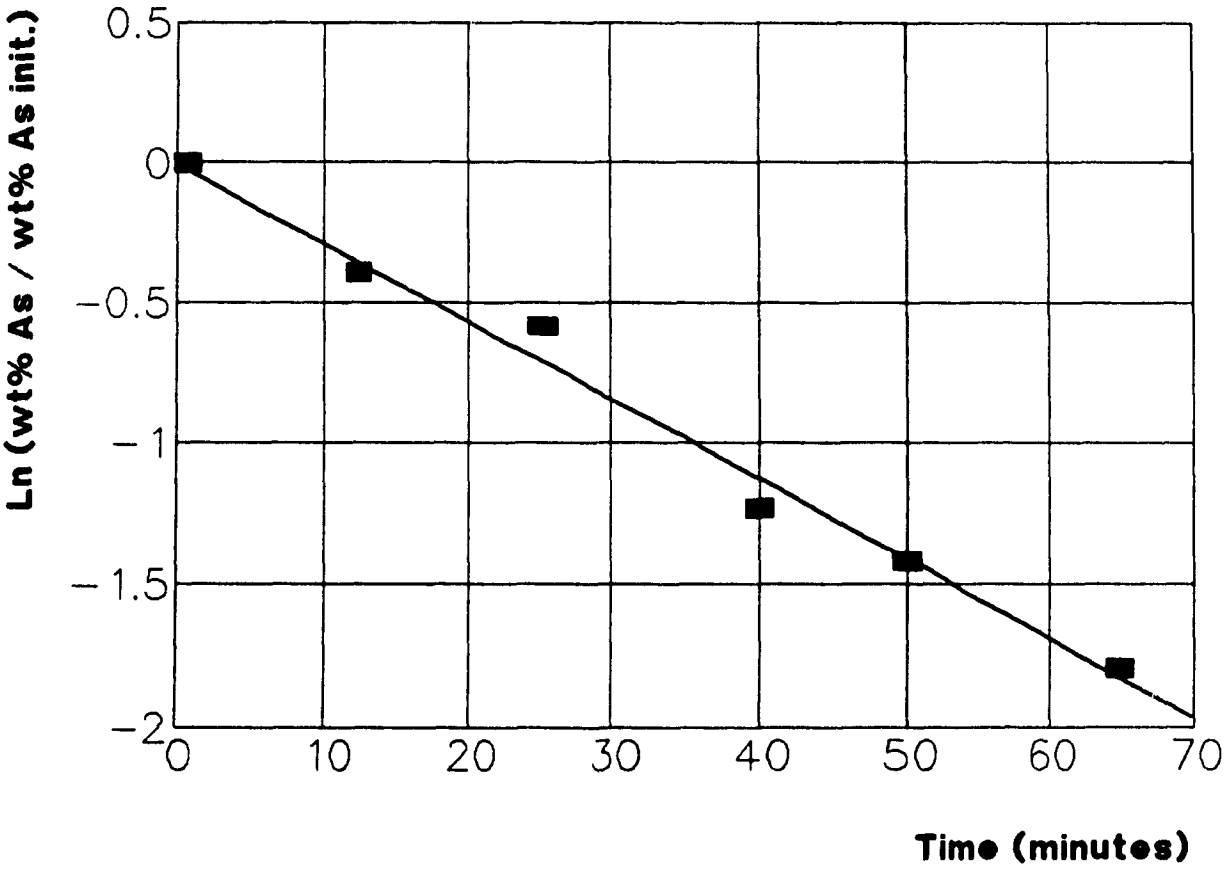

$y = -0.0281 x - 0.00163$

$R^2 = 0.99$

Fig. 7.54 : Antimony Concentration vs Time Experiment #12

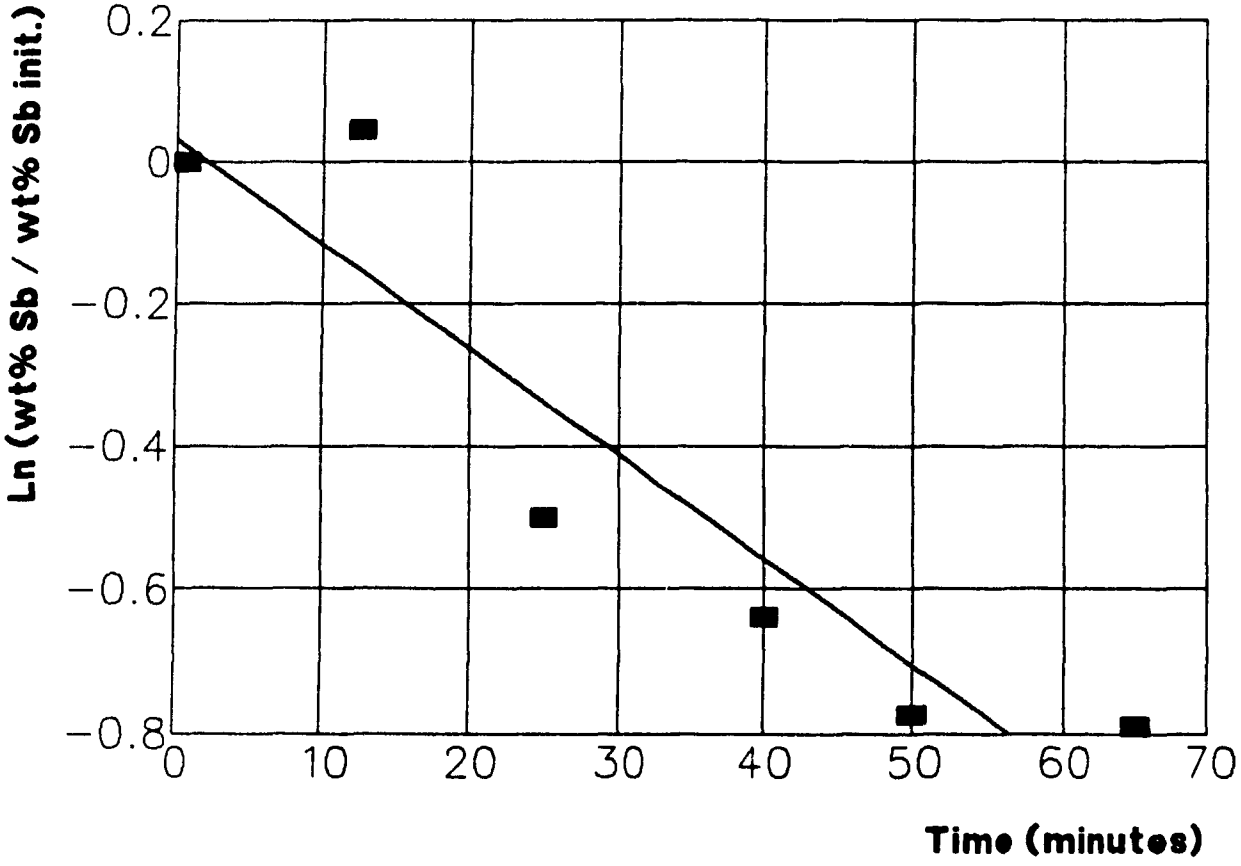

$y = -0.01453x + 0.02147$

$R^2 = 0.87$

Fig. 7.55 : Lead Concentration vs Time, Experiment #13

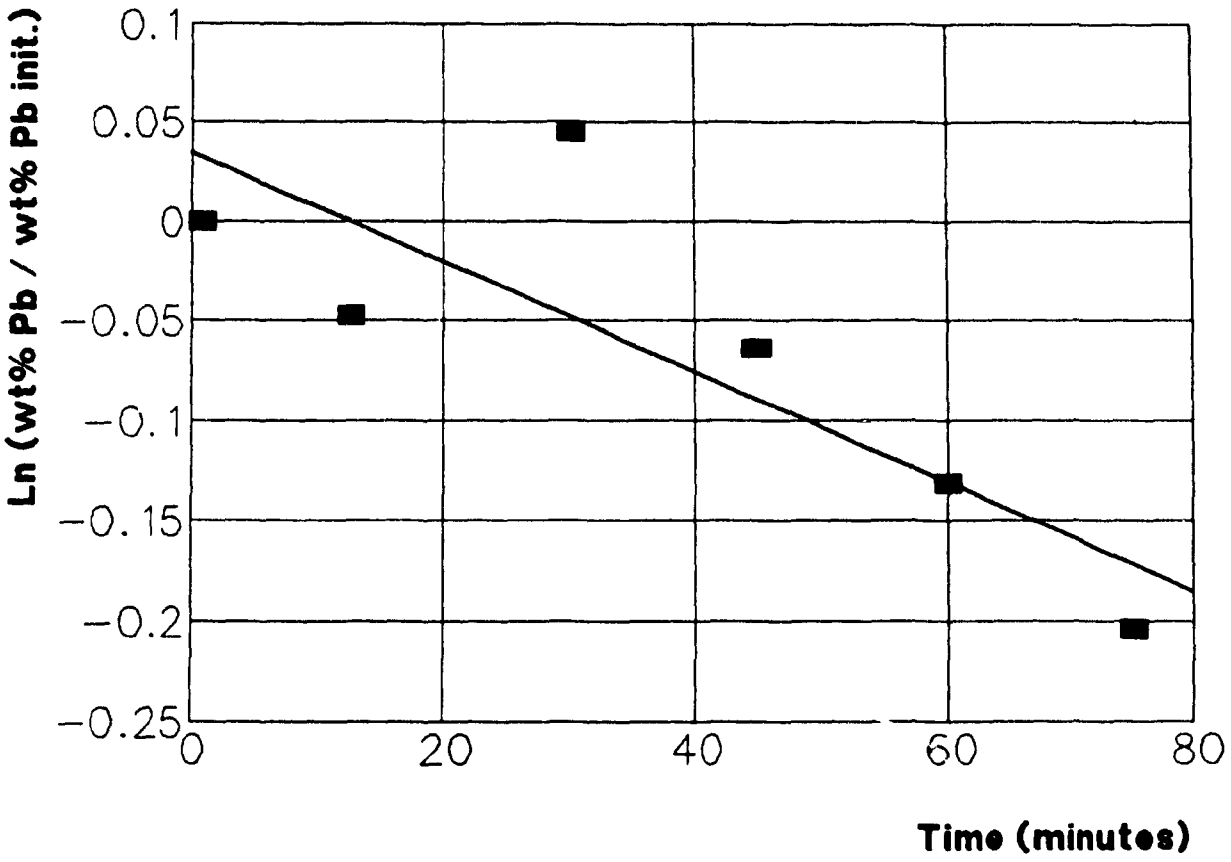

$y = -0.00257 x + 0.02834$

$R^2 = 0.66$

Fig. 7.56 : Bismuth Concentration vs Time, Experiment #13

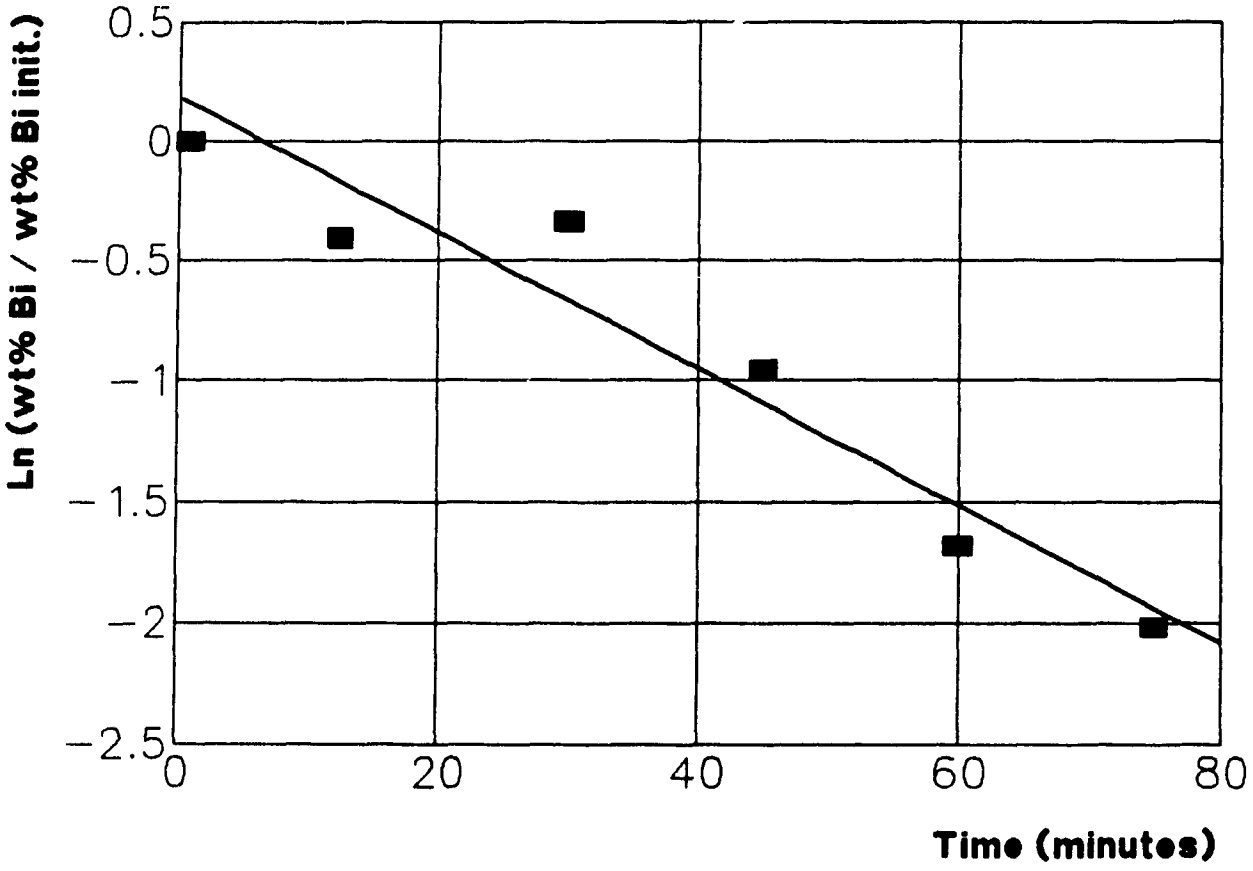

$y = -0.02717x + 0.1086$

$R^2 = 0.93$

Fig. 7.57 : Arsenic Concentration vs Time, Experiment #13

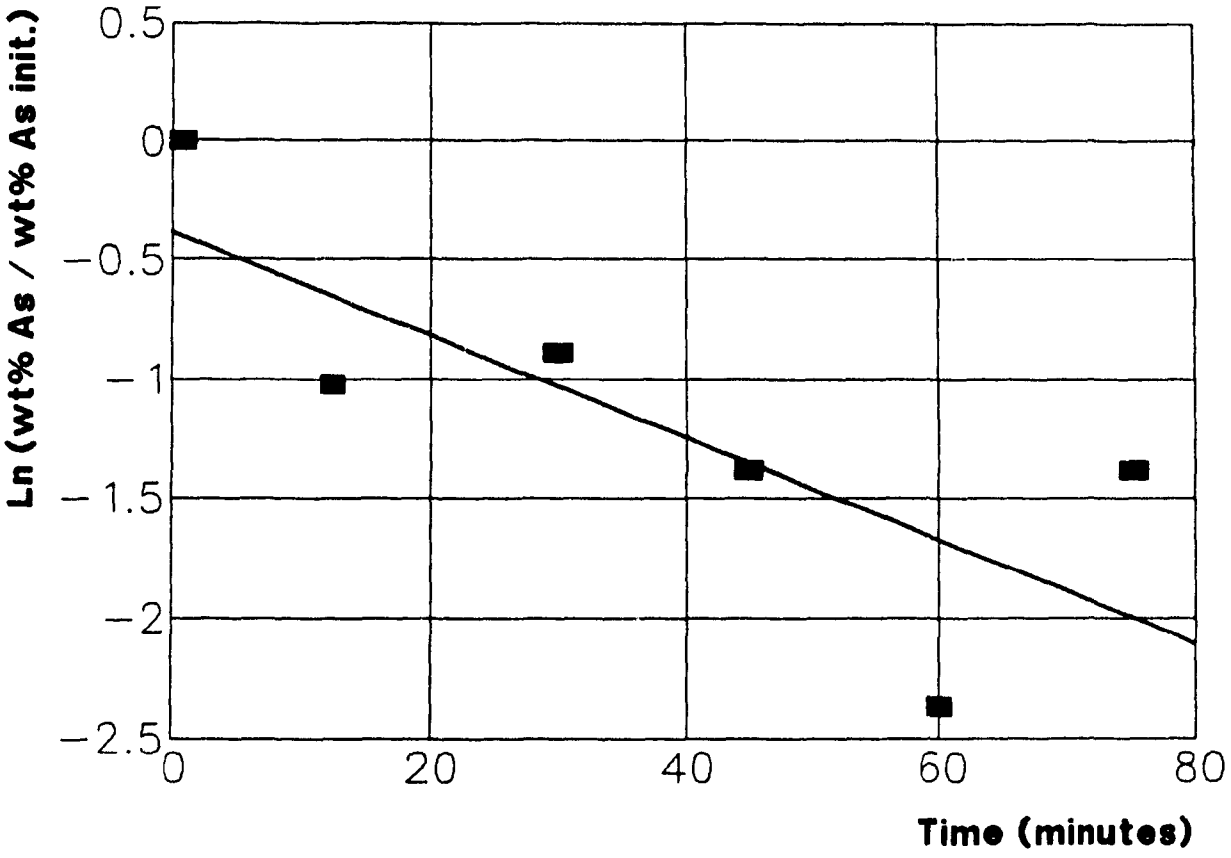

$y = -0.02128 x - 0.3859$

$R^2 = 0.61$

Fig. 7.58 : Antimony Concentration vs Time

Experiment #13

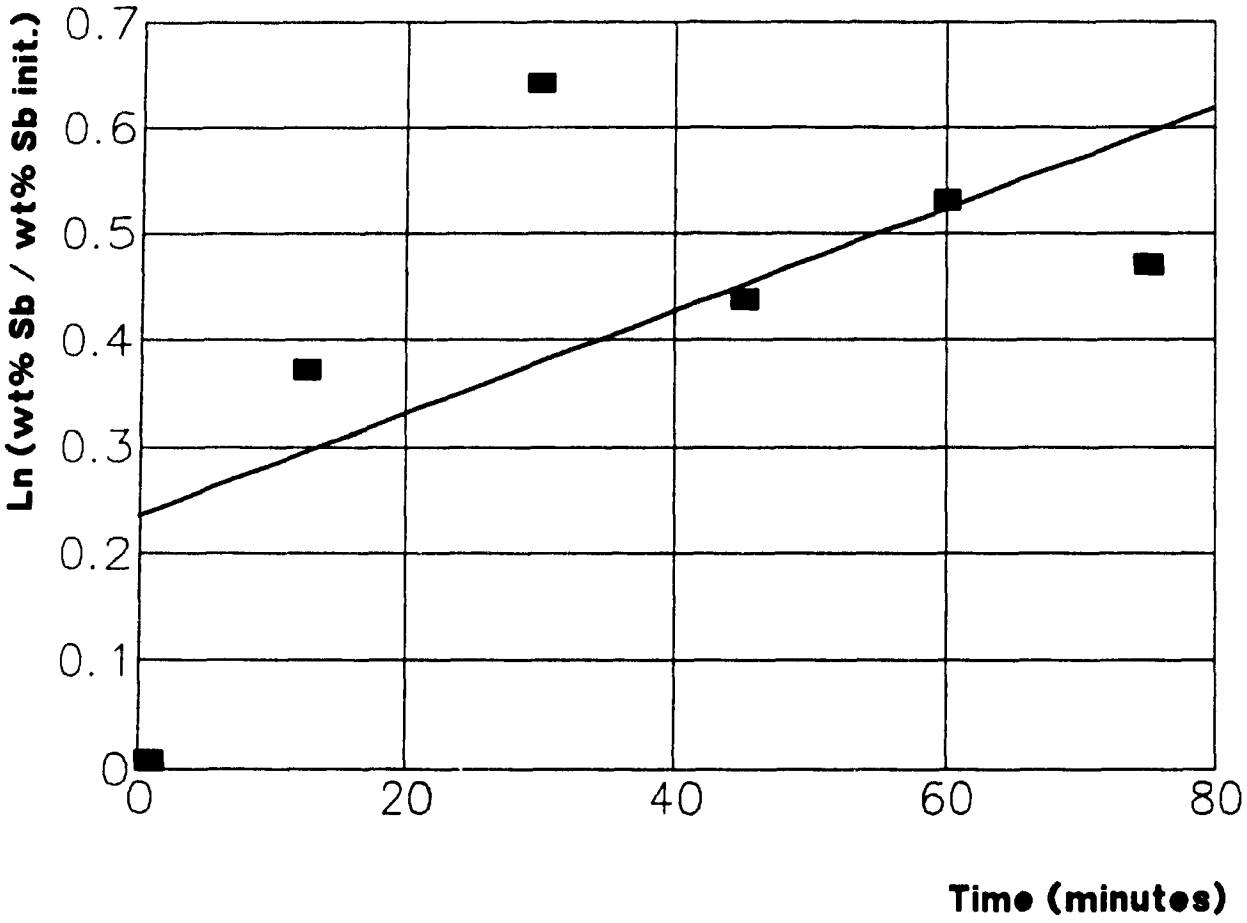

$y = 0.004875x + 0.2279$

$R^2 = 0.40$

Fig. 7.59 : Lead Concentration vs Time, Experiment #14

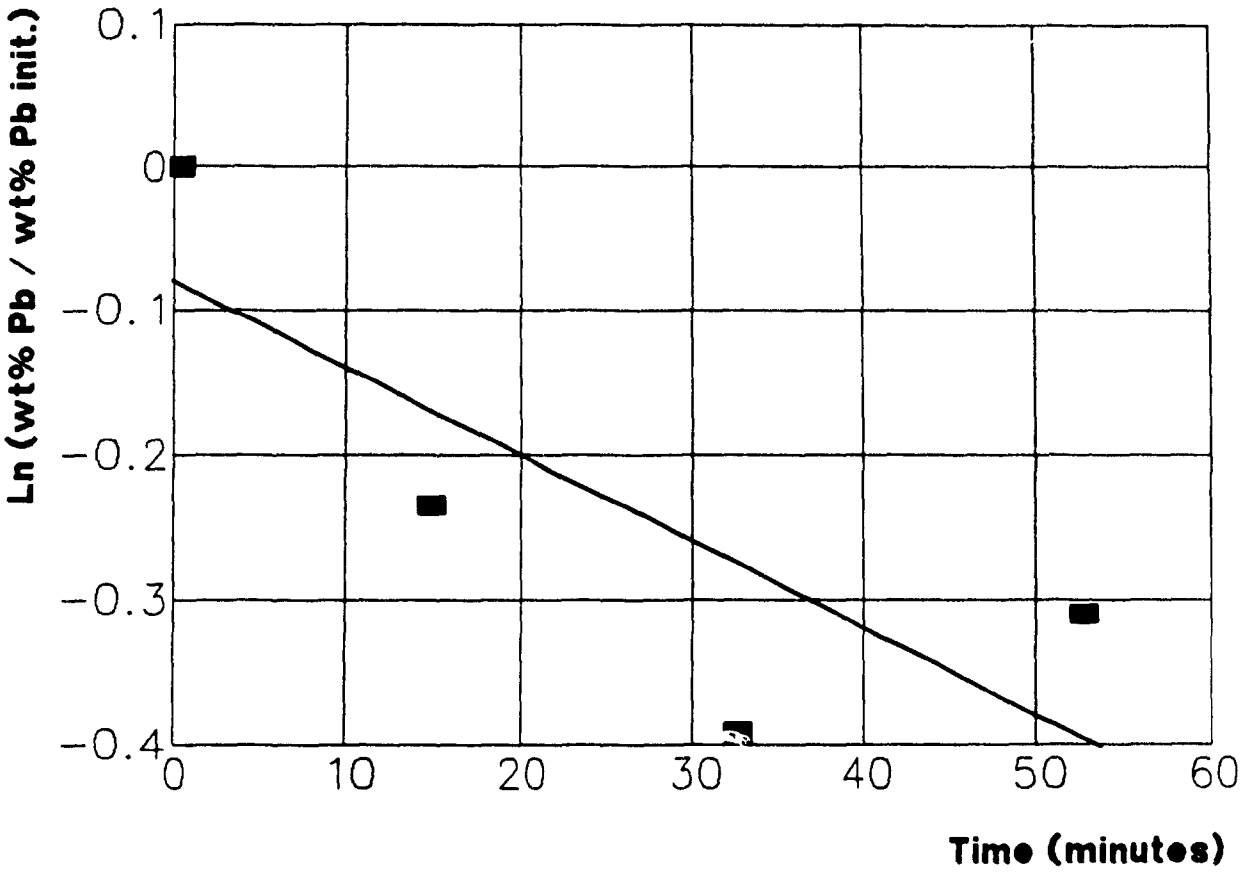

$y = -0.00593\,x - 0.08597$

$R^2 = 0.63$

Fig. 7.60 : Bismuth Concentration vs Time, Experiment #14

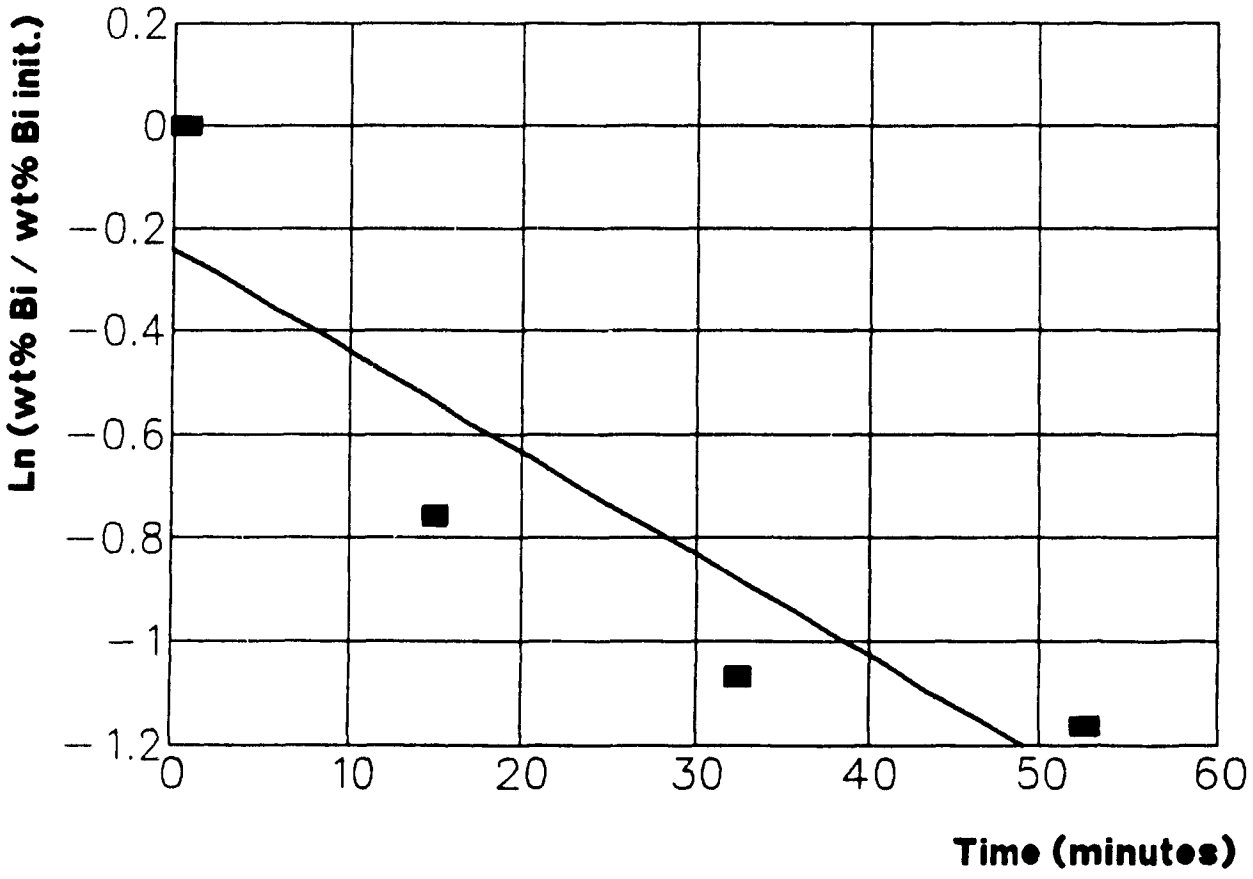

$y = -0.02109x - 0.2200$

$R^2 = 0.82$

Fig. 7.61 : Arsenic Concentration vs Time, Experiment #14

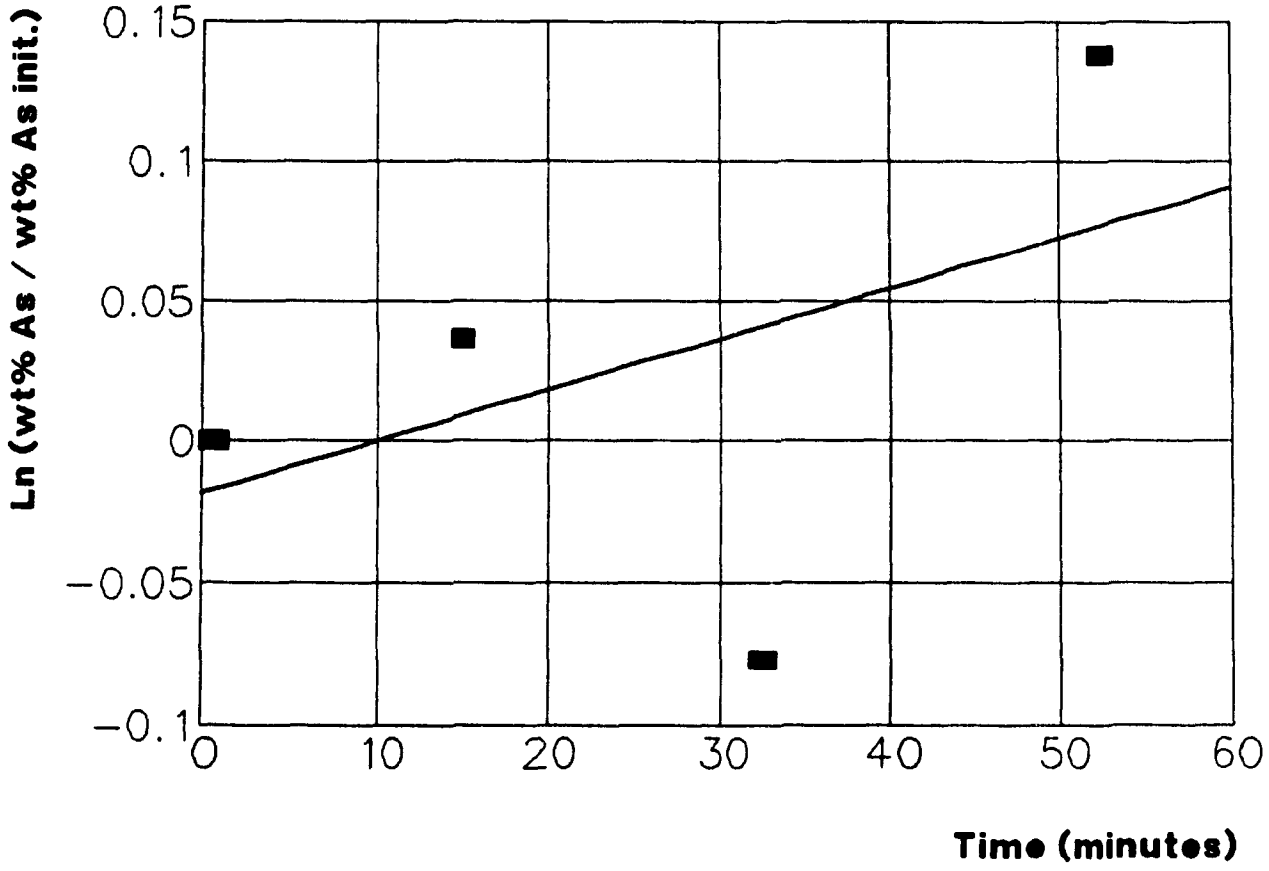

$y = 0.001859x - 0.02209$

$R^2 = 0.22$

Fig. 7.62 : Antimony Concentration vs Time

Experiment #14

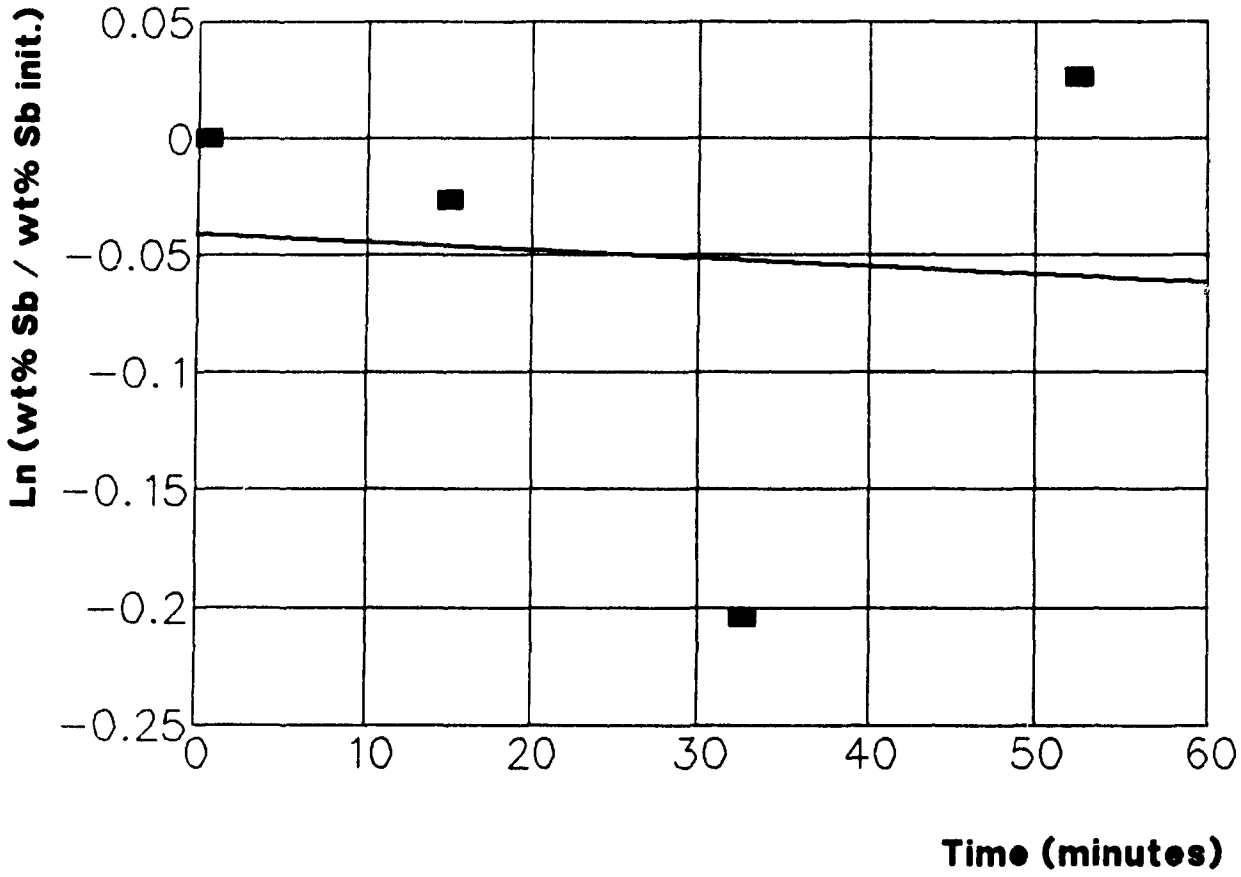

$y = -0.00036\,x - 0.0422$

$R^2 = 0.01$

Fig. 7.63 : Lead Concentration vs Time, Experiment #15

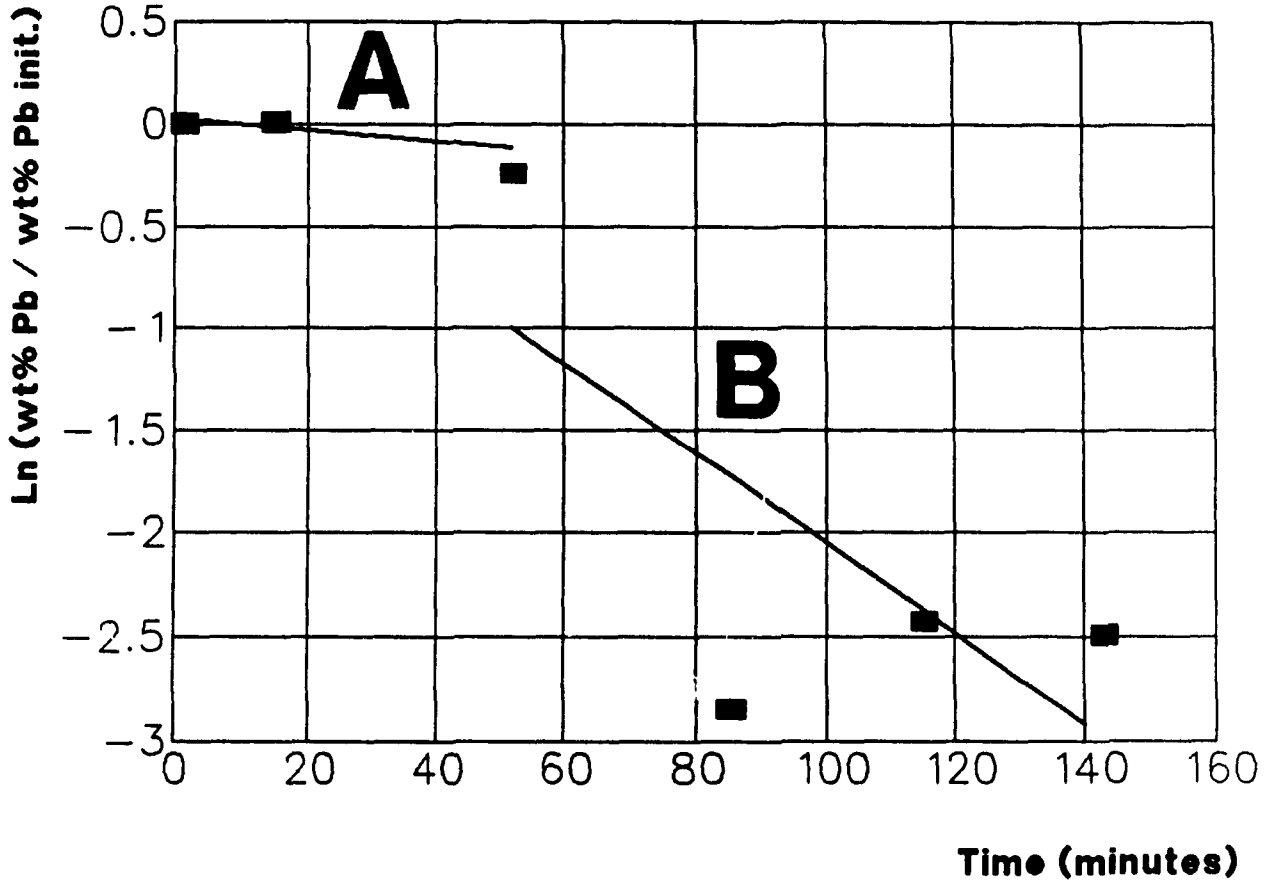

A $y = -0.00507 x + 0.0350$

$R^2 = 0.905$

B $y = -0.0216 x + 0.128$

$R^2 = 0.506$

Fig. 7.64 : Bismuth Concentration vs Time, Experiment #15

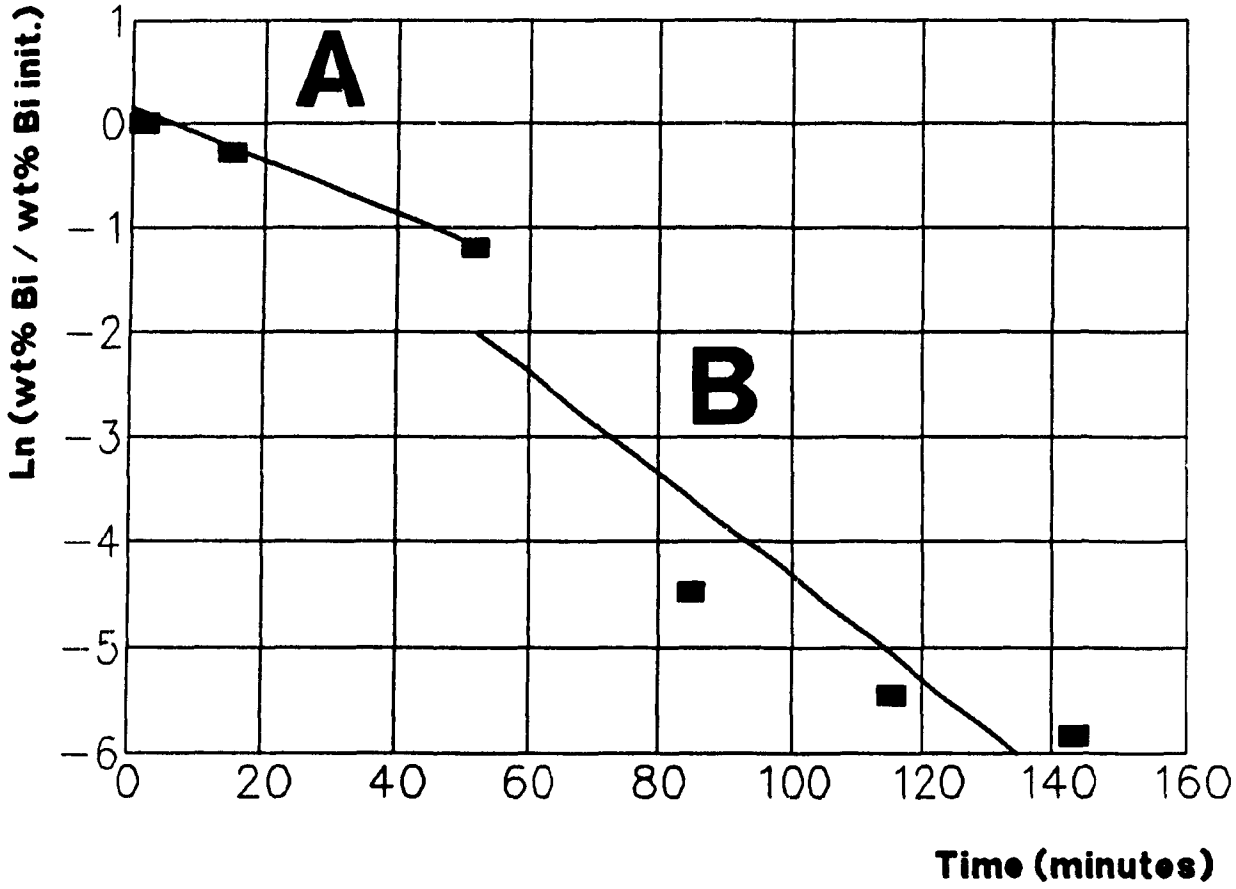

A $y = -0.02334x + 0.0291$

$R^2 = 0.997$

B $y = -0.0499x + 0.685$

$R^2 = 0.858$

Fig. 7.65 : Arsenic Concentration vs Time, Experiment #15

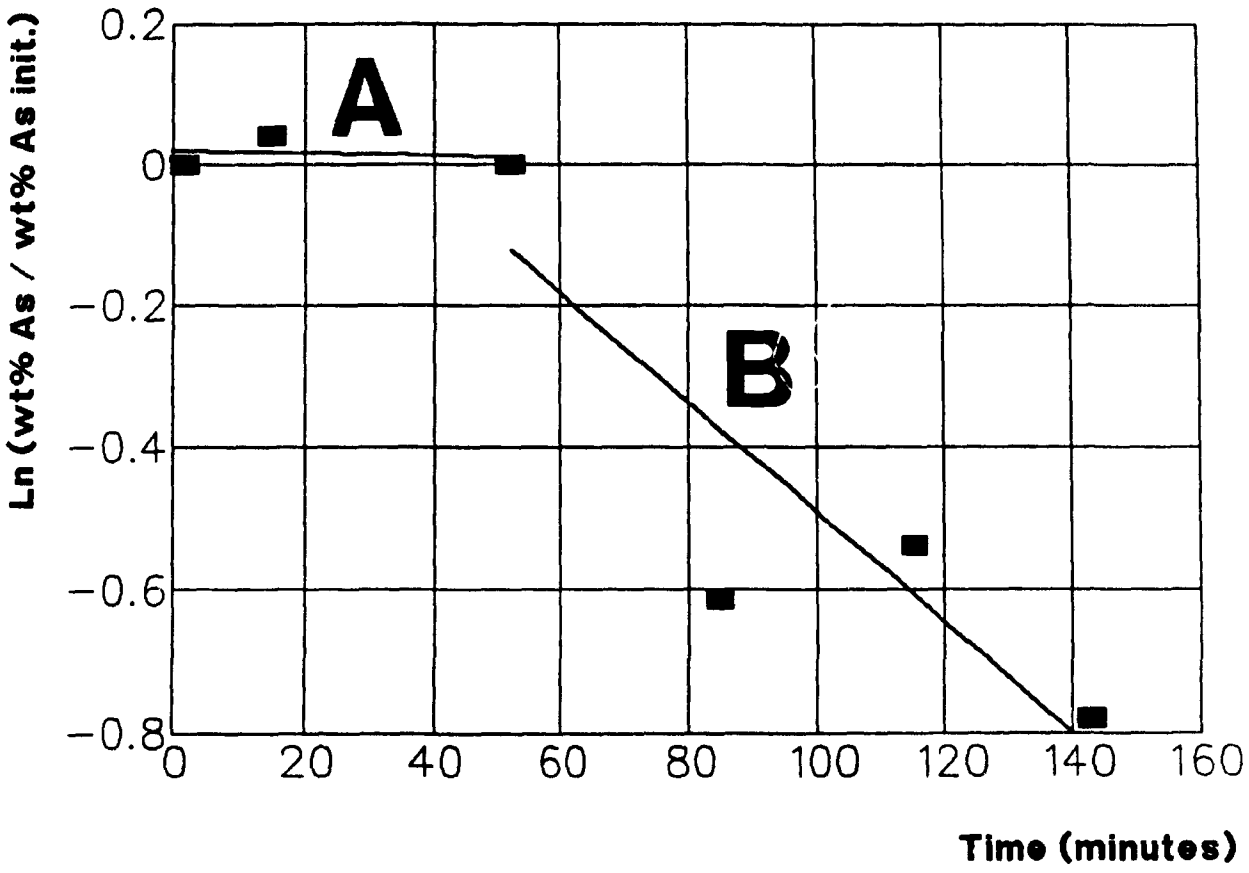

A $y = -0.00021x + 0.0183$, $R^2 = 0.056$

B $y = -0.00758x + 0.266$, $R^2 = 0.773$

Fig. 7.66 : Antimony Concentration vs Time

Experiment #15

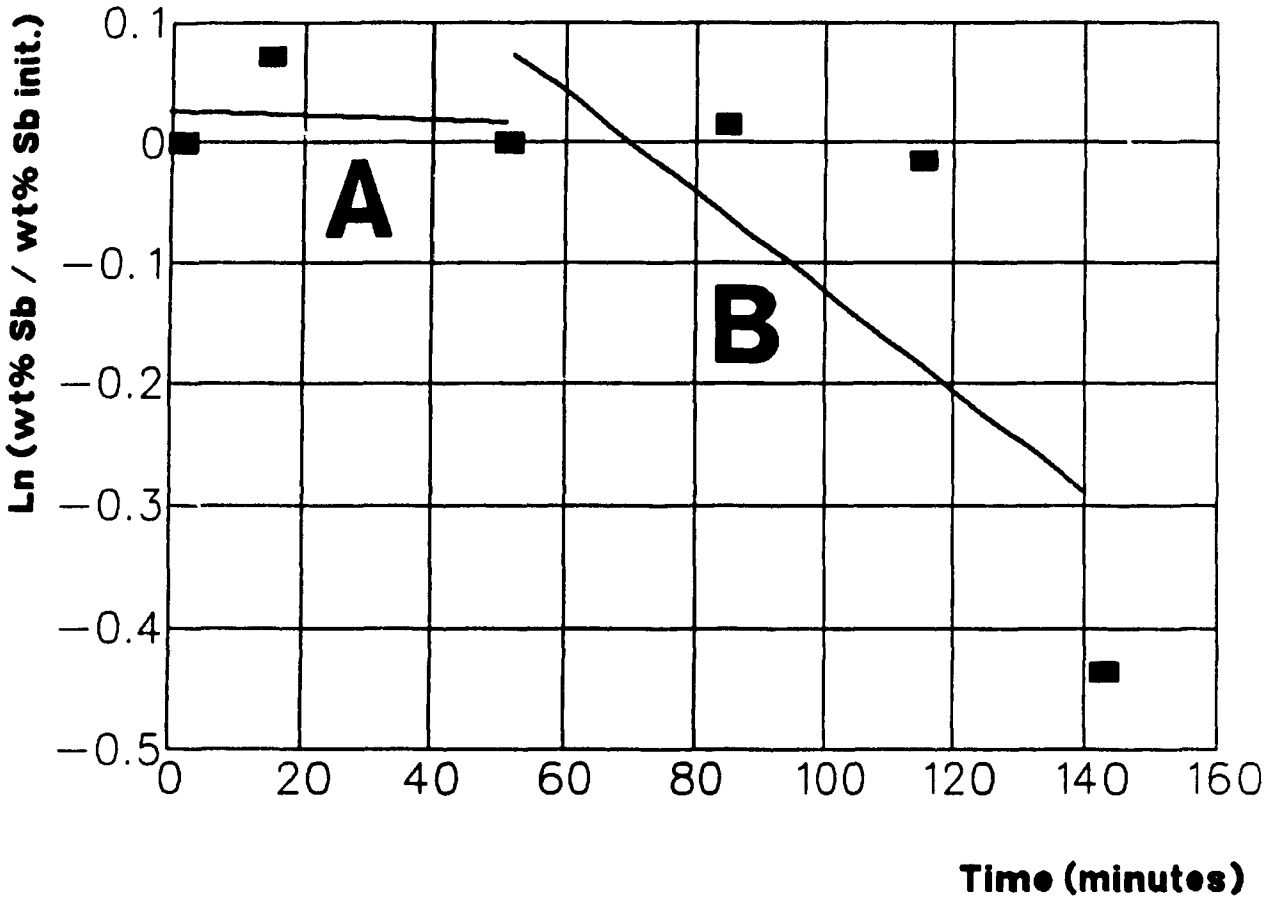

A $y = -0.00036\,x + 0.0318$

$R^2 = 0.056$

B $y = -0.00429\,x + 0.314$

$R^2 = 0.593$

7.6 Discussion of the Problems and Advantages Associated With the Experimental Procedure

Several problems were encountered during the experiments. One major problem was the large amount of splashing occurring during the degassing period. To minimize splashing, gradual depressurization was performed. Despite this, matte losses of up to 20 % were unavoidable.

Another major problem was the difficulty found in evaluating the lift ratio. The surface area produced by the spray was strongly affected by the lift ratio. Due to the melt losses (evaporation and splashing) during the experiment, the lift ratio increased and thus the spray decreased. Since it was not possible to control the lift ratio, strong variations in the surface area produced by the same gas flow rate were recorded.

Lastly, difficulties were encountered when assaying for antimony. Samples sent out twice for assaying returned with large variations in analytical results. The copper matte could have been doped with Sb, but then the evaporation of Sb_2 or Sb_4 vapours would have been possible and would have resulted in high evaporation rates when compared to typical industrial concentrations.

Several advantages were associated with the experimental set up. One great feature was the possibility of sampling without

breaking the vacuum. This allowed for sampling early in the experiment when impurity volatilization was at its maximum improving the accuracy of the kinetic data obtained. It further allowed for a long depressurization time to occur which avoided excessive splashing.

The windows on the vacuum furnace permitted visual observations. This enabled the experimenter to better control the melt splashing and observe the presence or absence of a slag layer.

The graphite versus alumina apparatus permitted the observation of evaporation under two completely different chemical situations. It allowed for the verification of the effect of two different levels of oxygen activity upon the rate of evaporation of the impurities. The relative proportion of the oxide vapours to the sulphide and monoatomic metal vapours changed with oxygen activity. Thus, the possibility existed of truly testing the thermodynamic data on the energy of formation of the oxide and sulphide vapours of the impurities.

The possibility of observing the simultaneous evaporation of several impurities permitted comparisons of refining rates and gave the opportunity to gain further insight into the copper matte system.

CHAPTER 8

Discussion and Interpretation of the Results

8.1 Introduction

The discussion of the experimental results will be subdivided into two main areas. Firstly, a discussion on the results of the dust characterization and the selective condensation of the vacuum refining vapours will be undertaken. Secondly, the overall refining rates in the graphite and alumina LSV apparatus will be discussed.

The dust characterization will provide useful information concerning its formation. This information gives an insight on how the copper content in the dust can be controlled as well as how separate products may be obtained.

The refining rates will be examined to gain an understanding on the predominant variables affecting the rates of evaporation. The experimental rates will be compared to the calculated rates. The strengths and weaknesses of the model will be discussed to ascertain if confident predictions can be carried out and if an industrial size scale up is possible.

8.2 Characterization of the Vacuum Refining Dust

One of the major concerns regarding the use of vacuum refining to purify copper matte is how to handle the dust produced. The dust cannot be recirculated into the smelting unit because it contains the undesirable impurities removed from the melt. However, if it is to be discarded, the dust should not contain copper in excess of 1 to 2 percent by weight.

8.2.1 Dust Characteristics

The dust was collected at the end of each experiment. All samples were analyzed individually for the content of copper, lead, bismuth, arsenic and antimony. Table 6.1 (Chapter 6) summarizes the results of the chemical analysis. It is evident that the copper content of the dust was larger than 2 weight percent. Thus, it would be wasteful to discard it.

To evaluate what treatment is suitable for processing the dust, it was decided to perform a size fraction analysis and mineralogical determination. The dust was found to be composed of three main species, lead sulphide (PbS), zinc sulphide (ZnS) and metallic lead (Pb). The fifty percent passing size on dry screen analysis was 80 μm (Figure 6.1, Chapter 6). However, scanning electron microscopy showed that the dust particles were clusters of smaller sub micron particles. Thus, it is inconceivable to treat the dust by froth flotation.

Each size fraction was analyzed for copper, lead, bismuth, arsenic and antimony. The results are presented in Figures 6.2 and 6.3. From Figure 6.2, it is seen that the copper content of the dust decreased as the particle size decreased. The +28 mesh dust contained 45 percent copper which was similar to the grade of the matte refined. This result, and the spherical appearance of the large grains under the

microscope (round solid spheres), led to the conclusion that the large grains of dust were prills of matte ejected during the experiments. This was in accordance to visual observations during the LSV experiments, where one could readily see matte particles ejected from the apparatus. In fact, 80 percent of the copper present in the dust (calculated) was present in the +48 mesh size fractions. The -200 mesh size assayed only 1 to 3 percent copper by weight.

Figures 6.2 and 6.3 showed that lead, bismuth, arsenic and antimony demonstrated the inverse of the behavior shown by copper and reported mainly in the fine size fractions. It is thus concluded that the dust was composed of two kinds of particles. The large particles were formed by prills of matte ejected from the LSV apparatus and the small particles (clusters of sub micron particles) were formed by the homogeneous condensation of the lead, zinc, bismuth, arsenic and antimony vapours. Some copper evaporated and condensed in fine particles. This was seen by the presence of approximately 1 percent copper in the -200 mesh fraction.

These results imply that with a proper LSV apparatus design, which would impede the ejection of copper prills, the dust produced would have a low enough copper content to justify its being discarded or sent to a lead smelter.

8.2.2 Selective Condensation Experiments

Five experiments were performed on the selective condensation of the vacuum refining vapours. The experimental procedure and the apparatus were described in Chapter 6, Section 3.

Table 6.4 shows the chemical analysis of the samples taken in the condenser and in the vacuum chamber. Taking note of Experiment E, it can be seen that the condensate contained 49.1 percent zinc, 26.2 percent sulphur and 1 percent lead. The chamber dust contained 32.0 percent lead, 15.1 percent zinc and 15.9 percent sulphur. Thus, it was possible to separate the zinc from the lead vapours by controlling the cooling process of the vapours. Point E on Figure 6.7 shows that the condenser temperature and the chamber pressure were located above the ZnS equilibrium condensing curve but below the PbS and Pb condensing curve. Thus, ZnS condensed while Pb and PbS did not. The zinc content in the chamber dust was still high (15% zinc) due to the short length of the condenser and lack of time available for the condensation of the zinc sulphide vapours.

It was observed during the experiments that the zinc condensed into a hard and crusty material. This would prove problematic if a condenser was built at an industrial scale due to the difficulty involved in retrieving the zinc from the condenser wall or plates. Zinc sulphide sublimates or

condenses to a solid phase and thus any attempts to control the wall temperature of the condenser could not result in the production of a liquid phase.

8.3 LSV Vacuum Refining Experiments

8.3.1 Impurity Removal during the LSV Refining Experiments

Table 8.1 shows a summary of the experimental conditions for the fifteen experiments. Table 8.2 presents a summary of the percent impurity elimination for the fifteen LSV experiments carried out in this study. The first nine experiments were performed in a graphite apparatus and the last 6 in an alumina apparatus (see Figures 8.1 and 8.2).

The graphite apparatus experiments showed that lead and bismuth removals were possible for matte grades ranging from 35 to 80 percent copper. Arsenic and antimony removals were lower than those for lead and bismuth. Furthermore, for a matte grade of 78 percent copper (white metal), the arsenic and antimony removal was null.

Comparing the graphite and alumina apparatus experiments (Tables 8.3 and 8.4), it was observed that lead and bismuth removals were identical in both sets of experiments. However, arsenic removal in the alumina apparatus was larger than in the graphite apparatus. Antimony removal as well was superior in the alumina apparatus.

At chamber pressure of 600 pascals or more, arsenic and antimony removal was negligible in both the alumina and the

graphite apparatus (Experiments 13, 14 and 15A).

Silver assays were taken during Experiment 5, selenium assays during Experiments 1, 2, 5 and 6, and nickel assays during Experiments 10, 11, 12, 13, 14 and 15. No removal of any of these elements were recorded.

Figure 8.3 shows the equilibrium vapour pressure of various selenium species versus the activity coefficient of selenium in the melt. The activity coefficient of selenium at the onset of an experiment was calculated at 10^{-3} and the starting oxygen activity in an alumina crucible was lower than 10^{-7} atmosphere for both 35 and 65 percent copper matte. Under these conditions, the selenium dioxide (SeO_2) and monoxide (SeO) vapour pressure were lower than the metallic selenium (Se) pressure. Thus, even if the selenium assays were done using samples from graphite crucible experiments, theoretically the results would have been the same as if the assays would have been carried out using samples from alumina crucibles experiments. However, in blister copper, where the oxygen activity is three to four orders of magnitude higher, the selenium oxide vapour pressure would have been significantly higher than the metallic selenium pressure. Thus, vacuum refining might be a feasible method and experiments on blister copper saturated with oxygen are recommended.

Table 8.1 : Summary of the Experimental Conditions for the LSV Experiments

Exp. #	Chamber Press.	App. Const.	Const. Material	Matte Source	Lifting Gas	Oxygen Potential Measured
1	High	A	Graphite	Rv.	N_2	No
2	Medium	A	Graphite	Rx.	N_2	No
3	Medium	A	Graphite	Rv.	N_2	No
4	Low	B	Graphite	Rx.	N_2	No
5	Low	B	Graphite	Rx.	N_2	No
6	Low	B	Graphite	Rx.	N_2	No
7	Low	B	Graphite	Rx.	N_2	No
8	Low	B	Graphite	W.M.	N_2	No
9	Low	B	Graphite	W.M.	N_2	No
10	Medium	C	Alumina	Rv.	Air	No
11	Medium	D	Alumina	Rv.	N_2	No
12	Medium	D	Alumina	Rx.	N_2	No
13	High	D	Alumina	Rv.	N_2	Yes
14	High	E	Alumina	Rx.	None	Yes
15a	High	E	Alumina	Rx.	None	Yes
15b	Low	E	Alumina	Rx.	None	Yes

Legend : Rv. = Reverberatory Furnace Matte (35 % Cu)
Rx. = Noranda Reactor Matte (60 % Cu)
W.M. = White Metal (80 % Cu)
High = High Chamber Pressure (> 500 Pa)
Medium = Medium Chamber Pressure (> 50 Pa, < 100 Pa)
Low = Low Chamber Pressure (< 20 Pa)
N_2 = Nitrogen Gas
None = No Lifting Gas Used
For Configuration A, B, C, D, and E, See Figure 8.1

Fig 8.1: Schematic Diagram of Graphite LSV Apparatus Used in Experiments 1 to 9.

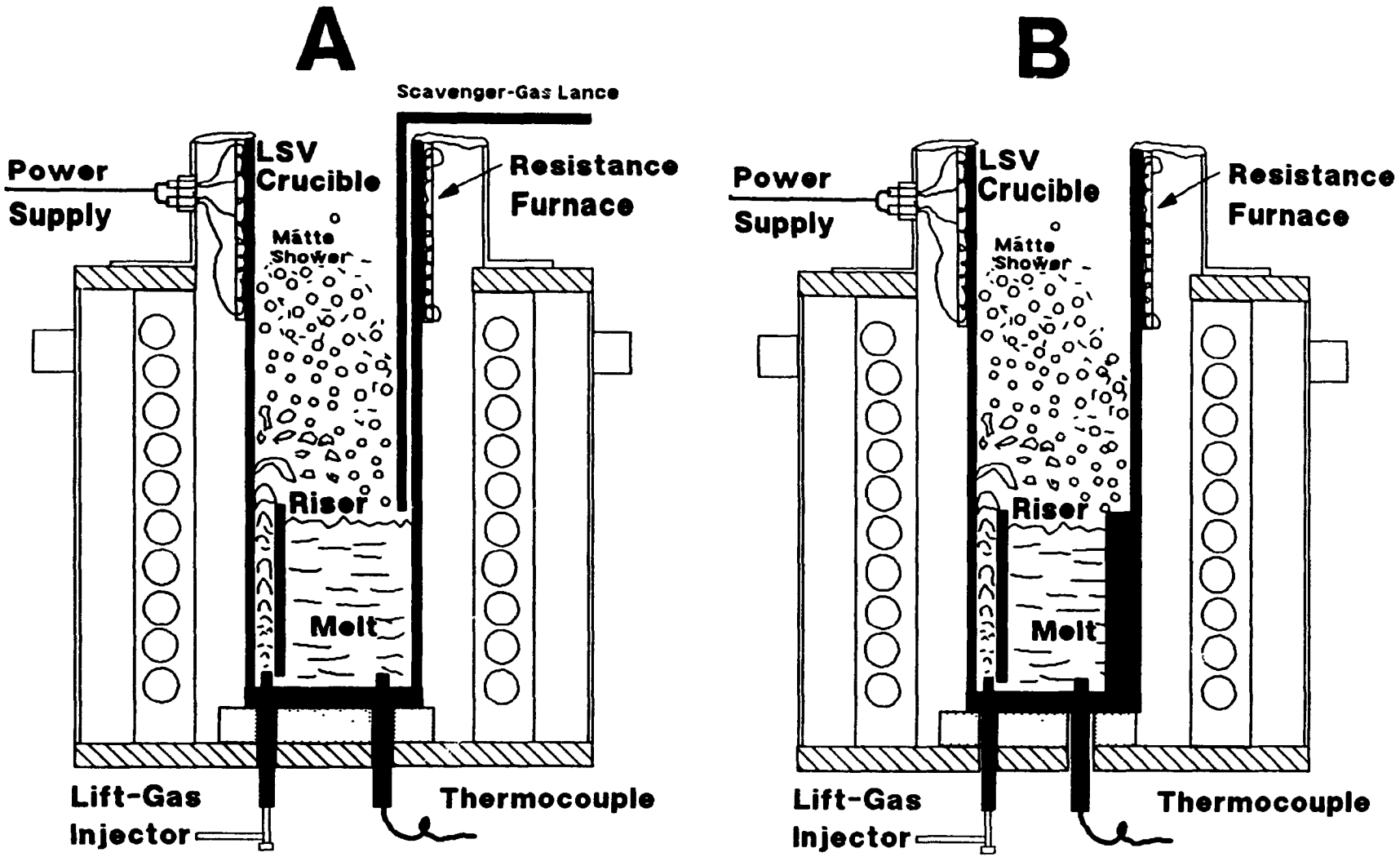

Fig 8.2 : Schematic Diagram of Alumina LSV Apparatus Used in Experiments 10 to 15.

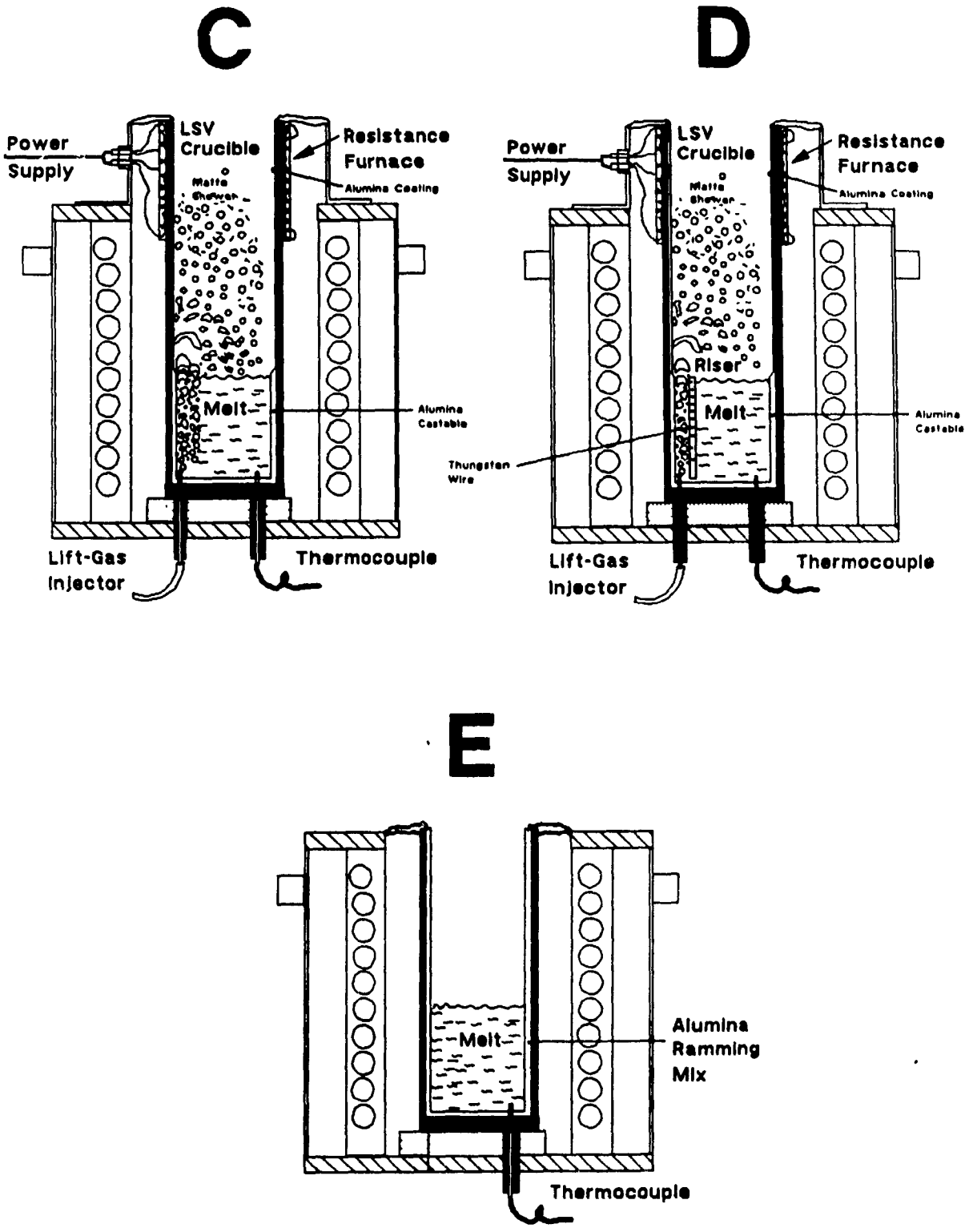

Table 8.2: Summary of Experimental Conditions and Percent Impurity Elimination in the LSV Graphite and Alumina Lined Apparatus.

					Impurity Elimination			
Exp. #	Matte	Cu (%)	Temp. (K)	Press. (Pa)	Pb (%)	Bi (%)	As (%)	Sb (%)
1	Rv.	38	1423	1300	72	85	14	18
3	Rv.	36	1473	100	99	90	43	35
7	Rv.	40	1523	13	99	94	59	71
2	Rx.	65	1523	65	94	75*	32	40
4	Rx.	59	1533	20	98	67*	76	45*
5	Rx.	60	1533	13	92	>79	76	58
6	Rx.	63	1523	20	99	65	77	62
8	WM.	78	1523	13	95	71*	0	0
9	WM.	78	1533	13	98	70*	0	0
11	Rv.	35	1493	91	96	95	>97	20
10	Rv.	37	1473	78	97	97	>97	73
13	Rv.	30	1473	600	18	87	0*	0*
12	Rx.	61	1483	78	95	97	83	56
14	Rx.	60	1533	600	27	69	0	0
15A	Rx.	60	1473	600	22	70	0	0
15B	Rx.	60	1600	13	89	99	54	35

Notes : Mass balances performed on these experiments* considering the melt and condensate masses, and assays indicate that the percent elimination of the impurity should have been higher. Experiments 1 to 9 in graphite apparatus and Experiments 10 to 15 in alumina apparatus.

Table 8.3 : Summary of Impurity Elimination in the Graphite Apparatus Experiments, At 50 to 100 Pa Pressure.

Experiment #	Matte Source	Percent Impurity Removal			
		Pb	Bi	As	Sb
3	Rv.	99	90	43	35
2	Rx.	94	75*	32	40
8 & 9	W.M.	96	71*	0	0

Notes : Mass balances performed on these experiments* considering the melt and condensate masses, and assays indicate that the percent elimination of the impurity should have been higher.

Table 8.4 : Summary of Impurity Elimination in the Alumina Apparatus Experiments, At 50 to 100 Pa Pressure.

Experiment #	Matte Source	Percent Impurity Removal			
		Pb	Bi	As	Sb
10 & 11	Rv.	97	96	>97	47
12	Rx.	95	97	83	55

Fig. 8.3: Equilibrium Vapour Pressure of Selenium versus the Activity of Selenium in a Melt at 1473 K.

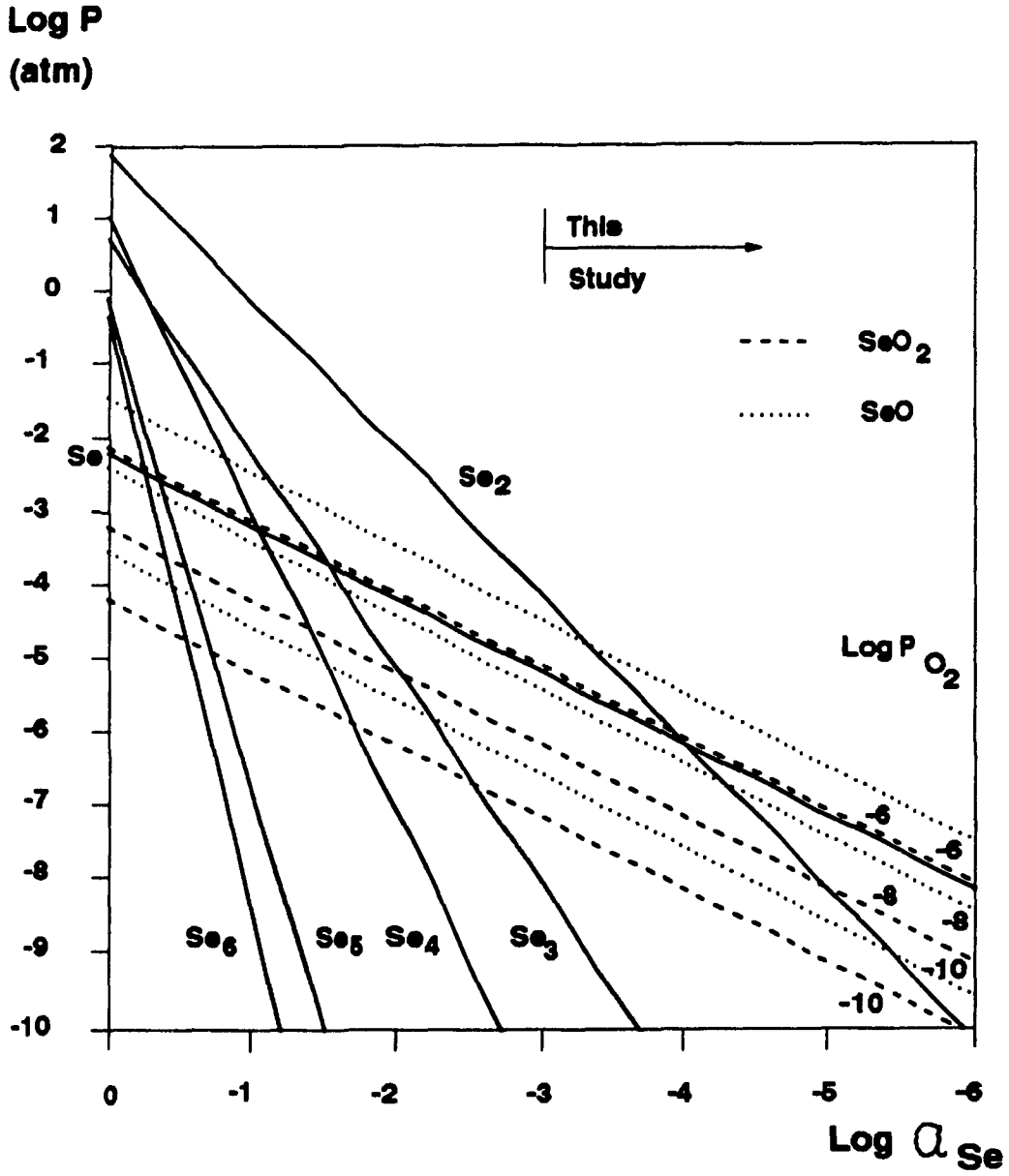

8.3.2 Surface Area Enhancement by the LSV Refining Apparatus

In Chapter 7, the chemical assays for each impurity in the matte samples were plotted semi-logarithmically against time. Linear regressions were calculated for the data to find the slope of the lines. Assuming evaporation of lead follows first order kinetics, then:

$$\ln\left(\frac{(\%\ \text{lead at time} = T)}{(\%\ \text{lead at time} = 0)}\right) = -K_{ov}\cdot(a/v)\cdot t$$

Since the initial weight of the matte (or volume) was known at the beginning of the experiment and remained essentially constant throughout the experiment, the surface area for evaporation was calculated assuming that the lead evaporation rate coefficient was liquid phase controlled at chamber pressures of less than 100 pascal.

The estimated surface areas for evaporation calculated for some of the experiments are shown in Table 8.5. The spray surface area was deduced by subtracting the crucible surface area. As can be observed, the spray surface area increased as the lifting gas flow rate increased.

Table 8.5 :Summary of the Estimated Surface Area for Evaporation in the LSV Apparatus Based on $-K_{ov}^{Pb} = 2 \times 10^{-4} ms^{-1}$.

Experiment #	Nominal Area (m^2)	Lifting Gas Flowrate ($Nmls^{-1}$)	Estimated Area (m^2)	Spray Area (m^2)
5 to 9	0.014	8	0.022	0.008
10 to 12	0.020	16	0.032	0.012
2 to 3	0.032	30	0.051	0.019

8.3.3 Oxygen Activity in Copper Matte Subjected to Vacuum

Table 8.6 :Summary of Oxygen Activity Measurements Taken During Experiments # 13, 14 and 15.

Exp. #	Time from Start (min.)	Copper in Matte (%)	Chamber Press. (Pa)	Temp. (K)	Oxygen Activity (atm.)
13	0	30	101000	1423	1×10^{-8}
	75		600	1553	1.8×10^{-10}
14	0	60	101000	1585	1×10^{-7}
	15		600	1577	8.6×10^{-9}
	60		600	1527	7.4×10^{-9}
15	0	60	101000	1415	1×10^{-7}
	20		600	1503	1.9×10^{-8}
	60		600	1527	5.1×10^{-9}
	120		13	1556	1.2×10^{-9}

Table 8.6 summarizes the oxygen activity measurements taken during Experiments 13, 14 and 15. The starting oxygen activity data was obtained from the literature (16). The Emf recordings from the (Ni/NiO) Temp-Q-Tip probes were then used to calculate the oxygen activities (see Section 7.3.2). From the observed values, it can be seen that the oxygen activity fell by a factor of ten during the degassing period (first 15 minutes of the experiment). During the subsequent refining period, the oxygen activity fell by a further factor of two to ten, for a total of a twenty to one hundred fold fall. This oxygen activity drop was taken into account when modeling the different behaviors of some species in alumina crucible vacuum refining experiments.

8.3.4 Vacuum Refining Elimination Rates

Selection of the Data Points for Regression

A simple, unbiased system was used in selecting which of the experimental points would be used for further analysis. It functioned as follows, either an experiment was accepted and all the experimental points were retained for the regressions or the experiment was rejected due to some identifiable technical problems.

Two experiments, # 1 and # 13, were rejected. Experiment 1 was rejected due to a broken window during the depressurization period. There were not enough points available to perform a regression. Experiment 13 was rejected because the chamber pressure exceeded 600 pascal. At such high pressures, lead evaporation is not liquid phase controlled and thus, no reference was available to calculate the evaporation rate coefficients (i.e., the area in the LSV experiment was unknown).

Experiment 15 was divided into two parts for analytical purposes. For the first 60 minutes of the experiment, the chamber pressure was maintained around 600 pascal. For the following 90 minutes the chamber pressure averaged 13 pascal. Thus, the experiment was subdivided into parts A and B depending on the chamber pressure used.

Shape of the Curves

The plots of the logarithm of the concentration ratio versus time could generally be divided into three regions. During the first 10 or 20 minutes of the experiment the graph takes on a concave shape. This was due to the slow depressurization at the start of the experiment required to prevent excessive splashing of the melt during degassing.

The graph then becomes linear once the pressure stabilized to the desired level. Here, the process followed first order kinetics, thus the rate of evaporation was calculated from the slope of the line.

Finally, on some experiments, there was a tendency by the impurity concentration to level out after an hour of treatment. This was explained by the vapour pressure of the impurities in the melt approaching the pressure in the chamber, i.e., the pressure difference term in Equation 10 became negligible.

Refining Rates, Alumina versus Graphite Experiments

Table 8.7 shows the overall experimental refining rate coefficient for bismuth, arsenic and antimony. These values are based on a lead removal rate of 2×10^{-4} ms^{-1} at chamber pressures of less than 100 pascal.

Experiments 10, 11 and 12 showed that lead, bismuth and arsenic removal were liquid phase controlled (>1.5 X 10^{-4} ms^{-1}) when the chamber pressure was below 100 pascal (alumina apparatus). Antimony removal was somewhat slower at 0.6 X 10^{-4} ms^{-1} and exhibited a combination of liquid and gas phase mass transfer control. In Experiments 2 to 7, which were performed in graphite apparatus, the removal rates of bismuth, arsenic and antimony were slower. Since the oxygen activity was 10^{-6} to 10^{-8} times lower in the graphite apparatus, we would expect the activity of the oxide vapours of bismuth, arsenic and antimony to be negligible in the graphite apparatus.

Experiments 8 and 9 were performed on white metal (78 % Cu). No arsenic or antimony removal was observed, which is consistent with the low activity coefficient of these impurities at high matte grade (> 70 % Cu).

Table 8.7 : Summary of the Impurity Overall Refining Rate for all the Vacuum Refining Experiments.

					Overall Refining Rate($X10^4$)			
Exp. #	Matte	Cu (%)	Temp. (K)	Press. (Pa)	K_{Bi} (ms^{-1})	K_{As} (ms^{-1})	K_{Sb} (ms^{-1})	K_{Pb} (ms^{-1})
1	Rv.	38	1423	1300	—	—	—	—
2	Rx.	65	1523	65	1.0	0.24	0.36	2.0
3	Rv.	36	1473	100	1.14	0.35	0.27	2.0
4	Rx.	59	1533	20	0.69	0.63	0.23	2.0
5	Rx.	60	1533	13	0.75	0.80	0.42	2.0
6	Rx.	63	1523	20	0.28	0.63	0.42	2.0
7	Rv.	40	1523	13	1.02	0.40	0.27	2.0
8	WM.	78	1523	13	0.88	0.0	0.0	2.0
9	WM.	78	1533	13	0.65	0.0	0.0	2.0
10	Rv.	37	1473	78	1.78	2.32	0.66	2.0
11	Rv.	35	1493	91	1.75	1.83	0.10	2.0
12	Rx.	61	1483	78	1.92	1.12	0.58	2.0
13	Rv.	30	1473	600	--	--	--	--
14	Rx.	60	1533	600	0.41	0.0	0.0	0.12
15A	Rx.	60	1473	600	0.46	0.0	0.0	0.09
15B	Rx.	60	1600	13	1.30	0.17	0.10	0.68

Note : Experiments 1 to 9 in Graphite Apparatus.
Experiments 10 to 15 in Alumina Apparatus

Table 8.8: Overall Experimental Removal Rates; Comparison Between Alumina and Graphite Apparatus. (%Cu = 35, C.P. = 100 Pa and T = 1450 K)

Experiment #	Const. Material	Experimental Removal Rate (X 10^4 ms^{-1})			
		Pb	Bi	As	Sb
3	Graphite	2.0	1.14	0.35	0.27
10	Alumina	2.0	1.78	2.32	0.66
11	Alumina	2.0	1.75	1.83	0.10

Table 8.9 : Overall Experimental Removal Rates ; Comparison Between Alumina and Graphite Apparatus. (% Cu = 65, C.P. = 100 Pa and T = 1500 K)

Experiment #	Const. Material	Experimental Removal Rate (X 10^4 ms^{-1})			
		Pb	Bi	As	Sb
2	Graphite	2.0	1.00	0.24	0.36
12	Alumina	2.0	1.92	1.12	0.58

8.4 Mathematical Modeling of the LSV Refining Experiments

The mathematical modeling of the LSV refining experiments was carried out in two phases. Firstly, a model was written to calculate the overall mass transfer coefficient using the equations developed in Chapter 4. Secondly, a mathematical simulation of the LSV process was developed taking into account the spray area, starting impurity concentration, melt volume, etc.

8.4.1 Theoretical Overall Mass Transfer Coefficient

In general the mathematical model was in accordance to the measured refining rate coefficients. For example, Figure 5.1 (Chapter 5) shows the effect of matte grade on the removal rates of lead, bismuth, arsenic and antimony for a chamber pressure of 100 pascal using an alumina crucible. Similarly to what was observed in the experiments, the removal rates of arsenic and antimony decreased to small values when the matte grade increased to 80 % copper. The lead and bismuth removal rates remained greater than 1.5×10^{-4} ms^{-1} .

The observed behavior of arsenic was complex; the predicted removal rate increased along with the matte grade (up to 70 % Cu) due to the increase in oxygen activity in the melt. Then, it decreased due to the sharp drop in the activity coefficient when the matte grade increased from 70 to 80 % copper. No increase in the removal rate was observed in these experiments due to a lack of precision in the experimental method.

Figures 5.3 and 5.4 show that as the pressure increased from 10 to 1000 pascal, the lead and bismuth refining rates fell to approximately 0.5×10^{-4} ms^{-1}, as observed in the experiments. Arsenic and antimony rates reached values of less than 0.1×10^{-4} ms^{-1} and no removal was found in Experiment 14 and 15A.

8.4.2 LSV Refining Simulation

An LSV simulation was developed (Section 4.3.7). The simulation predicted removals of 98 percent for lead, bismuth and arsenic for a 60 minute refining period using a 65 % copper grade at a chamber pressure of 100 pascal. Under the same conditions, 70 % removal of antimony was expected. This was in accordance with the impurity removal previously observed for Experiments 10, 11 and 12.

Figures 5.8 to 5.11 show some deviation from linearity for lead, bismuth, arsenic and antimony concentration versus time plots. However, no leveling off of the impurity content of the melt as seen in the experiments was predicted by the model. It was observed during the experiments that, when the sum of of all impurity vapour pressures decreased to the same level as the chamber pressure, the refining process came to a stop. The impurities must be transported away from the LSV apparatus by bulk flow which resembles water vapour exiting from the mouth of a boiling kettle. To quickly transport the impurities away from the LSV apparatus, the inner pressure must be slightly higher than the outer pressure. Thus, the mathematical model should be modified to include a transport step to take into account the impurity bulk flow from the interface to the vacuum chamber. This updated model will facilitate the prediction of the cessation of the refining process due to the equalization of the impurity vapour and

chamber pressures.

8.4.3 Strength and Weaknesses of the Models and simulation

The main problem with the model, which was based on thermodynamic data, was that it depended on the reliability of the data input to the model. In order for the model to predict the lower evaporation rates in the graphite apparatus as compared to the alumina apparatus, the author had to lower the Gibbs energies of formation of AsS and SbS and raise the energies of formation of AsO and SbO vapours. These changes imply that the thermodynamic data on the energy of formation of AsS, SbS, AsO and SbO is not accurate in the literature.

Gibbs energy data for arsenic and antimony vapour formations is usually determined by transportation methods (55, 54, 44, 45, 46) performed in silica or alumina crucibles. However, experiments should also be performed in both graphite and alumina crucibles, and the results compared to obtain valuable data for both sulphide and oxide vapours. In graphite crucibles, the oxygen activity would be maintained between 10^{-14} to 10^{-16} atmosphere and thus, the amount of AsO and SbO vapours above the melt would be negligible and true measurements of AsS and SbS vapour concentration would be forthcoming. Thus, reliable energy of formation of AsS and SbS could be calculated from the mass spectrometer measurements. To obtain the data to calculate the energy of

formation of AsO and SbO vapours, experiments using alumina crucibles with controlled oxygen activity could be performed. In conclusion, the author believes that further work in this area should be pursued.

CHAPTER 9

Scaling-Up the LSV Process to Industrial Size

9.1 Introduction

In this chapter, an example of scaling up the L.S.V. process for a hypothetical copper smelter is presented. Figure 9.1 shows the flow sheet of the process and the location of the L.S.V. refining step between the smelting and converting step. In this example, it was assumed that the smelting unit produces a matte grade of 65% copper. The total capacity of the smelter is 1,000 metric tons of copper per day. An 80% impurity removal of Bi, As, and Sb is desired.

Fig. 9.1 : Simplified Copper Sulphide Smelting Flowsheet and Location of an LSV Copper Matte Refining Unit.

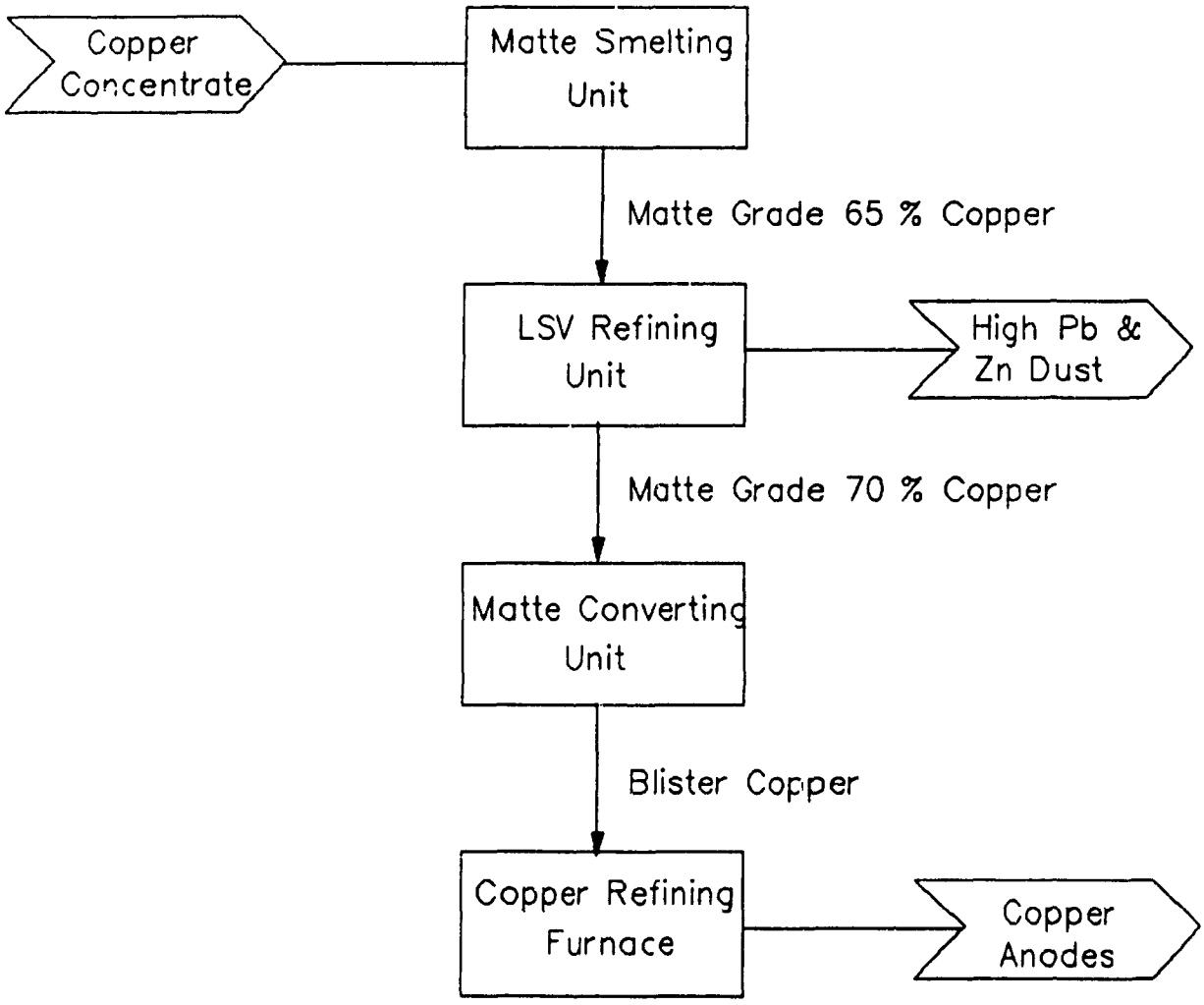

Table 9.1: Selected Parameters for Scale-Up Example of LSV Apparatus.

Cu Production:	1,000 T/day
Matte grade to L.S.V. unit:	70% Cu
Percent impurity Removal:	80% (Pb, Zn, Bi & As)
	40% (Sb)
Chamber pressure:	100 Pa
Overall removal rate :	$>1x10^{-4}ms^{-1}$ (Pb, Zn, Bi & As)
	$>0.5x10^{-4}ms^{-1}$ (Sb)
Ladle size:	$6m^3$, 30 Tonnes

Note: To achieve refining rates of Sb higher than $10^{-4}ms^{-1}$, a chamber pressure of 10pa or less must be chosen.

9.2 Calculation of Circulation Rates

9.2.1 Scale up parameters

The magnitude of several physical parameters were required to scale up the process to industrial size, shown in Table 9.2. Figure 9.2 shows a schematic diagram of the riser leg to help explain the scale up parameters. The **lift height**, L.H., is the length of the leg above the liquid level. The **lift ratio** is the lift height divided by the sum of the lift height plus the nozzle submergence. The **nozzle submergence**, N.S., is the depth under the liquid level, where the lifting gas is injected. Consultation with various operators of RH degassing units in the steel industry, indicated that a reasonable spray height of two meters could be achieved. The agreed upon spray height was then used to calculate the exposure time of the droplets in the vacuum assuming an unrestrained parabolic flight path under the action of gravity.

A lift ratio of 0.1 and a nozzle submergence of 0.70 meters were selected from the work of Lee (86). These values represent the optimum conditions for maximum spray areas according to Lee. The required riser diameter and gas flow rate could then be calculated.

Table 9.2 : Scale-Up Parameters for Riser.

Spray Height :	2 m
Lift Ratio :	0.1
Nozzle Submergence :	0.70 m
Tube Diameter :	?
Gas Flow Rate :	?

Fig. 9.2 : Schematic Diagram of the Riser Leg from an LSV Refining Apparatus.

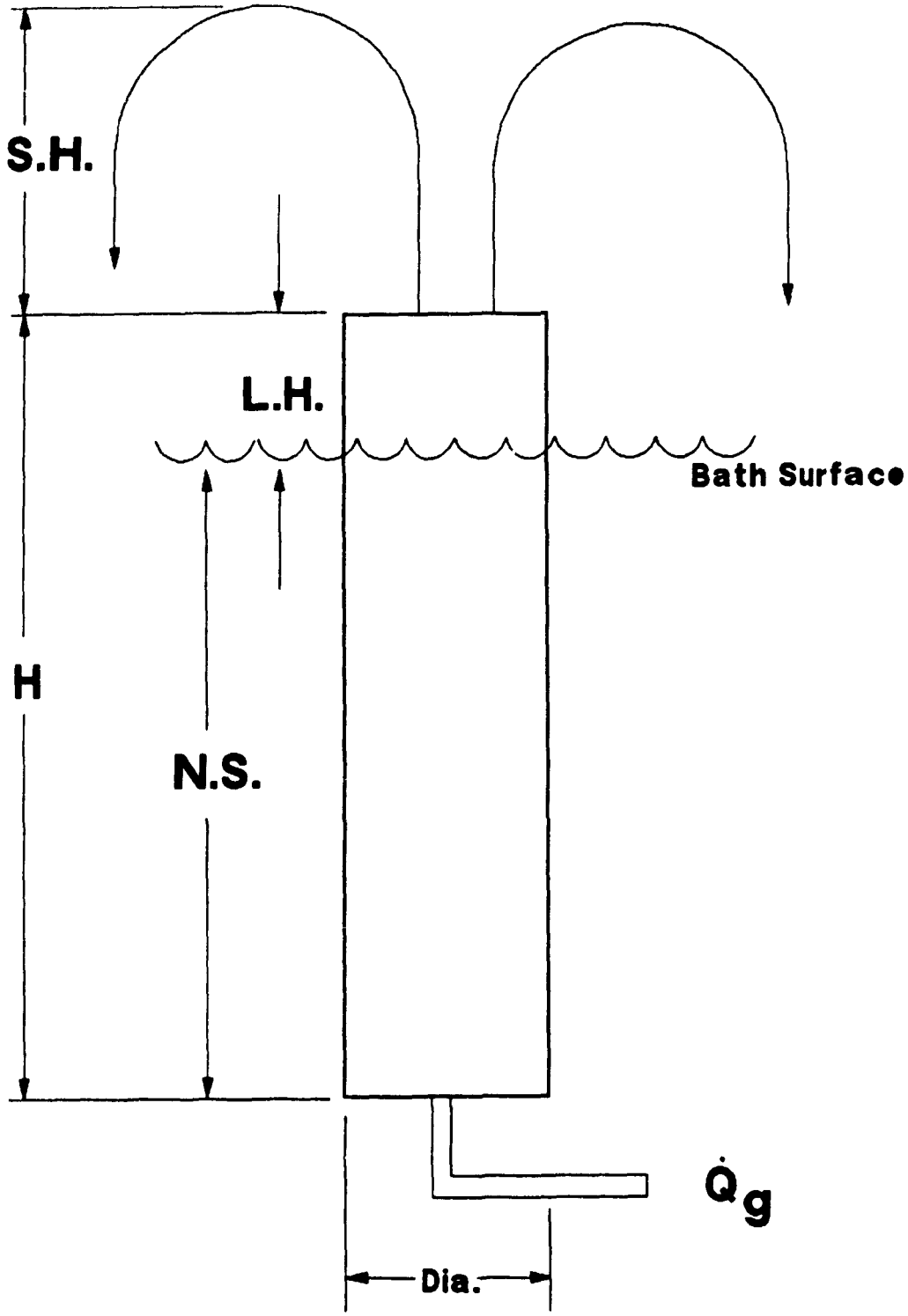

9.2.2 Calculations of Riser Diameter

A smelter producing 1,000 tonnes/day of copper produces a 30 tonne ladle of 70% matte every 30 minutes (V = 6 m^3). Thus, a maximum refining time of a 30 minutes seems reasonable. This time was substituted into Equation 37 for a batch vacuum refining operation. The ratio of the final to initial concentration was set at 0.2 (80 % impurity removal), an overall rate of refining of 10^{-4} ms^{-1} was chosen as was a ladle volume of 6 m^3. The surface area required was calculated to be 54 m^2 (Fig. 9.3).

Assuming a parabolic flight path and a spray height, S.H., of 2 meters, the exposure time, t_e, was calculated from the formula, S.H. = 0.5 g t_e^2, where g is the gravitational acceleration (9.8 ms^{-2}). The calculated time was doubled to account for the rise and fall of the droplets back into the melt. The calculated time of flight, i.e. the exposure time, was 1.3 seconds.

The volume of liquid suspended in the vacuum (V.S.) at any point in time was given by the flow rate of copper matte up the riser leg multiplied by the exposure time, t_e. Assuming the droplets were spherical, the volume suspended multiplied by three and divided by the radius of one droplet was equal to the surface area of the droplets suspended. The area required for the desired refining was calculated at 54 m^2 and

the stable droplet diameter at 0.01 meters (from visual observation of copper matte LSV experiments and calculation of the stable droplet size, Section 4.3.6). Thus, the volumetric flow rate of matte was calculated to be 0.07 m^3s^{-1} or 21 tonnes per minute.

Figure 9.4 plots the superficial liquid velocity versus the superficial gas velocity (86). It can be seen that for a liquid velocity of 0.5 ms^{-1}, a gas velocity of 1.2 ms^{-1} is required. This figure was obtained from a LSV water model representing a fifth of the actual industrial size. The modeling study showed the fastest refining rates at lift ratios between 0.1 to 0.2 .

Since, the superficial liquid velocity was equal to the volumetric flow rate of matte divided by the cross-sectional area of the riser leg, a riser diameter of 0.42 m (16 inches) was calculated. Using the riser cross-sectional area, the superficial gas velocity (1.2 ms^{-1}), the melt temperature (1473 K) and the head of copper matte (0.35 m), the necessary gas flow rate of 5.20 ls^{-1} NTP was calculated.

Fig. 9.3 : Sample Calculations to Scale-Up the LSV Apparatus to Industrial Size.

$$1\ \text{Ladle} \longrightarrow 30\ \text{minutes}$$

$$\ln(0.2) = (10^{-4}) \cdot \frac{A}{6} \cdot (1800) \longrightarrow A = 54\ m^2$$

$$S.H. = 0.5\ a\ t^2 \longrightarrow t = 0.64\ s$$
$$te = 1.3\ s$$

$$Q_l \times te = V.S. \longrightarrow V.S. \times 3/R = A$$

$$Q_l = 0.07\ m^3 s^{-1} \longrightarrow J_l = 0.5\ ms^{-1}$$
$$J_g = 1.2\ ms^{-1}$$

$$J_l = Q_l/\pi R^2 \longrightarrow D = 0.4\ m$$
$$Q_g = 5.20\ ls^{-1} NTP$$

R.H. Degassing of Steel (92)

$$Q_g = 13.2\ ls^{-1} \longrightarrow D.Tube = 0.4\ m$$

Fig. 9.4 : Superficial Gas Velocity versus Superficial Liquid Velocity in Riser Leg. Graph Plotted from 1/5 Industrial Water Model from Reference 86.

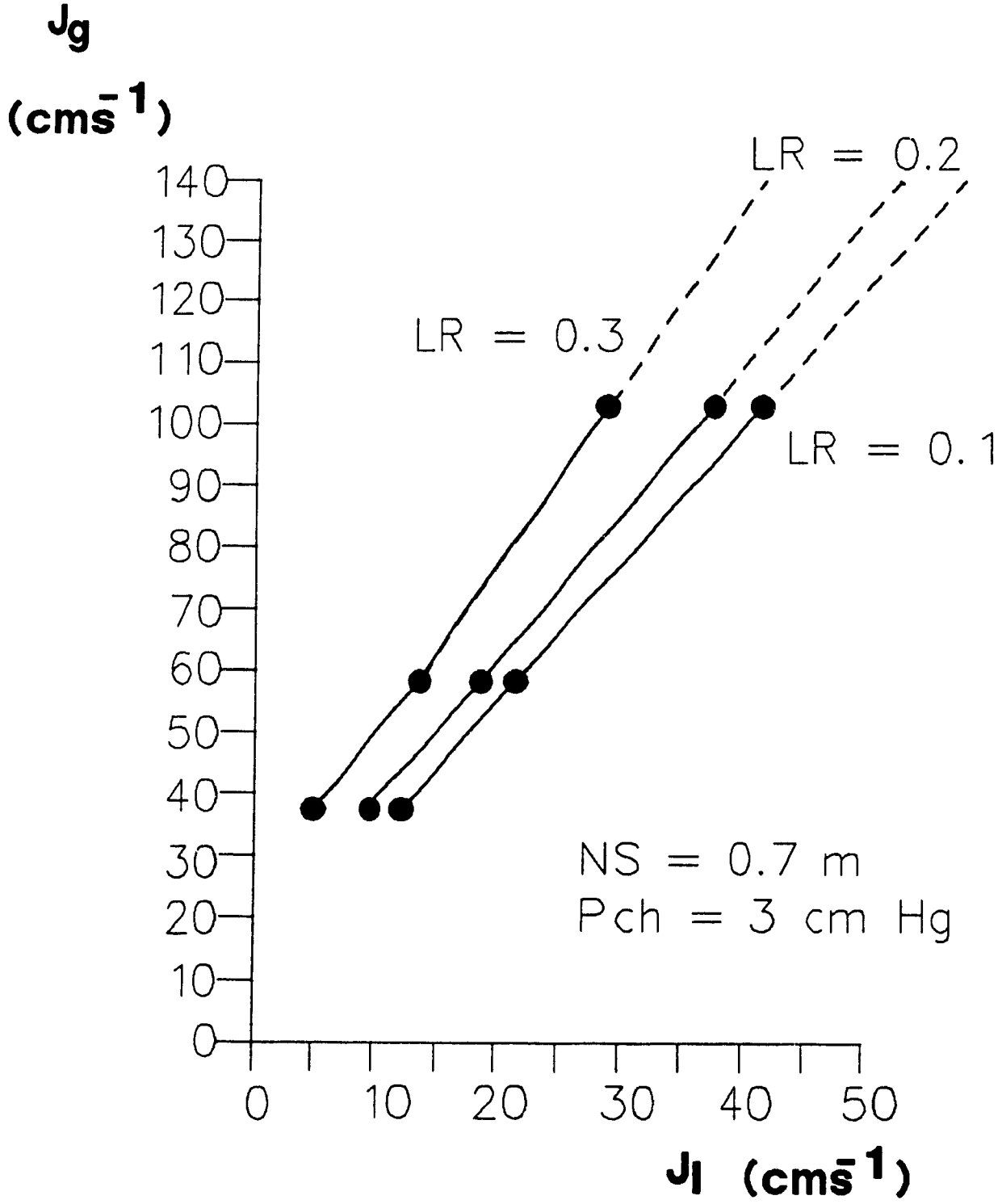

9.3 Comparison with RH Degassing Units

Typical data for RH degassing units were obtained from interviews with people in the steel industry (92). In a RH degasser for example, 60 tonnes per minute of steel is circulated with a gas flow rate of 13.2 Nls^{-1} up a leg of 0.4 m in diameter. This gives a volumetric flow rate of about 0.13 m^3s^{-1} and a superficial liquid velocity of 1.0 ms^{-1}. These values are double those calculated in section 9.2.2 thus, LSV refining is well within today's engineering expertise.

Figure 9.5 shows a schematic diagram of what an L.S.V. apparatus would look like and with its dimensions. It can be constructed like an RH type unit with a minor modification to the riser leg which would be made to extend into the vacuum chamber, above the liquid matte level. The vessel's diameter would be 3.2 meter to accommodate the minimal one meter radial dispersion of the spray (discussion with RH degassing unit operators). The free board would be 2 meters above the spray to avoid excessive splashing into the exit vacuum duct. An alternative would be to construct a baffle in front of the vacuum exit to deflect the splashes. The lifting gas would be nitrogen because of the small NTP flow rates and because when air was used in a pilot trial (Experiment 10), the gas flow rate was erratic and the injetor blocked after 45 minutes.

Nitrogen could be injected into the down leg to control liquid levels in the chamber. The vacuum chamber walls would have to be kept at a temperature of 1,050^{o}C to avoid matte splashes from freezing and impurities from condensing in the upper part of the chamber.

The gas pumping could be carried out using steam ejectors or mechanical pumps depending on the pressure desired in the chamber. The gas pumping rate should be sufficient for rapid degassing of the melt (< 10 minutes) and to maintain a chamber pressure of 100 pascal with the lifting gas flowrate plus the system's air infiltration.

Fig. 9.5 : Schematic Diagram of Possible Industrial Size LSV Copper Refining Unit (not to Scale).

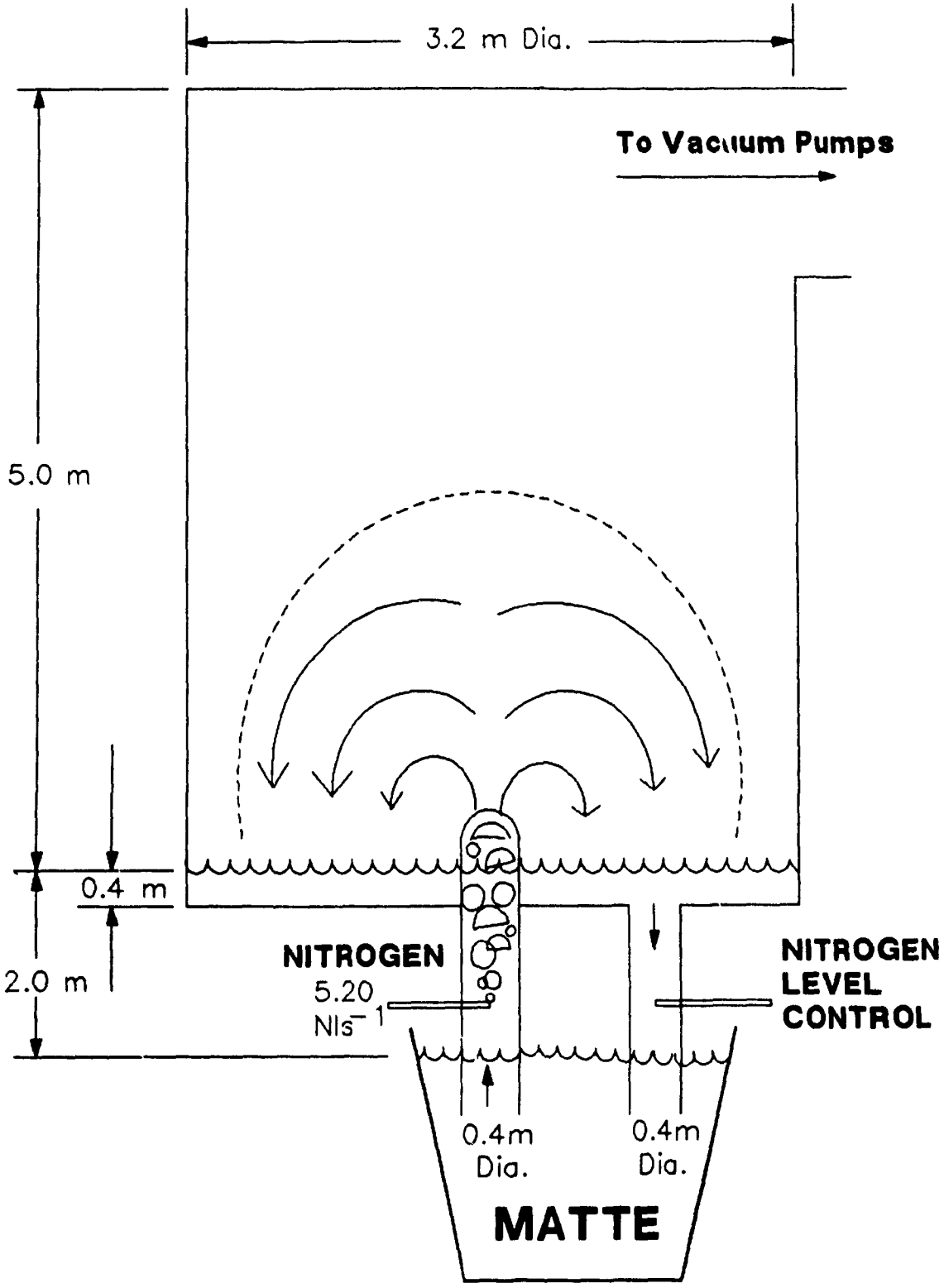

CHAPTER 10

Conclusions

The feasibility of using the Lift-Spray Vacuum refining apparatus to enhance the rate of vacuum refining copper matte melts was demonstrated in these small scale pilot trials. More specifically, the vacuum refining rates of lead, bismuth arsenic and antimony were monitored. Removal rates were not measured for silver, nickel and selenium.

From the dust characterization and selective condensation experiments, it was found that :

1- The main mineralogical species in the condensate were metallic lead, lead sulphide and zinc sulphide. The copper present in the dust was the result of copper matte prills ejected during the experiments.

2- The mean size of the dust particles (d_{50}) was eighty microns. However, from scanning electron microscopy, it was observed that the condensate particles were clusters of smaller sub-micron particles.

3- By removing the large copper matte particles, or preventing their transport outside the LSV apparatus, a condensate of less than two percent copper might be produced.

From the Lift-Spray Vacuum refining experiments, it was concluded that:

4- The LSV apparatus significantly increased the surface area available for impurity evaporation from the copper matte melt.

5- When air was used as a lifting gas instead of nitrogen, the gas flow rate was erratic and the injector blocked after a few minutes.

6- Rapid overall rates of refining of lead, bismuth and arsenic (larger than 1.5×10^{-4} ms^{-1}) were measured in an alumina lined apparatus at chamber pressures of less than 100 pascal. For the same conditions, antimony removal rate was observed between 0.5 and 1.0×10^{-4} ms^{-1}.

7- In a graphite apparatus, where the oxygen activity is 10^{-8} times lower than in alumina lined apparatus, only the lead removal rate remained above $1.5 \times 10^{-4} ms^{-1}$. The removal rates of bismuth and arsenic decreased as compared to the alumina apparatus to between 0.5 and 1.1×10^{-4} ms^{-1}.

8- Fourty to sixty minutes into the refining process, the evaporation rate of all impurities started to drop and the impurity content of the matte leveled off. This occurred when the sum of the impurities vapour pressures dropped down to

the level of the chamber pressure.

9- A mathematical model was developed to predict lead, bismuth, arsenic, antimony and zinc removal rates using metallic, sulphide dimer and oxide dimer vapour pressures. Concordance between the model and the measured removal rates of the impurities was observed for both the alumina and graphite apparatus.

Using both the pilot plant data generated during this study and the data from Lee's water model (86), it is now possible to scale up the LSV refining unit to industrial size. The calculated dimensions compared well to the R.H. degassing units used in the steel industry.

CHAPTER 11

Suggestions for Future Work

Future studies should extend into two areas, the development of the LSV vacuum refining process and the thermodynamic properties of arsenic and antimony.

The future work on the LSV process would include :

1) Modifying the LSV configuration to reduce the matte losses ejected from the melt.

2) Comparison of the LSV process configuration to the RH degassing unit or a plume of inert gas in a ladle under vacuum.

3) Perform still vacuum refining experiments with antimony doped copper matte to obtain more reliable data on antimony evaporation rate.

4) Carry out pilot scale size LSV processing to study riser design materials, i.e. refractory. Further examine the effect of bath depth on the dissolved oxygen content of the copper matte.

5) Investigate the use of SO_2 as a lifting gas to keep the oxygen activity in the melt as high as possible.

6) Determine the heat losses associated with the vacuum refining process to gain knowledge of the energy requirements needed to keep the melt temperature constant at the desired level.

7) Do still vacuum refining experiments with selenium doped

copper matte and blister copper in alumina crucibles to confirm whether or not it is possible to remove selenium by vacuum refining.

8) Modify the vacuum refining theory and mathematical model to take into account the levelling off of the impurity concentrations.

The future work on the thermodynamic properties of arsenic and antimony would involve the following :

1) Develop an experimental technique where the oxygen and sulphur potential of the copper matte could be controlled.

2) Carry out transportation experiments (at very low oxygen activity in the melt) on synthetic Cu_2S-FeS copper matte to gain reliable data on the activity coefficient of arsenic and antimony in copper matte.

3) Carry out transportation experiments on copper matte with a controlled amount of dissolved oxygen to gain knowledge of the contribution of the arsenic and antimony oxide vapours and thus, be able to calculate reliable Gibbs Free energy of formation of the diatomic arsenic and antimony oxides and sulphides.

CHAPTER 12

Original Contributions

The following is a list of the original contributions accomplished during this study :

1) The three step mass transport theory to explain the evaporation of monoatomic vapours from metallic melts was extended to a multi component evaporation model. The model explains how minor elements (less than one weight percent) such as zinc, lead, arsenic, antimony, bismuth, etc, evaporate from copper matte melts in the form of monoatomic ($i_{(g)}$), diatomic sulphide ($iS_{(g)}$) and diatomic oxide ($iO_{(g)}$) vapours. The model based on fundamental thermodynamic data such as Gibbs energy of formation and activity coefficient, can be applied to copper matte, blister copper and other metal, metal oxide and metal sulphide mixtures.

2) A series of experimental procedures was developed to characterize and selectively condense the vacuum refining dust. These experiments proved that the zinc and lead fractions can be condensed separately by controlling the temperature of the condenser wall and the total chamber pressure. The vacuum refining dust was shown to be composed mainly of sub-micron particles of zinc sulphide (ZnS), lead sulphide (PbS) and metallic lead (Pb) clustered into larger particles having a mean diameter of eighty microns.

3) A new vacuum refining experimental procedure was developed where two sets of experiments were carried out, one in a graphite apparatus and one in an alumina apparatus. During the alumina apparatus experiments, the oxygen activity in the melt was measured at different chamber pressures and refining times.

4) The experimental procedure and vacuum refining model mentioned above was used as a novel transportation technique to verify the consistency of the thermodynamic data of the volatile impurities i.e., activity coefficient and Gibbs energy of formation of the diatomic sulfide and diatomic oxide species. Analysis of the experimental data showed that the arsenic and antimony vapour pressures are higher than the arsenic and antimony sulphide pressures above copper matte melts saturated with oxygen. This result contradicts the free energy of formation data presently published in the literature for arsenic and antimony.

6) Using the water modeling work of H.S.Lee (86) and the copper matte LSV vacuum refining experiments, the scale-up calculations of the LSV refining apparatus to a full size copper smelter were performed. The calculated dimensions as well as the required lifting gas flow rate were found to be comparable to RH degasser technology used in the steel industry. Thus the LSV process can now be confidently scaled-up and commercialized.

References

1. Davenport, W.G. and Biswas, A.K., "Extractive Metallurgy of Copper", Pergamon Press, Oxford, England, 1976.

2. Ozberk, E. and Guthrie, R.I.L., "Vacuum Melting of Copper - Evaporation of Impurities", Proc. 6th Intl.Vacuum Metallurgy Conf., San Diego, Apr. 1979, Amer. Vac. Soc., New York, N.Y., pp 248-267, 1979.

3. MacKey, P.J., McKerrow, G.C. and Tarsassoff, P., "Minor Elements in the Noranda Process", Paper Presented at 104th AIME Annual Meeting, New York, NY, Feb. 1975, Met. Soc. AIME Annual Meeting, Warrendale, P.A., 1975.

4. Suzuki, T. and Shibasaki, T., "Behavior of Impurities in Mitsubishi Cont. Copper and Converting Process", Paper A75-40, 104th AIME Annual Meeting, New York, NY, Feb. 1975, Met. Soc. AIME, Warrendale, P.A., 1975.

5. Player, R.L., "Removal of Impurities from Copper Matte by Vacuum Treatment", Proc. 6th Intl. Vac. Met. Conf., San Diego, CA, April 1979, Amer. Vac. Soc., New York, NY, pp 214-224, 1979.

6. Harris, R., "Vacuum Refining Copper Melts to Remove Bismuth, Arsenic and Antimony", Metall. Trans. B, Vol. 15B, June, pp 251-257, 1984.

7. Hiroshi, K., Haruhiko, A., Toshihiko, I. and Takashi, S., "Behavior of Minor Elements in Onahama Smelter", Met. Rev. MMIJ, Vol. 3, #1, April, pp 145-157, 1986.

8. Persson, S.A. and Harris, R., "Tin Elimination from Melted Scrap Steel", Erz Metall, Vol. 37, No. 4, pp 174-178, 1984.

9. Kametami, H. and Yamauchi, C., "Vacuum Lift Refining in Copper Smelting", Transaction of National Research Institute for Metals, Japan, Vol. 20, No. 1, 1978.

10. Itagaki, K. and Yasawa, A., "Thermodynamic Evaluation of Distribution Behavior of Arsenic, Antimony and Bismuth in Copper Smelting", Advances in Copper Smelting, ed by H.J. Sohn, D.B. George and A.D. Zunkel, Met. Soc. AIME, Warrendale, P.A., pp 119-142, 1083.

11. Nagamori, M. and MacKey, P.J., "Thermodynamics of Copper Matte Converting: Part I Fundamentals of the Noranda Process", Metall. Trans., Vol. 9B, June, pp 255-265, 1975.

12. Nagamori, M. and MacKey, P.J., "Thermodynamics of Copper Matte Converting: Part II. Distribution of Au, Ag, Pb, Zn, Se, Te, Bi, Sb, and As between Copper Matte and Slag in the Noranda Process", Metall. Trans., Vol. 13B, Sept., pp 319-329, 1982.

13. Nagamori, M. and Chaubal, P.C., "Thermodynamics of Copper Matte Converting: Part III. Steady State Volatilization of Au, Ag, Pb, Zn, Ni, Se, Te, Bi, Sb, and As from Slag, Matte and Metallic Copper", Metall. Trans. Vol. 13B, Sept., pp 319-329, 1982.

14. Nagamori, M and Chaubal, P.C., "Thermodynamics of Copper Matte Converting: Part IV. A Priori Predictions of the Behavior of Au, Ag, Pb, Zn, Ni, Se, Te, Bi, Sb and As in the Noranda Process Reactor", Metall. Trans., Vol. 13B, Sept., pp 331-338, 1982.

15. Tarassof, P., "Process R + D - The Noranda Process", Metall. Trans. B, Vol. 15B, pp 411-432, 1984.

16. Mackey, P.J., "The Physical Chemistry of Copper Smelting Slags - A Review", International Symposium on Metallurgical Slags, Halifax, Nova Scotia, Aug. 1980, p70, Can. Inst. Min. Metall., Montreal, P.Q., 1980.

17. Harris, G., "Treatment of Non-Ferrous Smelter Dust by Hydrometallurgical Processes", Seminar on Processing of Metallurgical Residues, May 13-15, 1985, McGill University, Montreal, P.Q., 1985.

18. Geiger, S.H. and Poirier, D.R., "Transport Phenomena in Metallurgy", Addison-Wesley Publishing Company, Reading, Mass., pp 463-546, 1980.

19. Higbie, R., "The Rate of Absorption of a Pure Gas into a Still Liquid During Short Periods of Exposure", Trans. Am. Inst. Chem. Engs., Vol. 31, pp 365-389, 1935.

20. Ward, R.G., "Evaporative Losses During Vacuum Induction Melting of Steel", J. Iron Steel Inst., pp 11-15, Jan. 1963.

21. Balfour, G.C., Vogt, J.A. and Mackey, P.J., "Current Converter Practice at the Horne Smelter", Proceedings of 108th AIME Meeting, Feb. 19-21, 1979, Met. Soc. AIME, Warrendale, P.A..

22. Roine, A. and Jalkanen, H., "Activities of As, Sb, Bi and Pb in Copper Mattes", Metall. Trans. B, Vol. 16B, pp 129-141, 1985.

23. Irons, G.A., Chong, C.W., Guthrie, R.I.L. and Szekely, J., "The Measurement and Prediction of the Vaporization of Magnesium from an Inductively Stirred Melt", Metall. Trans. B, Vol. 9B, March, pp 151-154, 1978.

24. Schmitt, P. and Wuth, W., "Mass Transfer in Pyrometallurgical Top Blowing System", in 'Heat and Mass Transfer in Metallurgical System', D.B. Scalding and W.H. Afgan (eds), Hemisphere Publishing Corporation, Washington, pp 272-280, 1981.

25. Kraus, T., "The Mechanism of Material Exchange between a Highly Rarified Gas and its Solution in a Molten Metal", Schweizer Arch. Wiss. Tech., Vol. 28, pp452-468, 1962.

26. Treybal, Robert E., "Mass Transfer Operations", McGraw-Hill Book Company, New York, 1968.

27. Dimayuga, F., "Vacuum Refining of Molten Aluminum", PhD Thesis, McGill University, 1986.

28. Herbertson, J. and Harris, R., "Kinetics of Electron-Beam Refining of Liquid Metals", 8th ann. ICVM, Oct. 1985, Linz, Austria, Vac. Met. Soc. pp 273-282, USA, 1985.

29. Nakamura, T., Ueda, Y., Noguchi, F. and Toguri, J.M., "The Removal of Group Vb Elements (As, Bi, Sb) from Molten Copper Using a Na_2CO_3 Flux", Can. Met. Quart., Vol. 23, pp 413-419, 1984.

30. Yasawa, A. and Itagaki, K., "Thermodynamic Properties of Arsenic and Antimony in Copper Smelting Systems", Proc. CIM-AIME Complex Sulphide Symp., San Diego California, Met. Soc. AIME, Warrendale, P.A., Nov. 10-13, 1985, pp 705-722, 1985.

31. Herbertson, J., Dimayuga, F. and Harris, R., "Vacuum Refining as a Process Option in Recycling Aluminum Scrap", Proc. Int'l. Symp. Recycle and Secondary Metals, Florida, Met. Soc. AIME, Warrendale, P.A., Dec., pp 97-105, 1985.

32. Weisenberg, I.J., Bakshi, P.S. and Vervaert, A.E., "Arsenic Distribution and Control in Copper Smelters", Journal of Metals, Oct., pp 38-44, 1979.

33. Imris, I., Komorova, L. and Holmstrom, A., "Behavior of Antimony during the Roasting of Tetrahedrite Concentrates", Extractive Metallurgy '85, IMM London, Sept., pp 1015-1033, 1985.

34. Bryan, R., Pollard, D.M. and Willis, G.M., "Removal of Bismuth from Copper by Vacuum Refining", Australia Japan Ext. Met. Symp., Sydney, Australia, 1980, Aus.IMM, Sydney, pp 439-448, 1980.

35. Kubaschewski, O. and Alcock, C.B., "Metallurgical Thermochemistry", 5th ed., Pergamon Press, N.Y., 1979.

36. Danovitch, D., "Vacuum Refining of Copper Melts", M.Eng. Thesis, McGill University, Montreal, 1982.

37. Ozberk, E., "Vacuum Refining of Copper", M.Eng. Thesis, McGill University, Montreal, 1980.

38. Persson, H.A., "Vacuum Removal of Sulphur and Tin from Liquid Steel", M.Eng. Thesis, McGill University, Montreal, 1981.

39. Harris, R.L., "Vacuum Refining of Molten Steel", PhD Thesis, McGill University, Montreal, 1980.

40. Roth, A.,"Vacuum Technology", 2nd ed., North-Holland Publishing Co., N.Y., pp 1-120, 1982

41. Chaubal, P.C. and Nagamori, M., "Volatilization of Bismuth in Copper Matte Converting, Computer Simulation", Metall. Trans. B, AIME, Vol 13B, Sept., pp 339-348, 1982.

42. Ozberk, E. and Guthrie, R.I.L., "A Kinetic Model for the Vacuum Refining of Inductively Stirred Copper Melts", Metall. Trans. B, Vol 17B, March, pp87-102, 1986.

43. Sinha, S.H., Sohn, H.Y. and Nagamori, M., "Distribution of Lead between Copper Matte and the Activity of PbS in Copper Saturated Mattes", Metall. Trans. B, Vol 15B, Sept., pp 441-449, 1984.

44. Roine, A., "Activities of As, Sb, Bi and Pb in Copper Mattes - Effect of O, Ni and Co", Metall. Trans. B, Vol. 18B, pp 203-212, 1987.

45. Roine, A., "Activities of As, Sb, Bi and Pb in Copper Mattes - Impurity Elimination", Metall. Trans. B, Vol. 18B, pp213-223, 1987.

46. Roine, A., "Activities of As, Sb, Bi and Pb in Copper Mattes and their Effects on Impurity Elimination", PhD. Thesis, Helsinki University of Technology, 1988.

47. Chaubal, P.C. and Nagamori, M. ,"Thermodynamics for Arsenic and Antimony in Copper Matte Converting - Computer Simulation", Metall. Trans. B, Vol. 19B, pp547-556, 1988.

48. Harris, R. and Davenport, W.G., "Pilot Plant Scale Vacuum Distillation of Liquid Steel to Remove Copper", Can. Met. Quart., Vol. 18, pp303-311, 1979.

49. Harris, R., "Vacuum Refining Molten Tin to Remove Lead and Bismuth", Pyrometallurgy '87, Proc. Symp., 21-23 Sept., 1987, London, England, IMM, London, England, pp461-482, 1987.

50. Allaire, A. and Harris, R., "Vacuum Refining of Copper Matte", Proc. CIM-AIME Int'l Complex Sulphide Symp., Nov. 1985, San Diego, Ca., Met. Soc., AIME, pp683-702, 1985.

51. Ozberk, E. and Guthrie, R.I.L., "Vacuum Melting of Copper - Evaporation of Impurities", Proc. 6th Intl Vacuum Metallurgy Conf., San Diego, Apr. 1979, Amer. Vac. Soc., New York, N.Y., pp248-267, 1979.

52. Allaire, A., "Vacuum Refining of Copper Matte", M.Eng. Thesis, McGill University, Montreal, 1986.

53. Harris, R. and Davenport, W.G., Canadian Patent No. 1178142 and USA Patents Nos. 4378242 and 4456479.

54. Hino, M., Toguri, J.M. and Nagamori, M., "The Gibbs Free Energy of Gaseous AsS", Can. Met. Quart., Vol. 25, pp 195-197, 1986.

55. Hino, M., Toguri, J.M. and Nagamori, M., "Thermodynamics of Gaseous SbS", Metall. Trans., Vol. 17B, pp913-914, 1986.

56. Harris, R., Dimayuga, F. and Pouliquen, B., "Lift-Spray Vacuum Processing (LSV) of Molten Aluminum", Trans. IMM, Sect. C, Vol. 95, ppC199-C205, 1986.

57. Harris, R., "Numerical Simulation of Vacuum Refining of Liquid Metal", Can. Met. Quart., Vol.27 ,pp 169-178 , 1988.

58. Kaiser, D.L. and Elliott, J.F., "Solubility of Oxygen and Sulphur in Copper Iron Mattes", Metall. Trans. B, Vol. 17B, pp147-157, 1986.

59. Kaiura, G.H. and Toguri, J.M., "Densities of the Molten FeS, FeS-Cu_2S and Fe-S-O System - Utilizing a Bottom-Balance Archimedean Technique", Can. Met. Quart., Vol. 18, pp155-164, 1979.

60. Otsuka, S. and Chang, Y.A., "Activity Coefficient of Oxygen in Copper-Sulphur Melts", Metall. Trans. B, pp 337-344, 1984.

61. Harris, R., McClincy, R.J. and Rielbling, E.F., "Bismuth, Arsenic and Antimony Removal from Anode Copper via Vacuum Distillation", Can. Met. Quart., Vol. 26, pp1-4, 1987.

62. Ayhan, M., Dengher, K.W., Krone, K.W. and Kruger, J.G., "Vacuum Distillation of Copper Alloy Scrap and Lead Copper Matte", Proc. 8th ICVM Intl Conf., Sept 30-Oct 4, Linz, Austria, pp877-896, 1985.

63. Celmer, R., Yamamoto, M. and Toguri, J.M., "Vapour Pressure of Arsenic", Can. Met. Quart., Vol. 23, pp169-172, 1984.

64. Hino, M. and Toguri, J.M., "Antimony Activities in Copper Mattes", Metall. Trans. B, Vol. 18B, pp189-193, 1987.

65. Hino, M. and Toguri, J.M., "Arsenic Activities in Molten Copper and Copper Sulphide Melts", Metall. Trans. B, Vol. 17B, pp755-761, 1986.

66. Alcock, C.B., Itkin, V.P. and Horrigan, M.K., "Vapour Pressure Equations for the Metallic Elements: 298-2500K", Can. Met. Quart., Vol. 23, pp309-313, 1984.

67. Smale-Adams, K.B., "The Mineral Industry, the Institution and Everything", Trans. IMM, Sect. C, Vol. 92, ppC29-C34, 1983.

68. Ozberk, E. and Guthrie, R.I.L., "Evaluation of Induction Melting for Copper Refining", Trans. IMM, Sect. C, Vol. 94, ppC146-C157, Sept., 1984.

69. Ozberk, E and Guthrie, R.I.L., "Application of Vacuum Refining in Copper Production", Mat. Sci. Tech., Vol. 1, pp12-18, Jan., 1985.

70. Kametami, H., Yamauchi, C., Murao, K. and Hayashida, M., "A Fundamental Study on the Vacuum Treatment of Molten Matte and White Metall", Trans. Jap. Inst. Met., Vol. 14, pp218-223, 1973.

71. Pouliquen, B. and Harris, R., "Gas Injection into Liquids Exposed to Reduced Pressure", ERZ Metall., Vol. 39, pp31-36, 1986.

72. Holzgruber, W., "An Overview on Secondary Liquid Metal Refining Processes and Outlook", 8th ann. ICVM, Oct., 1985, Linz, Austria, Vac. Met. Soc., USA, pp477-496, 1985.

73. Frurip, D.J. and Bauer, S.H., "Homogeneous Nucleation in Metal Vapors. 4. Cluster Growth Rates from Light Scattering", The Journal of Physical Chemistry, Vol. 81, No. 10, pp1007-1015, 1977.

74. Larrain, J.M., Lee, S.L. and Kellogg, H.H., "Thermodynamics Properties of Copper-Sulphur Melts", Can. Met. Quart., Vol. 18, pp395-400, 1979.

75. Pomfret, R.J. and Grieveson, P., "The Kinetics of Slag-Metal Reactions", Can. Met. Quart., Vol. 22, pp287-299, 1983.

76. Bjorkman, B. and Eriksson, G., "Quantitative Equilibrium Calculations on Conventional Copper Smelting and Converting", Can. Met. Quart., Vol. 21, pp329-337, 1982.

77. Kumar, M.L., Li, K. and Warren, G.W., "Gas-Phase Chlorination of Chalcopyrite", Can. Met. Quart., Vol. 24, pp335-343, 1985.

78. Turkdogan, E.T., Grieveson, P. and Darken, L.S., "Enhancement of Diffusion-Limited Rates of Vaporization of Metals", The Journal of Physical Chemistry, Vol. 67, pp1647-1654, 1963.

79. Turkdogan, E.T., "The Theory of Enhancement of Diffusion-Limited Vaporization Rates by a Convection-Condensation Process. Part I - Theoretical", Trans. Met. Soc. AIME, Vol. 230, pp740-749, 1964.

80. Turkdogan, E.T., "The Theory of Enhancement of Diffusion-Limited Vaporization Rates by a Convection-Condensation Process. Part II - Experimental", Trans. Met. Soc. AIME, Vol. 230, pp750-753, 1964.

81. Szekely, J. and Themelis, N.J., "Rate Phenomena in Process Metallurgy", Wiley-Interscience, New York, 1971.

82. Soejima, T., Saito, T., Matsumoto, H., Shinozaki, K. and Minura, T., "Mechanism of Vacuum Decarburization during RH Treatment (Development of RH Refining Process - III)", Trans. ISIJ, Vol. 25, p B-146, 1985.

83. Ohno, R., "Kinetics of Evaporation of Various Elements from Liquid Iron Alloys Under Vacuum", "Liquid Metal Chemistry and Physics, ed. S.Z. Beer, , Marcel-Decker, New York, pp38-79, 1972.

84. Ranz, W.E. and Marshall, W.R., "Evaporation from a Drop", Chem. Eng. Prog., Vol. 48, pp141-146, pp173-180, 952.

85. Clift, R., Grace, J.R. and Weber, M.E., "Bubbles Drops and Particles", Academic Press, New York, NY, pp339-342, 1978.

86. Lee, H.S., "Spray Generation by Gas-Lift Pumps", M.Eng. Thesis, McGill University, Montreal, 1988.

87. Lau, K.H., Lamoreaux, R.H. and Hildenbrand, D.L., "Vapor Pressure Determination of Arsenic Activity in a Molten Cu-Fe-S Matte", Metall. Trans. B, Vol. 14B, pp 253-258, 1983.

88. Fruehan, R.J., "An Introduction to Vacuum Degassing", Iron and Steelmaker, Vol. 17, No. 6, p 42, June 1990.

89. Fruehan, R.J., "An Introduction to Vacuum Degassing", Iron and Steelmaker, Vol. 17, No. 7, pp 42-43, July 1990.

90. Fruehan, R.J., "An Introduction to Vacuum Degassing", Iron and Steelmaker, Vol. 17, No. 8, p 40, August 1990.

91. Fruehan, R.J., "An Introduction to Vacuum Degassing", Iron and Steelmaker, Vol. 17, No. 9, pp 48-49, 1990.

92. Fruehan, R.J., "An Introduction to Vacuum Degassing", Iron and Steelmaker, Vol. 17, No. 10, pp 70-71, 1990.

93. Allaire, A. and Harris, R., "Vacuum Distillation of Copper Matte to Remove Lead, Arsenic, Bismuth and Antimony", Metall. Trans. B, Vol. 20B, pp 793-804, 1989.

Appendix I

List of Equipment and Materials

Copper Matte	Reverberatory and "Noranda Reactor" matte, and converter white metal from the Norande Horne Smelter were provided by the Norande Technology Center in Pointe-Claire, Québec.
Graphite	Graphite of electrode grade was supplied by Speer Carbon Inc., St-Laurent, Québec.
Refractories	Alumina castable cement and alumina clay ramming mix (Thermogen 90 F plastic) were provided by Duquesne Refractory, Montréal, Québec.
Furnace	100kW, 3000Hz, "Tocco" induction furnace; coil diameter, 35 cm; manufactured by Inductoterm Inc., Rancocas, N.J..
Power Supply	100kW, 3000Hz, variable frequency power supply, model # 100-3-600. Manufactured and supplied by Bradley Controls Ltd, Withby, Ontario.
Vacuum Chamber	Cylindrical; volume of 2.25 m^3; diameter 1.5 m; length 1.8 m. Manufactured and supplied by Deltec Systems Inc. Primarose, Pa.
Pumping System	i)"Stokes" mechanical pump; nominal capacity of 0.142 m^3s^{-1}. Supplied by Deltec Systems Inc. ii)"Roots" blower; nominal capacity 0.614 $\cdot m^3s^{-1}$. Supplied by Deltec Systems Inc.
Pressure Gauge	"McLeod" gauge, 0 to 5 mm Hg. Supplied by Fisher Scientific Co., Montréal, Quebec.

Temperature Gauges	i)Ten chanels digital thermometer model DSS-660. Supplied by Omega Engineering Inc., Stanford, CT. ii)Two channel strip chart recorder model RD-199. Supplied by Omega Engineering Inc. Stanford, CT. iii)Analogic digital thermometer #AN467A-RC. Supplied by Thermo-Kinetics Ltd, Ville Lemoyne, Québec.
Thermocouples	i)Chromel Alumel "Type K" thermocouple with Nextel 312 ceramic fiber insulation. Supplied by Omega Engineering Inc., Stanford, CT. ii)Platinum Rhodium "Type R" thermocouple gauge 20. Supplied by Thermo-Kinetics, St-Laurent, Québec.
Oxygen Probe	Temp-O-Tips, Ni/NiO, "Type S", Platinum Rhodium Thermocouple. Supplied by Leeds and Northrup, Missisauga, Ontario.
Gases	Commercial purity nitrogen and dry air. Supplied by Welding Products Ltd, Montréal, Québec.
Resistive Heater	Heater # RH2007, 230 volts, embedded coil. Supplied by Thermcraft Inc., Winston-Salem, N.C. .
Insulators	Mulite ceramic insulators and protection tubes for thermocouples #MXRD-1204-12 and #42-1080-12. Supplied by Thermo-Kinetics Ltd, Ville Lemoyne, Québec.
Ceramic Glue	Aremco high temperature ceramic adhesive #503. Supplied by Subtec Ltd, Nepean, Ontario.

Appendix II

LSV Computer Simulation Program (Written by Frank Buijsen)

```
/INC WATFIV
      IMPLICIT REAL*8 (A-Z)
      DIMENSION OPSL(15,5),NULB(15),EPS(15),CONC(15,7)
      DIMENSION TEST(15),MASS(15),CB(15)
      INTEGER I,E,ES,J
      READ(5,*)E,T,PERCCU,MA,AR,PRCH,FML,FAUL,ENDTIM,STEPS,PSTEPS
      ES=E*3
      READ(5,*)(TEST(I),I=1,ES)
      TIME=0.
      PRTIME=0.
      F=FML*4.0907E-8
      RO=4100+22*(PERCCU-30)
      KL=2.E-4
      RT=8314*T
      BETA=(144.7/PERCCU)-1.81
      MASMT=(159.08+BETA*87.85)/(1+BETA)
      DT=ENDTIM/STEPS
      VOL=MA/RO
      WRITE(9,3)
    3 FORMAT('0','   **REFINING OF NORANDA COPPER-MATTE**')
      PRINT5,ES,T
    5 FORMAT('0',' NUMBER OF SPECIES:  ',I2,'     TEMP:'  ,F8.2)
      PRINT6,PRCH,MA
    6 FORMAT('0',' PRESSURE CHAMBER: ',F7.2,'     MASS:'  ,F8.2)
      PRINT7,PERCCU,F
    7 FORMAT(' 0','PERCENTAGE OF COPPER:   ',F6.2,'   SCAVENGING
     #GAS:  ',E14.5)
      PRINT8,ENDTIM,DT
    8  FORMAT('0','   TIME OF REFINING:',F8.2,'     STEP SIZE:'
     #,F8.2)
      DO 20 I=1,ES
      IF (TEST(I).EQ.1.) GOTO 15
      DO 10 J=1,5
      MASS(I)=0.0
   10 OPSL(I,J)=0.0
      GOTO 20
```

```
 15 READ(5,*) A,B,C,GO,PRESS,MI,ALPHA
    MASS(I)=MI
    OPSL(I,1)=A+B*T*DLOG10(T)+C*T
    OPSL(I,2)=GO*MASMT*DEXP(-OPSL(I,1)/(RT*1E-3))*DSQRT(PRESS)*
   #101350./RO
    OPSL(I,3)=DSQRT(RT/(2*3.141593*MI))*ALPHA
    OPSL(I,4)=(1.4E-4*(T**1.5))/(PRCH*1.E-2)
    CPSL(I,5)=1./((OPSL(I,3))+(1./OPSL(I,4)))
 20 CONTINUE
    AS=0
    WRITE(9,25)
 25 FORMAT('0','   DGO      U      KE      KG      KEG')
    PRINT30,((OPSL(I,J),J=1,5),I=1,ES)
 30 FORMAT('0',5E13.5)
    READ(5,*) (CB(I),I=1,ES,3)
    DO 35 I=1,ES,3
    NULB(I)=(CB(I)*RO)/(MASS(I)*100)
 35 CONTINUE
    PRINT36,TIME
 36 FORMAT('0','   TIME=',F10.2)
    PRINT37,(NULB(I),I=1,ES,3)
 37 FORMAT('0','INITIAL CONCENTRATION= ',E15.7)
    D=AR/RT
 40 SIGN=0
    DO 45 I=1,ES,3
    CONC(I,3)=(2.E-4*NULB(I)*RT)/(OPSL(I,5)*OPSL(I,2)+OPSL(I+
   #1,5)*OPSL(I+1,2)+OPSL(I+2,5)*OPSL(I+2,2)+2.E-4*RT)
    CONC(I+2,3)=CONC(I+1,3)=CONC(I,3)
    CONC(I,4)=CONC(I,3)
 45 CONTINUE
    DO 55 I=1,ES
    CONC(I,5)=D*OPSL(I,5)*CONC(I,3)*OPSL(I,2)
    IF(CONC(I,5).LT.0.) CONC(I,5)=0.0
    CONC(I,7)=CONC(I,5)
    SIGN=SIGN+CONC(I,5)
 55 CONTINUE
 65 DO 70 I=1,ES,3
    CONC(I,1)=(2.E-4*NULB(I)*RT)+PRCH*(OPSL(I,5)*(CONC(I,5)/
   #(SIGN+F))+OPSL(I+1,5)*(CONC(I+1,5)/(SIGN+F))+OPAL(I+2,5)*
```

```
     #(CONC(I+2,5)/(SIGN+F)))
      CONC(I,2)=(2.E-4*RT)+OPSL(I,5)*OPSL(I,2)+OPSL(I+1,5)*
     #OPSL(I+1,2)+OPSL(I+2,5)*OPSL(I+2,2)
      CONC(I,3)=CONC(I,1)/CONC(I,2)
      CONC(I+2,3)=CONC(I+1,3)=CONC(I,3)
  70  EPS(I)=DABS(CONC(I,3)-CONC(I,4))
      DO 85 I=1,ES
  85  CONC(I,4)=CONC(I,3)
      DO 90 I=1,ES,3
  90  IF (EPS(I).GT.FAUL) GOTO 100
      GOTO 130
 100  DO 105 I=1,ES
      CONC(I,6)=D*OPSL(I,5)*(CONC(I,3)*OPSL(I,2)-(CONC(I,7)/
     #(SIGN+F))*PRCH)
      IF(CONC(I,6).LT.0.) CONC(I,6)=0.0
      CONC(I,7)=CONC(I,6)
 105  CONTINUE
      SIGN=0
      DO 120 I=1,ES
      SIGN=SIGN+CONC(I,6)
 120  CONTINUE
      GOTO65
 130  IF(PRTIME.LT.PSTEPS) GOTO 155
      WRITE(9,135)
 135  FORMAT('0','    FLUX')
      PRINT145,(CONC(I,6),I=1,ES)
      WRITE(9,140)
 140  FORMAT('0',    CIF')
      PRINT146,(CONC(I,3),I=1,ES,3)
 145  FORMAT('0',3E13.5)
 146  FORMAT('0',5E13.5)
 155  IF(PRTIME.GE.PSTEPS) PRTIME=0
      TIME=TIME+DT
      PRTIME=PRTIME+DT
      DO 160 I=1,ES,3
      NULB(I)=NULB(I)-((CONC(I,6)+CONC(I+1,6)+CONC(I+2,6))/VOL)*DT
 160  CONTINUE
      IF(PRTIME.LT.PSTEPS) GOTO 165
 162  PRINT163,TIME
```

```
163 FORMAT('0',' TIME= ',F10.4)
    PRINT164,(NULB(I),I=1,ES,3)
164 FORMAT('0','NEW INITIAL CONCENTRATION= ',E17.9)
165 DO 166 I=1,ES,3
    VOL=VOL-((CONC(I,6)*MASS(I)+CONC(I+1,6)*MASS(I+1)+
   #CONC(I+2,6)*MASS*I+2))/RO)*DT
166 CONTINUE
    IF(TIME.GE.ENDTIM) GOTO 180
    GOTO 40
180 STOP
    END
```